

## 8. SITE 1124: REKOHU DRIFT—FROM THE K/T BOUNDARY TO THE DEEP WESTERN BOUNDARY CURRENT<sup>1</sup>

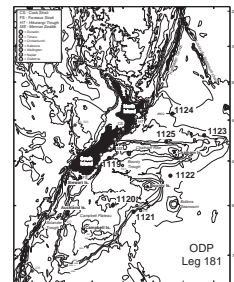
Shipboard Scientific Party<sup>2</sup>

### BACKGROUND AND OBJECTIVES

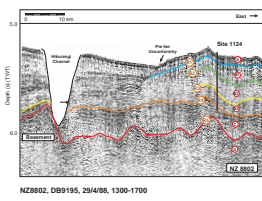
Site 1124 is located ~600 km east of Gisborne, North Island, New Zealand (Fig. F1), on the 250-km-long, north-south-trending ridge of Rekohu Drift, at a water depth of 3978 m. Seismic line NZ 8802 through the site (Fig. F2) shows that the main drift is onlapped from the west, with angular unconformity, by a sequence of turbidites that have over-spilled from the right bank of the Hikurangi Channel. These turbidites form part of the Hikurangi Fan Drift of Carter and McCave (1994), and are inferred to be of Pleistocene and perhaps late Pliocene age (cf. Lewis, 1994; Lewis et al., 1998). The Rekohu Drift ridge has clearly acted as a recent barrier to the eastward dispersal of terrigenous sediment from the Hikurangi Channel, which turns abruptly to the north against the drift. Until about the late Pliocene, the channel is thought to have flowed northeast directly along the axis of the Hikurangi Trough toward Kermadec Trench and to have become diverted eastward when a major slide blocked the trough-axis off Hawkes Bay (Lewis et al., 1998).

The Rekohu Drift sequence occurs above a regional reflector (R4), which before drilling was correlated with reflector X of presumed Oligocene age (Davey, 1977). Sediments of seismic Unit C, between R4 and the basement, are locally up to 200 ms thick, and overlie the basement (including fault-angle depression infills) as a simple drape. The upper part of Unit C is characterized by heavy, subparallel reflectors, indicating the probable presence of sands, cherts, or carbonates. As summarized in Table T1, the main Rekohu Drift comprises seismic Units A (65 m thick), B1 (78 m thick), B2 (150 m thick), and B3 (129 m thick). Unit B3 is characterized by the presence of “blotchy” reflecting zones within

F1. Locality map of Site 1224, p. 42.



F2. Portion of seismic line NZ 8802, p. 43.



T1. Summary of main seismic units and reflectors, p. 88.

<sup>1</sup>Examples of how to reference the whole or part of this volume.

<sup>2</sup>Shipboard Scientific Party addresses.

an otherwise almost transparent acoustic background. The seismic Unit A/B1 boundary may lie near the level of regional unconformity Y (Davey, 1977). A high-resolution 3.5-kHz profile (Fig. F3) indicates that the shallow stratigraphy comprises cyclic pelagic sediments, subparallel to the seafloor, with a particularly prominent reflector at a depth of 12 m (reflector  $\beta$  of Carter and McCave, 1994; McCave and Carter, 1997).

Before drilling, it was hoped that Site 1124 would yield a mainly biopelagic carbonate record of the Miocene paleohydrography of the Deep Western Boundary Current (DWBC). It was anticipated that in the upper part of the hole tephra would provide important information about the Neogene volcanic history of the active arc system in nearby North Island (e.g., Alloway et al., 1993; Shane et al., 1996). Finally, and if drilling penetrated reflector R4, the initiation of the DWBC and related current systems might be dated within the context of the regional stratigraphy.

## **OPERATIONS**

### **Hole 1124A**

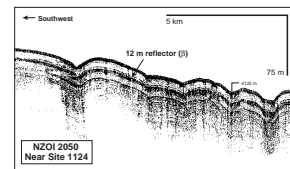
The vessel proceeded directly to the Global Positioning System coordinates of Site 1124 (proposed site SWPAC-9B), where the positioning beacon was deployed and the hydrophones and thrusters were lowered. The advanced hydraulic piston corer/extended core barrel (APC/XCB) bottom-hole assembly (BHA) was assembled using a 9 $\frac{7}{8}$ -in PDC bit and deployed. Hole 1124A was spudded with the APC at 0610 hr on 26 September. The core barrel was full and required a second attempt at recovering a mudline.

### **Hole 1124B**

The bit was positioned at 3962.5 m below sea level (mbsl), which was 5 m higher than the bit position of Hole 1124A. The initial attempt at a mudline core on this hole was thwarted when the core barrel was recovered with a shattered liner and no core. Another core barrel was deployed and Hole 1124B was spudded with the APC at 0507 hr on 26 September. At 0610 hr the second piston core in Hole 1124B was shot with the bit at 3972.0 mbsl (5.4 meters below seafloor [mbsf]). Because of an incomplete stroke, the drill string pressure had to be manually bled off. The core barrel could not be retrieved with 10 kips of overpull being applied. Various attempts to free the stuck core barrel proved unsuccessful. After the sinker bar assembly was recovered with the wireline, the top drive was racked, and the BHA with the stuck APC barrel was retrieved. At 1745 hr on 26 September, the bit was at the rotary table. The APC corer was found in a fully stroked out position and the bottom section of the inner barrel was extended below the bit and bent ~1 m below the BHA, which prevented retrieving the core barrel through the bit.

It was concluded that the piston corer impacted a thick layer of tephra at a shallow depth which forced the BHA to displace horizontally and bend the core barrel. Because of the shallow penetration (4.5 m), the sediment provided very little lateral support to the BHA when the piston corer advanced into the hard layer of tephra. The situation can be compared to trying to balance a full bottle of soda in the air with a plastic straw.

F3. Portion of 3.5 kHz line NZOI 2050, p. 44.



## **Hole 1124C**

Because of the incident in Hole 1124B, it was decided to drill the first two cores in Hole 1124C with the XCB. Hole 1124C was spudded at 0220 hr on 27 September and washed to 8.0 mbsf, where XCB coring was initiated. XCB coring advanced from 8.0 to 27.2 mbsf with 74% recovery (Table T2, also in [ASCII format](#)). The coring system was then switched to the APC and piston coring advanced from 27.2 to 159.2 mbsf, which was considered APC refusal. The Adara heat-flow shoe was affixed to the APC corer for Cores 5H (55.7 mbsf), 7H (74.7 mbsf), 9H (93.7 mbsf), and 11H (112.7 mbsf). The data from the last three runs were used to compute a temperature gradient of 51.9°C/km.

XCB coring deepened the hole from 159.2 to 473.1 mbsf (Table T2), which was considered the depth objective for this hole.

---

T2. Site 1124 coring summary,  
p. 89.

---

### **Logging Operations in Hole 1124C**

In preparation for logging, an aluminum go-devil was dropped and the hole swept with 60 barrels of high-viscosity mud. The bit was pulled back in the hole to 447 mbsf, and the hole was displaced with 175 barrels of sepiolite mud. The bit was then positioned at the logging depth of 96 mbsf.

Logging operations began at 2100 hr on 29 September and lasted for 19 hr. Logging was conducted from the bottom of the hole at 474 mbsf to the bit at 78 mbsf (picked up from 96 mbsf). Three standard tool string configurations were run: the triple combination, the FMS-sonic, and the GHMT (see “[Downhole Measurements](#),” p. 29, in the “Explanatory Notes” chapter for details). The NMRS tool on the GHMT failed to operate. The condition of the borehole was good and the quality of the data is excellent. By 1545 hr on 30 September, the Schlumberger equipment was disassembled, and the drill bit cleared the seafloor at 1630 hr.

## **Hole 1124D**

The vessel was offset 30 m to the north of Hole 1124C. An attempt was made to wash down to 13 mbsf, but was given up when very hard formation (possibly cemented ash) was encountered. The vessel was offset an additional 10 m to the west where Hole 1124D was spudded with the XCB at 1917 hr on 30 September. The bit was drilled ahead to 22.6 mbsf with no difficulty and the XCB wash barrel was recovered. APC coring was initiated at this depth and continued to the planned depth objective of 155.6 mbsf (Table T2).

The drill string was pulled to the surface with the bit clearing the seafloor at 1325 hr. As soon as the bit cleared the seafloor, the beacon was recalled. After the BHA was inspected, the drilling equipment was secured and the vessel was under way to Site 1125, the last site of Leg 181, at 2330 hr on 1 October.

## **LITHOSTRATIGRAPHY**

### **Introduction**

As the northward-flowing DWBC passes the eastern end of Chatham Rise, it swings northwestward along a region of moderate to low relief. The effect of this weak western boundary is to decelerate the flow, thereby instigating sediment deposition (McCave and Carter, 1997).

Part of this load has accumulated to form Rekohu Drift, which extends north from 41°S to 39°S. Apart from a few 3.5-kHz and single-channel seismic profiles, the only other control of the drift sediments is a kasten and a piston core collected at National Institute of Water and Atmospheric Research (NIWA) Station S931, just north of Site 1124. The barrel of the kasten core was bent during coring, presumably as a consequence of striking a consolidated tephra layer. The piston corer, however, penetrated 2.6 m and recovered a cyclic sequence of carbonate-bearing (interglacial) and carbonate-poor (glacial) mud, which, on the basis of the carbonate curve and two dated tephra layers—the Kawakawa Tephra of 22,590 radiocarbon years (Carter et al., 1995) and Omataroa Tephra of ~28,000 radiocarbon years (Froggatt and Lowe, 1990)—extended back to isotope Stage 5. Even though the 4001-m depth of Site 1124 approaches the regional Carbonate Compensation Depth (CCD) of ~4500 m, a reasonable carbonate record was obtained in piston core S931 with a maximum value of 73% (isotope Stage 5e). Hence, the site was anticipated to provide a carbonate-based record of Lower Circumpolar Deep Water entry into the Pacific.

## Description of Lithostratigraphic Units

Cores from Site 1124 showed that the sedimentary sequence is composed mainly of clay-bearing nannofossil ooze and chalk with interbeds of more terrigenous sediment and, in the top half of the core, frequent layers of tephra. A total of six lithostratigraphic units are recognized on the basis of the core visual descriptions supplemented with data from smear slides, carbonate analyses, X-ray diffraction (XRD), and physical properties including light reflectance. The generalized characteristics of the lithostratigraphic units are summarized in Figure F4 with a more specific set of logs, combining biostratigraphic and magnetostratigraphic data, presented in Figure F5.

With respect to reflectance, values at 550-nm wavelength were plotted as the dependent variable against  $\text{CaCO}_3$  percentage (Fig. F6). The resultant correlation was sufficiently robust to allow use of reflectance as a proxy for carbonate concentrations for most of Site 1124 cores. As reflectance measurements were made at 2-cm intervals, the data provided a detailed and accurate measure of carbonate cyclicity and fluxes (e.g., Mix et al., 1995) (Fig. F7). An exception was the dark brown mudstone of Unit IV, which had anomalously high reflectance relative to its 50% carbonate content. A downcore plot of reflectance as a ratio of 700/400 nm produced a profile that outlined the boundaries of the main lithostratigraphic units (Fig. F7).

### Unit I

Unit I encompasses a succession of interbedded ooze, chalk, and silty clay extending from the seafloor to 300 mbsf. Three subunits, IA to IC, are recognized (Fig. F4).

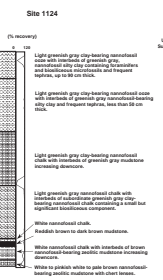
#### Subunit IA

Interval: Section 181-1124A-1H-CC; Sections 181-1124B-1H-1 through 2H-CC; Sections 181-1124C-1X-1 through 6H-4; Sections 181-1124D-1H-1 through 4H-CC

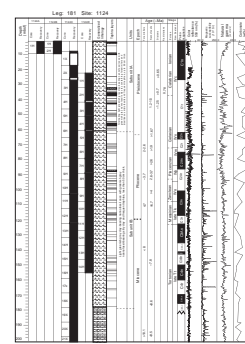
Depth: 0–9.5 mbsf (Hole 1124A); 0–9.9 mbsf (Hole 1124B); 8–60.6 mbsf (Hole 1124C); 22.6–60.6 mbsf (Hole 1124D)

Age: Pleistocene

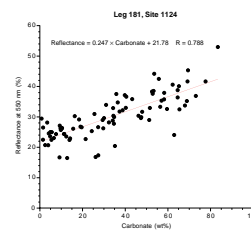
F4. Lithostratigraphic summary from Site 1124, p. 45.



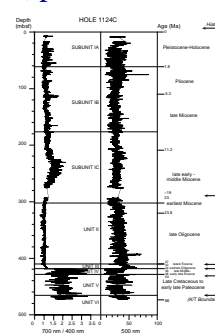
F5. Summary of lithostratigraphic, biostratigraphic, and magnetostratigraphic data, p. 46.



F6. Carbonate vs. reflectance with regression equation, p. 49.



F7. Downcore profiles of color reflectance, p. 50.



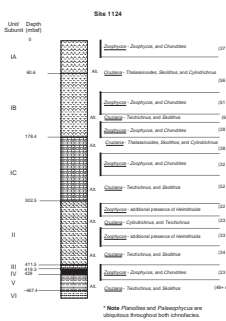
Commencing at the seafloor as an oxidized, light yellowish brown (10YR 6/4) nannofossil silty clay, Subunit IA continues downcore as a sequence of light and darker colored layers. The light layers are light greenish gray (5GY 7/1) to white (5Y 8/1) clay-bearing nannofossil ooze and nannofossil ooze, with a small component of foraminifers. These carbonate-dominant sediments are interpreted as representing interglacial periods. By comparison, darker layers are mainly greenish gray (5GY 5/1 to 5GY 6/1) silty clay to nannofossil-bearing silty clay, which are regarded as glacial period deposits. The darker layers are further distinguished by a small but significant biosiliceous component of radiolarians, diatoms, and spicules, as well as fewer foraminifers and less quartz/feldspar. Both foraminifers and biosiliceous elements help distinguish Subunit IA from the underlying subunits. Judging by the 500-nm reflectance profile (Fig. F7), there is a general increase in carbonate toward the base of the subunit. This change is accompanied by a small increase in quartz and feldspar indicating either higher terrigenous or volcanic fluxes or both of these inputs. Obviously, the carbonate flux outstripped the other increments, suggesting either higher production or lower dissolution (e.g., see Weaver et al., 1998).

Bioturbation is pervasive and is manifested in two ichnofacies. The upper part of Subunit IA has a *Zoophycos* facies of *Zoophycos* and *Chondrites* together with the less facies-specific *Planolites* and *Palaeophycus*. In contrast, the lower part of the subunit bears the *Cruziiana* facies of *Thalassinoides*, *Skolithos*, and *Cylindrichnus* again with *Planolites* and *Palaeophycus* (Fig. F8).

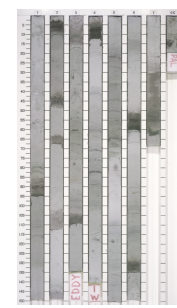
Another feature is layers of typically pinkish gray (5YR 5/1 to 5YR 6/1) to light pinkish gray (5YR 7/1) macroscopic tephra up to 92 cm thick (181-1124C-3H-3 to 3H-4) (Fig. F9). However, this may not be the largest deposit encountered as Core 181-1124A-1H failed to fully penetrate a tephra of >81 cm thickness. A typical tephra layer has a sharp base, normal grading and, frequently, a bioturbated top (Fig. F10). Such attributes are consistent with both airfall deposits and turbidites, but the purity of the ash, the absence of Bouma-type sedimentary structures, and the location of the site on the crest of a ridge well above Hikurangi Channel collectively favor the airfall hypothesis. Sixty-eight tephra layers were recorded, mainly within four clusters throughout the subunit (Fig. F11). The total of 68 is, of course, a minimum value in light of unrecovered sediment, in particular the 8.15 m absent in Core 181-1124C-1X (Fig. F5). Furthermore, the total does not include the products of eruptions that produced smaller amounts of tephra. Carter et al. (1995) suggested that deposits <1 cm thick had a low rate of survival because of bioturbation. Certainly, layers <1 cm thick are few, whereas tephra-filled burrows are often present.

Dark green silty clay laminae are scattered throughout the core. Smear slides and XRD analyses from laminae indicate the presence of smectite and fragments of volcanic glass, suggesting formation by the alteration of thin layers of basic tephra. A similar conclusion was also reached by Gardner et al. (1986) and Nelson et al. (1986) for green layers at Deep Sea Drilling Project (DSDP) Site 593 on Challenger Plateau, west of New Zealand. Site 1124 green layers were excluded from the tephra count.

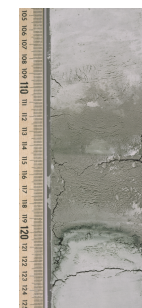
F8. Downcore distribution of *Zoophycos* and *Cruziiana* ichnofacies, p. 51.



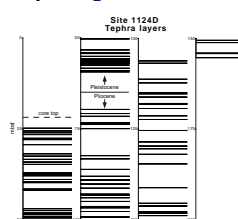
F9. Distribution of Pleistocene rhyolitic tephra, Subunit IA, p. 52.



F10. Typical tephra layer, upper Subunit IB, p. 53.



F11. Distribution of macroscopic tephra layers, p. 54.



***Subunit IB***

Interval: Sections 181-1124C-6H-4 through 19X-1; Sections 181-1124D-5H-1 through 14H-CC

Depth: 60.6–178.4 mbsf (Hole 1124C); 60.6–155.6 mbsf (Hole 1224D)

Age: early Pleistocene to late Miocene

Subunit IB consists of 0.2- to 1.0-m-thick beds of greenish gray (5GY 5/1 to 5GY 6/1) and light greenish gray (5GY 7/1) silty clay grading to nannofossil silty clay intercalated with light greenish gray (5GY 7/1 to 5BG 7/1) and white (5Y 8/1) clayey nannofossil ooze grading to nannofossil ooze. This lithologic and color layering is similar to that of Subunit IA. Likewise, the dominance of the *Zoophycos* and *Cruziana* ichnofacies is common to both subunits, although the Subunit IB *Cruziana* facies may be more diverse with the addition of *Teichichnus*. Furthermore, Subunit IB contained 60 macroscopic tephra layers, which is only two less than Subunit IA. Despite the similarities, there remain sufficient differences to warrant a separate Subunit IB. The distinguishing features follow:

1. Carbonate decreases downcore as inferred from reflectance profiles (Fig. F7) and confirmed by a downcore increase in more terrigenous sediments (e.g., silty clay and clayey nannofossil ooze).
2. Siliceous microfossils and foraminifers are rare or absent.
3. Tephra layers are thinner with a maximum thickness of <30 cm as well as a smaller total thickness of 5.75 m compared to 8.03 m for Subunit 1A.

***Subunit IC***

Interval: Sections 181-1124C-19X-1 through 31X-6

Depth: 178.4–302.5 mbsf (Hole 1124C)

Age: late Miocene to early Miocene

Subunit IC is heralded by a change from ooze to chalk. However, the sequence still retains the light and darker color banding characteristic of the overlying subunits, and it supposedly reflects a similar paleoclimatic cyclicity. At the top of the sequence, the differences between bands are subtle with light greenish gray (5GY 7/1) clay-bearing nannofossil chalk intercalated with greenish gray (5GY 6/1) clayey nannofossil chalk. Further downcore, the trend is toward less carbonate-rich sediments, although, as the carbonate curve shows, this trend is irregular (Fig. F5). At 226.5 mbsf, for example, a light/dark couplet comprises pale yellow (5Y 7/3) clayey nannofossil chalk and pale olive (5Y 6/3) nannofossil mudstone, and at 255 mbsf the dark couplet is replaced by mudstone. This downcore change is accompanied by an increase in the amounts of quartz, feldspar, and mica.

The subunit is further distinguished from its younger counterparts by a paucity of tephra layers. Only eight thin layers, with a total thickness of 29 cm, were detected in the upper part of Subunit IC. The oldest recognized tephra is at 207 mbsf and has an estimated age of 12 Ma. Since that time, it and any older tephra have altered, mainly to clay.

The ichnofacies are again alternations of *Zoophycos* and *Cruziana*, the latter having slightly different assemblages comprised of *Thalassinoides*, *Skolithos*, and *Cylindrichnus* in the uppermost 30 m of Subunit IC and *Teichichnus* and *Skolithos* in the basal 52 m (Fig. F8).

## **Unit II**

Interval: Sections 181-1124C-31X-6 through 43X-2

Depth: 302.5–411.5 mbsf (Hole 1124C)

Age: early Miocene to late Oligocene

The top of Unit II is positioned near the base of Core 181-1124C-31X on the basis of abrupt changes in sediment characteristics recorded by the wireline logging tools (see “**Downhole Measurements**,” p. 36). Core 181-1124C-31X was the first section below a zone of very poor recovery in interval 181-1124C-29X to 30X, in which there is an abrupt change in lithology. By comparison, the base of the unit is well constrained by what we interpret to be the Marshall Paraconformity. The actual boundary is present in Core 181-1124C-43X. It appears as a well-defined contact separating light greenish gray (5BG 7/1) clay-bearing nannofossil chalk from underlying white (5Y 8/1) nannofossil chalk. *Planolites* and *Zoophycos* burrows mix sediment across the contact (Fig. F12).

The upper part of Unit II is white (5Y 8/1) to light greenish gray (5GY 7/1) nannofossil chalk with interbeds and laminae of greenish gray (5G 6/1) clay-bearing nannofossil chalk that grades downcore through a nannofossil-bearing mudstone to a plain mudstone. These greenish gray beds have a conspicuous biosiliceous component of radiolarians, diatoms, and spicules, the last component sometimes having high enough concentrations to warrant the term “spicule bearing.” Of note is the presence of finely laminated, flaser-like beds, which is the first evidence of bottom current activity in the unit (Fig. F13).

Regularly alternating zones characterized by the *Cruziana* and *Zoophycos* ichnofacies occur through Unit II. The *Zoophycos* ichnofacies is particularly well developed (Fig. F14) and is further distinguished by the presence of *Helminthoida*.

## **Unit III**

Interval: Sections 181-1124C-43X-2 through 44X-1

Depth: 411.5–419.3 mbsf (Hole 1124C)

Age: early Oligocene

Unit III is composed of a uniform white (5Y 8/1) clayey nannofossil chalk. The white color belies the presence of a significant clay content, which may be as high as 45% as suggested by a single carbonate determination (Fig. F5). Smear slides reveal a dominance of nannofossils with abundant clay and accessory amounts of feldspar, mica, and foraminifers. The unit is massive and is probably bioturbated, although the lack of color differentiation precludes identification of individual trace fossils.

The top of the unit is bounded by the Marshall Paraconformity, whereas the base is a sharp contact with the multihued mudstones of Unit IV.

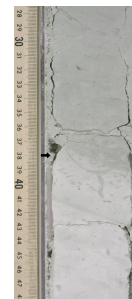
## **Unit IV**

Interval: Sections 181-1124C-44X-1 through 44X-8

Depth: 419.3–429.0 mbsf (Hole 1124C)

Age: middle to late Eocene

F12. The Marshall Paraconformity, p. 55.



F13. Dark green, flaser-like laminae, Unit II, p. 56.



F14. Well-developed *Zoophycos* trace fossils, lower Unit II, p. 57.



Unit IV marks an abrupt change to mudstone in various hues of reddish brown (5YR 6/6 – 6/5), pink (5YR 8/3), yellowish brown (10YR 6/4–5/4), and dark brown (10YR 4/3) toward the unit's base. Contacts between the various colored layers tend to be gradational, and bioturbation is pervasive with a *Zoophycos* ichnofacies and a strong representation by *Planolites* and *Palaeophycus*. Smear slides reveal a dominance of clay and quartzofeldspathic silt, with the latter tending to decrease toward the dark brown mudstone at the unit's base. Nannofossils also decrease toward the dark brown mudstone, whereas zeolites tend to increase downcore and become ~25% of the sediment. X-ray diffraction of the mudstone reveals a high content of expandable, dioctahedral clay minerals possibly Na-montmorillonite. No chlorite was found, but traces of illite and small amounts of quartz and silica were detected. The clinoptilolite is the most likely candidate.

## **Unit V**

Interval: Sections 181-1124C-45X-1 through 48X-5

Depth: 429.0–467.4 mbsf (Hole 1124C)

Age: early Paleocene

The main lithology in Unit V is a nannofossil-bearing mudstone that, near the top of the section, is in various shades of light brown (light brownish gray = 10YR 6/2; pale brown = 10YR 6/3 to 7/3). Isolated beds of nannofossil chalk also occur near the top of the section, whereas the lower section includes pinkish white (7.5YR 8/2) mudstone and nannofossil mudstone laminae. The contacts between the light brown beds and light laminae are often knife-edge sharp and appear to represent chemical fronts whose brownish hue may be related to manganese in the sediments. The basal sedimentary rock is reddish brown (5YR 6/4) mudstone with chert layers or lenses. Smear slides indicate that the light brown mudstone is composed mainly of clay, nannofossils, and needle-like crystals of zeolite that are tentatively identified as clinoptilolite on the basis of a single XRD analysis. Foraminifers are also present and help differentiate Unit V from underlying rocks.

Differences in sediment color at bed and laminae contacts highlight the trace fossils, which mainly belong to the *Zoophycos* ichnofacies containing *Chondrites* and the ubiquitous *Planolites* and *Palaeophycus*. Some burrow fillings are dark pink to red (2.5YR 4/8), suggesting the possible the onset of chert formation.

The base of Unit V is the Cretaceous/Tertiary (KT) boundary which, on the basis of the biostratigraphy, is positioned between Cores 181-1124C-48X-5 and 49X-1. The inferred position of the boundary coincides with a strong spike in the wireline resistivity logs (see “[Downhole Measurements](#),” p. 36).

## **Unit VI**

Interval: Sections 181-1124C-49X-1 through 49X-5

Depth: 467.4– 473.1 mbsf (Hole 1124C)

Age: Late Cretaceous

Rocks of Unit VI are nannofossil-bearing mudstones in various colors that include (passing downcore) brown, gray, white, and pink. Munsell notations and detailed distribution of the different colored beds and laminae are summarized in the appropriate barrel sheet. The main com-

ponents are clay, zeolites (clinoptilolite?), and nannofossils. Foraminifers are absent.

Bioturbation is present throughout with trace fossils best seen near the contacts of differently colored beds. Burrows appear to be vertically compressed but the fossils are still recognizable. Compared to Unit V, Unit VI has a *Cruziana* ichnofacies of *Teichichnus* and *Skolithos*, together with *Palaeophycus* and *Planolites* (Fig. F8). Some burrows have a distinct reddish brown color (2.5YR 6/4) that presumably highlights the presence of chert.

## **Discussion**

The sedimentary record postdating the Marshall Paraconformity encompasses the last 27 m.y. Apart from a 5-m.y. hiatus in the lower Miocene, this record is expected to provide a long-term history of deep-water sedimentation beneath the DWBC. The following is a brief interpretation of the paleoceanographic events beginning from the base of the Site 1124 sequence.

Over the past 27 m.y., sedimentation at Site 1124 has exhibited marked cyclicity as shown in the 500-nm reflectance proxy for calcium carbonate (Fig. F7). Furthermore, the cycles are superimposed on longer term changes exemplified by the general increase in reflectance/carbonate up through the lower Pliocene (Fig. F7). Whether or not the cycles have Milankovich frequencies must await an astronomically tuned time scale for the site. Whatever the case, the cycles display changes in sediment composition that may be interpreted in terms of oceanographic variability, tectonism, and volcanism.

The Marshall Paraconformity is a regional feature formed by widespread erosion of the ocean floor around 32 Ma (e.g., Kennett et al., 1985; Carter, 1985; Fulthorpe et al., 1996). In the case of Site 1124, it probably heralds the inflow of the DWBC to the Southwest Pacific Ocean (Kennett, 1977; Carter and McCave, 1994). Waning of the flow following its initial incursion may be recorded in the sediments directly above the paraconformity. Basal sediments of Unit II have elevated terrigenous contents that coincide with the appearance of the *Cruziana* ichnofacies. This assemblage, according to Pemberton and MacEachern (1995), is indicative of an energetic, well-ventilated, deep-water environment. Furthermore, the appearance of a small but diverse biosiliceous component of radiolarians, diatoms, and spicules indicate cold-water conditions that would be consistent with an inflow from Antarctic reaches. This cold inflow appears to diminish in the late Oligocene, as manifested by the prevalence of nannofossil ooze (chalk) and by the occurrence of the *Zoophycos* ichnofacies, which indicates a quiet, deep-water environment. Further cycles of a terrigenous, energetic setting and a pelagic, quiet-water setting occur through Unit II, but in a more subdued form compared to the cycle near the Marshall Paraconformity.

Immediately following the erosional event responsible for the early Miocene (19–23.8 Ma) unconformity at the top of Unit II, the basal beds of Subunit IC reveal an increased input of terrigenous sediment that is coupled with a switch to the energetic *Cruziana* ichnofacies. Like Unit II, the terrigenous component decreases and nannofossil ooze (chalk) increases further upsection in consort with a change to the *Zoophycos* ichnofacies. Nevertheless, a higher frequency cyclicity, as identified from the reflectance profiles, is expressed in the carbonate content. The causes of these fluctuations are unclear. It may simply be a response to variations in terrigenous load carried by the DWBC. Significantly,

this load contains mica. This mineral is interpreted to be an indicator of a southern source, in particular, the Bounty Trough, which receives sediment from the mica-rich, metamorphic terrain of the South Island (Carter and Mitchell, 1987). This would mean that the Bounty Channel was actively injecting sediment into the DWBC in early Miocene times. It is unlikely that the other main sediment supplier, Hikurangi Channel, was contributing to the DWBC and Rekohu Drift, because the channel had probably not yet diverted from its original course toward Kermadec Trench (Lewis, 1994, 1998; this report, see “[Background and Objectives](#),” p. 1).

Carbonate cyclicity may also have been influenced by dissolution, as suggested by the paucity and poor preservation of the nannofossil and planktonic foraminiferal fauna. Dissolution may be related to changes in the regional CCD. Site 1124 is only 500 m above the modern CCD and is thus exposed to relatively small fluctuations of this boundary. Such changes may be related to large-scale incursions of cold water carried north by the DWBC and/or changes in the global CCD. But direct evidence for the postulated incursions is equivocal. Biosiliceous microfossils, indicators of cold water masses, are few at Site 1124. Their paucity, however, may be related to corrosion, as suggested by the poor condition of the few specimens observed (see “[Biostratigraphy](#),” p. 12). This poor preservation of microfossils extends through Subunit IC.

For the lower part of Subunit 1C, incursions of cold corrosive waters is at odds with the paleoclimatology, which reveals a climatic optimum from 19.5 to 16.5 Ma in high southern latitudes (Kennett and von der Borch, 1986). However, following this event there appears to have been a major expansion of the East Antarctic ice sheet and cooling of bottom waters, which presumably extended into the Southwest Pacific under the DWBC.

Terrigenous sediment increases towards the top of Subunit IC and on to the middle of Subunit IB at the base of the Pliocene (~5.3 Ma). The trend is consistent with the increased tempo of uplift onshore that followed instigation of a collisional plate boundary through the New Zealand region (e.g., Rait et al., 1991). Although the long-term trend is one of terrigenous increase, it is superimposed on a cyclicity that is well displayed in color reflectance and other physical parameters (Fig. F5; also see “[Composite Depths](#),” p. 27) as well as by the alternations of light-colored nannofossil ooze and darker colored silty clay. In view of the prominence of the terrigenous signal, such cyclicity would have been strongly influenced by changes in sediment supply from south of Chatham Rise. Supply may be affected by bouts of erosion under the DWBC and Antarctic Circumpolar Current (ACC), as indicated by the intensely eroded sediment cover at Site 1121, or by variations in the sediment supply via Bounty Channel (e.g., Carter and Carter, 1993), or by both these processes. Furthermore, there is a suggestion that the cycles may be climatically driven. Dark layers have a biosiliceous component of radiolarians, diatoms, and spicules that is typical of glacial periods, whereas the light-colored nannofossil oozes are more interglacial in character (e.g., Griggs et al., 1983; Weaver et al., 1998).

The Pliocene sediments display a reversal in the earlier compositional trend, with a gradual increase in carbonate content extending from 5.3 to ~2.3 Ma (Fig. F7). This trend is consistent with a mid-Pliocene increase in biogenic carbonate productivity that resulted from a general warming of Southwest Pacific surface waters, concomitant with increased upwelling (Kennett and von der Borch, 1985). From 2.3

Ma to the late Quaternary, the compositional trend inferred from the 550-nm reflectance data suggests a slight change back to a more terrigenous sediment (Fig. F7). This change is not clear in the carbonate record (Fig. F5), but this record is based on widely scattered data points and is not definitive. Again, a series of cycles are superimposed on the general trend, and these are regarded as glacial/interglacial cycles on the basis of their microfossil contents and lithology. The overall change to more terrigenous and, in the case of glacial period sediments, to more biosiliceous sediments, reflects the combined influence of large paleoclimatic fluctuations, increased uplift along the New Zealand plate boundary, and increased volcanism. Specifically,

1. A combination of colder waters and increased upwelling under strong glacial wind regimes (e.g., Stewart and Neall, 1984) encouraged the production of biogenic silica that is reflected in the improved diatom and radiolarian contents of the upper Pliocene–Pleistocene section (see “[Biostratigraphy](#),” p. 12).
2. Increased uplift, together with the progressive uncovering of readily erodible schists on the South Island, ensured an increasing sediment supply to the DWBC and ACC via the Solander, Bounty, and possibly Hikurangi Channels (e.g., Carter et al., 1996). Certainly, the increase in sedimentation around 2 Ma on the Bounty Fan (see the “[Site 1122](#)” chapter) coincides with a similarly timed increase in sedimentation at Sites 1123 and 1124. The way in which Hikurangi Channel is involved is, however, unclear. Although the modern channel is proximal to Rekohu Drift, there is little evidence from Site 1124 visual core data to show that turbidity currents overspilled the channel levees and extended onto the drift. More likely is the wafting of any residual turbidity current plumes onto Rekohu Drift by the DWBC. These turbidity currents would only have come to the Rekohu Drift area after diversion of Hikurangi Channel to the east (Lewis et al., 1998). This probably occurred in the early Pleistocene and may well be marked by the sharp increase in sedimentation rate at around 1.5–1.2 Ma (see “[Magnetostratigraphy](#),” p. 24).
3. The size and frequency of volcanic eruptions increased through the Pliocene and into the Pleistocene (Shane et al., 1996). Seventy macroscopic tephra layers were recorded in the Pliocene to give an average frequency of one tephra per 50 k.y. The total thickness of tephra was ~5% of the Pliocene sequence. In contrast, tephras compose 13% of the Pleistocene sequence and have an average frequency of one tephra per 29 k.y.
4. Although the timing is uncertain, Rekohu Drift probably also received sediment derived from Chatham Rise via Rekohu Canyon (see Carter and McCave, 1994). The canyon feeds a small, turbidite-filled basin to the south of Rekohu Drift, which, therefore, will only receive that part of the turbidite plume transported by the DWBC. Furthermore, the contribution is liable to be small, as Rekohu Canyon has no obvious sediment source apart from Chatham Rise sediment, which is most likely to be remobilized only during maximum lowstands of sea level.

# BIOSTRATIGRAPHY

## Summary

Site 1124, drilled on the Rekohu Drift in 4000-m water depth, proved a challenge for dating because of the poor preservation of microfossils in the Oligocene and Neogene strata; despite this, the nannofossils proved the most useful for dating throughout the hole. Foraminifers provided good resolution in the uppermost Miocene–Pliocene and in the Cretaceous and Paleogene. Good radiolarian faunas are present in the upper Neogene, upper Oligocene, and Cretaceous–Paleocene and were particularly useful in resolving the Oligocene/Miocene boundary. Diatoms are poorly preserved and of little value in the Paleogene and Cretaceous but provided additional biostratigraphic resolution and evidence of sediment provenance in the upper Neogene. The biostratigraphy of Site 1124, as determined by the various microfossil groups, is summarized in Figures F15 and F16.

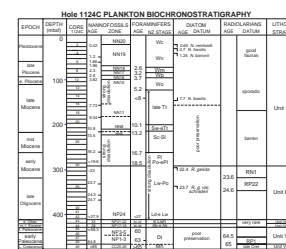
The following major intervals have been determined by combining results from all groups:

Pleistocene–Holocene (0–1.8 Ma), 0 to ~65 mbsf, lithostratigraphic Subunit IA;  
Pliocene (1.8–5.3 Ma), 65 to ~115 mbsf, lithostratigraphic Subunit IB (upper);  
late Miocene (5.3–11.2 Ma), 115 to ~210 mbsf, lithostratigraphic Subunits IB (lower) and IC (upper);  
late early–middle Miocene (~11.2–19 Ma), 210 to 290 mbsf, lithostratigraphic Subunit IC (lower);  
hiatus (~3.4 m.y.), 290 mbsf;  
earliest Miocene (~22.4–23.6 Ma), 290 to 322 mbsf, lithostratigraphic Unit II;  
late Oligocene (23.6–~27 Ma), 322 to 412 mbsf, lithostratigraphic Unit III;  
hiatus = Marshall Paraconformity (3–5 m.y.), 412 mbsf;  
early Oligocene ([? 30] 32–34 Ma), 412 to 419 mbsf, lithostratigraphic Unit IV;  
hiatus (~2 m.y.), 419 mbsf;  
late middle–early late Eocene (36–38 Ma), 419–428 mbsf, lithostratigraphic Unit V;  
hiatus (>20 m.y.), 428 mbsf;  
Late Cretaceous to early late Paleocene (59–~66 Ma), 428–473 mbsf, lithostratigraphic Unit VI; and  
Cretaceous/Tertiary boundary, lost between 463–467 mbsf.

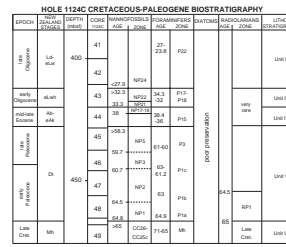
## Age

The micropaleontological biostratigraphy of Site 1124 is mostly based on the onboard study of core-catcher samples. Samples from Holes 1124A and 1124B were used for the uppermost part of the section, and Samples from Hole 1124C for the majority. Additional samples were taken from within selected cores to address specific age and paleoenvironmental questions. The absolute ages assigned to biostratigraphic datums follow the references listed in Tables **T2**, p. 59; **T3**, p. 60; **T4**, p. 63; **T5**, p. 64; all in the “Explanatory Notes” chapter.

F15. Biostratigraphic summary chart, p. 58.



F16. Biostratigraphic summary chart for the Paleogene and Late Cretaceous, **p. 59**.



### Calcareous Nannofossils

Samples obtained from Hole 1124C, together with several samples taken from Holes 1124A and 1124B, were examined for nannofossil biostratigraphy (Tables T3, T4; Fig. F17). Well-preserved nannofossils were found only in the upper sections of this site. Differential dissolution becomes stronger from Sample 181-1124C-11H-CC (112.95 mbsf) and downward. In some of the samples, only dissolution-resistant forms, such as discoasterids and large-sized coccoliths, including *Cyclicar-golithus floridanus* and *C. abisectus*, were left. Thirty-four age-diagnostic datum levels were identified as summarized in Table T4. The preliminary biochronology suggests that this site recovers a continuous 410-m-long record from the upper Oligocene (~27 Ma) to the Pleistocene (Fig. F17). The lower part of Hole 1124C (410 to 473 mbsf) records parts of the Paleogene and uppermost Cretaceous with several hiatuses. There are at least four hiatuses truncating the record, leaving less than 50% of the mid-Oligocene to the lowermost Cretaceous preserved.

#### Neogene

Signs of dissolution were observed even at the very top of the sequence. The first two commonly used datums (the reversal of dominance between *Gephyrocapsa oceanica* and *Emiliania huxleyi* and the first occurrence [FO] of *E. huxleyi*) for the uppermost Pleistocene cannot be identified because of dissolution effects, which have dissolved the bridge structures of gephyrocapsiids and the I-shaped elements of the distal shields of *Emiliania huxleyi*. The only reliable age datum we could find for the uppermost Pleistocene was the last occurrence (LO) of *Pseudoeemiliania lacunosa* (0.24 Ma) in Sample 181-1124C-2X-1, 146 cm (21.06 mbsf).

The Pleistocene is ~60 m thick, as marked by the FO of medium-sized *Gephyrocapsa* (1.67 Ma) in Sample 181-1124C-5H-CC (56.09 mbsf). In the same sample, the LO of *Calcidiscus macintyreii* (1.60 Ma) was found. In the next downcore sample (Sample 181-1124C-7H-CC, 75.09 mbsf) observed was the LO of *Discoaster brouweri* (1.96 Ma). Well-preserved discoasterids were found in the next three cores, facilitating a good correlation of this interval to the standard zonation of the late Pliocene. The zonal markers of the top boundaries of the Zones NN17, NN16, and NN15 were found in Samples 181-1124C-8HCC to 10H-CC (84.35–102.72 mbsf), respectively (Fig. F15; Table T4).

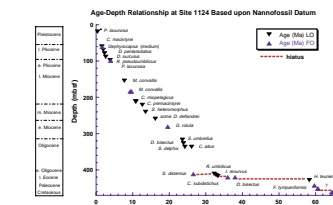
From Sample 181-1124C-11H-CC (112.95 mbsf) to 30X-CC (284.3 mbsf), nannofossils are poorly to moderately preserved. The absence of marker species belonging to *Ceratolithus*, *Amaurolithus*, *Discoaster*, *Sphenolithus*, and *Helicosphaera* makes it impossible to make an unambiguous correlation of this interval with the standard zonal scheme. It is hard to pinpoint where the Miocene/Pliocene boundary is. The presence of *Minylitha convallis*, a short-ranged late Miocene dissolution-resistant species, indicates that the interval between 154.92 and 183.22 mbsf was deposited between 7.7 and 9.3 Ma. The presence of the short-ranged *Catinaster calyculus* (LO 9.64 Ma) and *C. coalitus* (FO 10.8 Ma, marker of the base of Zone NN8) in the next three samples from Sample 181-1124C-19X-CC through 21X-CC further confirms the correlation.

The boundary between the middle and late Miocene (11.2 Ma) is bracketed by the LO of *Coccolithus miopelagicus* (10.94 Ma) in Sample 181-1124C-22X-CC (216.96 mbsf) and the LO of *Calcidiscus premacintyreii* (12.65 Ma) in Sample 181-1124C-23X-CC (226.59 mbsf). Within the middle Miocene, the LO of *Sphenolithus heteromorphus* in Sample 181-

T3. Identification and abundance of nannofossils, p. 103.

T4. Nannofossil datum levels, p. 107.

F17. Age-depth relationships at Site 1124, based upon nannofossil datums, p. 60.



1124C-25X-CC (245.88 mbsf) marks the top of Zone NN5 at 13.52 Ma. Below this level, the nannofossils are poorly preserved. Strong dissolution has caused many samples to be barren of nannofossils or to contain only fragments and few robust specimens. The lack of *Sphenolithus* and *Helicosphaera* in the interval between Samples 181-1124C-25X-CC (245.88 mbsf) and 33X-CC (322.68 mbsf) almost precludes any possibility of correlation. The poorly preserved discoasterids in this interval, however, show a transition from the *Discoaster deflandrei* complex to the *D. variabilis* group at ~260 mbsf (between Samples 181-1124C-26X-CC and 27X-CC; 255.4 to 264.95 mbsf). This level indicates approximately the boundary of the middle and early Miocene at ~16.4 Ma. The trace but persistent occurrence of *Geminilithella rotula* down to Sample 181-1124C-29X-CC (276.41 mbsf) suggests that this level still belongs to the early Miocene younger than 19.6 Ma. The sudden termination of *D. druggii* in Sample 181-1124C-31X-CC (303.08 mbsf) indicates that this level is near the first appearance of this marker species at the top of Zone NN2 at 23.2 Ma. The sudden appearance of a diverse group of Oligocene *Sphenolithus* three samples downward (Sample 181-1124C-34X-CC; 322.49 mbsf) also supports this interpretation. The interval between 276.41 and 303.08 mbsf is either a condensed lower Miocene section of the early Miocene or it contains a small hiatus with less than 3 m.y. missing. The absence of nannofossils in the core catcher of this core (Sample 181-1124C-30X-CC; 284.3 mbsf), and the general poor preservation of the flora in samples below and above, makes it difficult to evaluate which interpretation is correct. It is likely that there is a disconformity in Core 181-1124C-30X (Fig. F15).

#### **Paleogene and Cretaceous**

The topmost Paleogene is recorded in Cores 181-1124C-34X to 42X, as marked by the presence of age-diagnostic late Oligocene assemblages. The common occurrence of *Sphenolithus delphix* (LO 23.8 Ma), *S. capricornutus* (LO 23.7 Ma), *S. conicus* (LO 21.8 Ma), and *S. umbrellus* (LO 23.6 Ma) (Berggren et al., 1995) in Samples 181-1124C-34X-CC to 36X-CC (322.68–351.71 mbsf) provides a suite of excellent biochronologic markers for this interval. Sample 181-1124C-34X-CC (332.49 mbsf) is older than 23.8 Ma, based upon the co-existence of *Sphenolithus delphix* and *S. capricornutus*. The same sample (Sample 181-1124C-34X-CC at 332.49 mbsf) records the LO of *Reticulofenestra bisectus*, indicating an age of 23.9 Ma. The FO of *Sphenolithus delphix* in Sample 181-1124C-36X-CC marks an age of 24.3 Ma, whereas the LO of *Chiasmolithus altus* at 26.1 Ma in Sample 181-1124C-35X-CC (342.34 mbsf) further strengthens the biochronologic determination of this interval. The occurrence of *S. ciperoensis*, together with the absence of *S. distentus* in Samples 181-1124C-39X-CC (380.95 mbsf) through 43X-1, 66 cm (410.36 mbsf), suggests that the bottom of this interval (i.e., 410.36 mbsf) is not the true FO of *S. ciperoensis*; rather, it is still younger than the datum level of the LO of *S. distentus* (27.5 Ma).

Four reliable markers of the earliest Oligocene all occur consecutively in the next several sections in Core 181-1124C-43X: the LO of *Reticulofenestra umbilicus* (31.3 Ma) and the LO of *Isthmolithus recurvus* (31.8–33.1 Ma; Berggren, 1995) in Sample 181-1124C-43X-2, 57 cm (411.77 mbsf), the LO of *Ericsonia formosa* (32.8 Ma), and the acme of *Clausicoccus subdistichus* (33.3 Ma) in Sample 181-1124C-43X-6, 66 cm (417.86 mbsf). However, the disappearance of *I. recurvus* (range ~32 to 35.5 Ma) and *Dictyococcites bisectus* (FO 38 Ma) in Sample 181-1124C-44X-1, 100 cm, and downcore, indicates that there is a stratigraphic break between

this sample and the sample above (i.e., between Samples 181-1124C-44X-1, 7 cm, at 419.36 mbsf and 44X-1, 100 cm, at 420.3 mbsf). We interpret this to mean that there might be a hiatus of at least 4.5 m.y. duration (from 33.3 to 38 Ma).

The assemblages contained in Sample 181-1124C-44X-1, 100 cm, to 44X-6, 50 cm (420.3 to 427.3 mbsf) is of middle Eocene age, as characterized by *Discoaster barbadiensis*, *Coccolithus eopelagicus*, *Cyclicargolithus floridanus*, *Ericsonia formosa*, and *Reticulofenestra umbilicus* (FO 43.7 Ma). As constrained by the absence of *Dictyococcites bisectus* and the presence of *Reticulofenestra umbilicus*, this interval is bracketed between 38 and 43.7 Ma.

In the very bottom of the core-catcher of Core 181-1124C-44X (428.97 mbsf), just below the black mudstone, a moderately preserved nannofossil assemblage indicative of the middle Paleogene was found. The presence of *Fasciculithus tympaniformis* in this sample clearly indicates that the sample is older than at least 55.3 Ma. An additional sample taken from the very top of the next core (Sample 181-1124C-45X-1, 29 cm, 429.29 mbsf) contains abundant, well-preserved nannofossils of middle Paleocene age. The presence of *Hornbrookina teuriensis* suggests that this level is older than its LO at 58.3 Ma. It is evident that in, or at the base of, the dark brown mudstone in Sample 181-1124C-44X-CC exists a major hiatus that separates the middle Paleocene below (>58.3 Ma) from the middle Eocene (between 38 and 43.7 Ma) above.

The nannofossils in sediments below the unconformity are generally abundant and moderately preserved. The abundant occurrence of *Fasciculithus tympaniformis*, *F. ulii*, and *F. pilateaus* and the absence of any *Helicolithus* in the three samples of Core 181-1124C-45X (429 to 438.62 mbsf) suggest strongly that this interval is within Zone NP5 with an age older than 58.4 Ma (FO *Helicolithus*) and younger than 59.9 Ma (FO of *F. ulii*). The FO of the first *Sphenolithus* species, *S. primus*, in Sample 181-1124C-46X-CC (445.83 mbsf) marks the age of 60.6 Ma. Within this core, the FO of *Chiasmolithus bidens* occurs in Sample 181-1124C-46X-5, 59 cm, indicating an age of 60.7 Ma. These two datum levels collectively suggest that this core (1124C-46X, 438.62 to 445.83 mbsf) belongs to the Zone NP3. Without finding the marker species for the base of NP4, it is difficult to evaluate whether this zone is missing. In the next two lower samples, three age-diagnostic datums were found: *Cruciplacolithus tenuis* (the marker of the base of Zone NP2 at 64.5 Ma) in Sample 181-1124C-47X-CC (457.46 mbsf), *Cruciplacolithus primus* (FO 64.8 Ma), and *Hornbrookina teuriensis* (FO 64.9 Ma) in Sample 181-1124C-48X-CC (463.32 mbsf). The presence of these species suggests that this interval is very near to the base of the Tertiary (65 Ma).

The next two samples from Core 181-1124C-49X, the last core in the sequence, contain typical flora of the Late Cretaceous (>65 Ma) as characterized by abundant occurrence of *Micula* spp., *Arkhangelskiella cymbiformis*, *Prediscosphaera cretacea*, and *Bronsonia enormis*. However, it appears that the contact between Cretaceous and Tertiary was not recovered, and occurs between Sample 181-1124C-48X-CC and the top of Core 181-1124C-49X.

## **Foraminifers**

Throughout most of the Site 1124 section, the planktonic foraminiferal assemblages show evidence of variable, selective dissolution. Selective dissolution of planktonic foraminifer tests affected our ability to find all of the regionally expected taxa of potential use in the site

biostratigraphy and to have confidence in the distribution of some of the observed events (Tables T5, T6, T7).

#### **Late Pliocene–Quaternary**

At this site, the Quaternary interval is not easy to recognize or subdivide biostratigraphically, using foraminifers. The stratigraphic range of some taxa is different from that found south of the Subtropical Convergence.

Sediments down to Sample 181-1124C-5H-5, 88–93 cm (0–53.5 mbsf), are younger than 2.6 Ma (late Pliocene–Recent, Nukumaruan [Wn], Castlecliffian [Wc], and Haweran [Wq] Stages), because they contain sporadic *Globorotalia crassula* (FO 2.6 Ma).

These faunas contain common *Globorotalia inflata*. *Globorotalia puncticuloides* morphotypes are particularly common in Core 181-1124A-1H to Core 181-1124C-5H, in contrast to southern Leg 181 sites, where their last appearance was consistently ~0.6–0.7 Ma. *Globorotalia puncticuloides* morphotypes become much rarer below Core 181-1124C-5H. No *G. cavernula* (FO 0.2 Ma) were found, but *Globorotalia hirsuta* (FO 0.45 Ma) occurs in the surface sample (Sample 181-1124B-1H-1, 0–2 cm).

A crude subdivision of this interval is provided by the sporadic occurrences lower down of the *Globorotalia tosaensis*–*G. truncatulinoides* lineage. Keeled *G. truncatulinoides* morphotypes (FO ~2 Ma in tropics and subtropics) occur down to Sample 181-1124C-5H-CC. Unkeeled morphotypes of *G. tosaensis* (3.2–1 Ma) occur in Samples 181-1124C-5H-5, 88–93 cm, and 7H-4, 98–100 cm. Based upon this, Core 181-1124C-5H is 1–2 Ma. Common *Globorotalia inflata triangula* (LO ~2 Ma) are present in Sample 181-1124C-7H-CC.

#### **Pliocene**

Samples 181-1124C-8H-3, 140–142 cm, and 8H-5, 10–12 cm (80.1 mbsf), are of late Pliocene age (2.6–3.0 Ma, Mangapanian Stage), because of the presence of dextral, unkeeled *Globorotalia crassaformis* (3.0–2.1 Ma) and lack of *G. crassula* or *G. crassacarina* (FO 2.6 Ma).

Samples 181-1124C-8H-CC to 9H-CC (84.4–94.1 mbsf) are mid-Pliocene in age (3.0–3.6 Ma, Waipipian Stage), based on the occurrence of abundant *G. inflata* (FO 3.7 Ma) and *G. inflata triangula* (FO 3.6 Ma), sinistral *Globorotalia crassaformis* (LO 3.0 Ma, Samples 181-1124C-8H-CC and 9H-CC), *G. puncticuloides* (FO 3.6 Ma, Sample 181-1124C-9H-4, 107–109 cm), and *G. crassaconica* (LO 3.0 Ma, Sample 181-1124C-9H-CC). In southern Leg 181 sites, *Globorotalia inflata* occurred in low numbers and as small specimens down to this level. It was not as dominant in the late Pliocene as it was in the temperate latitudes at Site 1124.

Sample 181-1124A-10H-1, 76–78 cm (94.5 mbsf), is of mid-Pliocene age (~3.6–3.7 Ma, late Opoitian Stage), based on the occurrence of *Globorotalia inflata triangula* (FO 3.6 Ma), common *G. pliozea* (last common occurrence [LCO] 3.6 Ma), common *G. inflata* (FO 3.7 Ma), and sparse *G. puncticulata* (LO 3.7 Ma).

Samples 181-1124C-10H-CC to 11H-CC (102.7–113 mbsf) are of early Pliocene age (3.7–4.7 Ma, Opoitian Stage), based on the occurrence of common *Globorotalia puncticulata* (FO 5.2 Ma, LO 3.7 Ma) and *G. crassaconica* (FO 4.7 Ma), and supported by the sporadic presence of *G. pliozea* (3.6–5.4 Ma, Sample 181-1124C-110H-1, 89–91 cm).

T5. Significant foraminiferal and bolboformid datums, [p. 108](#).

T6. Identification and abundance of planktonic foraminifers, [p. 109](#).

T7. Identification and abundance of benthic foraminifers, [p. 111](#).

***Miocene and late Oligocene***

Samples 181-1124C-14H-2, 100–102 cm, to 17X-CC (134.2–168.7 mbsf) are of largely undifferentiated late Miocene age (5.6–9.9 Ma, late Tongaporutuan and early Kapitean Stages), based on the presence of sinistral *Globorotalia miotumida* (FO 10.5 Ma, LO 5.6 Ma) and the first downhole occurrence of the distinctive *Globoquadrina dehiscens* (LO 9.9 Ma) in Sample 181-1124C-20X-CC (335 mbsf). The interval can be coarsely subdivided on the presence of *Sphaeroidinella paenedehiscens* (FO ~8 Ma) in Sample 181-1124C-14H-CC (141.1 mbsf).

Samples 181-1124C-20X-CC to 21X-CC (197.57–207.36 mbsf) are of late middle Miocene to early late Miocene age (13.2–9.9 Ma, Lillburnian to early Tongaporutuan Stages), based on the presence of *Globoquadrina dehiscens* (LO 9.9 Ma) and sporadic *Globorotalia miotumida* and *Globigerina nepenthes* (FO 11.8 Ma) in Sample 181-1124C-21X-CC. Samples 1124C-22X-5, 124–128 cm, to 24X-CC are middle Miocene in age (late Clifdenian–Lillburnian Stages), based on the presence of sporadic, poorly preserved *Globorotalia praemenardii* (15.8–13.2 Ma), and one *Globorotalia amuria* (LO 13 Ma, in Sample 181-1124C-22X-5, 124–128 cm). A good population of *Orbulina suturalis* (FO 15.1 Ma, LO 10.5 Ma) occurs in Sample 181-1124C-22X-CC.

Samples 181-1124C-28X-CC and 29X-CC (274.6–276.4 mbsf) are of late early Miocene age (19–16.7 Ma, Altonian Stage), based on the presence of *Catapsydrax dissimilis* (LO 16.7 Ma), *Globigerinoides cf. trilobus* (FO 19 Ma) and one *Globorotalia incognita* (21.6–18.5 Ma) in Sample 181-1124C-29X-CC.

Samples 181-1124C-30X-CC to 42X-CC (284.3–409.7 mbsf) mostly contain low-diversity benthic foraminiferal faunas, with extremely rare planktonic forms occurring in fewer than 50% of the residues. In most instances, the only planktonic forms present are large specimens of the thick-walled *Catapsydrax dissimilis* (FO ~34 Ma, LO 16.7 Ma). In New Zealand sections, *C. dissimilis* is abundant in the uppermost Oligocene and lower Miocene (Waitakian and Otaian Stages). Sample 181-1124C-31X-CC has an assemblage with common *Cassidulina cuneata*, rare *Gyroidina soldanii*, *Pullenia* sp., *Cassidulina* sp., *Cibicidoides* sp., and isolated specimens of *Globigerina opima nana*.

Sample 181-1124C-40X-CC (390.1 mbsf) contains benthic foraminifers *Cibicidoides praemundulus* (LO 23.8 Ma), *Cassidulina cuneata* (FO 27 Ma) and planktonic *Catapsydrax unicavus*. This assemblage is tentatively assigned to the late Oligocene (27–23.8 Ma, Duntroonian–early Waitakian Stage).

***Eocene and Oligocene***

Sample 181-1124C-43X-CC is a calcareous plankton ooze, with abundant and robust specimens of *Subbotina angiporoides* LO 30 Ma), *Catapsydrax unicavus*, *Globigerina euapertura*, and also contains common small *Paragloborotalia gemma* (LCO 32 Ma, FO 35 Ma). In the absence of a continuous set of samples in this zone, it cannot be ascertained if we deal with *P. gemma* LCO (~32 Ma) or *P. gemma* LO (~30 Ma); hence, the 32 Ma date should be used with caution. If we deal with the *P. gemma* LO event, the age might be near 30 Ma. The sample lacks *Globigerinatheka index*, which in this region is abundant in samples older than 34.3 Ma, and *Subbotina linaperta*, which ranges up to near the top of the Eocene. Therefore, we conclude that the age of the sample is early Oligocene (34.3–32 Ma, early Whaingaroan Stage). This suggests a time gap of 5 m.y. (late Whaingaroan Stage) across the Marshall Paraconformity at 412 mbsf, between early Oligocene (>32 Ma) and late Oligocene

(<27 Ma).

Samples 181-1124C-44X-1, 67–69 cm, to 44X-6, 50–52 cm (420–427.3 mbsf), are of late middle to early late Eocene age (42–36 Ma, Bortonian to early Kaiatan Stages), based on the common presence of *Pseudogloboquadrina primitiva* (LO 36 Ma), *Globigerinatheka index* (FO 42 Ma), and *Nuttallides truempyi* (New Zealand LO 36 Ma). The upper part of this interval appears to have an age within the range 38.4–36 Ma, based on the occurrence of *Ponticulospaera semiinvoluta* (FO 38.4 Ma) in Samples 181-1124C-44X-1, 67–69 cm, and 44X-5, 93–95 cm.

Thus, there is a considerable hiatus (and lithologic change) between Sample 181-1124C-43X-CC and the top of Core 181-1124C-44X, with a minimum time gap of ~2 m.y., within the late Eocene (all Runangan and late Kaiatan Stages).

#### **Paleocene**

Samples from 181-1124C-44X-CC to 47X-CC (429.1–457.6 mbsf) are early Paleocene (65–60 Ma, early Teurian Stage). Sample 181-1124C-44X-CC (429.1 mbsf) contains two different lithologies: a dark brown mudstone and a pink-colored marl. The dark brown mudstone is barren of foraminifers and is probably of middle Eocene age, as it grades up into foraminifer-bearing, calcareous brown shales assigned to the interval above. The light-colored sample is rich in large benthic foraminifers, including *Gavelinella beccariiformis* and *Nuttallides "truempyi"*, which assigns the sample a Paleocene age, older than 55 Ma. There are no planktonic foraminifers in this sample, possibly the result of dissolution of carbonate in the water masses, before burial on the seafloor.

Sample 181-1124C-45X-CC (438.7 mbsf) contains a diverse and rich planktonic assemblage, including *Morozovella conicotruncata*, *M. angulata*, *M. praecursoria*, *M. aff. trinidadensis*, *Subbotina* spp., and the benthic forms *Aragonia ouezzanensis*, *Gavelinella beccariiformis*, *Pullenia coryelli*, *Gyroidinoides globosus*, and *Alabamina creta*. The assemblage correlates to the lower part of the standard planktonic foraminifer Zone P3 (60–61 Ma), Sealandian, early late Paleocene.

Samples 181-1124C-46X-CC through 47X-CC (445.8–457.5 mbsf) contain a totally different assemblage, largely composed of superabundant small globigerinids, typical of the early Paleocene (early Danian). In Sample 181-1124C-46X-CC occur abundant *Globanomalina compressa*, common *Globoconusa daubjergensis*, *Subbotina simplissima*, and *S. triloculinoidea*. No *S. pseudobulloides* were observed. Rare benthic forms include *Nuttallinella florealis* and *Spiroplectammina spectabilis*. The assemblages may be assigned to the upper part of standard planktonic foraminifer Zone P1 (61.2–63.0 Ma).

In Sample 181-1124C-47X-CC, the assemblage contains even smaller planktonic specimens than in the core-catcher immediately above, with rare *Globanomalina compressa*, *Globigerina fringa*, *G. simplissima*, *Globoco-nusa daubjergensis*, *Guembelitria cretacea*, and the same benthic forms as immediately above. The assemblage is assigned to the top of Subzone P1b or lower Subzone P1c (~63 Ma).

The pink and indurated limestone in Sample 181-1124C-48X-CC yields only isolated and tiny (63-µm fraction) planktonic forms. A tiny form with five chambers in the last whorl, slightly trochoid spire, and open umbilicus was found. We assign it to *Globigerina eugubina*, indicative of Subzone P1a (near 64.9 Ma).

The Cretaceous/Tertiary (K/T) boundary was not recovered. It occurs between Sample 181-1124C-48X-CC and the top of Core 181-1124C-49X.

**Late Cretaceous**

Samples 181-1124C-49X-3, 135–150 cm, and 49X-CC (471.7–473.1 mbsf) are Late Cretaceous in age (71–65 Ma, Maastrichtian and Hauterivian).

The two samples from this interval contain very few planktonic foraminifers. The only three specimens recovered are of *Rugoglobigerina rugosa* and *Hedbergella holmdelensis*, assigned a general Maastrichtian age. This agrees with the rich and diverse benthic assemblage, containing *Globorotalites michelinianus*, *Neoflabellina* aff. *semicirculata*, *Quadriflorina* sp., *Allomorphina* sp., *Gyroidinoides* sp., *Nuttallinella florealis*, *Bolivina incrassata*, *Loxostomum gemmum*, *Valvulinera* sp., *Gavelinella beccariiformis*, *Dorothia oxycona*, *Saccamina placenta*, *Hormosina ovula*, *Gaudryina healyi*, *Psammosphaera* sp., *Karrerulina conversa*, *Spiroplectammina spectabilis*, *S. dentata*, *Rhabdammina* sp., ?*Trochamminoides* sp., and unidentified agglutinated species.

A possible reason for the sudden appearance of calcareous planktonic forms immediately above the (not recovered) K/T boundary might be a drop in the level of the CCD, below the Late Cretaceous paleodepth of ~2–3 km of this site.

**Age Summary**

A summary of foraminiferal ages in terms of the New Zealand stage classification, and local chronological calibration of these stages, can be found in Table T2, p. 59, in the “Explanatory Notes” chapter.

1. Nukumaruan (Wn), Castlecliffian (Wc), and Haweran (Wq), late Pliocene to Holocene (0–2.6 Ma): down to Sample 181-1124C-7H-4, 98–100 cm (0–70.7 mbsf);
2. Mangapanian (Wm), late Pliocene (2.6–3.0 Ma): Sample 181-1124C-8H-3, 140–142 cm, to 8H-5, 10–12 cm (80.1 mbsf);
3. Waipipian (Wp), middle Pliocene (3.0–3.6 Ma): Samples 181-1124C-8H-CC to 9H-CC (84.4–94.1 mbsf);
4. Opoitian (Wo), early Pliocene (3.6–5.2 Ma): Samples 181-1124C-10H-1, 76–78 cm, to 11H-CC (194.5–113 mbsf);
5. Late Tongaporutuan and early Kapitean (late Tt–early Tk), late Miocene (9.9–5.5 Ma): Samples 181-1124C-14H-2, 100–102 cm, to 17X-CC (134.2–168.7 mbsf);
6. Late Lillburnian to early Tongaporutuan (late Sl–early Tt), middle to late Miocene (13.2–9.9 Ma): Samples 181-1124C-20X-CC to 21X-CC (197.57–207.36 mbsf);
7. Late Clifdenian to early Lillburnian (late Sc–eSl), middle Miocene (15.8–13.2 Ma): Samples 181-1124C-22X-5, 124–128 cm to 24X-CC;
8. Early and middle Altonian Stage (early–mid-Pl), late early Miocene (19–16.7 Ma): Samples 181-1124C-28X-CC and 29X-CC (274.6–276.4 mbsf);
9. Undifferentiated Duntroonian to early Altonian Stages, late Oligocene to early Miocene (~27–18.5 Ma): Samples 181-1124C-30X-CC to 42X-CC (284.3–409.7 Ma);
10. Duntroonian (Ld) to early Waitakian (early Lw) Stages, late Oligocene (27–23.8 Ma): Sample 181-1124C-40X-CC (390.1 mbsf);
11. Marshall Paraconformity (412 mbsf);
12. Early Whaingaroan Stage (early Lwh), early Oligocene (34.3–32 Ma): Sample 181-1124C-43X-CC (418.7 mbsf);
13. Unconformity between 181-1124C-43X-CC and top of Core 181-1124C-44X (419 mbsf);

14. Bortonian (Ab) and early Kaiatan (early Ak) Stages, late middle to early late Eocene (42–36 Ma): Samples 181-1124C-44X-1, 67–69 cm, to 44X-6, 50–52 cm (420–427.3 mbsf);
15. Unconformity in Sample 181-1124C-44X-CC (429 mbsf);
16. Early Teurian (early Dt) Stage, early Paleocene (65–60 Ma): Samples 181-1124C-44X-CC to 47X-CC (429.1–457.6 mbsf);
17. K/T boundary unseen, between 181-1124C-48X-CC and top of 49X (463–467 mbsf); and
18. Haumurian (Mh) Stage, latest Cretaceous (71–65 Ma): Samples 181-1124C-49X-3, 135–150 cm, and 49X-CC (471.7–473.1 mbsf).

### **Diatoms and Silicoflagellates**

Diatoms and silicoflagellates are present in sufficient numbers and good preservation in two core intervals at this site to base a stratigraphic assignment on them (Table T8): (1) upper Neogene (upper Miocene to Holocene) as at Site 1123 further east on the northern slope of the Chatham Rise; and (2) upper Oligocene to lowermost Miocene, from Core 181-1124C-31X to 41X.

In the Upper Cretaceous to lower Oligocene sediments below Core 181-1124C-42X, erosion and low sedimentation rates have resulted in dissolution of diatoms.

At this site even fewer stratigraphic marker species were encountered than at Site 1123, and most of the datums applied are last occurrences of these species (Fig. F15). Useful marker species for the late Neogene and early Miocene to late Oligocene can be found in Table T9.

Of these datums, the stratigraphic first occurrence of *Nitzschia fossilis* may originally have been slightly deeper than in Sample 181-1124C-14X-CC, but because of the poor preservation in the sediments below, its first occurrence can only be documented from this sample upsection. The poor preservation of diatoms in Cores 181-1124C-9X and 10X suggests that a hiatus may be present between Samples 181-1124C-8X-CC and 9X-CC.

Silicoflagellates are present but rare. Their abundance is not sufficient to recognize silicoflagellate zones. The few species found support the ages determined by the diatoms. Sample 181-1124C-3X-CC contains *Dictyocha lingii* and *Mesocena quadrangula* and, therefore, must be placed in the Pleistocene *Mesocena quadrangula* Zone. In Sample 181-1124C-16X-CC, the presence of *Paradictyocha apiculata* places this sample into the Miocene *Corbisema triacantha* Zone.

Reworking of Eocene and Oligocene diatom valves and silicoflagellate skeletons is present in the lower Miocene–upper Oligocene diatomaceous sediments. In the upper Neogene section, there are Eocene and Oligocene forms plus reworked Miocene and Pliocene specimens.

### **Radiolarians**

Radiolarian biostratigraphy at Site 1124 is based on the examination of 52 core-catcher samples and four core samples (Table T10). Radiolarian faunas are abundant and well preserved in the upper part of the section (Samples 181-1124A-1H-CC to 181-1124C-8H-CC, 4.7–84.35 mbsf), whereas the interval between Samples 181-1124C-9H-CC and 16H-CC (94.14–159.3 mbsf) contains rare, sporadic radiolarians. The lower part of lithostratigraphic Unit I (Samples 181-1124C-17X-CC to 30X-CC, 168.7–284.3 mbsf) is barren, which suggests extensive dissolu-

---

T8. Identification and abundance of diatoms and silicoflagellates, [p. 112](#).

---

T9. Significant diatom datum levels, [p. 116](#).

---

T10. Identification and abundance of radiolarians, [p. 117](#).

tion in this interval. The upper part of the lithostratigraphic Unit II (Samples 181-1124C-31X-CC to 42X-CC, 303.08–410 mbsf) contains moderately well-preserved early Miocene to late Oligocene radiolarians.

The last occurrence of *Axoprunum angelinum* occurs in Sample 181-1124C-3H-CC (37.1 mbsf), indicating an age younger than 0.78 Ma, based on its recorded datum in Sample 181-1123A-4H-CC (at the base of Brunhes normal epoch). Sample 181-1124C-5H-CC (56 mbsf) contains the FO datum of *Theocorythium trachelium* (FO 1.6–1.7 Ma in equatorial Pacific), which indicates an earliest Pleistocene age.

In Sample 181-1124C-7H-CC (75 mbsf), the first occurrence of *Cycladophora davisiana davisiana* (FO 2.91–3.08 Ma) indicates the sample is of late Pliocene age. The interval between Samples 181-1124C-8H-CC and 11H-CC (84.35–113 mbsf) is estimated to be of a late Miocene to Pliocene age, based on the occurrence of *Sphaeropyle langii* (FO 6.0–6.2 Ma). Samples between 181-1124C-12H-CC and 16H-CC (121.7–159.3 mbsf) contain *Stichocorys peregrina*, *Eucyrtidium calvertense*, and *Stylacontarium bispiculum*. They indicate a Miocene age.

Sample 181-1124C-32X-CC (313 mbsf) yields a radiolarian fauna including *Cyrtocapsella cf. tetrapera* (FO 23.62 Ma), *Lychnocanoma matakohe*, and rare *Phormocyrtis alexandrae*, which is assigned to the lower part of the *Cyrtocapsella tetrapera* (RN1) Zone of Sanfilippo and Nigrini (1998), based on the fauna from the next lowest sample (181-1124C-33X-CC). The estimated age is earliest Miocene.

In the interval between Samples 181-1124C-33X-CC and 35X-CC (322.68–342.34 mbsf), radiolarian faunas are highly diversified. They are characterized by the presence of few to abundant *Lychnocanoma elongata*, *Stichocorys negripontensis*, *Lychnocanoma conica*, *Anthocyrtidium mariaeae*, ?*Lophocyrtis inaequalis*, *Lophocyrtis galenum*, *Theocorys purii*, and *Phormocyrtis alexandrae*. The faunas are assigned to the *Lychnocanoma elongata* (RP22) Zone of Sanfilippo and Nigrini (1998), giving a latest Oligocene age (23.62–24.6 Ma). The faunas are very similar to those from calcareous siltstone of the Puriri Formation, Northland, in New Zealand (O'Connor, 1997a, 1997b).

Sample 181-1124C-39X-CC (381 mbsf) contains *Heliodiscus tunicatus* and *Eucyrtidium* sp. The former species ranges from the *Cryptocarpium ornatum* Zone to the *Theocyrtis tuberosa* Zone (O'Connor, 1997a, 1997b) and is of early Oligocene age.

Sample 181-1124C-42X-CC (409.69 mbsf) yielded a radiolarian fauna including *Lychnocanoma amphitrite*, *Lychnocanoma babylonis*, and *Lophocyrtis* sp., which indicate an Oligocene age.

The interval between Samples 181-1124C-47X-CC and 48X-3, 44–45 cm, yielded only a rare *Amphisphaera aotea*, which is assigned to the *Amphisphaera aotea* (RP1) Zone of Hollis et al. (1997). The estimated age is earliest Paleocene (64.5–65 Ma) for the interval.

## Paleoenvironment

### Foraminifers

#### *Late Oligocene and Neogene*

The foraminiferal faunas throughout the Neogene and upper Oligocene of Site 1124 show signs of strong to very strong dissolution, consistent with having accumulated below the foraminiferal lysocline. Dissolution appears to be strongest through the upper Oligocene and Miocene and slightly less in the Pliocene and Quaternary. Throughout this entire interval, the foraminiferal assemblages that remain are par-

ticularly sparse and required washing large core-catcher samples to obtain ~100 planktonic specimens in the Pliocene and Pleistocene or to obtain any planktonic specimens in many of the Miocene and Oligocene samples.

The hallmarks of dissolution are the reduced abundance of, first, planktonic and, to a lesser extent, benthic foraminifer specimens. Accompanying this is the large number of fragmented planktonic specimens and chambers and the decreasing planktonic percentage of the total foraminiferal assemblage. In terms of the planktonic composition of the fauna, there is a selective and progressive loss of the more solution-prone taxa (e.g., *Globigerina*, *Globigerinoides*, *Praeorbulina*, *Orbulina*, small *Globorotalia*) and of the smaller specimens. In many instances the small remaining assemblage is of low diversity, consisting of only one or two more solution-resistant taxa (e.g., *Catapsydrax*, *Globoquadrina*, *Globorotalia inflata*, *Sphaeroidinella*). The last, less-calcified chamber of many specimens is often dissolved away.

The benthic faunas also often appear to have a reduced diversity, having lost many of the smaller and more solution-prone taxa. The faunas often consist of 10–20 larger, thicker-walled taxa (e.g., *Oridorsalis*, *Globocassidulina*, *Dentalina*, *Melonis*, *Gyroidina*, *Pullenia*, and *Martiniella*).

A preliminary study of pairs of dark-colored (cool hemipelagic) and light-colored (warm pelagic) lithologies within the Pleistocene indicates that in the dark-colored intervals planktonic foraminifer percentages are lower (30%–70%) than in the lighter intervals (70%–95%) and that planktonic foraminiferal abundance in the darker intervals is ~30% of that in the light. Similarly, the number of planktonic test fragments, expressed as a ratio of the number of whole tests, is about twice as much in the darker intervals than the lighter.

In the Miocene and upper Oligocene, the darker horizons have planktonic percentages of 0%–20% compared with ~20%–50% in the lighter intervals. Many darker horizons have no planktonic forms present. Planktonic foraminiferal abundance is greatly reduced in both intervals compared with the Pleistocene, and the fragment-to-whole test ratio is greatly increased. These observations suggest that dissolution was stronger during the cooler periods than the warmer ones, and, possibly, planktonic productivity was higher during the warmer intervals. Dissolution is prevalent, however, throughout both cool and warm intervals.

The late Oligocene to Holocene benthic foraminiferal assemblages are relatively constant and typical of mid-bathyal to abyssal depths, above the CCD. More detailed quantitative work is required to see if these solution-impacted assemblages show changes that reflect water mass or other environmental shifts.

The evidence suggests that throughout most of the Neogene, Site 1124 was swept by corrosive bottom waters. This is most marked in the Miocene, where many assemblages have fewer than 10% planktonic foraminifers, compared with a normal oceanic assemblage above the lysocline, which would have >99% planktonic forms.

#### ***Eocene and Oligocene***

The early Oligocene foraminiferal assemblage in Sample 181-1124C-43X-CC, which has oceanic overhead conditions at upper abyssal depths, has normal planktonic foraminiferal assemblages in both abundance (~99% foraminifers) and composition. There is some evidence, however, for dissolution, seen in the presence of common planktonic

test fragments in the finer sand fractions.

The late middle to early late Eocene foraminiferal assemblages in Core 181-1124C-44X contain a normal upper abyssal or lower bathyal, benthic fauna (e.g., common occurrence of species of *Oridorsalis*, *Nuttallides truempyi*, *Gyroidina*, *Dentalina*), with 90%–99% planktonic forms showing no obvious signs of dissolution.

#### **Late Cretaceous and Paleocene**

This interval contains benthic foraminiferal assemblages typical of deep bathyal to abyssal paleo-water depth. Planktonic percentages are variable, between 0% and 100%. The extreme variation in planktonic concentration is an enigma: there are no planktonic forms, but diversified benthic foraminifers are abundant in Samples 181-1124C-49X-CC (Late Cretaceous) and 45X-CC (?late Paleocene), and planktonic oozes in the samples in between, of early Paleocene age. One explanation for no planktonic assemblages might be a relatively shallow CCD, with extreme dissolution of pelagic calcareous tests, and sufficiently oxic bottom water to yield high-diversity benthic assemblages, none of which show signs of mass-flow sorting or abrasion. Another possibility is a severely restricted and oxygen deficient mid-water mass, in a relatively restricted oceanic basin. Temporal expansion of this mid-water mass to the surface would prevent planktonic blooms; its expansion to the bottom of the basin might yield dark brown clays, as seen in the middle Eocene interval of Core 181-1124C-44X. An argument against a surface water-mass restriction is the fact that radiolarian and nannofossil assemblages persist.

Backtracking considerations for the area of this site, slightly landward of oceanic basement, with ~1 km of sediment fill, might place the paleo-water depth around 2000–3000 m in the Late Cretaceous through Paleocene. The diverse benthic assemblage with frequent and robust *Gavelinella beccariiformis*, *Nuttallides*, *Nuttallinella*, *Pullenia corylli*, *Aragonaria* (Paleocene), *Gyroidinoides* and *Globorotalites* (both Cretaceous), various deep-water agglutinated foraminifers, common ataxophragmids, and *Quadrimerphina*, are compatible with a deep-water setting.

#### **Diatoms**

Fluctuations in the abundance and preservation of diatoms in the sediment indicate two periods of increased primary productivity: the latest Miocene to Holocene and the late Oligocene to earliest Miocene.

The late Neogene diatom assemblages are composed of temperate to subtropical species, with an admixture of displaced subantarctic diatoms, which document the input of material picked up by the Lower Circumpacific Deep Water further south.

In the upper Oligocene to lower Miocene sediments, the assemblages are also characterized by temperate to subtropical species. During this period of sedimentation, an input of Antarctic-subantarctic species is not evident.

## **PALEOMAGNETISM**

Core archive halves from Holes 1124A, 1124B, 1124C, and 1124D were measured on the shipboard pass-through cryogenic magnetometer. Declination, inclination, and intensity of natural remanent magnetization (NRM) and 20-mT alternating field (AF) demagnetization steps

were measured at 5-cm intervals. The first few cores of each hole were also measured after a 10-mT demagnetization step; this step added little extra information and, because of time constraints, only the 20-mT step was continued. Because of a complex and hard overprint, XCB cores between 175 and 276 mbsf from Hole 1124C were also demagnetized at 40-mT, 60-mT, and 80-mT AF steps. In situ tensor tool data were collected for all APC cores, but a problem with the shipboard pass-through cryogenic magnetometer prevented the use of the declination for polarity determinations in these cores. Therefore, only inclination could be used to determine magnetic polarity in Holes 1124C and 1124D. At least two discrete oriented samples were collected from the working half of each core interval, but time constraints prevented any shipboard measurement of these. Whole-core magnetic susceptibility (MS) was measured on all cores using a Bartington susceptibility loop on the automated multisensor track (MST).

A composite paleomagnetic record was constructed for Site 1124 using data from Holes 1124C and 1124D. Holes 1124A and 1124B were not used in constructing a composite paleomagnetic record because of APC refusal immediately beneath the seafloor in a tephra layer (see “[Lithostratigraphy](#),” p. 3). XCB coring was used to penetrate this layer and then coring with the APC recommenced beneath. Paleomagnetic results for the uppermost 50 meters composite depth (mcd) in Holes 1124A and 1124B were not easy to interpret because recovery was poor and complicated by possible overlap and flow-in. For these reasons, a composite paleomagnetic record was constructed from below ~16 mcd in Holes 1124C and 1124D. Intensity of magnetic remanence varied markedly with depth in Hole 1124C (Fig. [F18](#)). The upper 280 mbsf have average NRM intensities that vary cyclically between  $4 \times 10^{-3}$  and  $8 \times 10^{-2}$  A/m. Between 290 and 420 mbsf, average NRM intensity is reduced to less than  $4 \times 10^{-3}$  A/m. Beneath 420 mbsf, NRM intensity increases to a range of  $8 \times 10^{-2}$  to 0.2 A/m and at 428 mbsf is similar to the upper 280 mbsf of the core (average NRM intensity =  $2 \times 10^{-2}$  A/m).

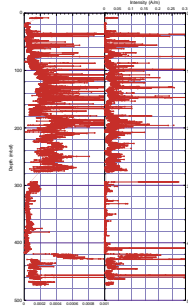
# Paleomagnetic Behavior

NRM measurements displayed consistent, steeply positive (down-core) inclinations ranging between  $+70^\circ$  and  $+80^\circ$ , consistent with a drill string overprint induced during coring. The 20-mT AF demagnetization step effectively removed this overprint above 185 mbsf and between 290 and 475 mbsf (base of Hole 1124C). However, the single 20-mT demagnetization step was not effective in removing the steep positive overprint from the core between 185 and 290 mbsf, and the overprint persisted to demagnetization steps of 40–60 mT. An 80-mT AF demagnetization step was therefore used to elucidate the primary remanence between 185 and 290 mbsf (Fig. F19B).

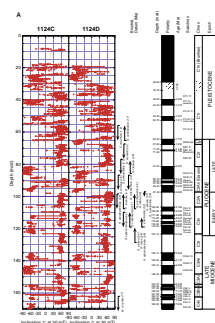
# Magnetostratigraphy

Interpretation of magnetic polarity from the composite inclination record for Site 1124 (Fig. F19) is well constrained by key foraminiferal and nannofossil datums for each of the core-catcher samples and for additional samples either side of the Cretaceous boundary in the lower-most part of the core (see “**Biostratigraphy**,” p. 12, and “**Biostratigraphy**,” p. 10, of the “Explanatory Notes” chapter). The inclination record for the upper 170 mcd of the composite record is taken from Holes 1124C and 1124D and, when compared with the Geomag-

## F18. Whole-core MS and NRM intensity, p. 61.



F19. Composite magnetostratigraphic record from Site 1124,  
p. 62.



netic Polarity Time Scale (GPTS) (Cande and Kent, 1995; Berggren et al. 1995), it provides a complete record of the Brunhes (C1n), Matuyama (C1r–C2r), Gauss (C2An), Gilbert (C2Ar–C3r), C3A, and C3B magneto-chrons (Fig. F19A). The interval between 19 and 28.85 mcd is of normal polarity and is inferred to represent the lower part of the Brunhes (C1n) Chron. The inclination record between 28.85 and 33.75 mcd is noisy and prevents an exact placing of the Brunhes (C1n)–Matuyama (C1r.1r) boundary. The characteristic normal-reversed-normal-reversed-normal pattern of the Gauss Chron (C2An) occurs between 81.60 and 97.30 mcd, constrained by the LOs of nannofossils *Discoaster surculus* (2.6 Ma) and *D. pentaradiatus* (2.3 Ma) and of foraminifers *Globorotalia puncticulata* (3.8 Ma), *G. pliozea* (3.7 Ma), and *G. crassaconica* (3.2 Ma), the FOs of the nannofossil *Pseudoemiliania lacunosa* (4.0 Ma), and foraminifers *G. puncticuloides* (3.4 Ma) and *G. crassula* (2.6 Ma). Between 33.75 and 81.60 mcd, the polarity is mostly reversed with four short normal polarity events. Two of these short normal polarity events immediately underlie the Brunhes (C1n) Chron and are assigned to the Jaramillo (C1r.1n) and Cobb Mountain (C1r.2r–1n) Subchrons, respectively. The other two short normal events occur between 64.50 and 71.60 mcd and, constrained by nannofossils *D. pentaradiatus* (LO, 2.3 Ma), *D. brouweri* (LO, 2.0 Ma), and *Calcidiscus macintyrei* (LO, 1.6 Ma) and foraminifer *G. caribbeanica* (FO, 1.7 Ma), are assigned to the Olduvai (C2n) Chron and Reunion (C2r.1n) Subchron, respectively.

The inclination record between 97.30 and 170 mcd (Fig. F19A) is very stable and well behaved after the single 20-mT cleaning step, and the overlap between Holes 1124C and 1124D contain a complete polarity record of Chrons C2Ar–C4n. Between 97.30 and 135.10 mcd, the polarity pattern is distinctive of the Gilbert Chron (mostly reversed with four short normal subchrons centered between two longer reversed subchrons, C2Ar–C3r) (Fig. F19A). Many nannofossil and foraminifer events confirm that this interval represents the Gilbert Chron (C2Ar–C3r). Nannofossil events include the LO of *Reticulofenestra pseudoumbilicus* (3.8 Ma) and the FO of *P. lacunosa* (4.0 Ma), and key foraminifer datums include the FO of *G. inflata* (3.8 Ma), the ranges of *G. puncticulata* (3.8–5.2 m.y.) and *G. sphericomiozea* (5.2–5.6 m.y.), and the FO of *G. pliozea* (5.4 Ma) and *G. mons* (5.5 Ma). Between 135.10 and 170 mcd, correlation with the polarity time scale is constrained only by the LO of the nannofossil *Minylitha convallis* (7.7 Ma) at ~165 mcd. However, the polarity is very distinctive and the normal-reversed-normal pattern of Chron C3An can be clearly recognized underlain by Chrons C3Ar, C3Bn, C3Br, and C4n (Fig. F19A).

The remaining polarity record is constructed only from Hole 1124C and is complicated by several large hiatuses that truncate foraminifer and nannofossil zones (see “**Biostratigraphy**,” p. 12) and further short hiatuses defined by missing and truncated polarity chronos or subchrons. A thick interval of normal polarity between 187.40 and 223.10 mbsf (Fig. F19B) contains the FO of the nannofossil *Catinaster coalitus* (10.8 Ma) and the LOs of the nannofossil *Coccolithus miopelagicus* (10.9 Ma) and foraminifer *G. dehiscens* (10.1 Ma) and is correlated with the characteristic long normal Chron C5n (9.74–10.95 m.y.) of the magnetic polarity time scale of Cande and Kent (1995). An interval of reversed polarity directly overlying C5n contains the nannofossils *M. convallis* (FO, 9.3 Ma) and *C. calyculus* (LO, 9.6 Ma) and is correlated with C4Ar. A very thin normal polarity excursion is recognized in the upper part of this reversed polarity interval and is correlated with Subchron C4Ar.1n. Subchrons C4Ar.2n and C5n.1r of the polarity time

scale are not recognized in Hole 1124C. They could be missing in core breaks or short unconformities that are not resolvable here. Above 173.80 mbsf in Hole 1124C, however, the polarity record is complete and Chrons C4An, C4r, and C4n complete the upper Miocene record.

Combined nannofossil events (see “[Biostratigraphy](#),” p. 12) and magnetostratigraphy define a short hiatus at ~226 mbsf in Hole 1124 (Fig. F19B). The LO of *Sphenolithus heteromorphus* (13.5 Ma) and *C. premacintyrei* (12.7 Ma) suggest that the reversed-normal-reversed-normal pattern above 226 mbsf correlates with C5Br–C5ADn and that ~3 m.y. is missing in the hiatus that juxtaposes the upper part of C5r (above) with C5ACr (below). A coring gap between 276 and 293 mbsf prevents any definitive correlation of the lower Miocene record in Hole 1124C with the polarity time scale. Some constraints are afforded, though; the acme of the nannofossil *D. deflandrei* (16.2 Ma) occurs at ~260 mbsf and the polarity between 257.60 and 276.40 mbsf, although noisy, is reversed and probably correlates with Chron C5Cr of the polarity time scale. The thin normal polarity interval between 256.96 and 257.60 mbsf most likely correlates with the base of Chron C5Cn. The upper part of C5Cn is truncated in a hiatus that is likely ~1.5 m.y. in duration (Fig. F19B).

Beneath the coring gap (276–293 mbsf), the inclination record, after 20 mT demagnetization, again defines a clear polarity pattern (Fig. F19C). The LOs of the nannofossils *S. umbrellus* (23.6 Ma), *Dictyococcites bisectus* (23.9 Ma), *S. delphix* (24.3 Ma), and *Chiasmolithus altus* (26.1 Ma) constrain the interval between 276 and 344 mbsf to the early Miocene and late Oligocene, but correlation with the polarity time scale is ambiguous. The interval between 305 and 344 mbsf most likely correlates with Chron C6Cn. The location of the Oligocene/Miocene boundary is also ambiguous. A thick interval of reversed polarity between 343.90 and 370.00 mbsf affords more control and is correlated with Chron C6Cr (Fig. F19C). The FO of the nannofossil *S. distentus* (27.5 Ma), within normal polarity at 408.90–411.05 mbsf, is correlated with Chron C9n of the polarity time scale. With these constraints there is a direct correlation of the polarity reversals between 370.00 and 408.90 mbsf with Chrons C7n through C8r.

Foraminifer and nannofossil events define a very complex stratigraphy beneath 411 mbsf (see “[Biostratigraphy](#),” p. 12) with several long hiatuses accounting for most of the lower Oligocene, upper Eocene, lower Eocene, and upper Paleocene record in Hole 1124C. The first hiatus occurs at 411.05 mbsf, has a duration of ~6 m.y., and is marked by a polarity transition separating Chron C9n (above) from Chrons C12r and C13n (below). Chrons C12r and C13n are defined by several nannofossil datums, including the LO of *R. umbilicus* (32.3 Ma) and *Ericsonia formosa* (32.8 Ma), and the acme of *Clausicoccus subdisticus* (33.3 Ma). The second hiatus (419.35 mbsf) is ~3 m.y. in duration and separates Chron C13n (above) from Chrons C18r, C19n, and C19r (below). The FO of the foraminifers *G. index* (42.9 Ma) and *Ponticulospaera semi-involuta* (38.4 Ma) constrain the interval below 419.35 mbsf to the middle Eocene and Chrons C18 and C19. A major hiatus of ~21 m.y. at 429.10 mbsf separates middle Eocene strata from upper Paleocene strata. It is defined by the LO of the nannofossil *Hornbrookina teuriensis* (58.3 Ma) and the LO of the foraminifer *Gavelinella beccariiformis* (55 Ma). Several nannofossil and foraminifer datums define the 430–463 mbsf interval as early–late Paleocene in age. At ~465 mbsf, a 3-m coring gap contains the K/T boundary (see “[Biostratigraphy](#),” p. 12). The inclination record is too poorly defined to allow unambiguous correla-

tion of the lower 45 m of Hole 1124C with the polarity time scale, but the lower 43 m of Hole 1124C is loosely correlated with Chrons C26–C30.

A complete list of depths and ages of magnetic polarity events for Site 1124 is given in Table **T11**. An age-depth model for Site 1124, using the GPTS reversal polarity ages of Berggren et al. (1995), is given in Figure **F20**. The average sedimentation rate for lithostratigraphic Subunits IA and IB (greenish gray clay-bearing nannofossil ooze and silty clay, see “**Lithostratigraphy**,” p. 3) is 21 m/m.y. However, the sedimentation rate is 44 m/m.y. down to 53 mcd, 21 m/m.y. below an inflection point at 1.2 Ma, and 16 m/m.y. below a second inflection point at 2.6 Ma (Fig. **F21**). Despite large changes in the sedimentation rate, the composite record of the upper 200 mcd of Site 1124 appears complete and contains all magnetic polarity chronos down to the base of Chron C5n. Some 139 discrete tephra horizons (see “**Lithostratigraphy**,” p. 3) are preserved in the composite 0–200 mcd record for Site 1124. A few tephra horizons are also preserved below 200 mcd. The age model presented in Figure **F21** affords very good constraints on the ages of these horizons. While the tephra horizons are distributed throughout, several phases of volcanism are noted (see “**Sedimentation Rates**,” p. 28).

Lithostratigraphic Subunit IC (a clay-bearing nannofossil chalk and mudstone; see “[Lithostratigraphy](#),” p. 3) is less complete and contains three hiatuses (Fig. F20): a middle Miocene hiatus at 238 mcd representing 3 m.y., a lower-middle Miocene hiatus at 269 mcd occupying 1.5 m.y., and a lower Miocene hiatus at 290 mcd occupying ~5 m.y. of missing time. Again in contrast, lithostratigraphic Unit II (a light greenish gray nannofossil chalk; see “[Lithostratigraphy](#),” p. 3) represents a near complete record of the upper Oligocene–lower Miocene with an average sedimentation rate of 28 m/m.y. Lithostratigraphic Units II and III (a white nannofossil chalk; see “[Lithostratigraphy](#),” p. 3) are separated by a hiatus representing ~6 m.y. of missing time (27–33 Ma) and is presumably correlative in part to the hiatus between lithostratigraphic Units III and IV at Site 1123 (see “[Paleomagnetism](#),” p. 26, in the “Site 1123” chapter) and with the Marshall Paraconformity (Carter, 1985; Fulthorpe et al., 1996). Two further hiatuses separate Miocene to lower Oligocene strata from upper Paleocene strata: a ~3-m.y.-long upper Eocene hiatus at 432 mcd within lithostratigraphic Unit IV (a reddish brown to dark brown mudstone, see “[Lithostratigraphy](#),” p. 3), and a ~21-m.y.-long Paleocene–Eocene hiatus at 441 mcd, which separates lithostratigraphic Unit IV from Unit V (a white nannofossil chalk and mudstone; see “[Lithostratigraphy](#),” p. 3). Sedimentation below this second unconformity is relatively continuous across the K/T boundary at ~472 mcd, which separates lithostratigraphic Unit V from Unit VI (a pinkish white to pale brown nannofossil mudstone and chert; see “[Lithostratigraphy](#),” p. 3). Unfortunately, the K/T boundary itself was lost in a break between coring intervals.

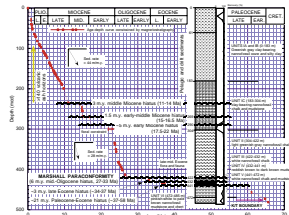
# **COMPOSITE DEPTHS**

## **Composite Section and Splice**

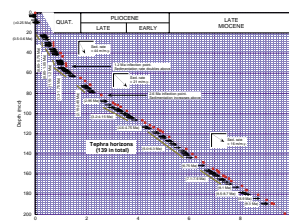
The composite section for Site 1124 yielded overlapping records for the upper ~171 mcd. Data from Holes 1124A and 1124B have been used to create a composite section between 0 and 11.66 mcd. Between 17.66 and ~174 mcd, a continuous section can be recreated using data from

T11. Compilation of age data,  
**p. 121.**

## F20. Site 1124 age model and correlation of composite magnetic polarity, p. 66.



F21. Age model and correlation of composite magnetic polarity,  
p. 67.



Holes 1124C and 1124D. Between 11.66 and 17.66 mcd there was no core recovered, perhaps because of the presence of thick, locally cemented tephra. Three high-resolution data sets proved most useful for correlation at this site: MS and gamma-ray attenuation porosity evaluator (GRAPE) density measured on whole cores on the MST and spectral reflectance at 550 nm (the center wavelength of the range measured), measured on split cores. Magnetic susceptibility and, unusually for this area, GRAPE records were useful for correlation between holes from 0 to 166 mcd. The least ambiguous record for correlation was reflectance, but below 124 mcd these data have a rather small variation and appear to be more noisy. The final composite section is illustrated in Figure F22.

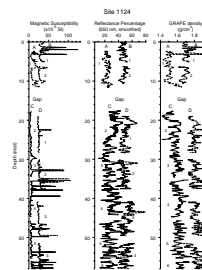
In the light of coring failure toward the top of the section, the top core in the lower part (17.66–174 mcd) of the composite section (Core 181-1124C-2H) was positioned so that the topmost point corresponds to the drillers' mbsf value. Above ~20 mbsf, offsets between mbsf and mcd do not follow a clear trend, probably because of the variable coring disturbance (Fig. F23). Data were edited to remove information collected over voids as identified by very low GRAPE density values and are shown in Figure F22. Below ~20 mbsf, downhole core offsets in the composite section parallel a model of 10% stretch between the mbsf and mcd depth scales (Fig. F23). Table T12 (also in [ASCII format](#)) contains the offsets between the mbsf and mcd scales, which result from composite section construction.

The continuous spliced record, based on MS and reflectance data (Fig. F24), extends to 171 mcd. The top portion of the splice is composed entirely of records from Holes 1124A and 1124B, but the bulk consists of intervals from Holes 1124C and 1124D. Wherever possible, splice tie points (Table T13, also in [ASCII format](#)) were picked at well-defined maxima or minima where the overlap in data from Holes 1124A and 1124B or 1124C and 1124D are strongly correlated. Typically, parameter values differed by less than 10% at tie levels. In all cases, ties were selected so that the spliced record was as free from noise (high-frequency variability) as possible.

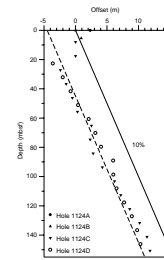
## AGE MODELS AND SEDIMENTATION RATES

The combined nannofossil, foraminifer, diatom, and radiolarian biostratigraphy at Site 1124, yielded ~91 event levels with a preliminary age assignment, using the shipboard stratigraphic framework (see "[Biostratigraphy](#)," p. 10, in the "Explanatory Notes" chapter). The 91 levels are shown in Table T14 and consist of 37 FO events, 50 LO events, and four LCO or acme events. All levels are plotted according to their observed depths at Site 1124 in Figure F25, and ages are defined in "[Biostratigraphy](#)," p. 10, in the "Explanatory Notes" chapter. The position of the arrows in Figure F25 may be extended uphole (downhole) for last occurrences (first occurrences) because of limited sampling density for shipboard analysis. For comparative purposes, the magnetostratigraphic age model (see "[Paleomagnetism](#)," p. 23) is shown as a line on Figure F25. All depths are reported in mcd rather than mbsf values. Poor preservation of the Neogene calcareous plankton limited stratigraphic resolution, in part because of the water depth of almost 4 km, which also resulted in selective dissolution of thinner walled Neogene planktonic foraminifers. The upper Miocene and upper Oligocene sections in particular yielded few stratigraphic data, although key radi-

F22. Composite sections for MS, color reflectance, and GRAPE density, [p. 68](#).

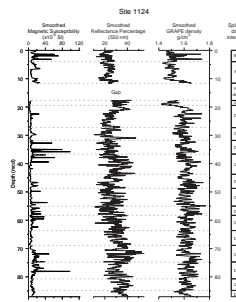


F23. Downhole depth offsets between the mbsf and mcd scales, [p. 71](#).



T12. Composite depth section, [p. 122](#).

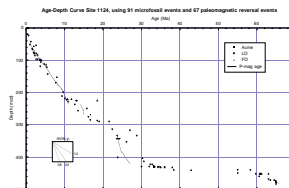
F24. Spliced record for Site 1124, [p. 72](#).



T13. Splice tie points, [p. 129](#).

T14. Biostratigraphic events, [p. 130](#).

F25. Age-depth plot, [p. 74](#).



olarian and diatom dates exist for the Miocene–Oligocene transition in Cores 181-1124C-31X through 41X.

As may be seen from the listing of biostratigraphic ages in Table T14, most of the dates have more than average uncertainty attached when compared to other sites drilled during Leg 181; many dates may be minimum or maximum ages. More intensive study of samples rich in radiolarians and diatoms, such as in the Oligocene and upper Miocene strata, may increase the stratigraphic resolution. Similarly, study of calcareous plankton in the more carbonate-rich, lighter colored intervals in the cores may assist in better definition of the hiatuses and mid-Cenozoic intervals with low rates of sedimentation.

Figure F20, the magnetostratigraphic age model for Site 1124, shows variation in rates of sedimentation from a low of 5 m/m.y. in early Paleocene, to over 25 m/m.y. in the period from late Oligocene to early Miocene. The main hiatuses are shown with undulating lines. The age-depth plot clearly illustrates severe sedimentary condensation in the pre-late Oligocene section, below the level equating to the Marshall Paraconformity in New Zealand, with much increased drift sedimentation after ~27 Ma. More study of samples around the 400 mbsf level may refine insight in the timing and waxing of drift sedimentation and erosion at Site 1124. The younger sediment below the drift sequence is ~33 Ma, whereas at Site 1123 it was of very similar age at ~32 Ma.

Sedimentary hiatuses occur in the lower Miocene (~17.5–22 Ma), the lower Oligocene (~27–33 Ma), in the upper Eocene (~34–37 Ma), and between the upper Paleocene and lower part of middle Eocene (~37–58 Ma). Lowermost Paleocene (early Danian) strata are present in Sample 181-1124C-48X-CC. Magnetic polarity at that depth is reversed and interpreted as Chron C29r. The K/T boundary beds occur in the coring gap at the top of Core 181-1124-49X-CC (and can be seen on the FMS log; see “[Downhole Measurements](#),” p. 36) and are immediately underlain by upper Maastrichtian strata with a normal polarity signature (Chron C30N; see “[Paleomagnetism](#),” p. 23).

The upper Cretaceous (upper Maastrichtian) through Paleocene mudstones were deposited at an average rate of ~5 m/m.y. The complex history of sedimentation, nondeposition, and erosion in Eocene time prevents an estimate of net sedimentation for the few meters of Eocene strata. Above the Marshall Paraconformity (~33–27 Ma), the thick upper Oligocene–lower Miocene section (~27–22 Ma) initially accumulated at 16.5 m/m.y., increased during the late Oligocene to ~41 m/m.y. and terminated at another disconformity with a hiatus of ~4 m.y. from 22 to 17.5 Ma. Middle Miocene drift sediments may be punctuated by at least two hiatuses recognized through omission of magnetochrons (see “[Paleomagnetism](#),” p. 23). Sedimentation is then very uniform at ~17 m/m.y. until ~1.2–1.5 Ma, when it increased sharply to ~42 m/m.y. This youngest sedimentation rate change at Site 1124 is not seen at Site 1123 and probably results from switching of Hikurangi Channel to the east, to directly supply fine terrigenous detrital sediment via turbidity current plumes. Volcanism becomes a significant feature in the record at Site 1124, as also recorded at Site 1123 (Figs. F20, F21; see “[Paleomagnetism](#),” p. 26, in the “Site 1123” chapter), and it is probably coincident with early compression at the New Zealand plate boundary (Walcott, 1998). Several phases occur in the lower and mid-Pliocene, and near continuous volcanism is observed from the lower Quaternary (>1.75 Ma) to the present. This was also recorded at Site 1123 (see “[Paleomagnetism](#),” p. 26, in the “Site 1123” chapter) and is coincident with the opening of the Taupo Volcanic Zone (Shane et al., 1996).

## INORGANIC GEOCHEMISTRY

### Interstitial Water

Twenty-four interstitial-water samples were collected from Site 1124, two from Hole 1124B at depths ranging from 2.90 to 8.30 mbsf, and 22 from Hole 1124C at depths ranging from 21.94 to 471.75 mbsf. One interstitial-water sample was taken from approximately every 10 m to a depth of 100 mbsf. From 100 mbsf to the bottom of the hole, every third core was sampled. Analytical results are summarized in Table T15 (also in [ASCII format](#)) and plotted in Figure F26.

### Salinity, Chloride, pH, and Sodium

Salinities of the interstitial-water samples generally show an increasing trend in the lower part of the core. From 2.90 to 299.90 mbsf (299.90 is the depth of the lithologic boundary between Subunit IC and Unit II), salinity varies between 34.5 and 35.0 and then increases to a maximum of 36.0 at 443.05 mbsf (Fig. F26). The high salinity in the lower part of the hole may be caused by enrichment of major ion concentrations including calcium, strontium, lithium, sodium, and chloride as described below.

The profile of chloride ( $\text{Cl}^-$ ) concentration is similar to that of salinity (Fig. F26). The  $\text{Cl}^-$  concentration increases from 556 mM at 2.90 mbsf to 572 mM at 80.60 mbsf and varies between 561 and 572 mM from 80.60 to 328.75 mbsf. Below 328.75 mbsf, the  $\text{Cl}^-$  concentration shows high values with a maximum of 579 mM at the same depth as the salinity maximum. Part of the chloride concentration profile may result from the hydration of clay minerals.

Interstitial water pH values generally decrease with depth, ranging between 7.01 and 7.41 (Fig. F26). The highest pH in Hole 1124C (7.50) occurs at 471.75 mbsf, but this value may be erroneous.

Concentrations of sodium ( $\text{Na}^+$ ) increase from 475 mM at 2.90 mbsf to 492 mM at 109.10 mbsf and then decrease toward the bottom of the hole (Fig. F26).

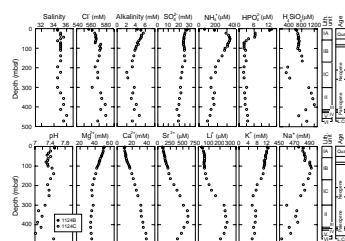
### Alkalinity, Sulfate, Ammonium, and Phosphate

The extent of oxidation, itself a function of the availability of organic matter, generally influences the concentrations of alkalinity, sulfate, phosphate, and ammonium. The profile of alkalinity in the interstitial water shows the typical pattern that results from organic matter oxidation and carbonate reprecipitation (Fig. F26). The alkalinity has a maximum (5.58 mM) at 21.94 mbsf, representing the peak of organic matter oxidation. The alkalinity then decreases gradually down to 193.90 mbsf, reflecting carbonate recrystallization and/or silicate reconstitution processes that use the bicarbonate ion from interstitial water (Gieskes, 1974). Below 193.90 mbsf, which is just below the lithologic boundary between Subunits IB and IC (see “[Lithostratigraphy](#),” p. 3), the variation of alkalinity is somewhat scattered, implying the occurrence of a variety of chemical reactions.

The sulfate ( $\text{SO}_4^{2-}$ ) concentration varies in a small range between 19.1 and 27.4 mM, which means that no active sulfate reduction occurred (Fig. F26). However, the  $\text{SO}_4^{2-}$  concentration generally decreases with depth, suggesting a limited amount of organic matter degradation. The main reason for the lack of sulfate reduction at this site is the pau-

T15. Summary of interstitial-water geochemistry results, [p. 132](#).

F26. Depth profiles of interstitial-water constituents at Site 1124, [p. 75](#).



city (and/or unavailability) of organic matter (see “[Organic Geochemistry](#),” p. 33), and the relatively slow sedimentation rate (see “[Age Models and Sedimentation Rates](#),” p. 28).

Ammonium ( $\text{NH}_4^+$ ) concentrations increase from 59 mM at 2.90 mbsf to a maximum of 330 mM at 52.10 mbsf (Fig. [F26](#)). This  $\text{NH}_4^+$  increase results from organic matter oxidation. Below this interval, the  $\text{NH}_4^+$  values steadily decrease down to 193.90 mbsf, which lies near to the lithologic boundary between Subunits IB and IC. The  $\text{NH}_4^+$  concentrations decrease continuously with depth, but a small enrichment in Unit II reflects an additional input into the pore water. The decrease of  $\text{NH}_4^+$  concentrations is caused by ion-exchange reactions on the surfaces of clay minerals and/or the subsequent incorporation of ions into interlayers of diagenetically formed clay minerals (Gieskes, 1981).

The phosphate ( $\text{HPO}_4^{2-}$ ) concentrations decrease with depth from the seafloor down to 71.10 mbsf (Fig. [F26](#)). Below 71.10 mbsf, the  $\text{HPO}_4^{2-}$  concentrations are relatively constant with a small variation. In the upper part of the hole, the phosphate profile is consistent with diagenetic uptake of dissolved phosphate, most likely into sedimentary mineral phases.

### **Calcium, Magnesium, and Strontium**

Calcium ( $\text{Ca}^{2+}$ ) concentrations generally increase with depth, except for at the top of the core, where  $\text{Ca}^{2+}$  concentrations are controlled by carbonate precipitation resulting from the buildup of alkalinity during organic matter oxidation (Fig. [F26](#)). The  $\text{Ca}^{2+}$  increase is attributed to the dissolution of carbonate-rich sediment in the interstitial waters. The gradual increase of  $\text{Ca}^{2+}$  concentrations ceases at ~300 mbsf, which is the lithologic boundary between Subunit IC and Unit II. Below this depth the  $\text{Ca}^{2+}$  concentrations remain relatively constant, but the lowermost part of hole shows another increasing trend.

The profile of magnesium ( $\text{Mg}^{2+}$ ) concentrations is almost opposite to that of the calcium concentration (Fig. [F26](#)). There is a gradual decrease of the  $\text{Mg}^{2+}$  concentration downhole to 200 mbsf, which can be explained by reactions that remove  $\text{Mg}^{2+}$  diagenetically from solution. Below 200 mbsf, which also marks the lithologic boundary, the  $\text{Mg}^{2+}$  concentrations remain at a consistent level.

Dissolved strontium ( $\text{Sr}^{2+}$ ) concentrations increase gradually from 93  $\mu\text{M}$  at 2.90 mbsf to a maximum of 598  $\mu\text{M}$  at 357.75 mbsf and then decrease with depth (Fig. [F26](#)). Strontium concentrations in interstitial waters are supplied by the recrystallization of biogenic carbonate. However, the decrease of  $\text{Sr}^{2+}$  concentrations in the lower part of the hole suggests that a different chemical reaction is occurring in addition to carbonate diagenesis. This reaction probably involves lithium and silica, as discussed below.

### **Dissolved Silica, Potassium, and Lithium**

Dissolved silica ( $\text{H}_4\text{SiO}_4$ ) concentrations increase slightly from 607  $\mu\text{M}$  at 2.90 mbsf to 816  $\mu\text{M}$  at 165.10 mbsf, which is the lithologic boundary between Subunits IB and IC (Fig. [F26](#)). The increasing silica concentration results from diagenetic dissolution of the biogenic silica in the sediments. At the interval of Subunit IC, silica concentrations become abruptly low and then increase again down to another lithologic boundary between Unit II and Unit III. Below Unit III, the dis-

solved silica decreases again to the bottom of the hole. The decrease of dissolved silica in the deeper part of the hole may be attributed to local chert formation (Gieskes and Lawrence, 1981; see “[Lithostratigraphy](#),” p. 3). In contrast to the bottom of the hole, the local decrease of silica in Subunit IC is not caused by chert formation. Instead, the low preservation of biogenic siliceous sediments suggests low paleoproductivity (see “[Biostratigraphy](#),” p. 12). In addition, the sudden decrease in tephra layers in Subunit IC is partly responsible for the low silica concentration (see “[Lithostratigraphy](#),” p. 3).

Potassium ( $K^+$ ) concentrations decrease gradually from 12.0 at 2.9 mbsf to 5.5 mM at 299.90 mbsf. Below 299.90 mbsf, the potassium concentrations are greater than 5.5 mM (Fig. F26). A depth of 299.90 mbsf coincides with the lithologic boundary between Subunit IC and Unit II (see “[Lithostratigraphy](#),” p. 3). The decrease of potassium in the interstitial water is a result of its removal into clay minerals that are forming within the sediments. However, below Unit II, the enrichment of potassium may reflect another chemical reaction.

The profile of dissolved lithium ( $Li^+$ ) concentrations is similar to that of strontium (Fig. F26). The  $Li^+$  concentrations increase slightly from 29  $\mu M$  at 2.90 mbsf to 66  $\mu M$  at 137.60 mbsf, which is just above the lithologic boundary between Subunits IB and IC. Throughout Subunit IC, the gradient of increasing  $Li^+$  concentrations becomes steeper down to the depth of 299.90 mbsf, which is the lithologic boundary between Subunit IC and Unit II. However, within Unit II, the  $Li^+$  concentrations remain relatively constant; below Unit II, the lithium decreases to the bottom of the hole. Generally, the  $Li^+$  concentrations depend on release of the element into the pore water from the sediments during recrystallization of biogenic sediments. Because the  $Li^+$  concentration is related to the biogenic silica content (Gieskes, 1981), the general increase indicates release of  $Li^+$  during diatom dissolution and silica transformation. However, based on the calcium, magnesium, and strontium concentrations, the decreasing pattern of lithium in the lower part of the hole, which is similar to strontium, may be caused by chert formation (Gieskes, 1983).

### **Summary of Interstitial Water Results**

The dominant chemical reactions controlling the interstitial-water element concentrations at Site 1124 include organic matter degradation, carbonate dissolution/precipitation, silica dissolution, chert formation, and reactions with clay minerals. Without active sulfate reduction, the element profiles of alkalinity, phosphate, and ammonia are typical, reflecting the organic matter oxidation and carbonate precipitation. The behavior of  $Ca^{2+}$ ,  $Mg^{2+}$ , and  $Sr^{2+}$  in the bottom part of hole implies the presence of another chemical reaction. The decrease of  $Sr^{2+}$  corresponds to the decrease of  $Li^+$ , which is related to silica utilization to form the chert observed in the lowermost part of core. However, low levels of dissolved silica in the middle of the core are attributed to the poor preservation of biogenic siliceous sediments, presumably because of low paleoproductivity. The general chemical zonations of interstitial waters at Site 1124 can be related to the lithostratigraphic units, paleontological age divisions, and the presence of hiatuses.

## ORGANIC GEOCHEMISTRY

### Volatile Hydrocarbons

As part of the shipboard safety and pollution-prevention monitoring program, hydrocarbon gases were analyzed in each core of Hole 1124B and in each core below 10 mbsf of Hole 1124C. The headspace methane concentrations are very low (<10 ppm), and gas pockets were not encountered. This result corresponds to low amounts of metabolizable organic matter in the sediments and high interstitial sulfate concentrations above 15 mM, which imply no significant sulfate reduction in the sediments (see “[Inorganic Geochemistry](#),” p. 30).

### Carbonate and Organic Carbon

The abundances of total, inorganic, and organic carbon and of calcium carbonate in sediments from Holes 1124A, 1124B, and 1124C are summarized in Table [T16](#) (also in [ASCII format](#)). Random sampling of all lithologies was performed for carbonate analysis, and for organic carbon measurements one sample per core was analyzed.

Carbonate contents vary between 0.1 and 88.3 wt% with an average of 36.3 wt% (Fig. [F27](#)). Variations are high in all sections. Between 100 and 200 mbsf, the average content is lower than in the rest of Hole 1124C. Below 300 mbsf, concentrations appear to be elevated, reflecting the transition from lithostratigraphic Unit II to Subunit IC (see “[Lithostratigraphy](#),” p. 3). The reddish brown to dark brown mudstone (lithostratigraphic Unit V) between 420 and 429 mbsf has a relatively low carbonate content, and the organic carbon content is not higher than in the rest of the sequence. Thus, this mudstone is not organic carbon rich, but rather has typical mudstone properties as indicated by natural gamma-ray intensity and magnetic susceptibility (see “[Downhole Measurements](#),” p. 36, and “[Paleomagnetism](#),” p. 23).

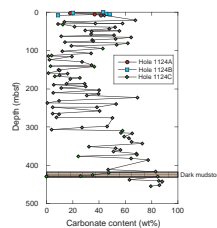
Sediments at Site 1124 average 0.31 wt% organic carbon (Fig. [F28](#)), which is in the normal range for deep-sea sediments as compiled by McIver (1975) from DSDP Legs 1 through 33. Variations are high without any apparent correlation with lithology. There is no indication of present-day bacterial degradation of organic matter as demonstrated by low methane concentrations. Thus, the organic matter may have been already degraded by bacteria, or large amounts are derived from terrigenous sources and are thus more refractory.

### Organic Matter Source Characterization

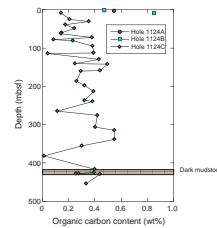
Organic carbon/nitrogen ratios were calculated for Site 1124 samples using organic carbon and total nitrogen concentrations to help identify the origin of their organic matter. The ratios vary from 0.2 to 12.6 with an average of 4.9 (Table [T16](#)). These low ratios are not accurate indicators of organic matter source. They may be an artifact of the low organic carbon content, combined with the tendency of clay minerals to adsorb ammonium ions generated during the degradation of organic matter (Müller, 1977). This interpretation is supported by unrealistically low atomic  $[C/N]_a$  values below 5.0 for organic carbon-poor samples (<0.3 wt%).

[T16. Organic chemistry data for sediments, p. 133.](#)

[F27. Carbonate contents in sediments from Holes 1124A, 1124B, and 1124C, p. 76.](#)



[F28. Organic carbon contents in sediments from Holes 1124A, 1124B, and 1124C, p. 77.](#)



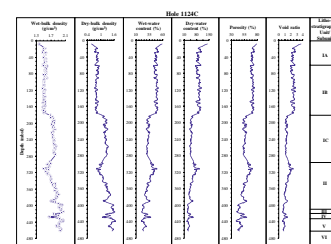
## PHYSICAL PROPERTIES

### Index Properties

Index properties measurements were made at a resolution of one sample for every two sections in the cores from all Site 1124 holes. Index properties were determined by a gravimetric method (see “Physical Properties,” p. 24, in the “Explanatory Notes” chapter). Values of measured index properties (void ratio, porosity, water content, bulk density, and grain density) are presented in Table T17 (also in [ASCII format](#)). The properties show two fairly homogeneous sediment sections occurring between 20 and 178 mbsf (lithostratigraphic Subunits IA and IB), and between 178 and 280 mbsf (lithostratigraphic Subunit IC; see “Lithostratigraphy,” p. 3). In both these units, the index properties profiles are nearly vertical with little variation (Fig. F29). No downhole increasing trend occurred in these two homogeneous sections. The porosity in Subunit IC is generally 15% lower than in Subunits IA and IB (above 178 mbsf), where sediments are apparently more compacted. An abrupt change in the index properties occurred at 178 mbsf; at this depth, lithification of the mud and nannofossil ooze into mudstone and nannofossil chalk, respectively, begins (see “Lithostratigraphy,” p. 3). Below 310 mbsf, wet-bulk density increases from 1.5 to 2.0 g/cm<sup>3</sup> downhole, while porosity decreases from 65% to 40% downhole. Two abrupt changes in the index properties occurred at 310 and 390 mbsf, possibly reflecting zones of depositional hiatuses or erosion, although this cannot be substantiated from the biostratigraphic results. Lithostratigraphic Unit IV, a dark mudstone (between 420 and 430 mbsf), is characterized by lower bulk density and higher porosity relative to the chalcs above and below.

T17. List of index properties measurements, [p. 135](#).

F29. Index properties measured from cores from Hole 1124C, [p. 78](#).

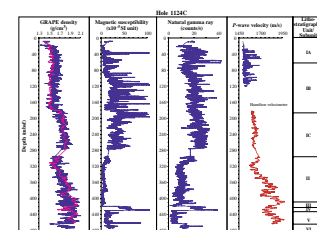


### Multisensor Track Measurements

The shipboard physical properties program at Site 1124 included nondestructive measurements of bulk density, magnetic susceptibility, and natural gamma-ray activity on whole sections of all cores using the MST (Fig. F30). Magnetic susceptibility was measured at 4-cm intervals and at high sensitivity (4-s measurement time) in all Site 1124 holes. High-amplitude fluctuations in magnetic susceptibility above 200 mbsf are associated with the occurrence of tephra layers (see “Lithostratigraphy,” p. 3). Magnetic susceptibility increases below 178 mbsf, the boundary between lithostratigraphic Subunits IB and IC, and then decreases below 310 mbsf. Lithostratigraphic Units II and III are characterized by very low magnetic susceptibility values; this finding is consistent with the high carbonate content of the nannofossil chalk (see “Organic Geochemistry,” p. 33). Below 420 mbsf, magnetic susceptibility increases abruptly corresponding to the high clay content of the dark mudstone in Unit IV. Below the dark mudstone (430 mbsf), magnetic susceptibility decreases again.

Natural gamma radiation was measured with a 15-s count every 14 cm in all Site 1124 holes. Natural gamma radiation values range from 0 to 40 counts/s. High values of natural gamma radiation indicate a relatively high clay mineral content. The low natural gamma radiation observed below 310 mbsf (except between 420 and 440 mbsf) indicates less clay-rich sediment than in the upper part of the core. The spikes in natural gamma radiation in the upper part of the section are probably a

F30. Multisensor track measurements from Hole 1124C, [p. 79](#).



result of the presence of abundant tephra layers. High natural gamma radiation values occurred between 420 and 430 mbsf and correlate with high magnetic susceptibility. These features are associated with the dark mudstone of Unit IV. Lithostratigraphic Unit VI is characterized by an abrupt increase in natural gamma radiation below 430 mbsf.

GRAPE bulk-density measurements were made at 4-cm intervals at all Site 1124 holes. A comparison of GRAPE density with the wet-bulk density determined from discrete samples shows general agreement although GRAPE density values are overall higher than bulk density obtained by index property measurements in the upper portion of the cores (APC cores). The *P*-wave velocity measurements (PWL) were made at 4-cm intervals at all Site 1124 holes. The PWL measurements were only collected from APC cores. High *P*-wave velocity peaks from Hole 1124C are associated with tephra layers.

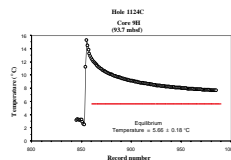
### **Compressional-Wave Velocity**

Compressional-wave (*P*-wave) velocity was measured perpendicular to the long axis of the core from XCB coring (below 178 mbsf) using the Hamilton frame velocimeter. *P*-wave velocity values are fairly constant in Subunit IC (between 178 and 280 mbsf). Nearly constant *P*-wave velocity can also be seen in the index properties record between 178 and 280 mbsf. Gradually increasing *P*-wave velocity values occurred below 310 mbsf. This change is not reflected in magnetic susceptibility and natural gamma radiation records, but a similar increase does occur in the GRAPE density profile. These changes indicate increasing overburden and lithification downhole. Lithostratigraphic Units II and III are distinguished by a reversal of *P*-wave velocity occurring at 410 mbsf. The dark mudstone of Unit IV is characterized by low *P*-wave velocities.

### **Thermal Conductivity and Heat Flow**

Four downhole temperature measurements with the Adara temperature tool were taken at the position of Cores 181-1124C-5H, 7H, 9H, and 11H. The Adara temperature tool yielded only one good-quality temperature estimate of 5.66°C from Core 9H (Fig. F31). Temperature records collected from Cores 7H and 11H were unusable. This bad reading might have been produced by sensor movement caused by the ship's motion. Accordingly, the temperature values from Cores 7H and 11H are provided only for reference (6.12°C and 6.56°C at Core 7H, and 6.87°C at Core 11H). On Core 9H (93.7 mbsf), the Adara temperature tool measured a value that reached 15.24°C just after the penetration, because of the effect of frictional heat production; in the same location, and at near equilibrium with the in situ sediments, it recorded 7.62°C just before pulling out. Based on temperature equilibration curves from Cores 7H, 9H, and 11H, the temperature estimate at the mudline is 0.92°C. Thermal conductivity was measured in the shipboard laboratory on the same core as the Adara temperature tool was used in; four measurements were made per core. A thermal gradient of 5.21°C/100 m was then calculated from the Adara tool and thermal conductivity measurements. Using an average thermal conductivity of 0.944 W/(m·K), heat-flow was estimated to be 0.049 W/m<sup>2</sup>. The thermal gradient and the estimated heat-flow value are both lower than those determined from sediments recovered from Site 1120. However, the values were only determined from two Adara temperature profiles and should be used with caution.

F31. Temperature measurement by the Adara temperature tool, p. 80.



## DOWNHOLE MEASUREMENTS

### Logging Operations

Downhole logging was performed in Hole 1124C. The drill string was placed at 95 mbsf as the logging tools were lowered to the bottom of the hole. During logging, the drill string was raised to 78.5 mbsf. The drill string had to be maintained at 78.5 mbsf to keep the upper hole wall from collapsing.

Three tool-string configurations were run in Hole 1123B in the following order: the triple combination, the FMS-sonic, and the GHMT (see “[Downhole Measurements](#),” p. 29, in the “Explanatory Notes” chapter). A repeat interval was measured with all three tool strings. Logging operations are summarized in Figure F32. Logging operations began at 2100 hr on 29 September 1998 and finished at 1600 hr on 30 September 1998. There was less than 2 m of heave throughout operations, and the wireline heave compensator was used during all measurements. The hole conditions were good, with a relatively uniform borehole diameter (~13 in) through the lower part of the hole and a more variable diameter in the upper portion (Fig. F33A). The NMRS (total field) sonde on the GHMT was again not working.

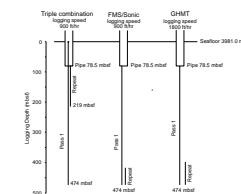
The Lamont temperature tool was left off the bottom of the triple combination to maximize the chances of recording the K/T boundary with the resistivity tool (DIT). The temperature tool is 1.3 m long. The sensors on the DIT are 1.6 m above the base of the tool. The location of the K/T boundary was estimated to be between Cores 181-1124C-48X and 49X (see “[Biostratigraphy](#),” p. 12), ~6–8 m above the base of the hole.

Observations of the core lithology detected horizons containing altered tephra. Altered tephra is frequently high in smectite, which is susceptible to swelling, and may cause constrictions downhole. With this in mind, clay-swelling tests were performed on two samples: a greenish clay, thought to contain very little smectite; and an altered tephra, thought to be almost entirely smectite. The results are shown in Figure F34. The greater the time shown on the y-axis the more susceptible the sample is to swelling. Figure F34 shows that the altered tephra sample was highly susceptible to swelling, but that the addition of KCl (an anti-swelling agent) considerably reduced the propensity of the sample to swell. Before logging operations, the borehole was flushed with a seawater-based drilling mud containing 276 kg/m<sup>3</sup> of sepiolite (an anti-swelling agent). This helped to reduce swelling of the altered tephra horizons in the borehole.

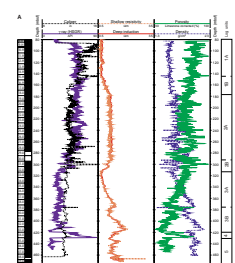
### Data Quality and Log/Core Correlation

Because of good weather and good hole conditions, the data quality is excellent. The uneven caliper in the upper portion of the hole may be caused by tephra bed washouts, as tephras were abundant in this part of the core (see “[Lithostratigraphy](#),” p. 3). Nevertheless, caliper deviation was generally no more than 1 to 2 in from the average (13 in). In some places, however, the caliper did exceed 15 in, and in these regions the FMS data are unreliable (see “[Downhole Measurements](#),” p. 29, in the “Explanatory Notes” chapter). For example, a washout can be seen on the FMS image at 300 mbsf. This point corresponds to a gap in core recovery.

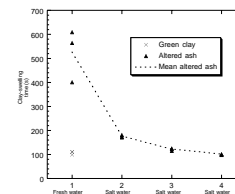
F32. Logging operations in Hole 1124C, [p. 81](#).



F33. Log data and logging units from Hole 1124C, [p. 82](#).



F34. Clay-swelling test results from Hole 1124C, [p. 84](#).



The log magnetic susceptibility data were correlated with the core magnetic susceptibility results (Fig. F35). Although core recovery was good for the majority of the hole, there was virtually no core recovered between 280–300 mbsf, and, consequently, the core-based magnetic susceptibility record is incomplete here. The log/core magnetic susceptibility correlation diagram shows a log susceptibility spike at 280–300 mbsf. The log/core susceptibility correlation also confirms that coring did not recover the K/T boundary. There is a small gap in the core-based magnetic susceptibility at 467 mbsf, which is the predicted location of the K/T boundary (see “**Stratigraphic Correlation: the K/T Boundary and the Brown Mudstone**,” p. 39).

Sonic traveltimes contained 5–10 cycle skips, which were edited from the log. The traveltimes were converted to velocities and used to create a depth-integrated travel time profile to compare with a pre-cruise seismic survey of the area. The profile demonstrates that the major lower seismic reflector correlates with the top of the brown mudstone at 419.5 mbsf (see “**Lithostratigraphy**,” p. 3).

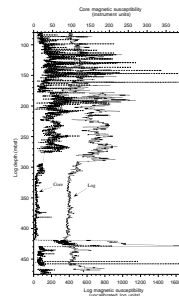
The predicted location of the K/T boundary, toward the base of the hole, was monitored by the lowest tool on each of the three tool strings. The tools that recorded the boundary were the resistivity tool on the triple combination, the FMS tool on the FMS-sonic, and the magnetic susceptibility tool on the GHMT. The sensor on the resistivity tool is 1.6 m above the base of the triple combination, the FMS is at the base of the FMS-sonic, and the susceptibility sensor is 3.96 m above the base of the GHMT.

## Logging Units

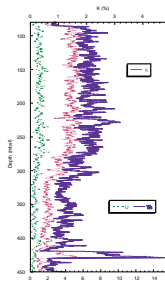
The log data from Hole 1124C show noticeable variations downhole (Fig. F33A, F33B), in response to fluctuating depositional environments. Distinct logging units can be identified on the basis of average log values and trends in the data. The range of values observed within the data from Hole 1124C is greater than that recorded from the previous two logged holes, possibly suggesting a more marked change in sedimentary environments through time. Magnetic susceptibility values vary from around  $390 \times 10^{-6}$  (uncalibrated log units) in log Subunits 3A and 3B, to more than  $1600 \times 10^{-6}$  at the base of the brown mudstone. Resistivity values are generally around  $0.5 \Omega\text{m}$  toward the top of the logged section, but exceed  $3 \Omega\text{m}$  near the base of the hole. Natural gamma-ray values reach a maximum of 88 API (American Petroleum Institute units) at the base of the brown mudstone, but drop to only slightly more than 10 API above and below this unit. As observed at Site 1123, downhole variations in thorium and potassium appear to correlate (Fig. F36). Uranium values often fluctuate independently of thorium and potassium (Fig. F36).

There is generally a good correlation between the log units identified in Hole 1124C and the main lithostratigraphic units (Figs. F33A, F33B). Log Subunits 1A and 1B correlate well with lithostratigraphic Subunit IB, and log Unit 4 (the brown mudstone) correlates well with lithostratigraphic Unit IV. There may be some correlation between log Subunits 2A and 2B and lithostratigraphic Subunit IC, and between log Subunits 3A and 3B and lithostratigraphic Unit II. The only major seismic reflector identified at this site occurs at the top of the brown mudstone (419.5 mbsf). The log units identified in Hole 1124C are outlined below and shown in Figures F33A, F33B.

F35. Comparison of log-based and core-based MS results, p. 85.



F36. Spectral gamma-ray results from Hole 1124C, p. 86.



### **Log Subunit 1A: Base of Pipe to 144 mbsf**

This subunit has a relatively low resistivity (shallow resistivity =  $0.64 \pm 0.04 \Omega\text{m}$ ) and high natural gamma values ( $54 \pm 5 \text{ API}$ ). Sonic traveltimes are consistently high ( $197 \pm 1.5 \mu\text{s}/\text{ft}$ ). Porosity, density, and photoelectric effect show relatively little long-term variation. Magnetic susceptibilities fluctuate regularly, by  $\sim 500 \times 10^{-6}$ . This is probably caused by the widespread occurrence of tephra horizons.

### **Log Subunit 1B: 144–176 mbsf**

Within this subunit, resistivities gradually increase with depth, and sonic traveltimes begin to decrease. However, the other log data are very similar in character to Subunit 1A, implying there is only a very subtle change from the subunit above.

### **Log Subunit 2A: 176–292 mbsf**

At the top of this subunit, both density and magnetic susceptibility show marked increases. Photoelectric effect values begin to show greater fluctuations, indicating that the composition of the sediment is more variable. Toward the base of Subunit 2A, natural gamma-ray values begin to decrease.

### **Log Subunit 2B: 292–313 mbsf**

Resistivity and magnetic susceptibility values begin to decrease from the top to the bottom of this subunit. In addition, magnetic susceptibility values show far less variability than those seen in the subunits above. This may be a result of the lack of tephra in this section of the hole (see “[Lithostratigraphy](#),” p. 3).

### **Log Subunits 3A (313–374 mbsf) and 3B (374–420 mbsf)**

Within both of these subunits, gamma-ray values are generally lower ( $43 \pm 5 \text{ API}$ ) than above. Magnetic susceptibility values are also low (mean =  $393 \times 10^{-6}$ ) and have a very small variation (standard deviation =  $24 \times 10^{-6}$ ). However, Subunits 3A and 3B can be subdivided using (1) resistivity, density, and photoelectric effect, which show two distinct cycles of increasing value downhole; and (2) sonic traveltimes and porosity, which show two cycles of decreasing value downhole. These log responses suggest that compaction and lithification increase in two steps, which overlap at the boundary of Subunits 3A and 3B.

### **Log Unit 4: 420–430 mbsf**

This log unit is noticeable by a sharp increase in magnetic susceptibility, sonic traveltimes, and gamma-ray values. Porosity increases within this unit and density decreases. The photoelectric effect also decreases, suggesting a change in the mineralogy within this unit. This unit correlates with the brown mudstone (see “[Lithostratigraphy](#),” p. 3).

### Log Unit 5: 430–474 mbsf

In Unit 5, all of the log data except for resistivity remain relatively constant. Gamma-ray values are at their lowest in this unit ( $14.5 \pm 3$  API). At 466.8 mbsf, however, there is a sharp increase in resistivity and an associated decrease in magnetic susceptibility, which reflect a sudden change in environmental conditions. These results are discussed in more detail below.

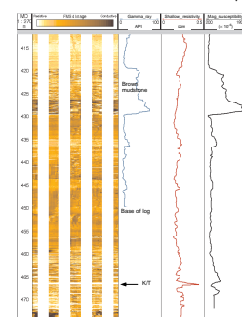
### Stratigraphic Correlation: the K/T Boundary and the Brown Mudstone

The drilling of Hole 1124C was of particular scientific interest, as it penetrated the K/T boundary (see “[Biostratigraphy](#),” p. 12). However, the exact contact between Cretaceous and Tertiary rocks is missing from the core. It lies between the base of the recovered section of Core 181-1124C-48X, which is Tertiary, and the top of Core 181-1124C-49X, which is Cretaceous. Three tools were able to take readings from the base of the hole (see “[Data Quality and Log/Core Correlation](#),” p. 36), where the first appearance of Cretaceous rocks was observed (see “[Biostratigraphy](#),” p. 12). The K/T boundary appears to occur at slightly more than 7 m above the base of the hole. This interpretation is based on a large spike in resistivity and a concomitant decrease in magnetic susceptibility at this point (Fig. F37). The FMS data show a 30-cm-thick resistive bed, with a sharp lower contact at 466.8 mbsf. Although the lithologic conditions responsible for these log responses are somewhat ambiguous (see below), they clearly represent a sudden and short-lived change in the environment at this point.

The sediment above and below the K/T boundary is highly lithified (see “[Lithostratigraphy](#),” p. 3). Although the low resistivity recorded in these lithified sediments appears incongruous, it may be explained by the presence of conductive clays. Terrigenous clays occur in varying amounts throughout the sediment column. High resistivities seen at the K/T boundary may represent the absence of these clays. Low magnetic susceptibility seen at the K/T boundary appears to support this interpretation, as it may be recording the absence of the terrestrially derived, clay-sized material that occurs above and below.

A distinct stratigraphic marker that was observed in the core was the brown mudstone (see “[Lithostratigraphy](#),” p. 3). The brown mudstone can also be clearly seen in the log data, as a horizon of increased natural gamma intensity and magnetic susceptibility between 420 and 430 mbsf (Fig. F37). Interestingly, the spectral gamma-ray values from the brown mudstone show no increase in uranium concentrations (Fig. F37), suggesting that the concentration of organic matter is low. Furthermore, the high magnetic susceptibilities and thorium concentrations at this point suggest an increased input of terrigenous clay.

F37. Selected logging results from the bottom of Hole 1124C, p. 87.



## **REFERENCES**

- Alloway, B.W., Pillans, B.J., Sandhu, A.S., and Westgate, J.S., 1993. Revision of the marine chronology in the Wanganui Basin, New Zealand, based on the isothermal plateau fission-track dating of tephra horizons. *Sediment. Geol.*, 82:299–310.
- Berggren, W.A., Kent, D.V., Swisher, C.C., III, and Aubry, M.-P., 1995. A revised Cenozoic geochronology and chronostratigraphy. In Berggren, W.A., Kent, D.V., Aubry, M.-P., and Hardenbol, J. (Eds.), *Geochronology, Time Scales and Global Stratigraphic Correlation*. Spec. Publ.—Soc. Econ. Paleontol. Mineral. (Soc. Sediment. Geol.), 54:129–212.
- Cande, S.C., and Kent, D.V., 1995. Revised calibration of the geomagnetic polarity timescale for the Late Cretaceous and Cenozoic. *J. Geophys. Res.*, 100:6093–6095.
- Carter, L., and Carter, R.M., 1993. Sedimentary evolution of the Bounty Trough: a Cretaceous rift basin, Southwestern Pacific Ocean. In Ballance, P.F. (Ed.), *South Pacific Sedimentary Basins*: Amsterdam (Elsevier), Sedimentary Basins of the World Ser., 2:51–67.
- Carter, L., Carter, R.M., McCave, I.N., and Gamble, J., 1996. Regional sediment recycling in the abyssal Southwest Pacific Ocean. *Geology*, 24:735–738.
- Carter, L., and McCave, I.N., 1994. Development of sediment drifts approaching an active plate margin under the SW Pacific deep western boundary current. *Paleoceanography*, 9:1061–1085.
- Carter, L., and Mitchell, J.S., 1987. Late Quaternary sediment pathways through the deep ocean, east of New Zealand. *Paleoceanography*, 2:409–422.
- Carter, L., Nelson, C.S., Neil, H.L., and Froggatt, P.C., 1995. Correlation, dispersal, and preservation of the Kawakawa Tephra and other late Quaternary tephra layers in the Southwest Pacific Ocean. *N. Z. J. Geol. Geophys.*, 38:29–46.
- Carter, R.M., 1985. The mid-Oligocene Marshall Paraconformity, New Zealand: coincidence with global eustatic sea-level fall or rise? *J. Geol.*, 93:359–371.
- Davey, E.J., 1977. Marine seismic measurements in the New Zealand region. *N. Z. J. Geol. Geophys.*, 20:719–777.
- Froggatt, P.C., and Lowe, D.J., 1990. A review of Late Quaternary silicic and ignimbrite stratigraphy of New Zealand: their stratigraphy, nomenclature, distribution, volume and age. *N.Z. J. Geol. Geophys.*, 33:89–109.
- Fulthorpe, C.S., Carter, R.M., Miller, K.G., and Wilson, J. 1996. The Marshall Paraconformity: a Southern Hemisphere record of a mid-Oligocene glacioeustatic lowstand. *Mar. Pet. Geol.*, 13:61–77.
- Gardner, J.V., Nelson, C.S., and Baker, P.A., 1986. Distribution and character of pale green laminae in sediment from Lord Howe Rise: a probable late Neogene and Quaternary tephrostratigraphic record. In Kennett, J.P., von der Borch, C.C., et al., *Init. Repts. DSDP*, 90 (Pt. 2): Washington (U.S. Govt. Printing Office), 1145–1159.
- Gieskes, J.M., 1974. Interstitial water studies, Leg 25. In Simpson, E.S.W., Schlich, R., et al., *Init. Repts. DSDP*, 25: Washington (U.S. Govt. Printing Office), 361–394.
- \_\_\_\_\_, 1981. Deep-sea drilling interstitial water studies: implications for chemical alteration of the oceanic crust, layers I and II. In Warme, J.E., Douglas, R.G., and Winterer, E.L. (Eds.), *The Deep Sea Drilling Project: A Decade of Progress*. Spec. Publ.—Soc. Econ. Paleontol. Mineral., 32:149–167.
- \_\_\_\_\_, 1983. The chemistry of interstitial waters of deep-sea sediments: interpretation of deep-sea drilling data. In Riley, J.P., and Chester, R. (Eds.), *Chemical Oceanography* (Vol. 8): London (Academic), 221–269.
- Gieskes, J.M., and Lawrence, J.R., 1981. Alteration of volcanic matter in deep-sea sediments: evidence from the chemical composition of interstitial waters from deep sea drilling cores. *Geochim. Cosmochim. Acta*, 45:1687–1703.
- Griggs, G.B., Carter, L., and Kennett, J.P., and Carter, R.M., 1983. Late Quaternary marine stratigraphy southeast of New Zealand. *Bull. Geol. Soc. Am.*, 94:791–797.

- Hollis, C.J., 1997. Cretaceous-Paleocene Radiolaria of eastern Marlborough, New Zealand. *Inst. Geol. Nucl. Sci. Monogr.*, 17:1–152.
- Kennett, J.P., 1977. Cenozoic evolution of Antarctic glaciation, the circum-Antarctic Ocean, and their impact on global paleoceanography. *J. Geophys. Res.*, 82:3843–3860.
- Kennett, J.P., and von der Borch, C.C., 1986. Southwest Pacific Cenozoic paleoceanography. In Kennett, J.P., von der Borch, C.C., et al., *Init. Repts. DSDP*, 90 (Pt. 2): Washington (U.S. Govt. Printing Office), 1493–1517.
- Lewis, K.B., 1994. The 1500-km long Hikurangi Channel: trench-axis channel that escapes its trench, crosses a plateau, and feeds a fan-drift. *Geo-Mar. Lett.*, 14:19–28.
- Lewis, K.B., Collott, J.-Y., and Lallemand, S.E., 1998. The dammed Hikurangi Trough: a channel-fed trench blocked by subducting seamounts and their wake avalanches (New Zealand-France GeodyNZ Project). *Basin Res.*, 10:441–468.
- McCave, I.N., and Carter, L., 1997. Recent sedimentation beneath the deep western boundary current off northern New Zealand. *Deep-Sea Res.*, 44:1203–1237.
- McIver, R.D., 1975. Hydrocarbon occurrences from JOIDES Deep Sea Drilling Project. *Proc. Ninth Petrol. Congr.*, 269–280.
- Mix, A.C., Harris, S.E., and Janecek, T.R., 1995. Estimating lithology from nonintrusive reflectance spectra: Leg 138. In Pisias, N.G., Mayer, L.A., Janecek, T.R., Palmer-Julson, A., and van Andel, T.H. (Eds.), *Proc. ODP, Sci. Results*, 138: College Station, TX (Ocean Drilling Program), 413–427.
- Müller, P.J., 1977. C/N ratios in Pacific deep sea sediments: effect of inorganic ammonium and organic nitrogen compounds sorbed by clays. *Geochim. Cosmochim. Acta*, 41:765–776.
- Nelson, C.S., Foggatt, P.C., and Gosson, G.J., 1986. Nature, chemistry, and origin of late Cenozoic megascopic tephras in Leg 90 cores from the Southwestern Pacific. In Kennett, J.P., von der Borch, C.C., et al., *Init. Repts. DSDP*, 90: Washington (U.S. Govt. Printing Office), 1161–1171.
- O'Connor, B., 1997a. Lower Miocene Radiolaria from Te Kopua Point, Kaipara Harbour, New Zealand. *Micropaleontology*, 43:101–128.
- \_\_\_\_\_, 1997b. New Radiolaria from the Oligocene and early Miocene of Northland, New Zealand. *Micropaleontology*, 43:63–100.
- Pemberton, S.G., and MacEachern, J.A., 1995. The sequence stratigraphic significance of trace fossils: examples from the Cretaceous Foreland Basin of Alberta, Canada. In Van Wagoner, J.C., and Bertram, G.T. (Eds.), *Sequence Stratigraphy of Foreland Basin Deposits*. AAPG Mem., 64:429–475.
- Rait, G., Chanier, F., and Waters, D.W., 1991. Landward and seaward-directed thrusting accompanying the onset of subduction beneath New Zealand. *Geology*, 119:230–233.
- Sanfilippo, A., and Nigrini, C., 1998. Code numbers for Cenozoic low latitude radiolarian biostratigraphic zones and GPTS conversion tables. *Mar. Micropaleontol.*, 33:109–156.
- Shane, P.A.R., Black, T.M., Alloway, B.V., and Westgate, J.A., 1996. Early to middle Pleistocene tephrachronology of North Island, New Zealand: implications for volcanism, tectonism, and paleoenvironments. *Geol. Soc. Am. Bull.*, 108:915–925.
- Stewart, R.B., and Neall, V.E., 1984. Chronology of palaeoclimatic change at the end of the last glaciation. *Nature*, 311:47–48.
- Weaver, P.P.E., Carter, L., and Neil, H., 1998. Response of surface watermasses and circulation to late Quaternary climate change, east of New Zealand. *Paleoceanography*, 13:70–83.

Figure F1. Locality map of Site 1124, showing location of seismic line of Figure F2, p. 43.

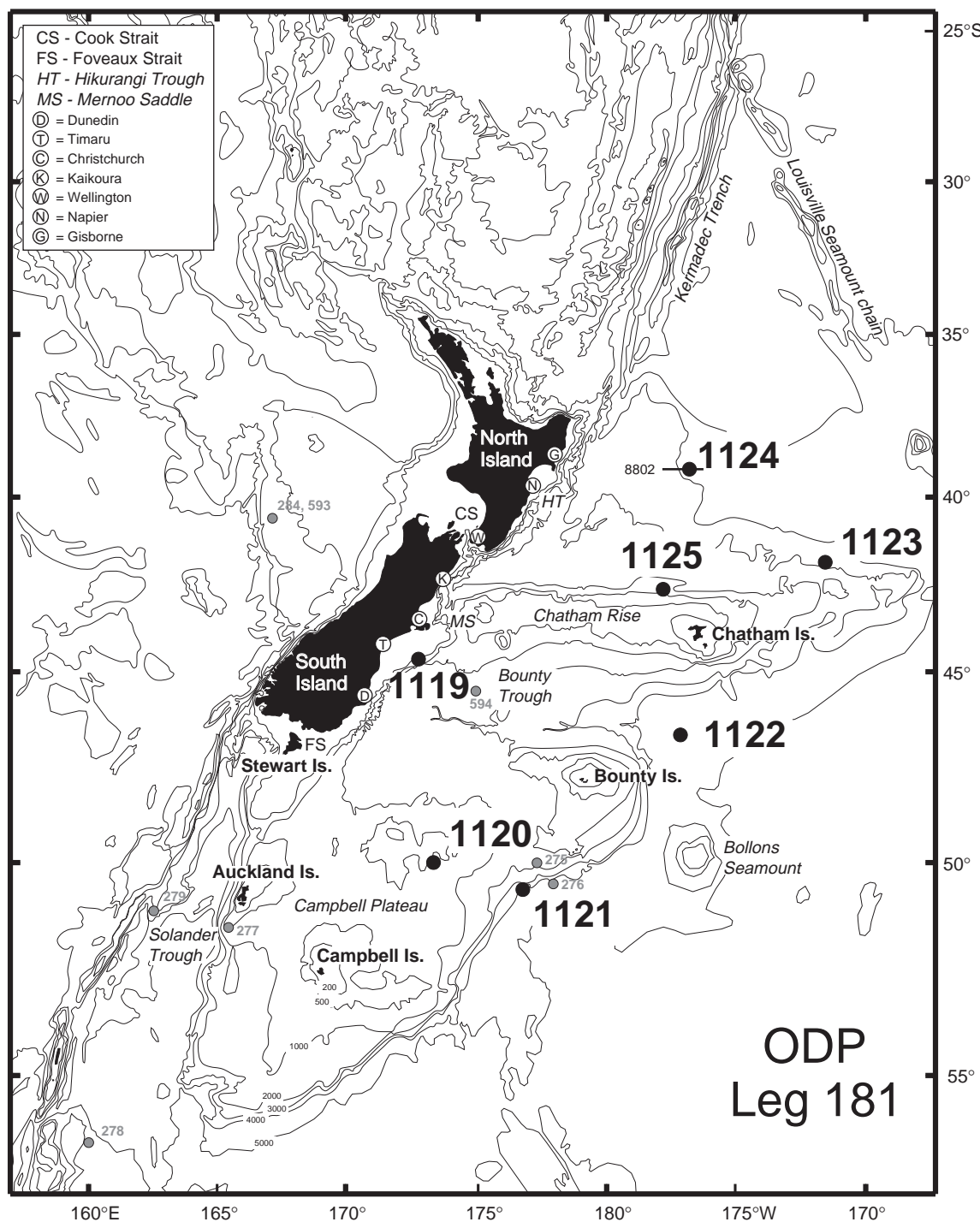
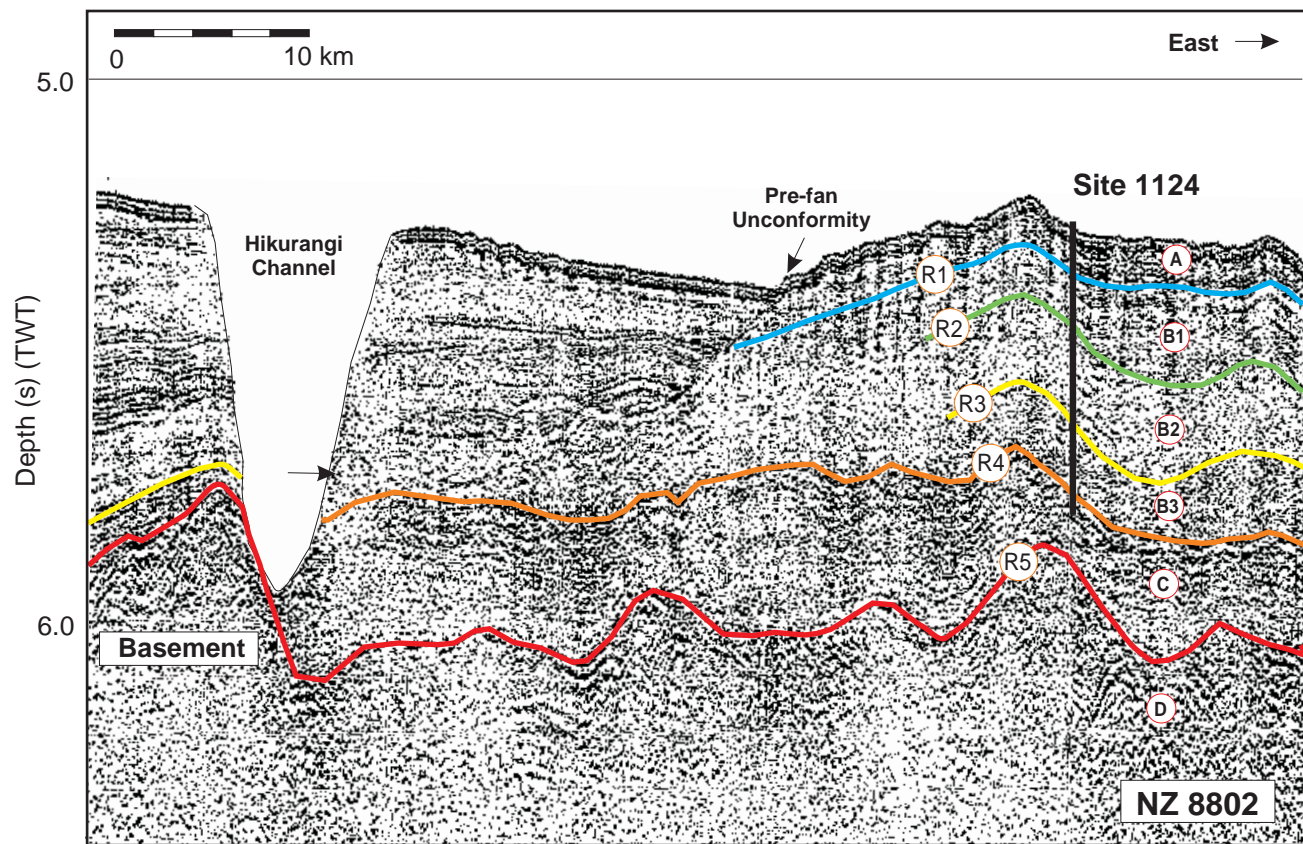


Figure F2. Portion of seismic line NZ 8802 through Site 1124 (1300–1700 hr, 29 April 1988).



NZ8802, DB9195, 29/4/88, 1300-1700

Figure F3. Portion of 3-kHz line NZOI 2050, near Site 1124.

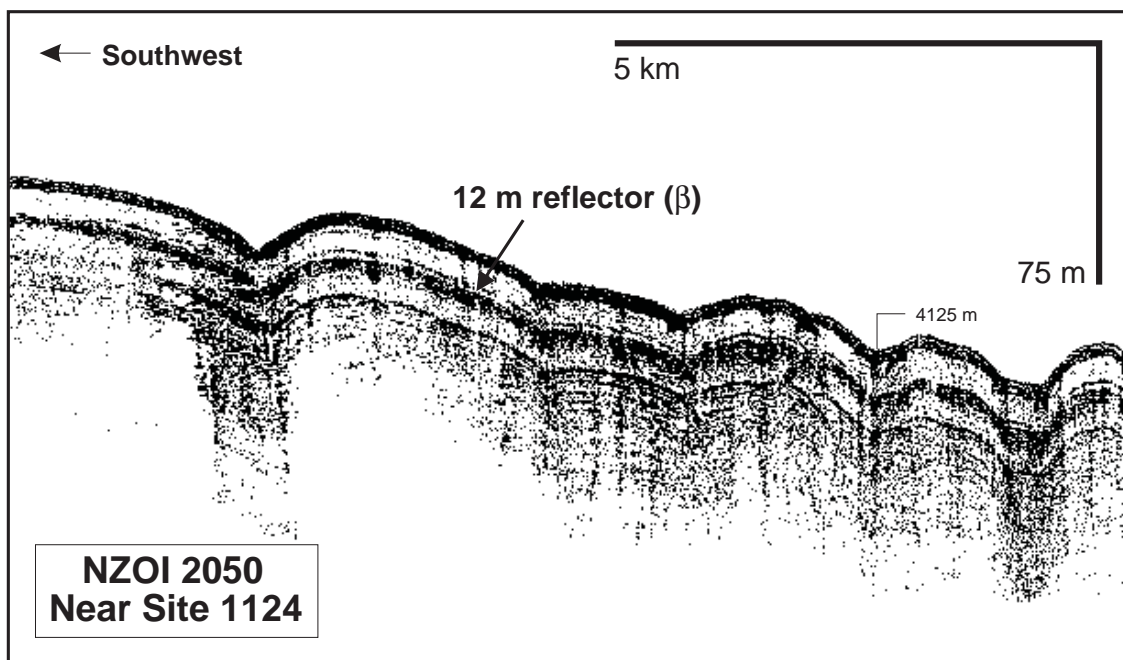
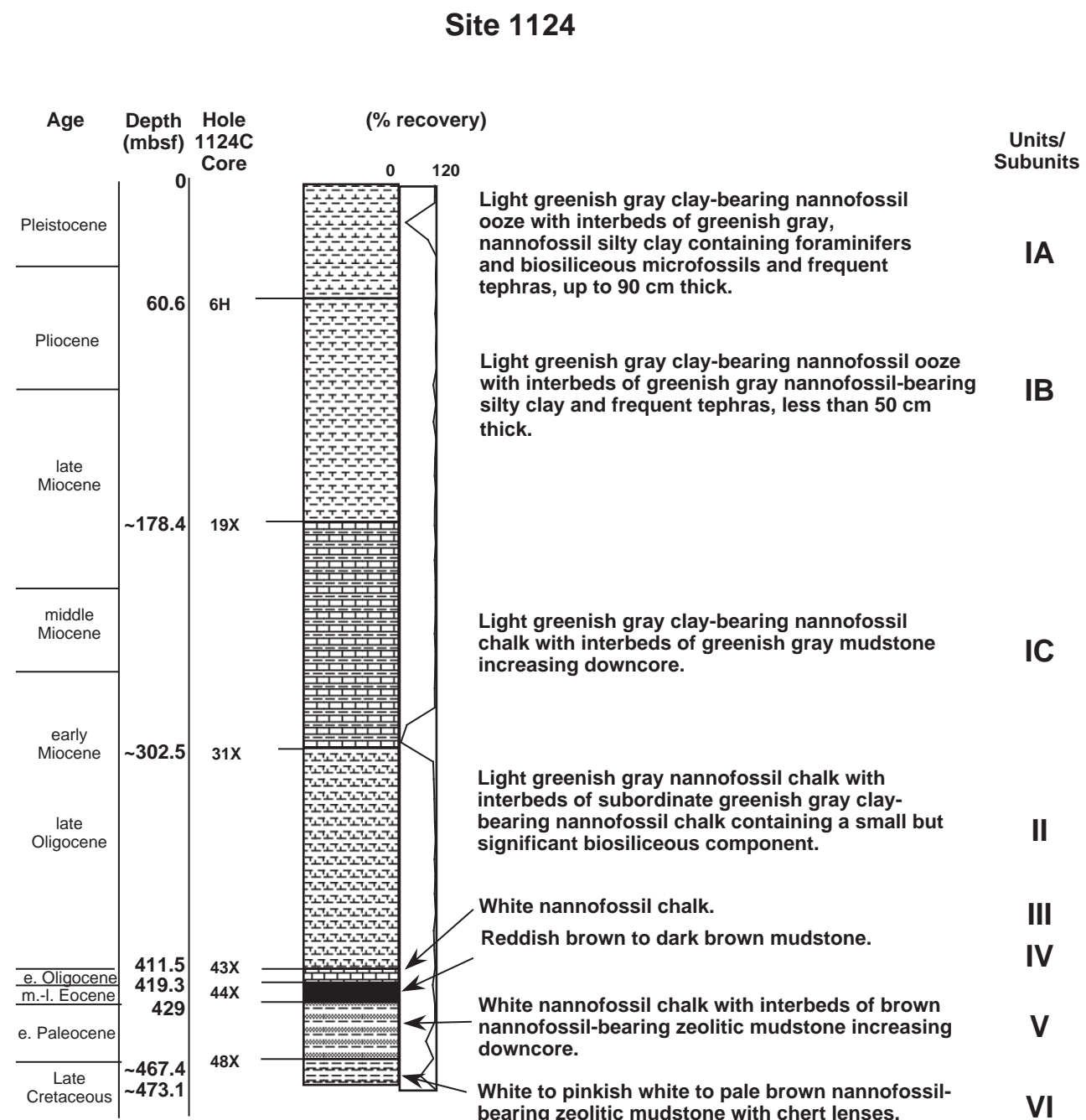
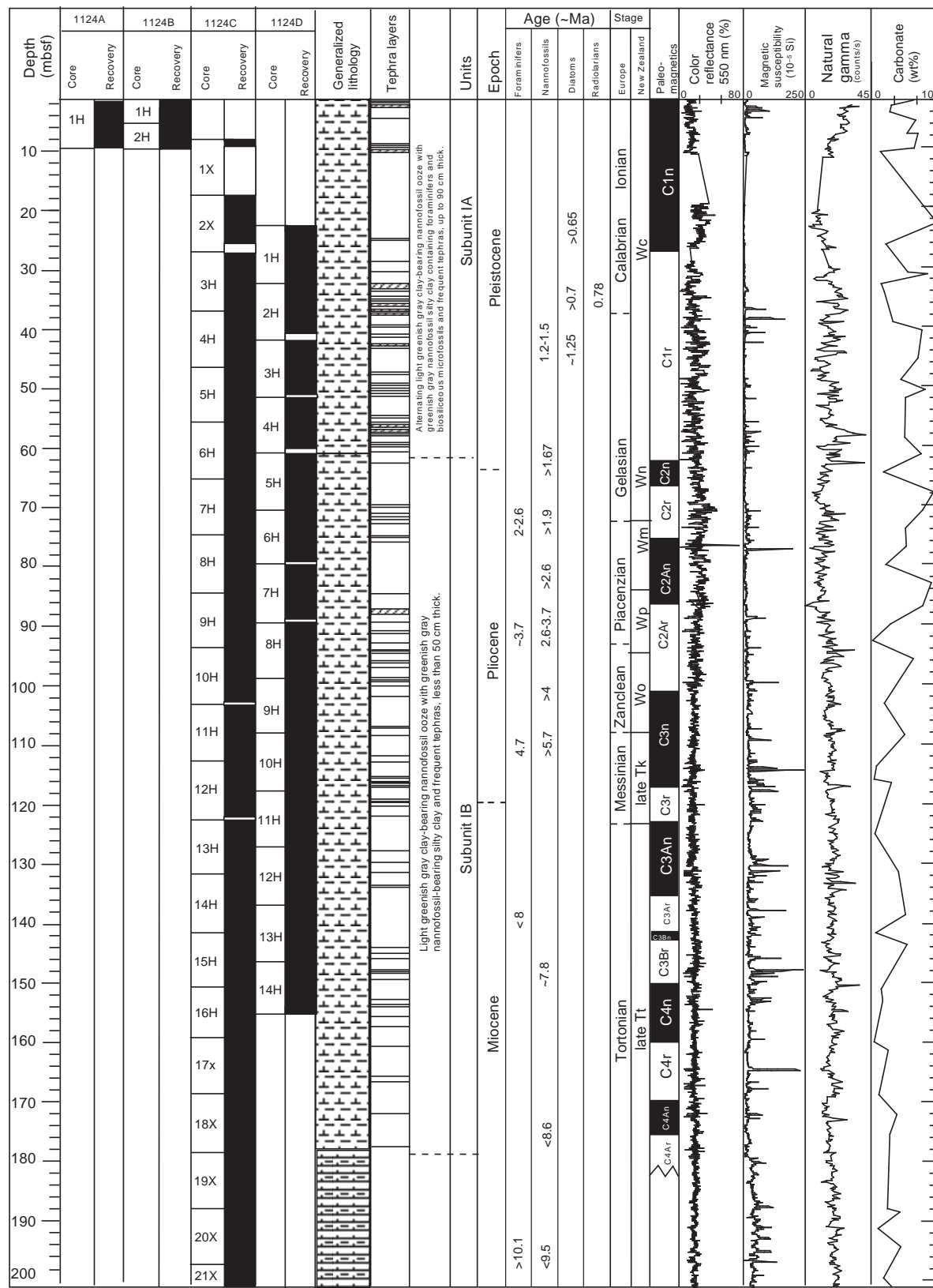


Figure F4. Summary of main lithologies found at Site 1124.



**Figure F5.** Summary of lithostratigraphic, biostratigraphic, and magnetostratigraphic data along with profiles of color reflectance, magnetic susceptibility, natural gamma ray, and calcium carbonate. (Continued on next two pages).

Leg: 181 Site: 1124



**Figure F5 (continued).**

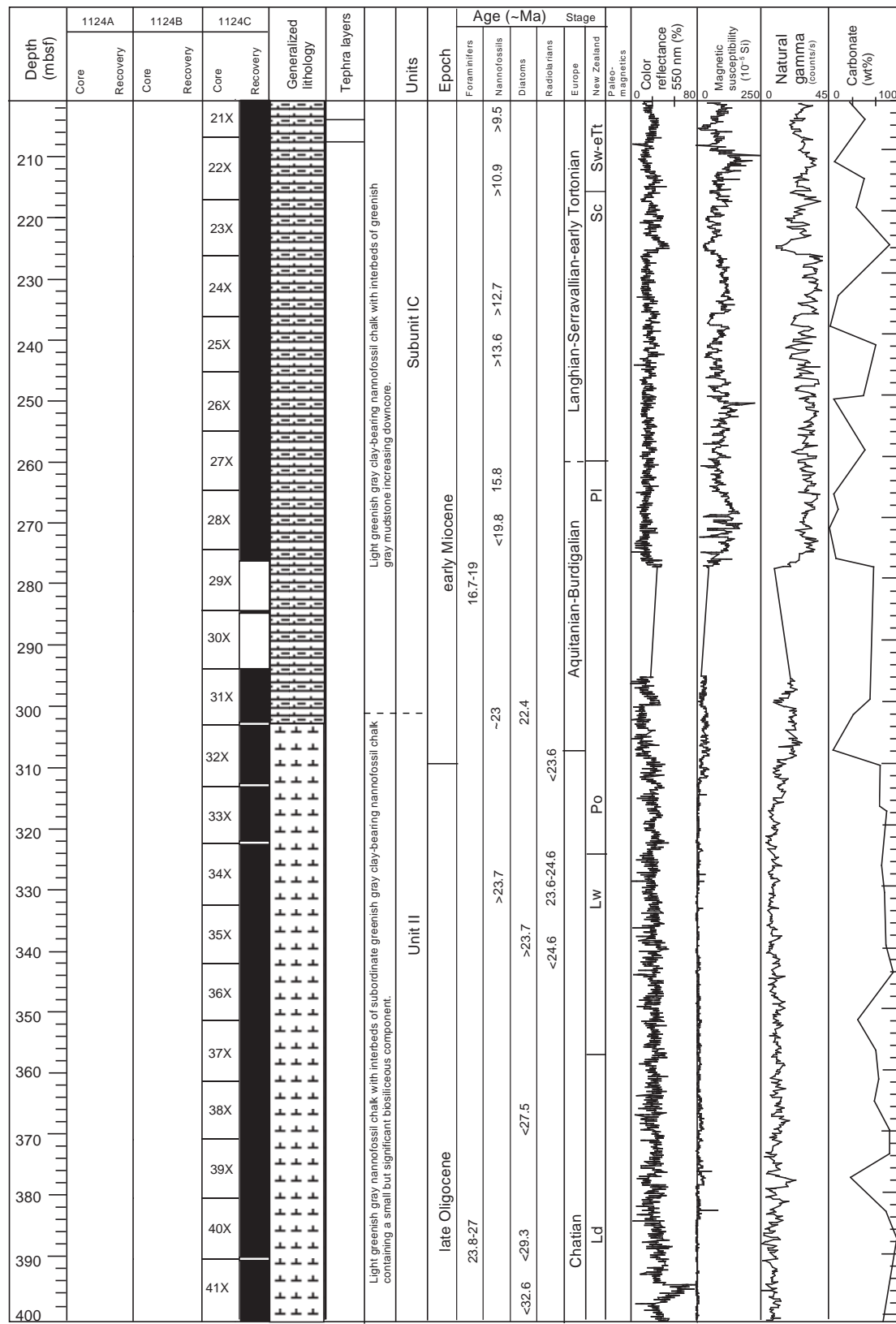


**Figure F5 (continued).**

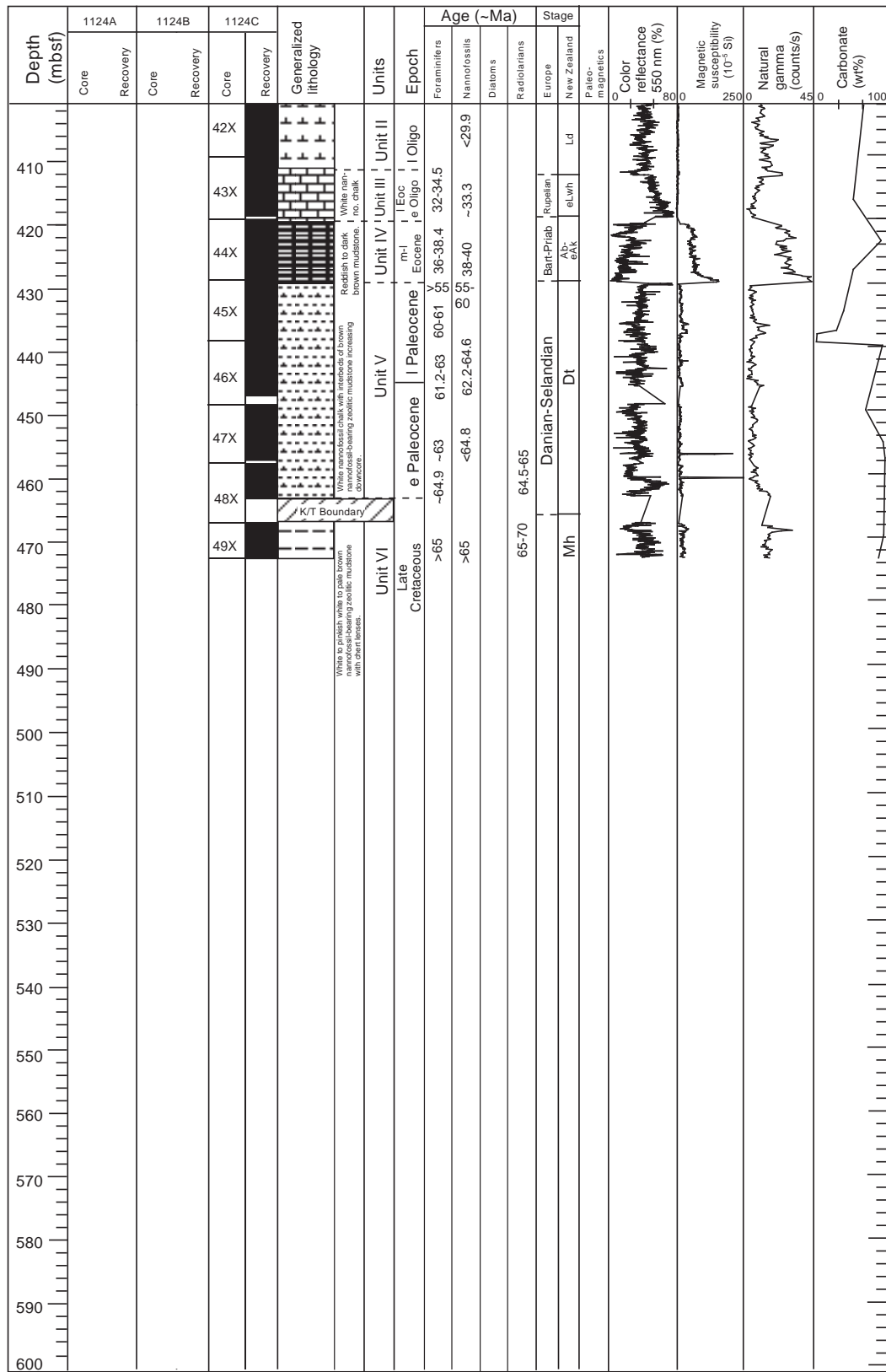


Figure F6. Carbonate vs. reflectance at 550 nm with regression equation.

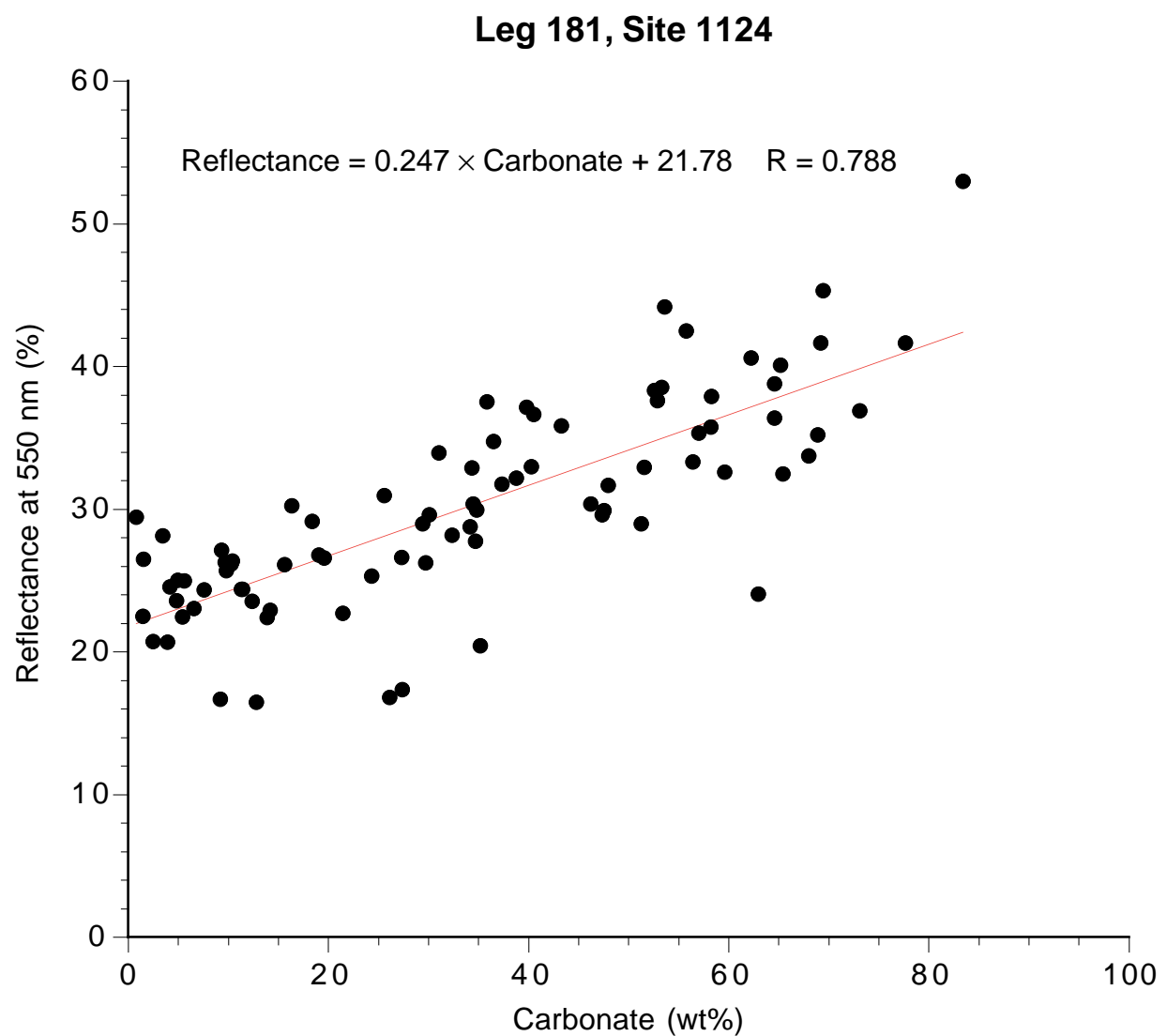
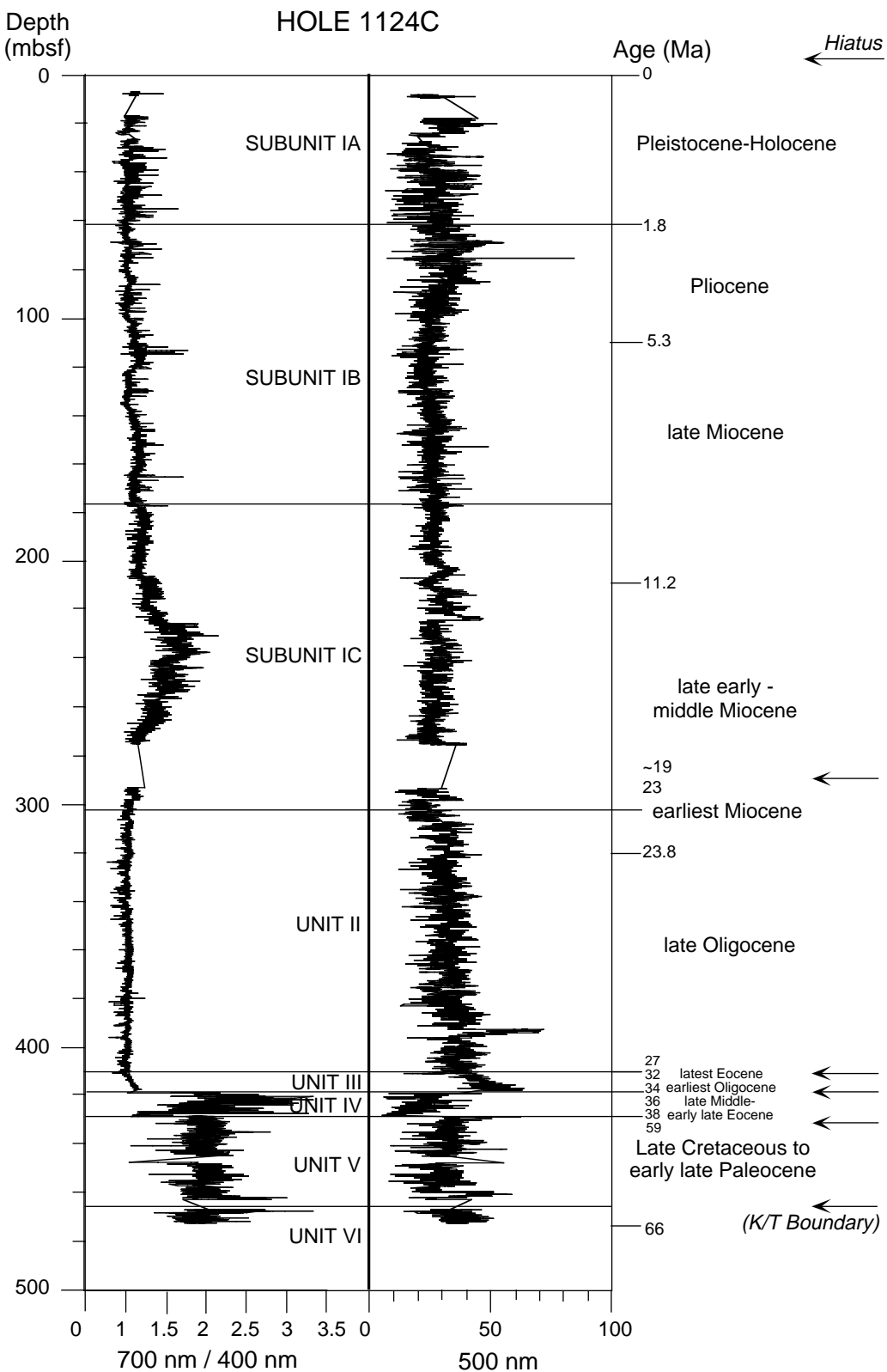
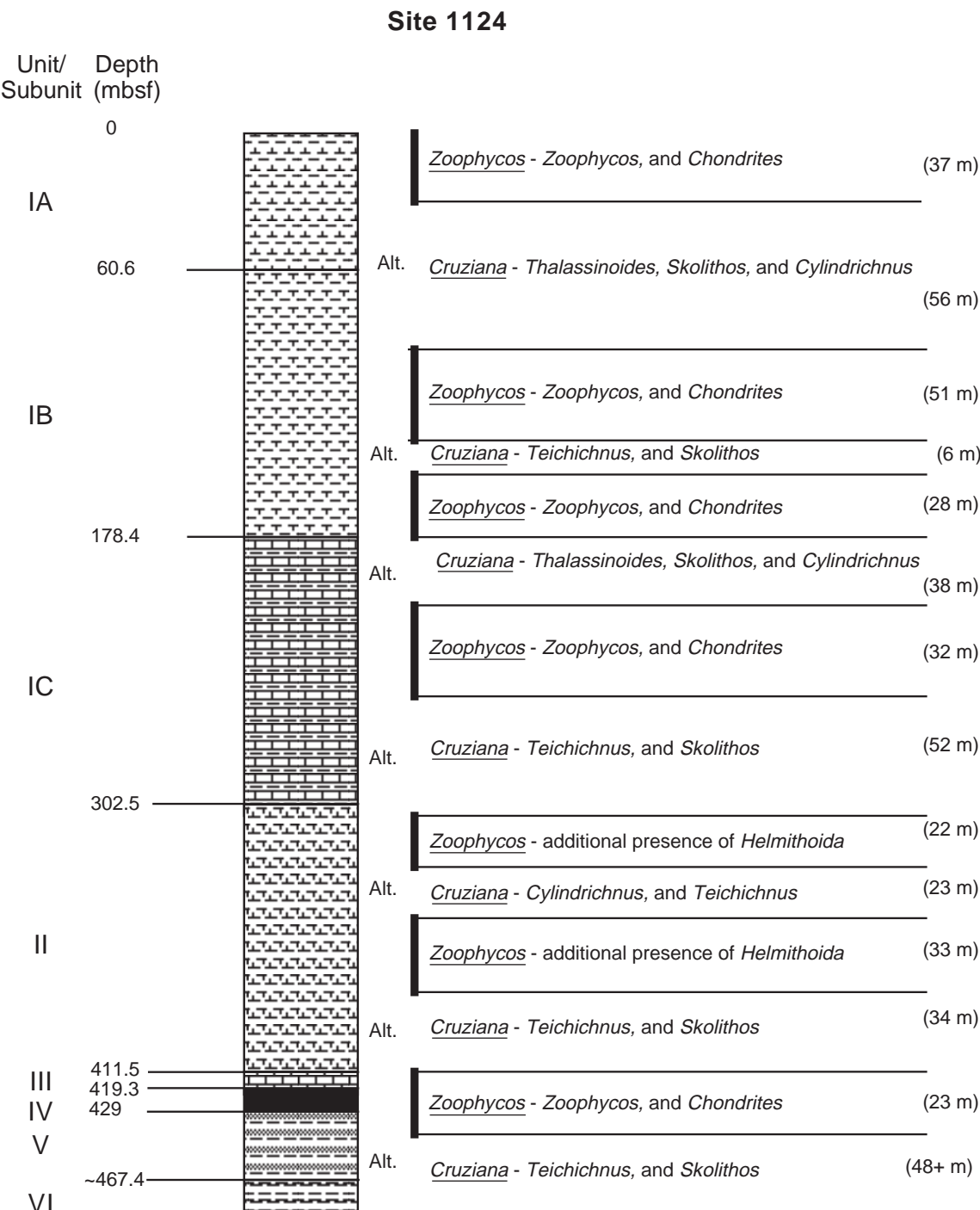


Figure F7. Downcore profiles of color reflectance with (left) the 700/400-nm ratio, which is essentially the red/blue ratio and (right) 550-nm band, which is a proxy for  $\text{CaCO}_3$ .



**Figure F8.** Downcore distribution of *Zoophycos* and *Cruziana* ichnofacies (underlined). Ichnofacies are alternating sequences of *Zoophycos* and a higher frequency of *Cruziana/Zoophycos* alternations (Alt.).



\* Note *Planolites* and *Palaeophycus* are ubiquitous throughout both ichnofacies.

**Figure F9.** Distribution of rhyolitic tephra in cyclic, color-banded sediment of early Pleistocene age in Sub-unit IA Core 181-1124C-5H (46.2–55.89 mbsf).

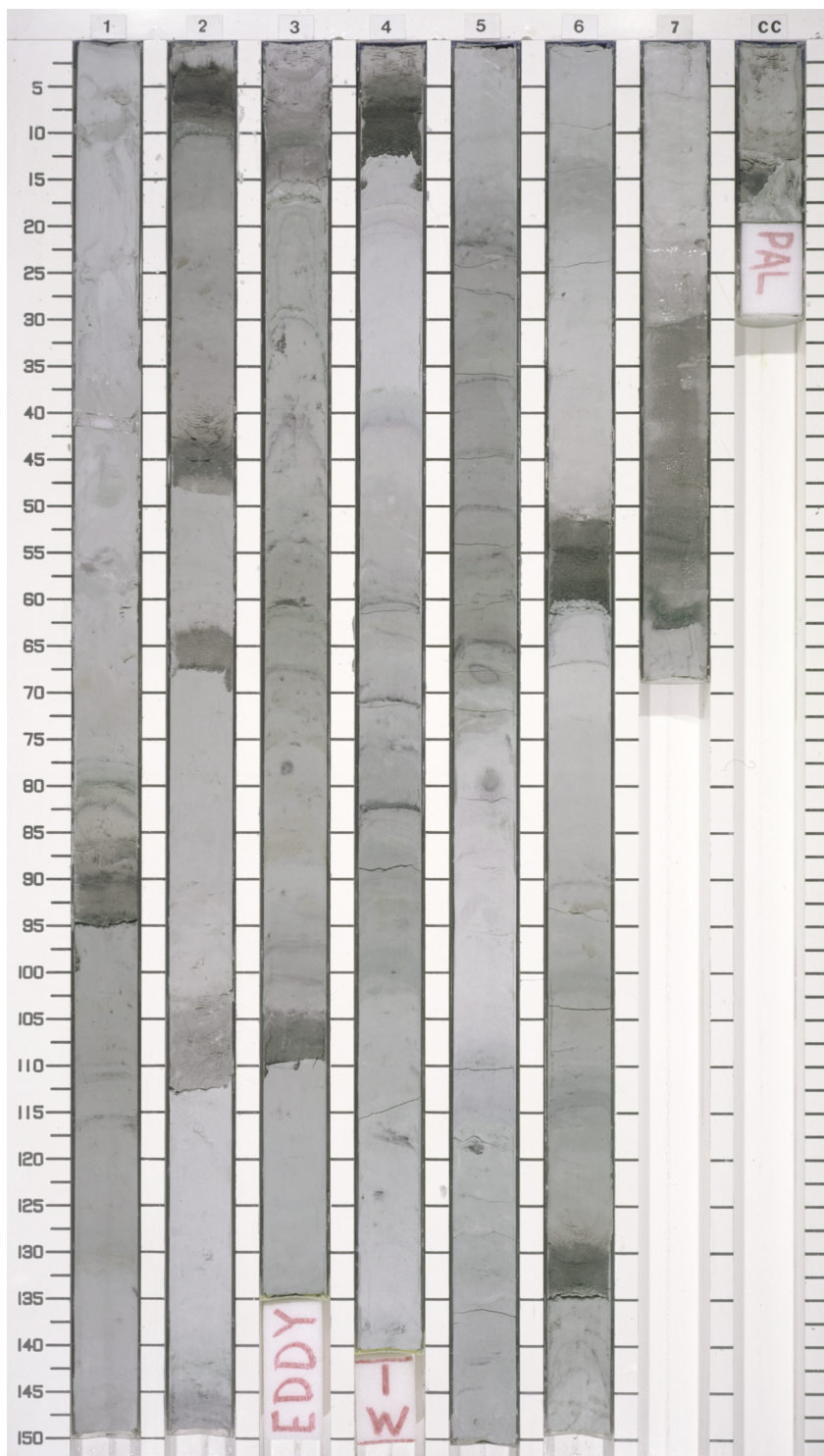


**Figure F10.** Typical tephra layer with sharp base, normal grading, and faintly bioturbated top, upper Sub-unit IB (interval 181-1124C-7H-3, 105–125 cm; 69.25–69.45 mbsf).

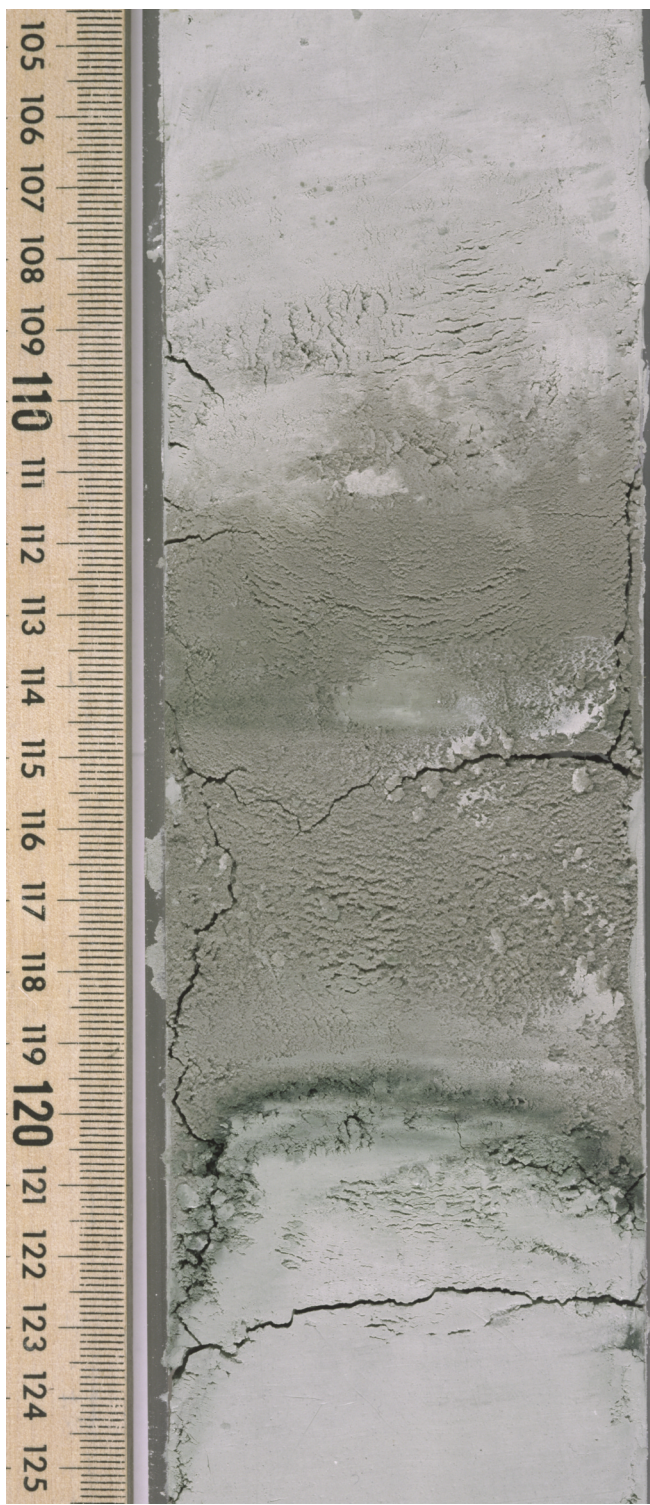
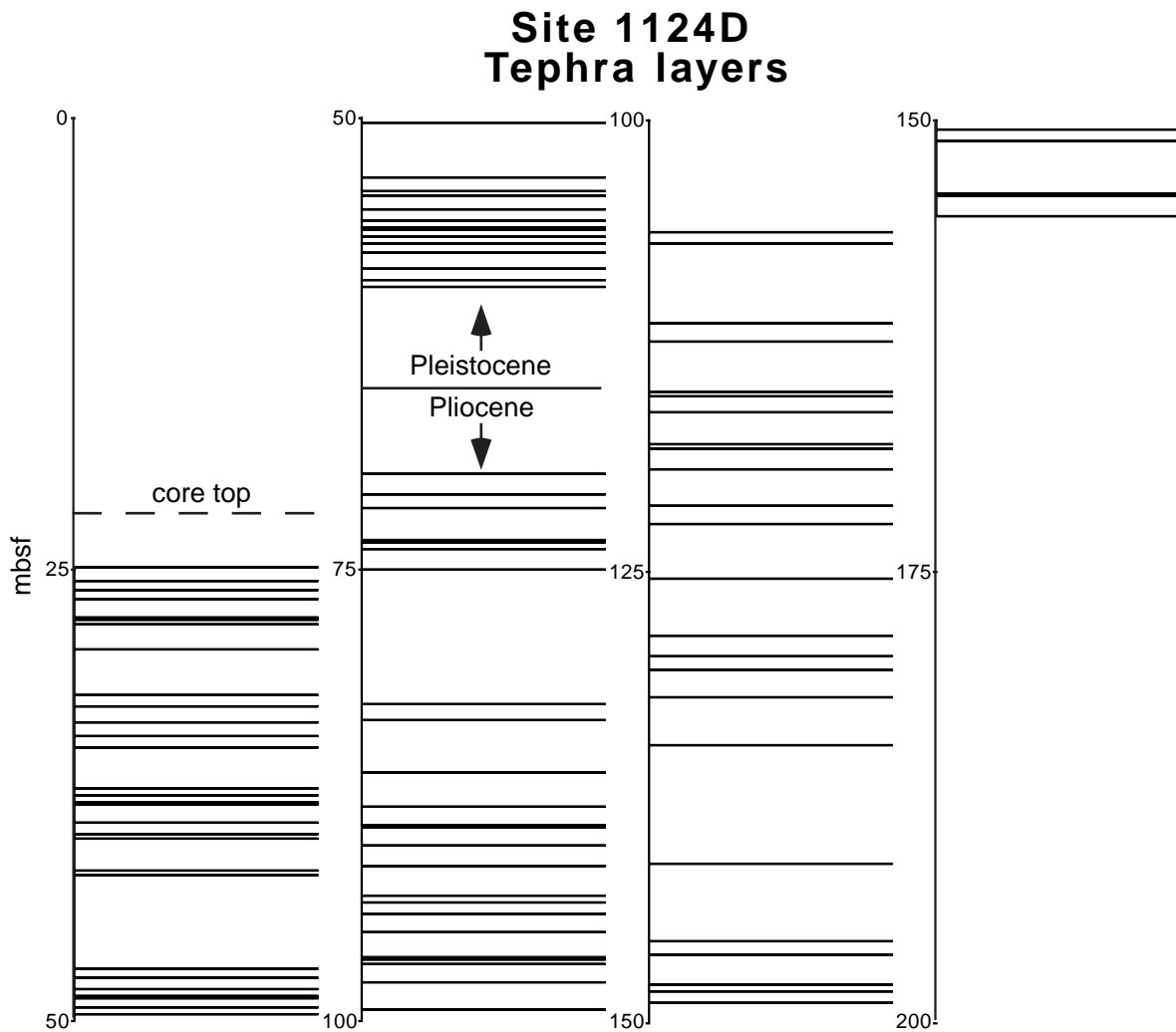
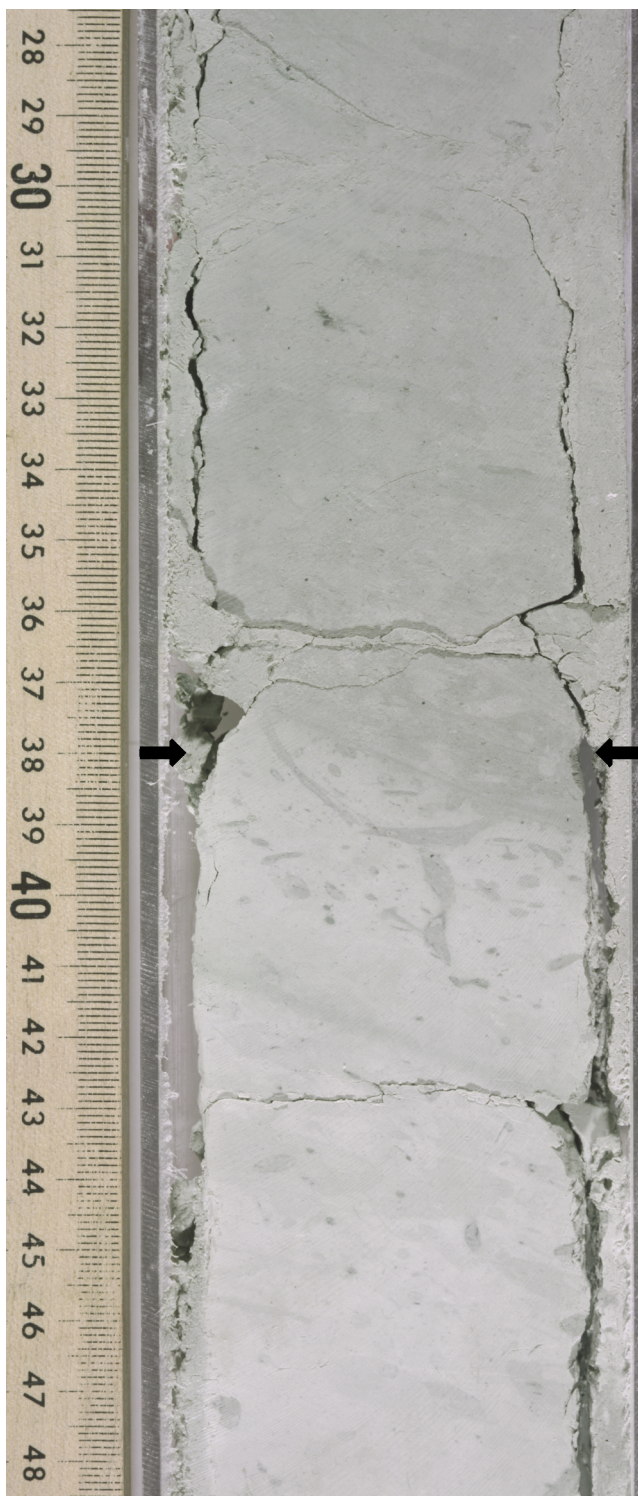


Figure F11. Distribution of macroscopic tephra layers in Hole 1124D, highlighting the grouping of eruptions through the Pliocene–Pleistocene. Top of hole is at 22.6 mbsf, above which tephras from Holes 1124A, 1124B, and 1124C have not been inserted.



**Figure F12.** The Marshall Paraconformity (38 cm), marked by the burrowed surface between basal Unit II Miocene (27 Ma) nannofossil-bearing mudstone and the top of Unit III late Oligocene (33 Ma) nannofossil chalk (interval 181-1124C-43X-2, 28–48 cm; 411.48–411.68 mbsf).



**Figure F13.** Dark green, flaser-like laminae in Unit II, suggesting the presence of sediment-moving bottom currents (interval 181-1124C-37X-2, 20–40 cm; 353.60–353.80 mbsf).

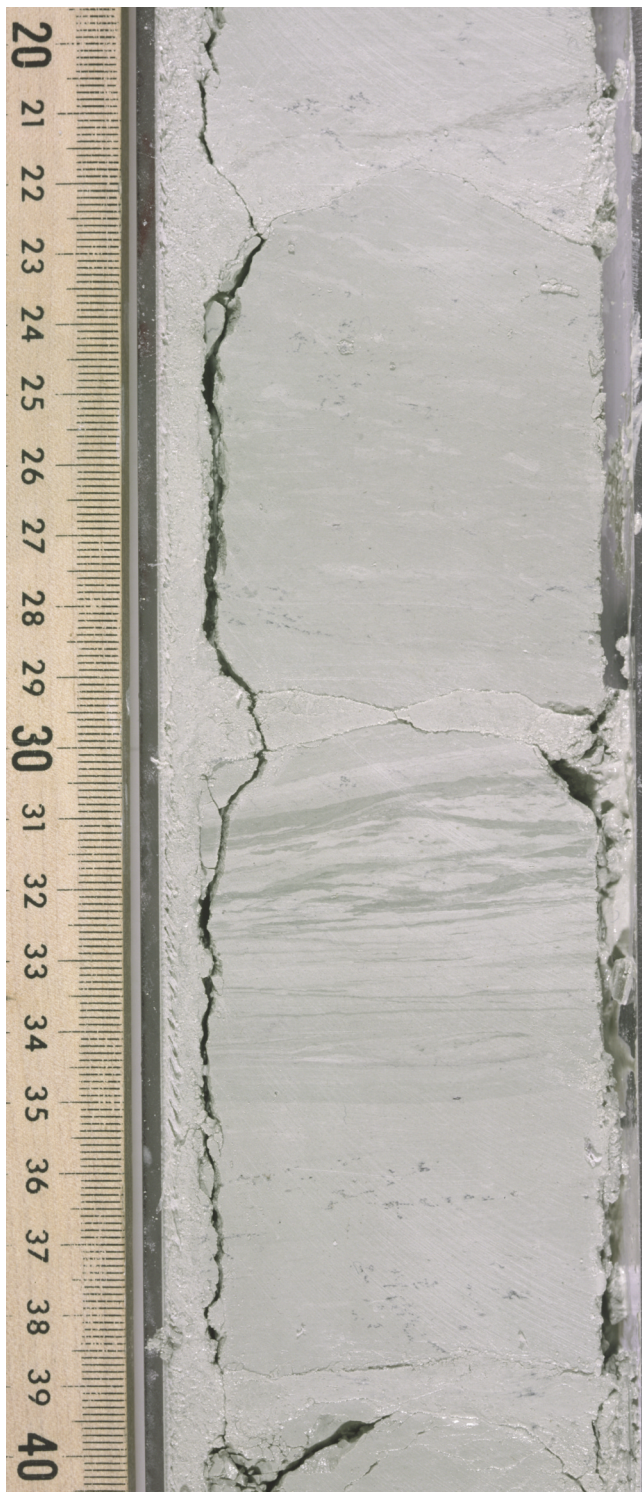


**Figure F14.** Well-developed *Zoophycos* trace fossils belonging to the ichnofacies with the same name, lower Unit II (interval 181-1124C-39X-4, 20–45 cm; 375.90–376.15 mbsf).

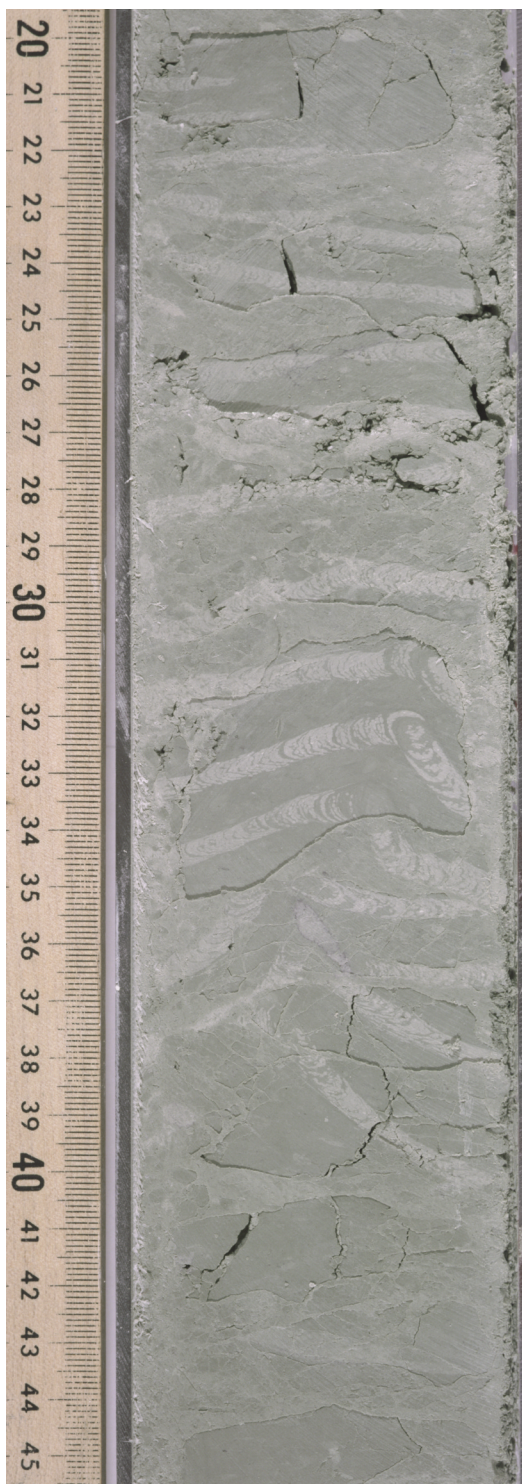


Figure F15. Biostratigraphic summary chart of Site 1124.

### Hole 1124C PLANKTON BIOCHRONOSTRATIGRAPHY

EPOCH	DEPTH (mbsf)	CORE 1124C	NANNOFOSSILS AGE ZONE	FORAMINIFERS AGE NZ STAGE	DIATOM AGE DATUM	RADIOLARIANS AGE DATUM	LITHO-STRAT	
Pleistocene	0 - 400 mbsf	2	0.42 NN20	Wc Wn Wm Wp Wo late Tt Sw-eTt Sc-SI Po-ePI Lw-Po Ld-e Lw	0.65 <i>N. reinholdii</i> 0.7 <i>N. fossilis</i> 1.25 <i>N. barronii</i>  7.7 <i>N. fossilis</i>  poor preservation	good faunas sporadic barren  RN1 RP22	Unit I	
		4	1.2 NN19					
		6	1.66 NN18					
		8	1.96 NN17					
		10	2.3 NN16					
		12	2.6 NN15					
		14	3.82					
		16	7.73					
		18	9.34					
		20	10.8 NN8					
late Pliocene		25	13.5 NN6					
		28	16.2					
		30	<19.6					
		35	~23					
		38	23.7					
e. Pliocene		40	24.3					
		41	24.7					
		42	<27.9					
		43	NP24					
		44	33 NP21-22	34-32 e Lwh		very rare	Unit III	
late Miocene		38	NP17-18	38-36 Ab-e Ak			Unit IV	
		45	>58.3	60 NP3-5 63 NP1-3	Dt poor preservation	64.5 65 RP1 late Cret	Unit V	
		46						
		47	64.8					
		48						
mid Miocene		49	>65	CC25-26	Mh		Unit VI	
		50						
		51						
		52						
		53						
early Miocene		54						
		55						
		56						
		57						
		58						
late Oligocene		59						
		60						
		61						
		62						
		63						
e. Oligo. m.-l. Eocene		64						
		65						
		66						
		67						
		68						
l. Paleocene		69						
		70						
		71						
		72						
		73						
early Paleocene		74						
		75						
		76						
		77						
		78						
L. Cretaceous		79						
		80						
		81						
		82						
		83						

**Figure F16.** Biostratigraphic summary chart for the Paleogene and Late Cretaceous lower part of Site 1124. See “[Late Cretaceous](#),” p. 19, for explanation of New Zealand stages.

## HOLE 1124C CRETACEOUS-PALEOGENE BIOSTRATIGRAPHY

Figure F17. Age-depth relationships at Site 1124, based upon nannofossil datums.

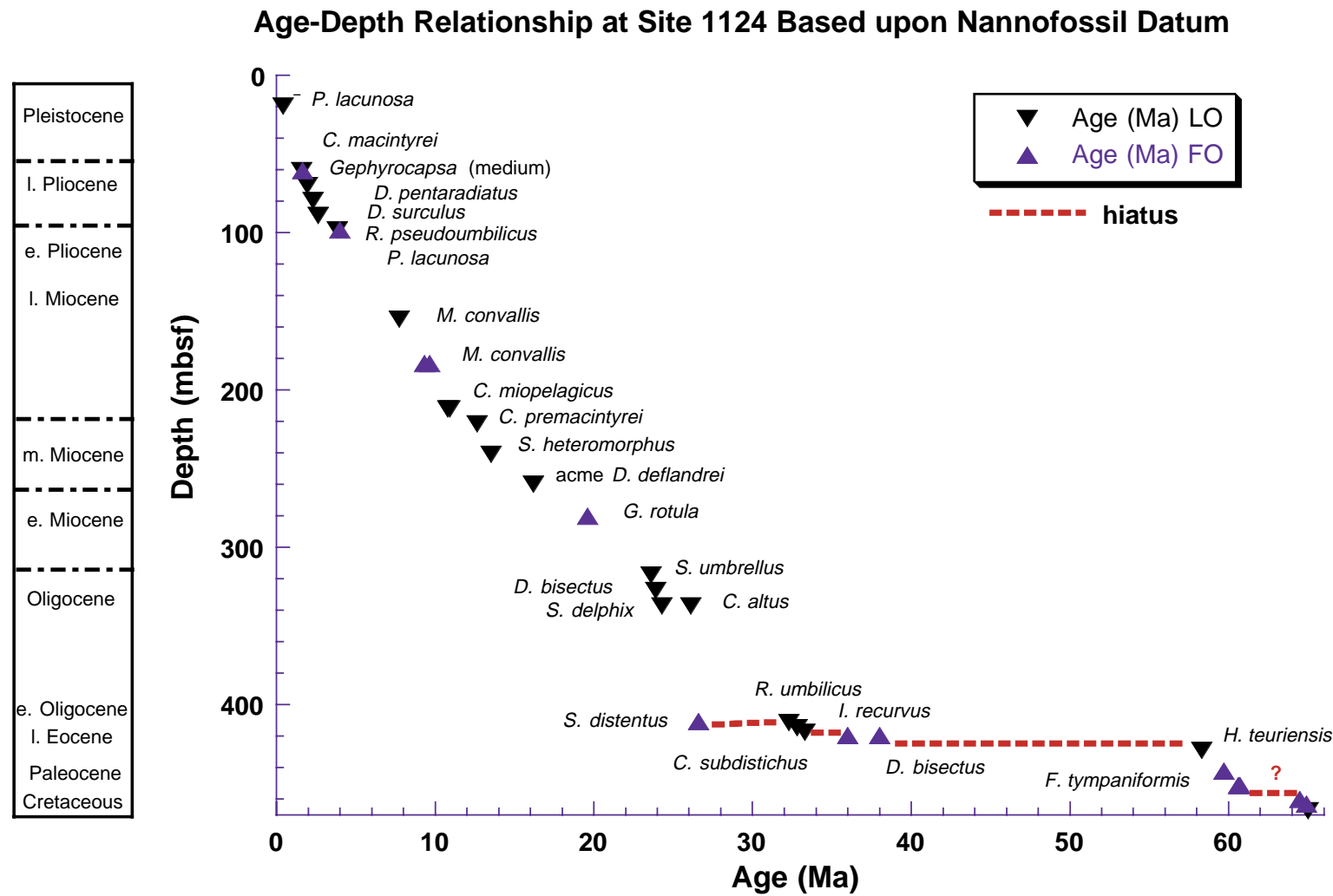


**Figure F18.** Whole-core magnetic susceptibility from the Bartington loop of the shipboard automated multisensor track and archive-half continuous measurement of NRM intensity from the pass-through cryogenic magnetometer for core from Hole 1124C. Vertical and subvertical lines at 10–20, 278–295, 445–448, and 463–470 mbsf indicate intervals where measurement was not possible because of poor core recovery or non-recovery.

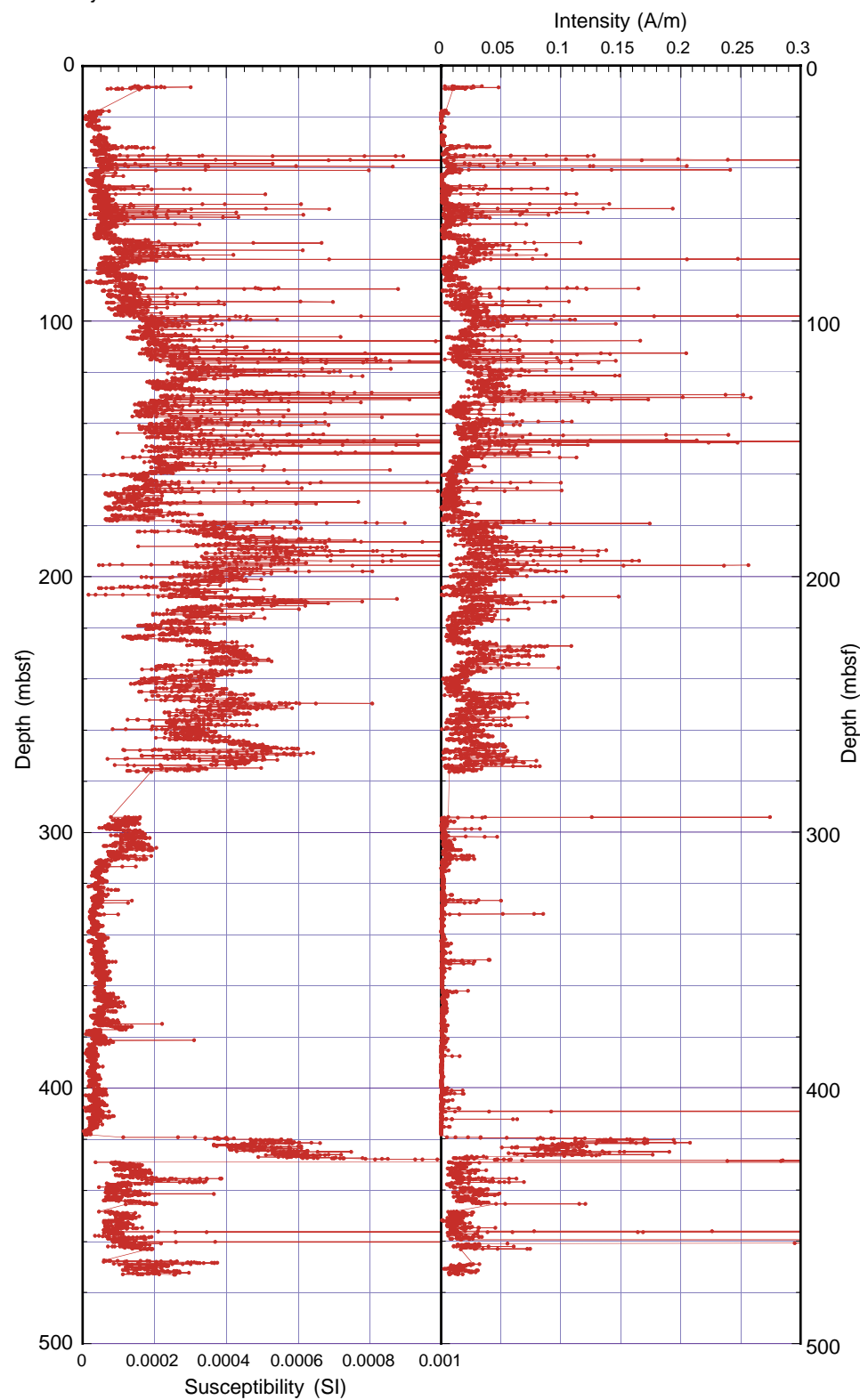


**Figure F19.** A–C. Composite magnetostratigraphic record from Site 1124. Depth scale is in meters composite depth (mcd) for the upper 170 mcd from correlation between Holes 1124C and 1124D using magnetic susceptibility and reflectance data in combination (see “[Composite Depths](#),” p. 27) and meters below sea-floor for 150–280 mbsf and 280–475 mbsf from Hole 1124C only. The inclination record is after a single demagnetization step of 20 mT for 0–175 mbsf/mcd and 290–475 mbsf, and an additional 80 mT step for the interval between 175 and 277 mbsf. Black (white) represents normal (reversed) polarity and hatching defines intervals where polarity could not be determined from the inclination record. Chron ages for polarity reversal datums are from Berggren et al. (1995). Arrowheads represent core-catcher depths for fossil datums and length of arrow represents possible error as a result of sampling intervals being confined to core-catcher samples (error bars extend up for last occurrences and down for first occurrences). Single occurrences and acme events have error bars extending to the core-catcher interval above and below. ([Figure shown on next three pages](#).)

Figure F19 (Caption on previous page.)

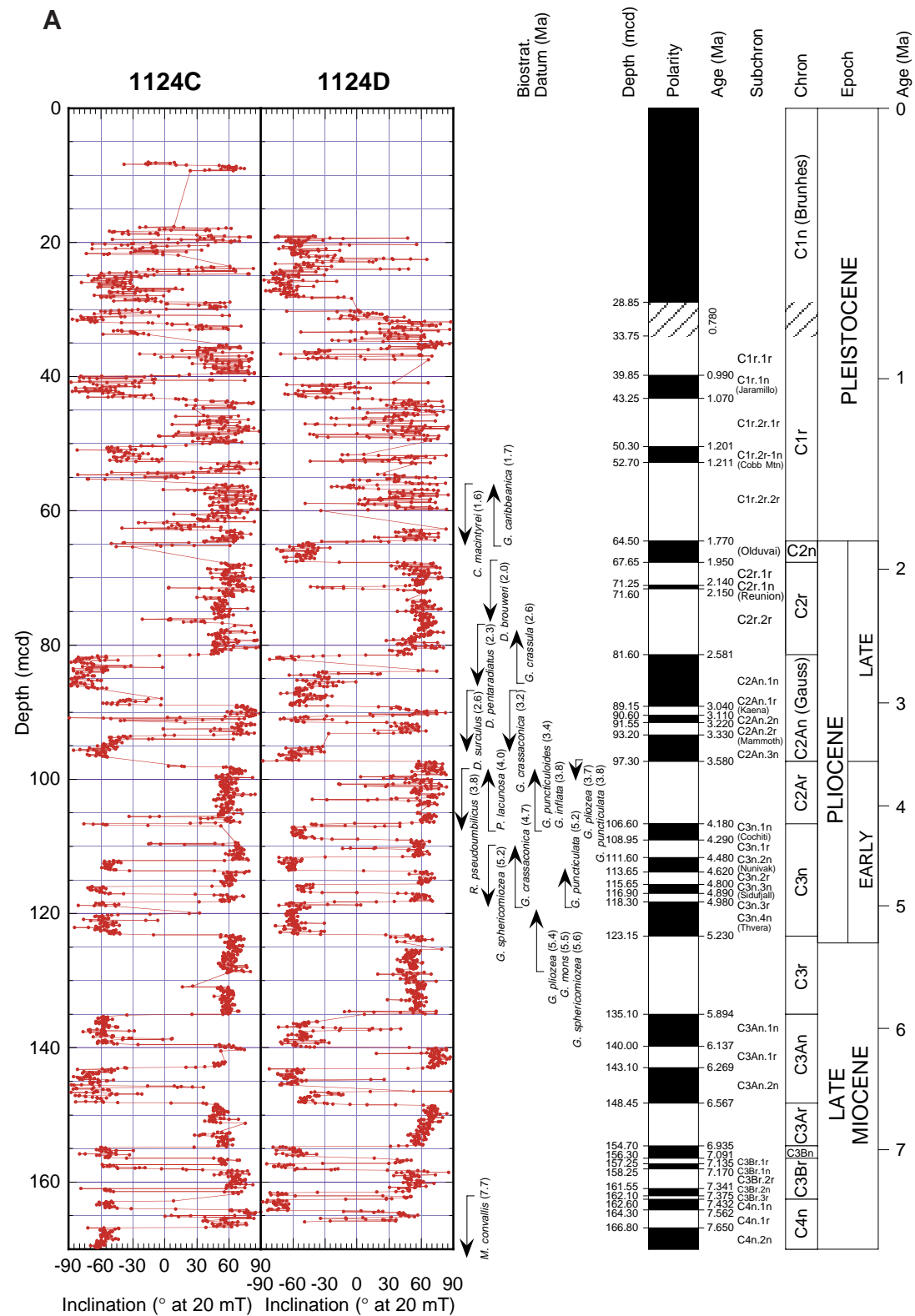
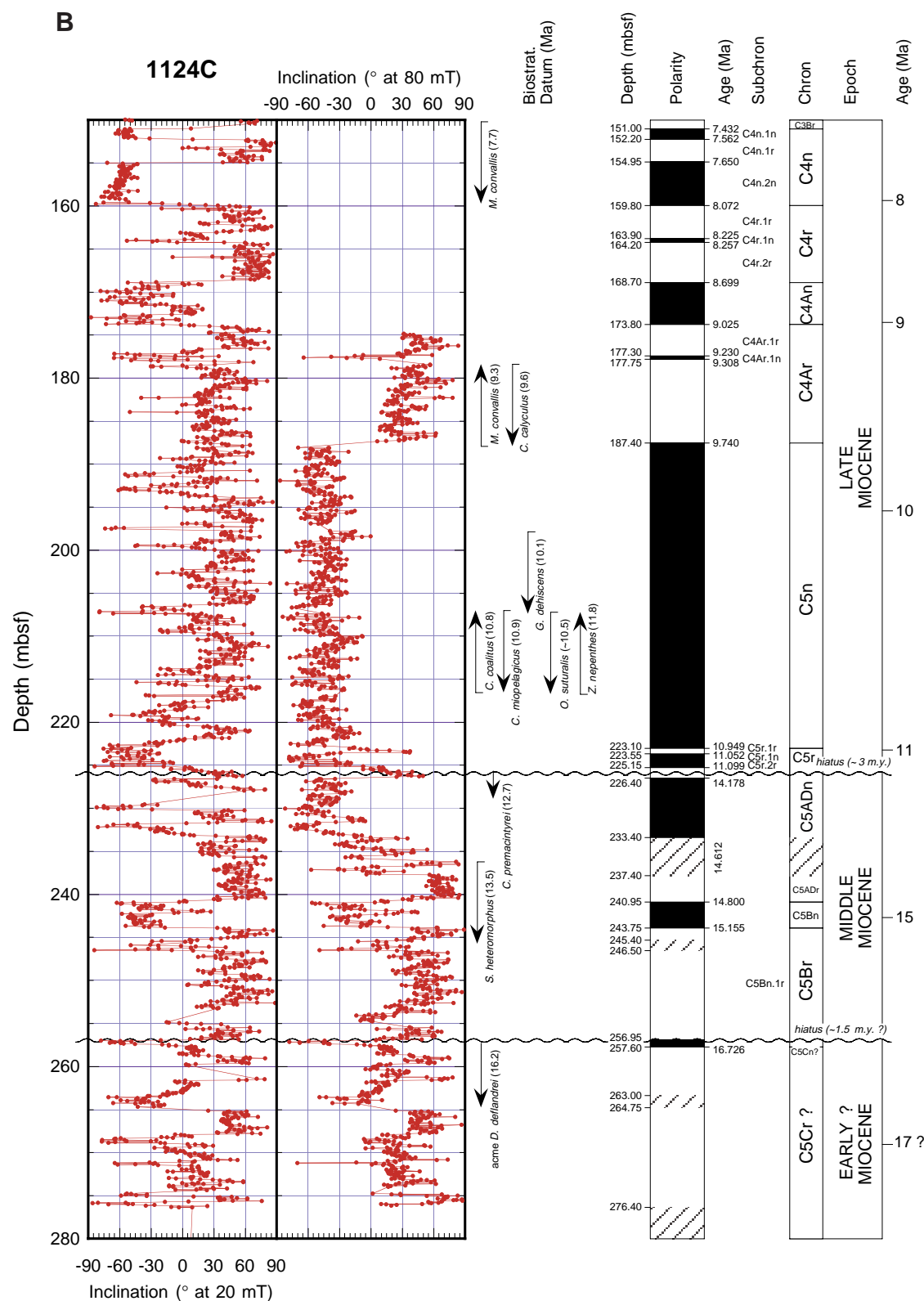
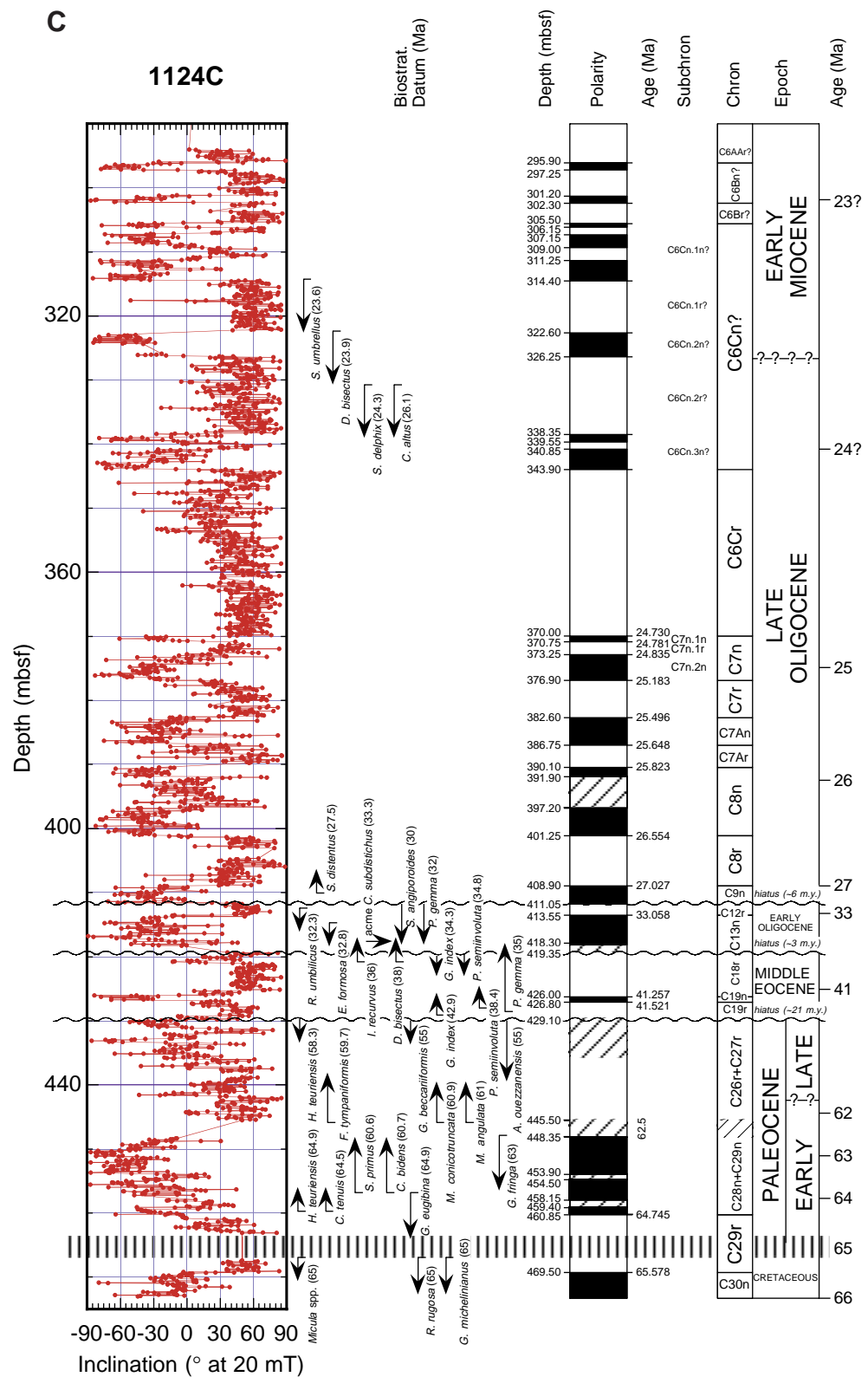


Figure F19 (continued).



**Figure F19 (continued).**



**Figure F20.** Age model and correlation of the composite magnetic polarity record for Site 1124. Magnetic polarity interpretations are given in Figure F19, p. 62, and individual reversal ages are from Berggren et al. (1995). Solid black line shows line of correlation. Undulating line indicates a hiatus. Lithostratigraphic summary is from “[Lithostratigraphy](#),” p. 3. The 0–200 mcd interval is enlarged in Figure F21, p. 67. The main features are discussed in the text.

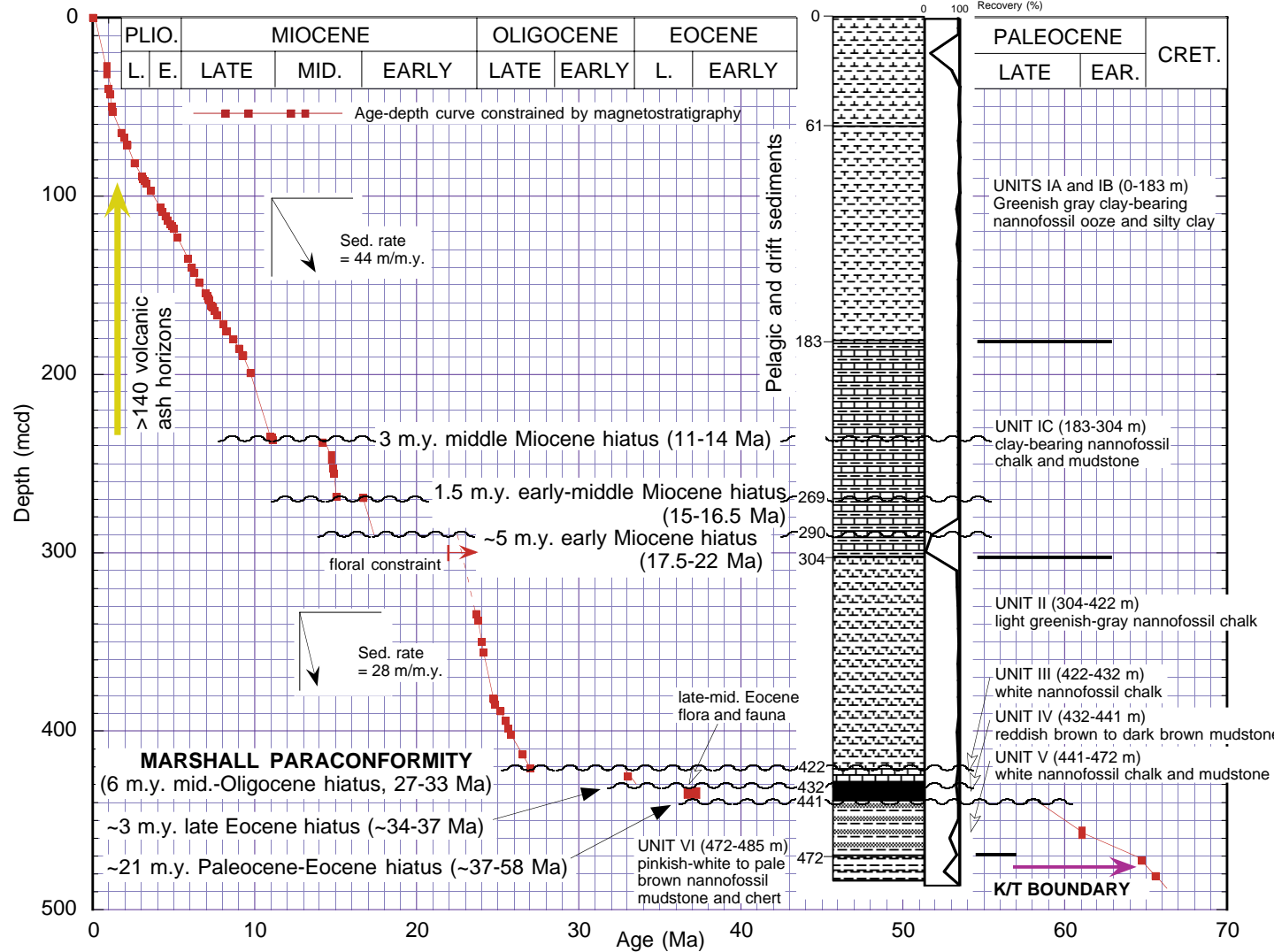


**Figure F21.** Age model and correlation of the composite magnetic polarity record for the upper 200 mcd of Site 1124. Magnetic polarity interpretations are given in Figure F19, p. 62, and individual reversal ages are from Berggren et al. (1995). Solid black line shows line of correlation. Ages of the tephra horizons are assigned from the age-depth model. The main features are discussed in the text.

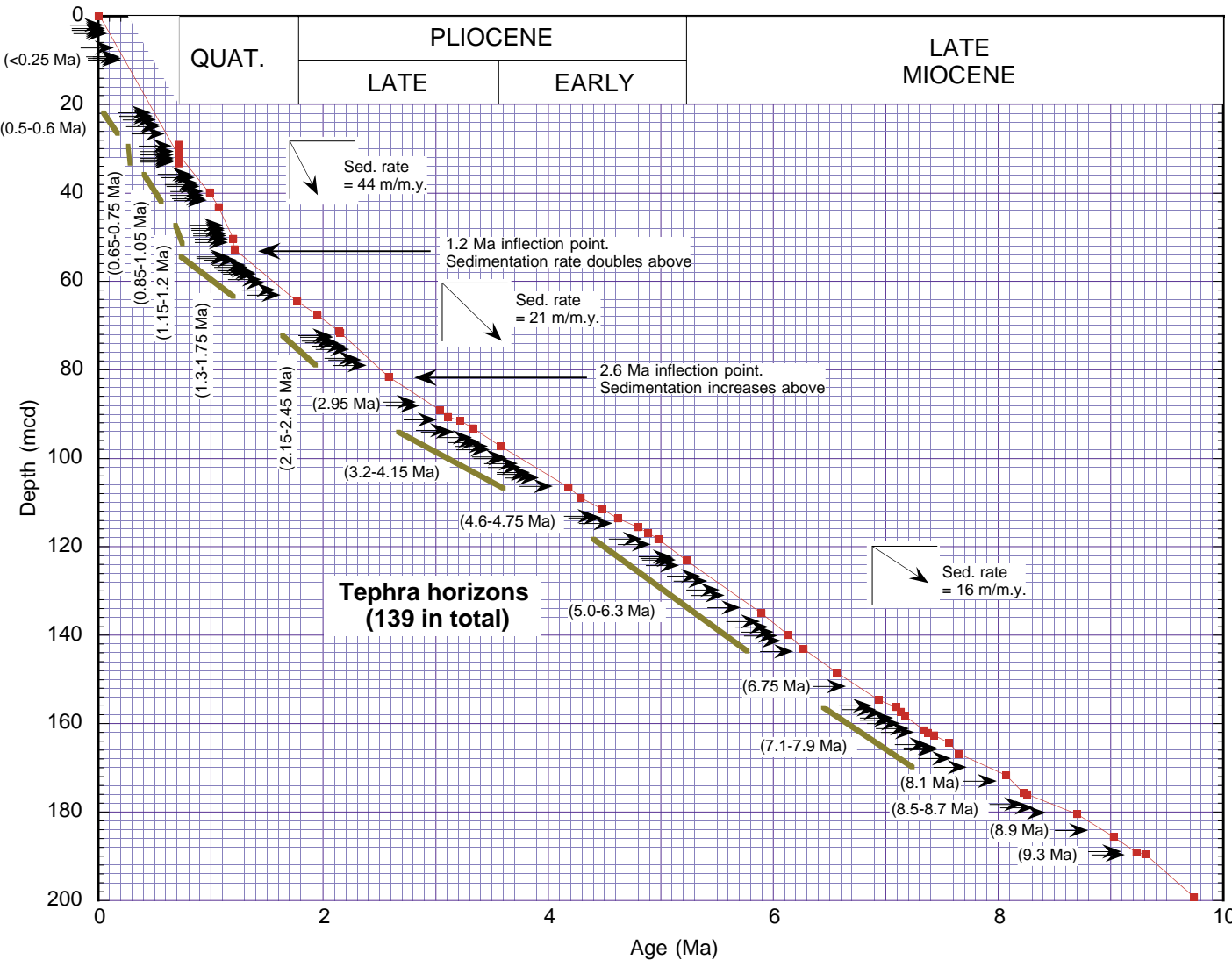


**Figure F22.** Composite sections for magnetic susceptibility, reflectance percentage at 550 nm, and GRAPE density. For convenience, MS values from Holes 1124B, and 1124D are offset by  $20 \times 10^{-5}$  relative to data from Holes 1124A and 1124C, respectively. Similarly, reflectance values are offset by 25% and GRAPE density values by  $0.2 \text{ g/cm}^3$ . Cores are indicated by small numbers. Data from disturbed intervals (typically "soupy" sediment at core tops and flow-in) have been removed. (Continued on next two pages.)

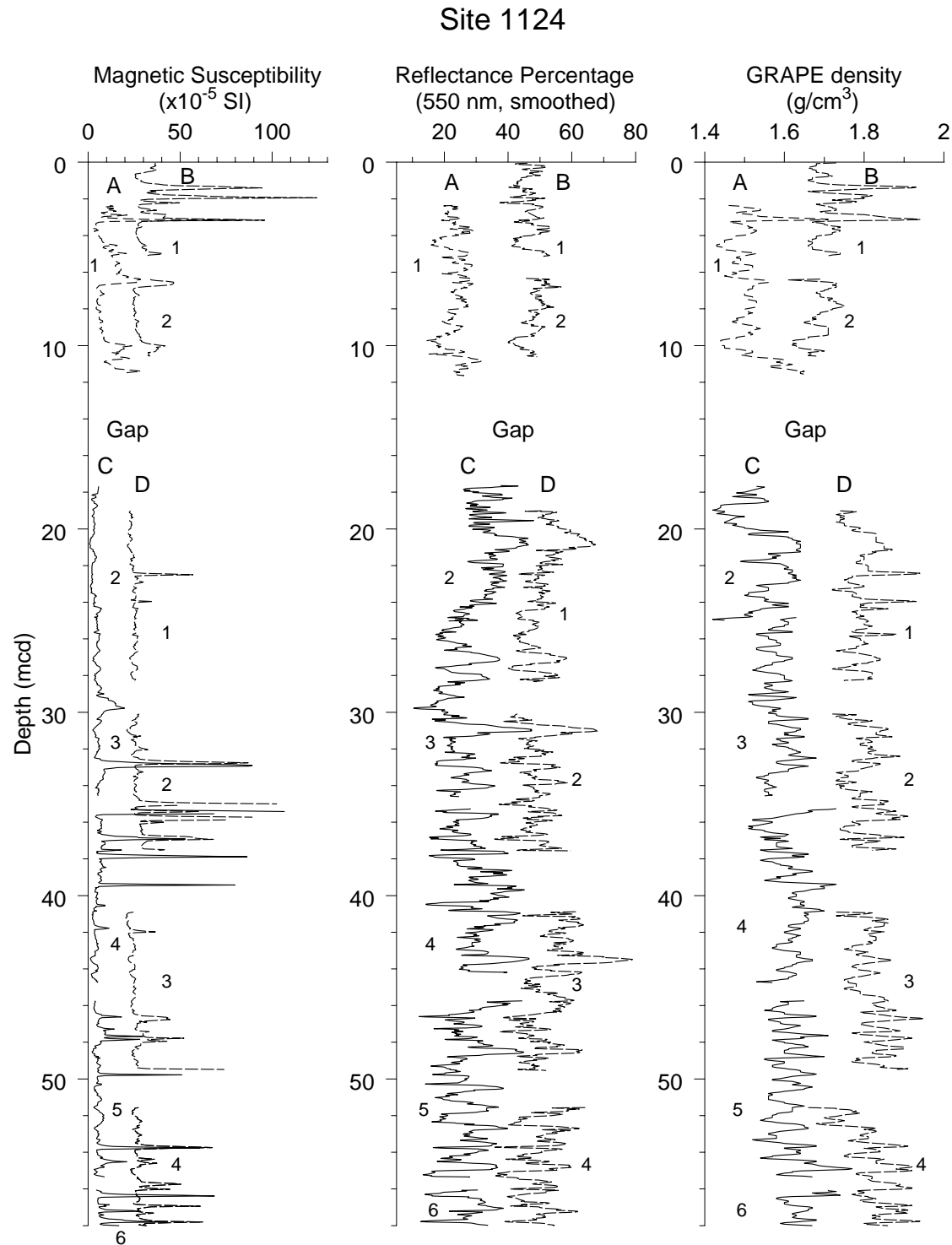


Figure F22 (continued).

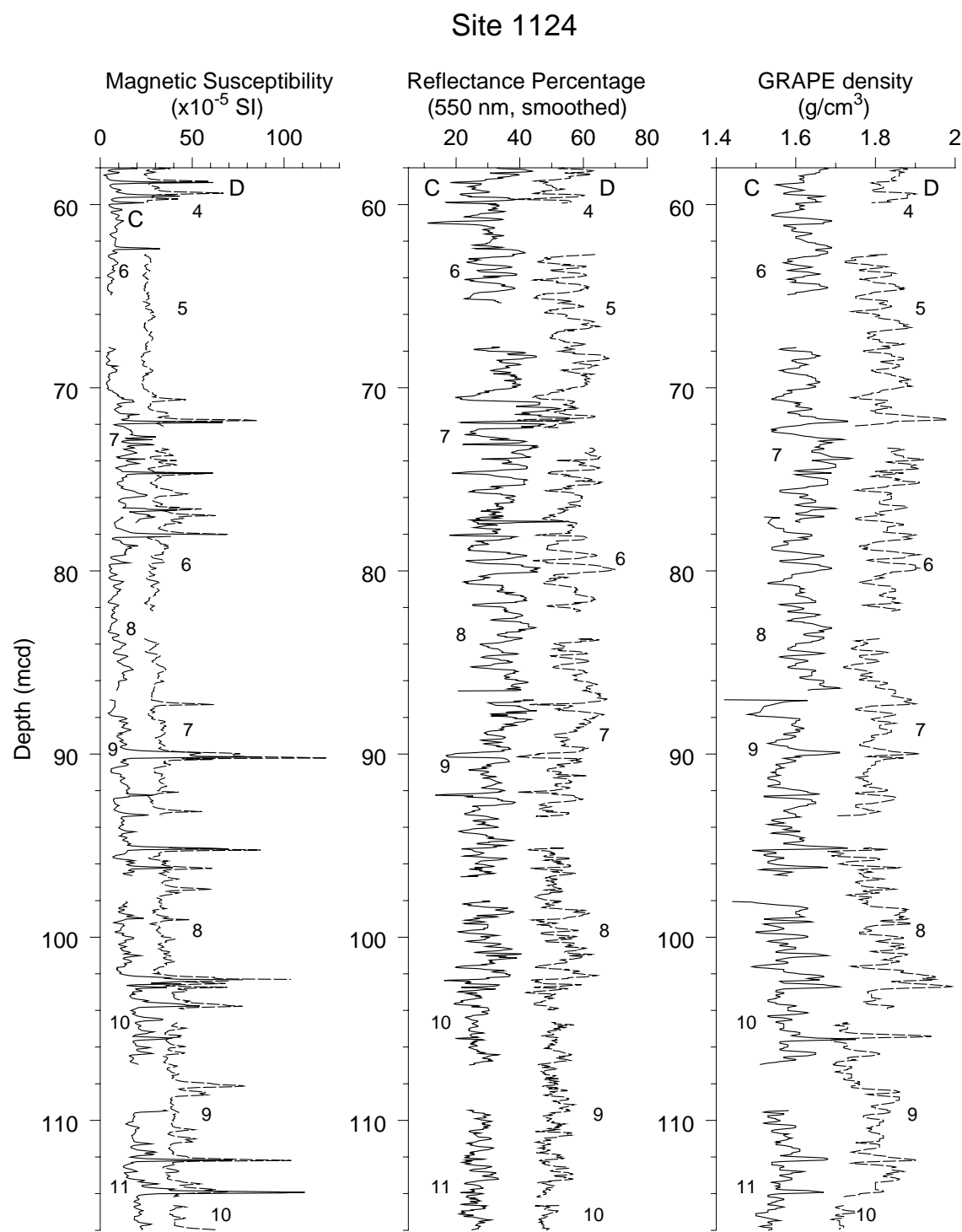
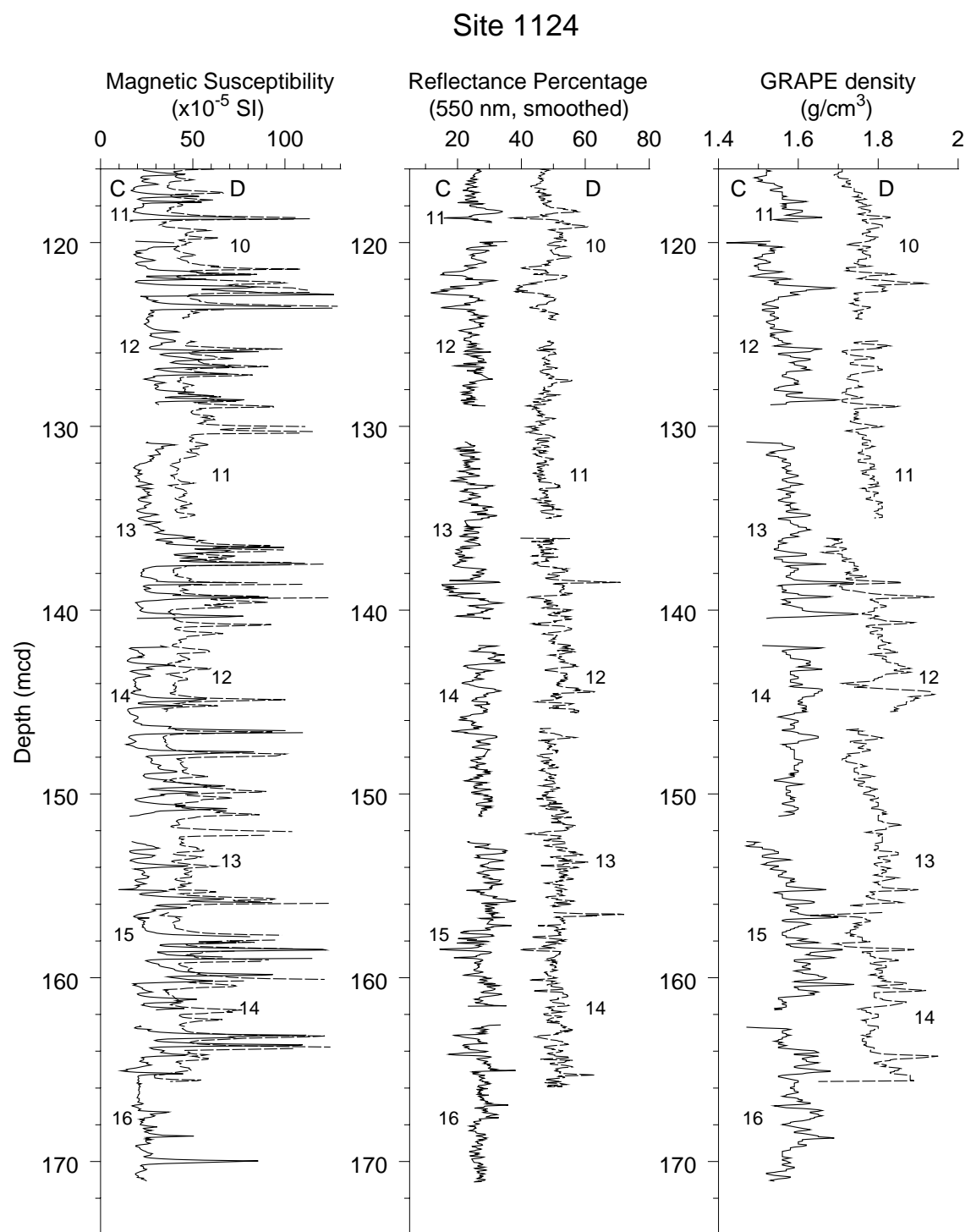
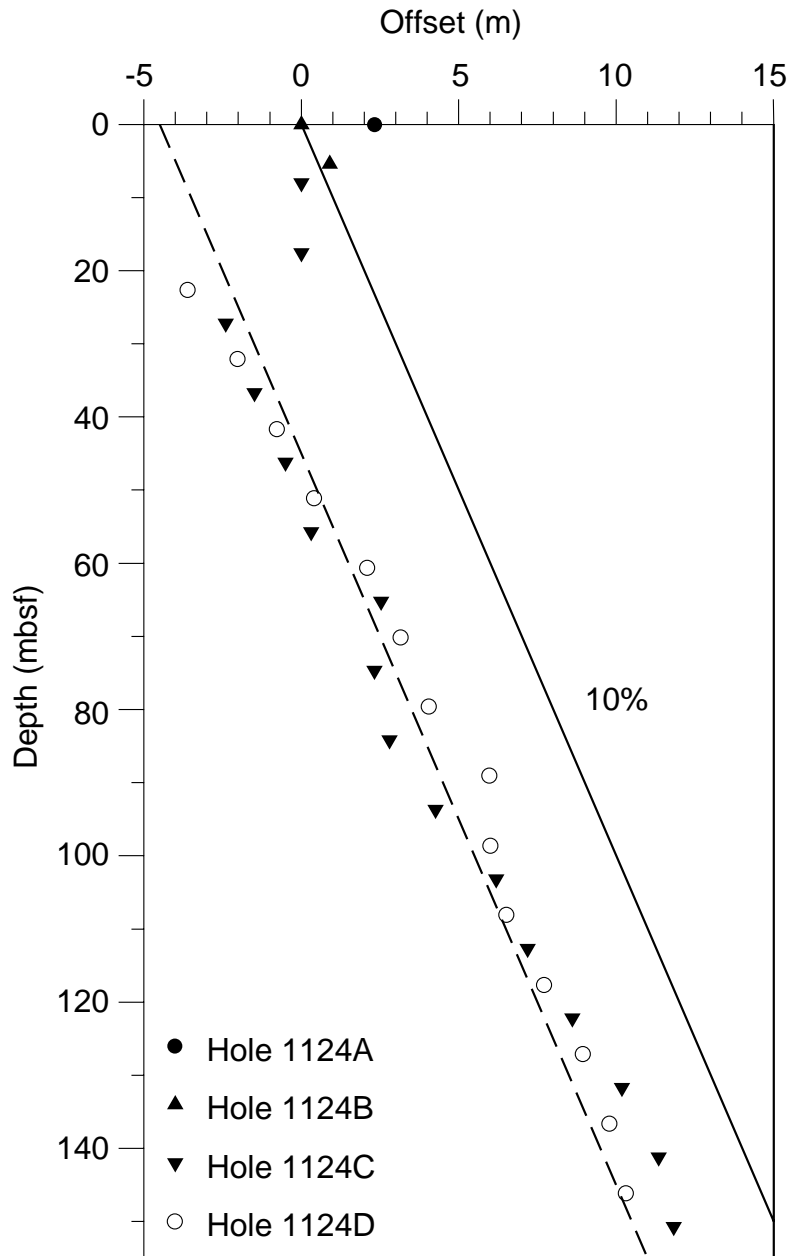


Figure F22 (continued).



**Figure F23.** Downhole depth offsets between the mbsf and mcd scales for Site 1124. The solid line indicates the trend for a typical 10% stretch model between mbsf and mcd depths; the dashed line parallels this trend. Composite depth offsets below ~20 mbsf parallel the 10% stretch model.



**Figure F24.** Spliced record for Site 1124. To reduce noise, all data illustrated were smoothed with a 5-point Gaussian window. Spliced data intervals: B1 = Core 181-1124B-1H, C2 = Core 181-1124C-2H, and so on. (Continued on next page.)

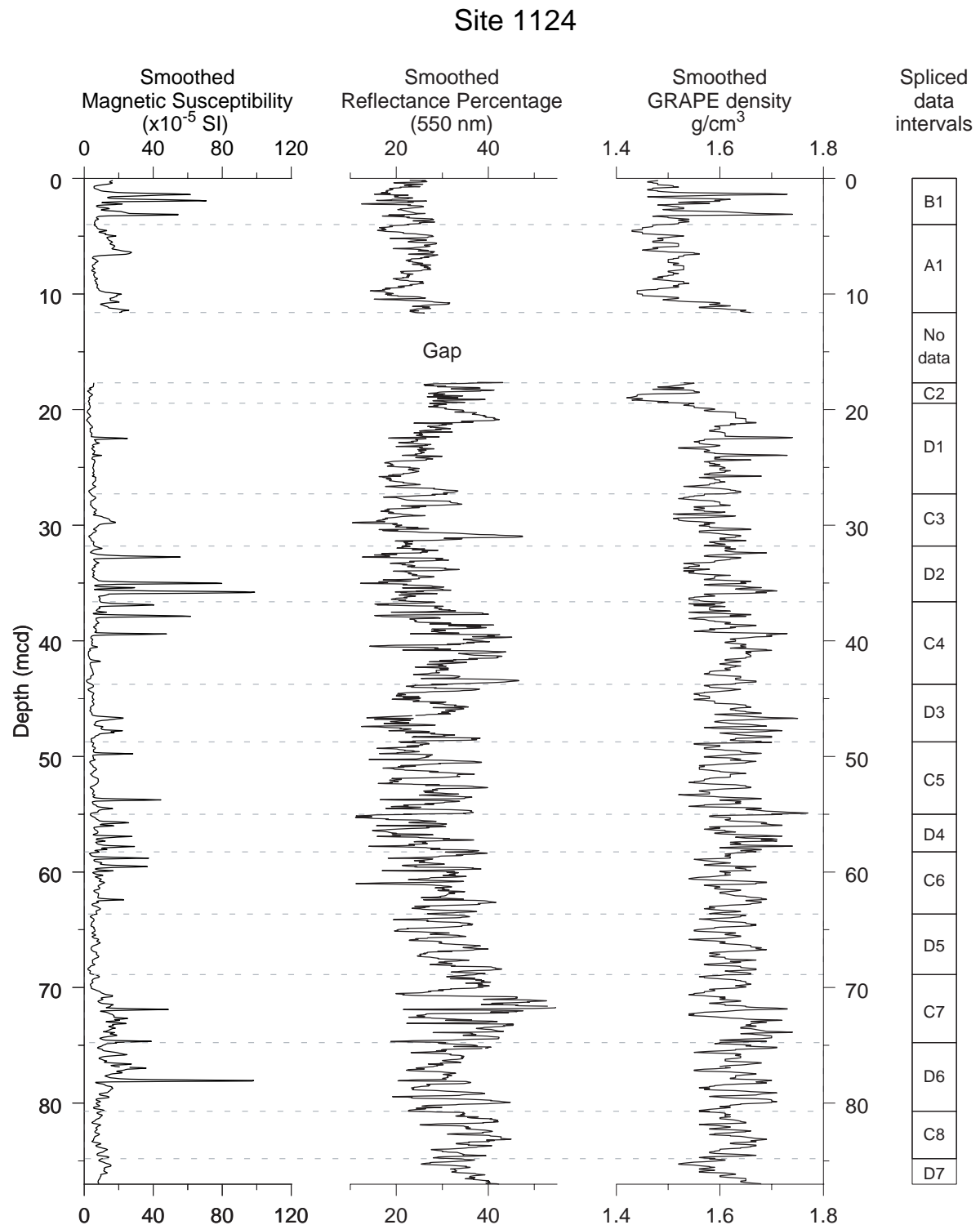
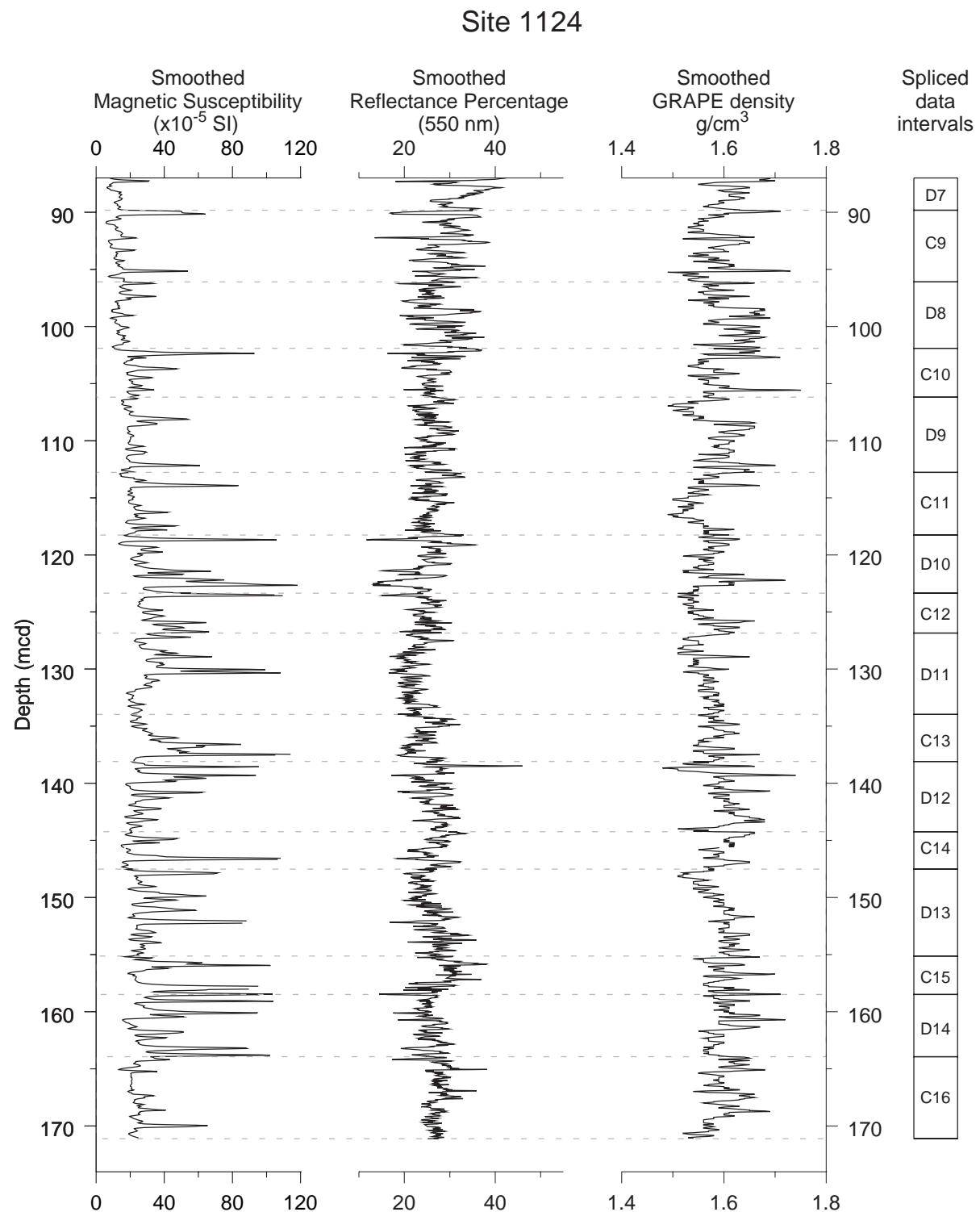


Figure F24 (continued).



**Figure F25.** Age-depth plot, using the diatom, radiolarian, foraminifer, and nannofossil age assignments for Site 1124, as shown in Table T14, p. 130. Because of the size of the plot, strongly or fully overlapping event positions may be obscured in the graph. All depths are reported in mcd values. The plot of events is tightly clustered and shows fairly good coherence. Solid line indicates the paleomagnetic age model from “[Paleomagnetism](#),” p. 26, in the “Site 1123” chapter.

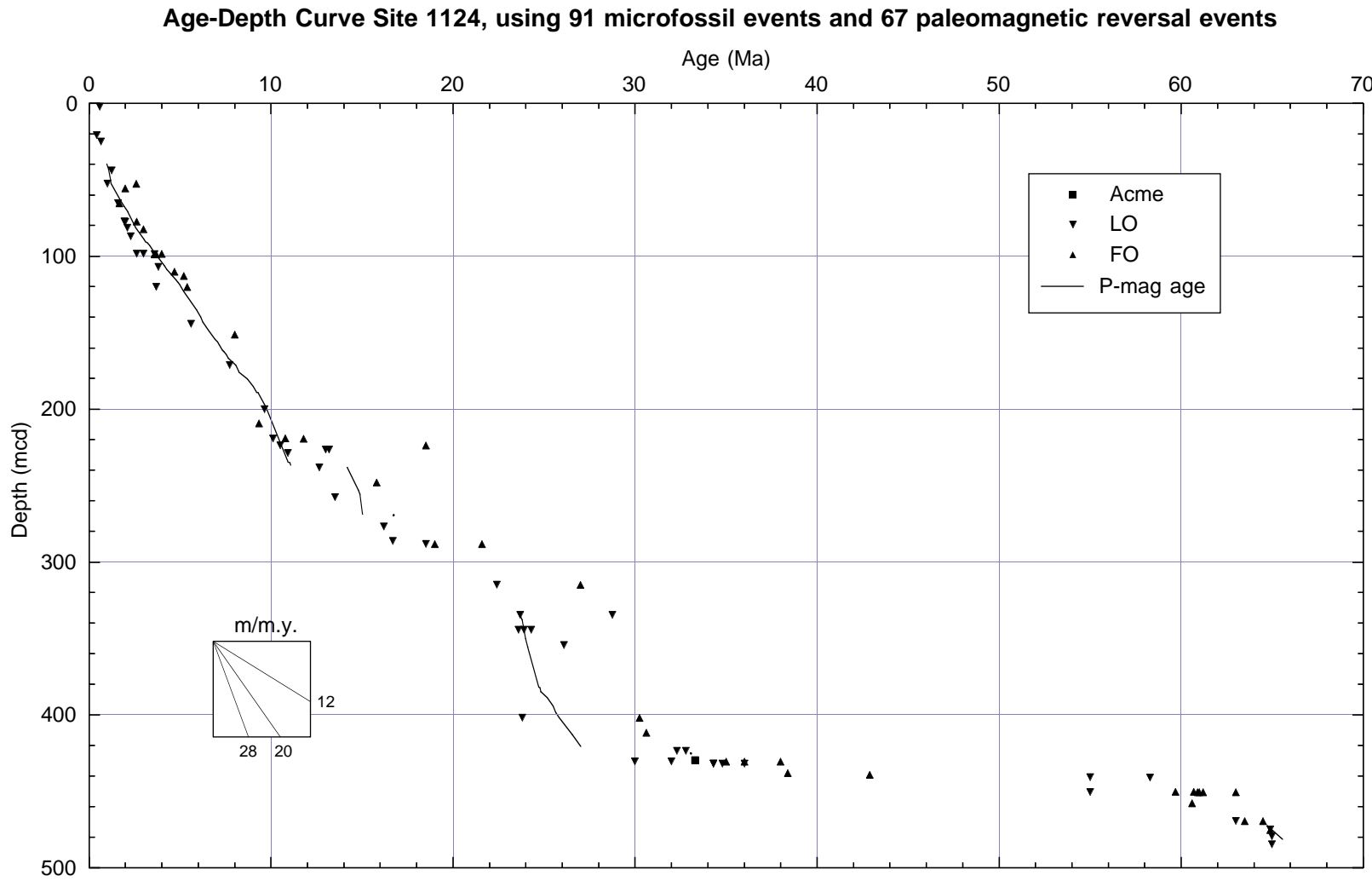


Figure F26. Depth profiles of interstitial-water constituents at Site 1124.

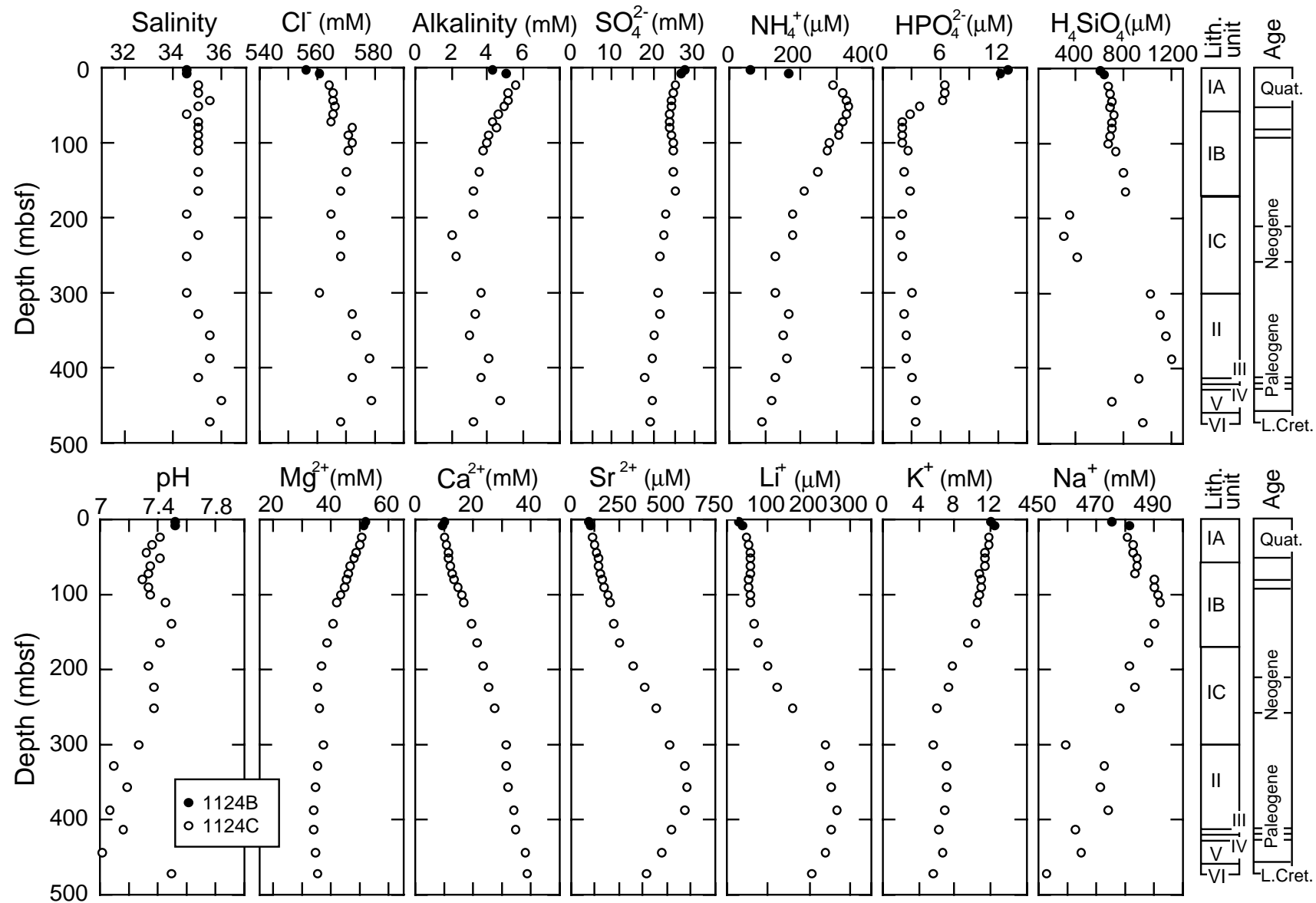


Figure F27. Carbonate contents in sediments from Holes 1124A, 1124B, and 1124C.

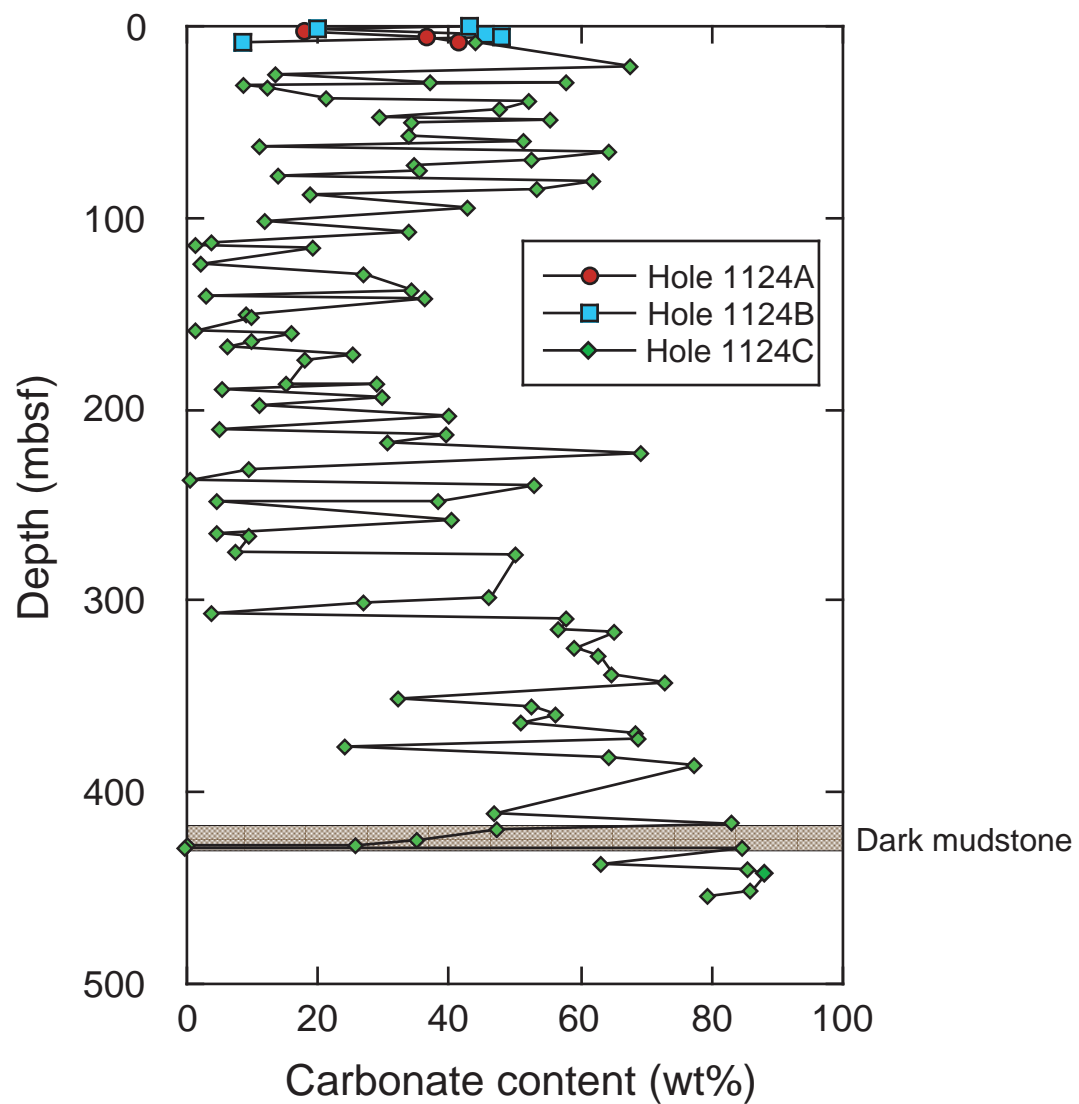


Figure F28. Organic carbon contents in sediments from Holes 1124A, 1124B, and 1124C.

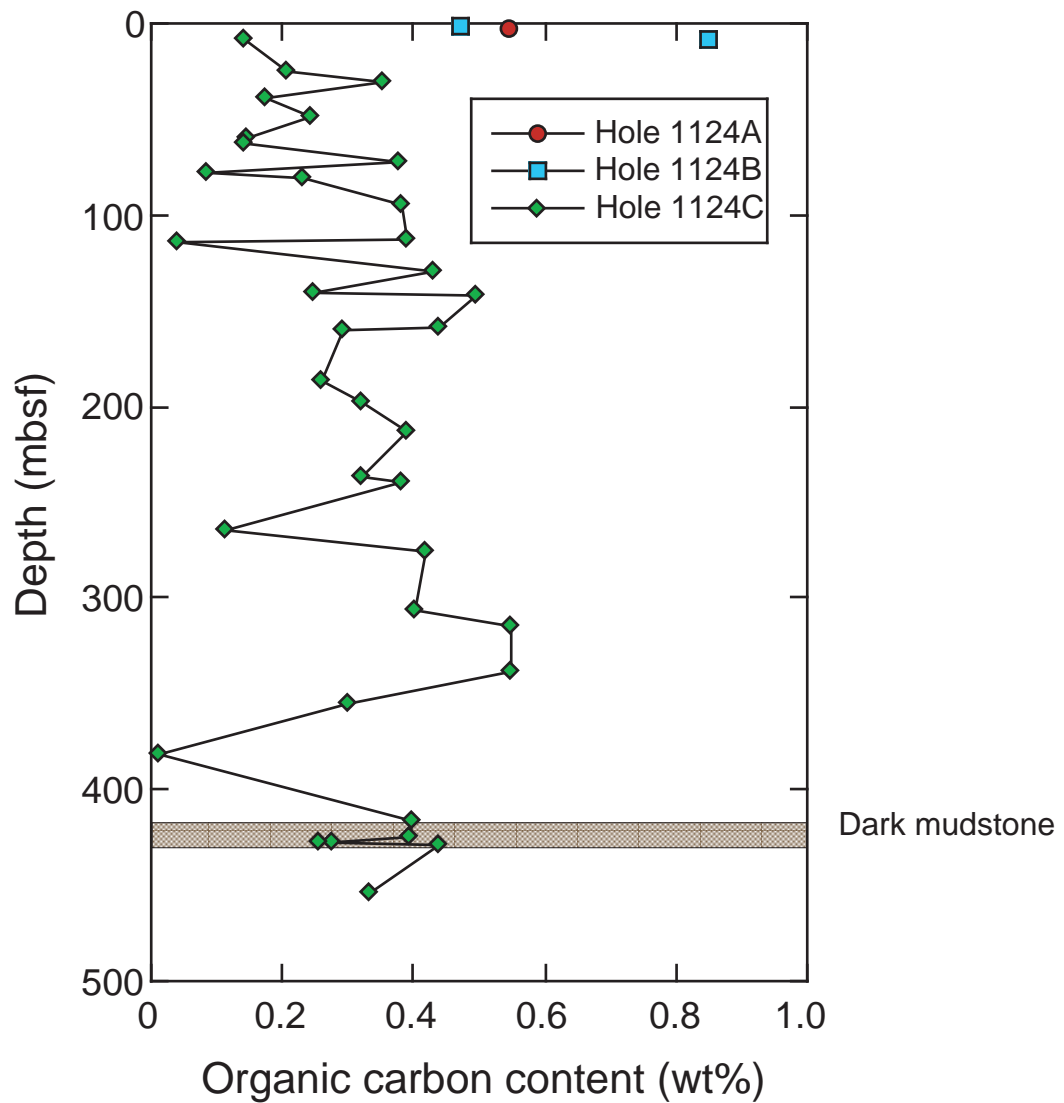
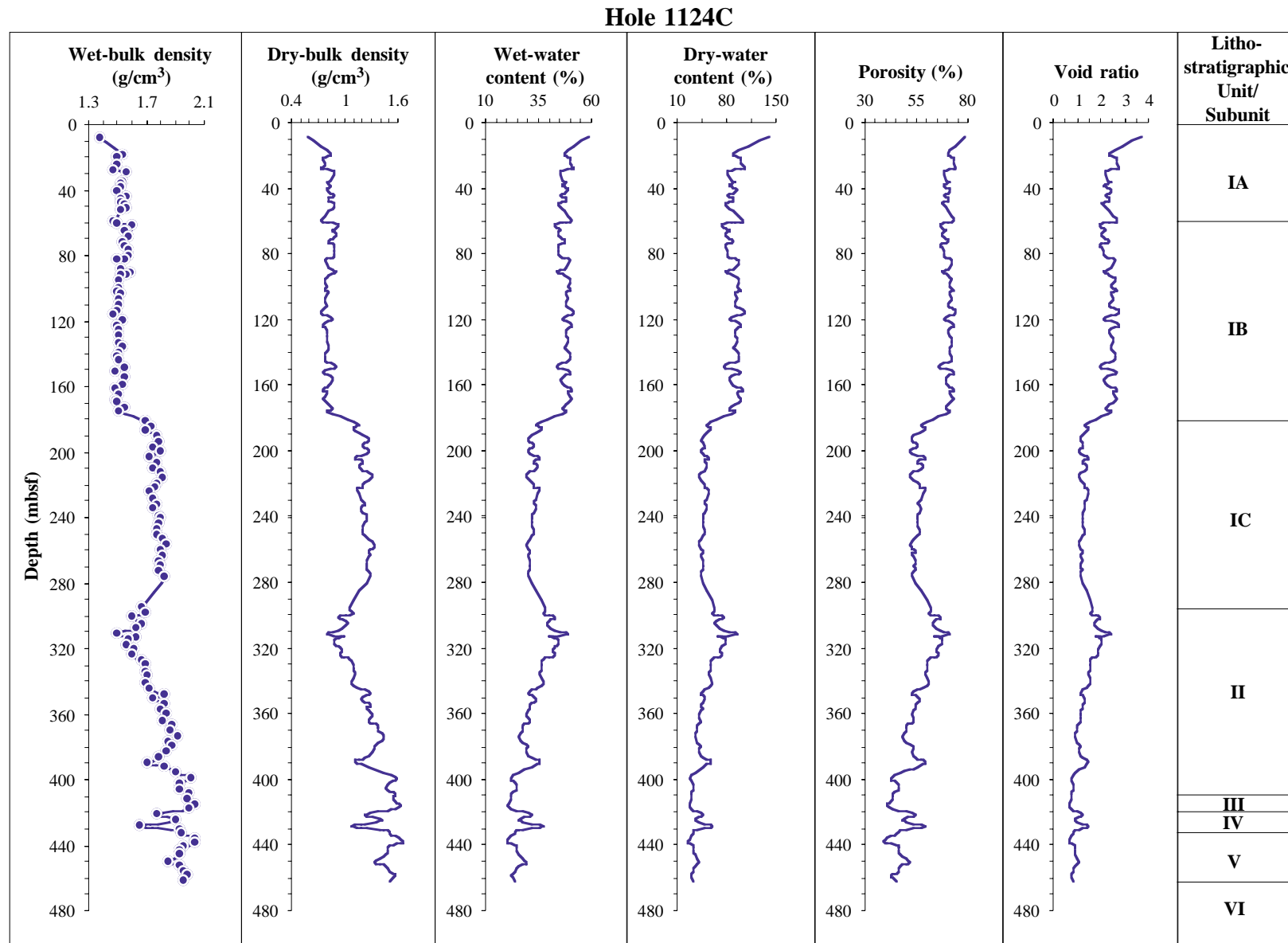


Figure F29. Index properties measured from cores from Hole 1124C.



**Figure F30.** MST measurements from Hole 1124C including MS, GRAPE density, natural gamma-ray intensity, and *P*-wave velocity. The smoothed *P*-wave velocity data were measured from split cores using the Hamilton frame velocimeter. The smoothed curve in the GRAPE density record indicates the distribution of wet-bulk density based on index properties measurements in Hole 1124C.

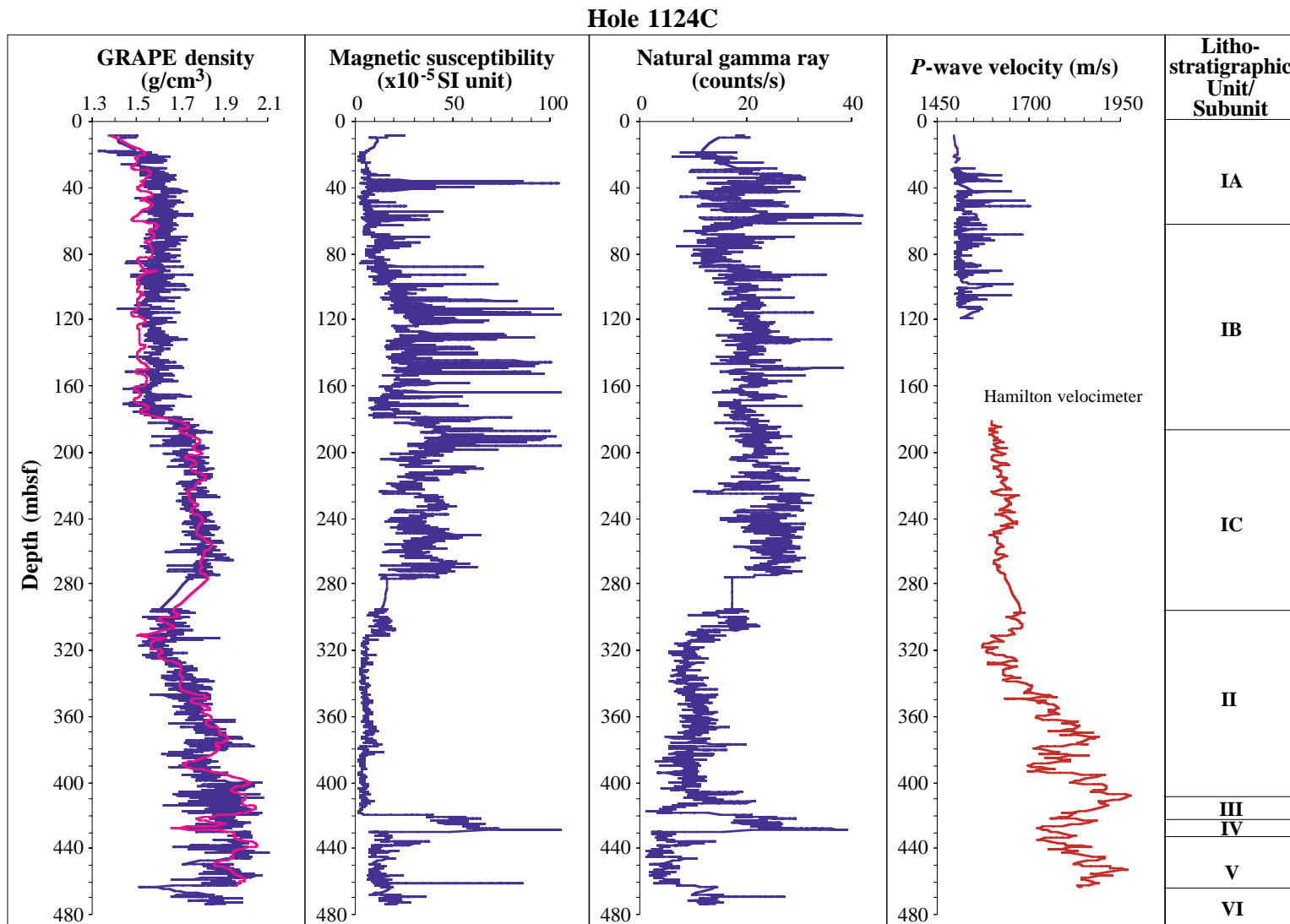
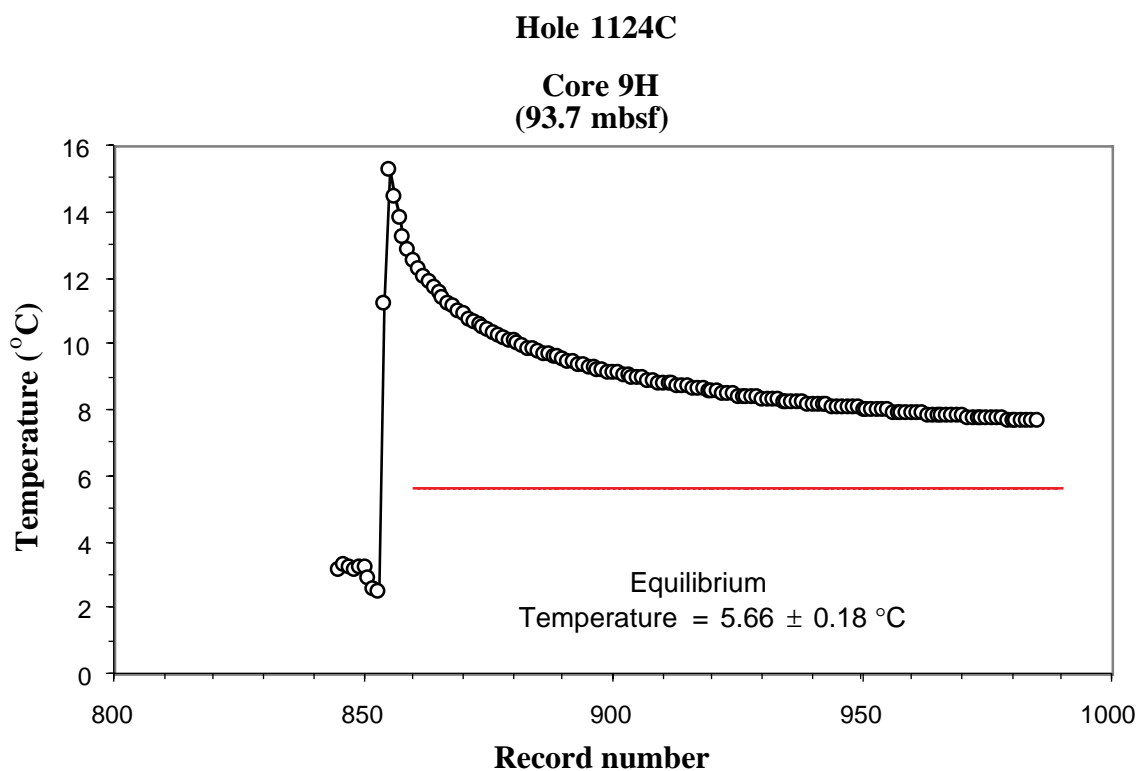
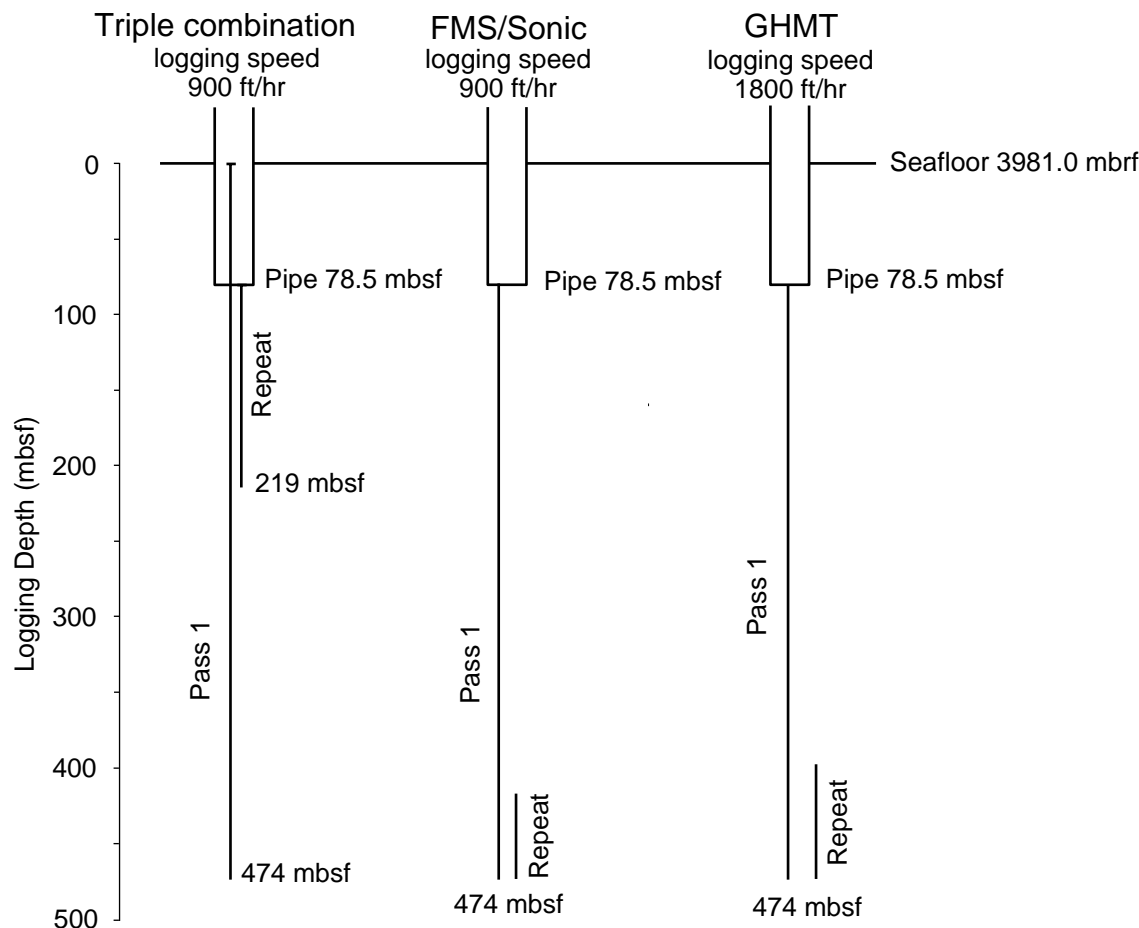


Figure F31. Temperature measurement by the Adara temperature tool on Core 181-1124C-9H.



**Figure F32.** Logging operations in Hole 1124C. The solid lines extending vertically from the pipe show the intervals that were logged. The top of each line represents where logging stopped, and the bottom shows where logging started.



**Figure F33.** Log data and logging units from Hole 1124C. A. Caliper, gamma-ray, resistivity, density, and porosity data. (Continued on next page.)

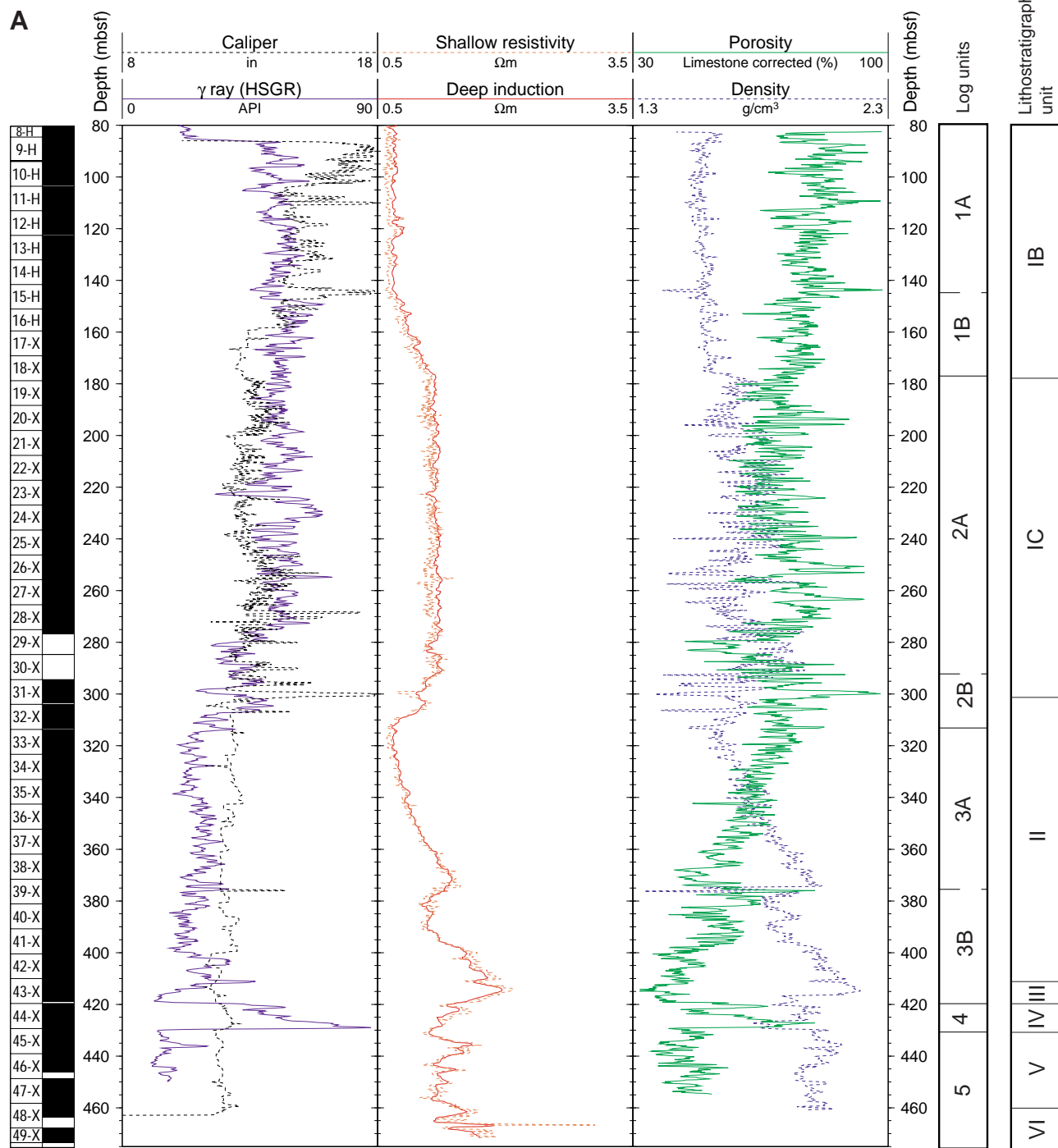
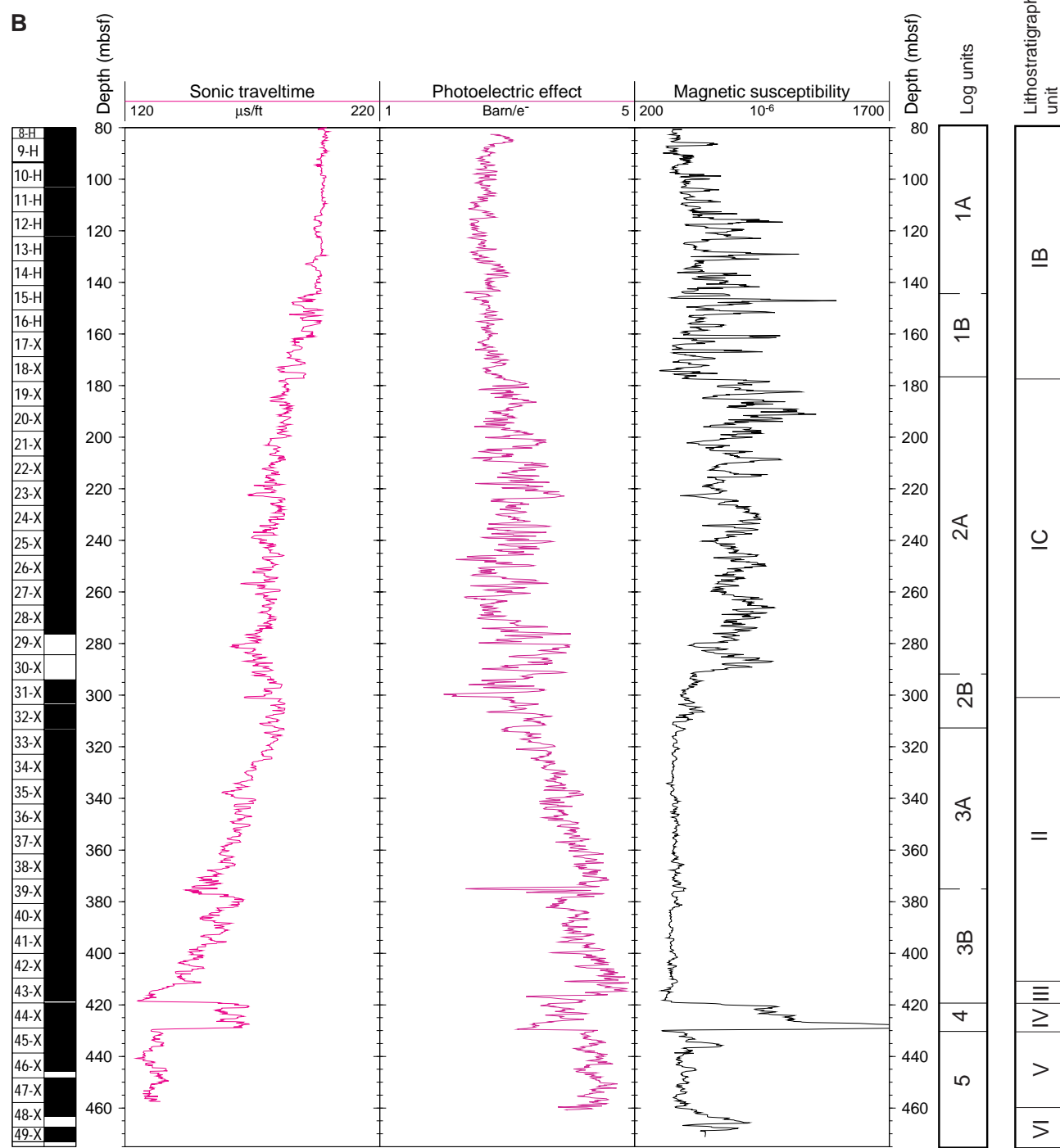


Figure F33 (continued). B. Sonic, photoelectric effect, and MS data.



**Figure F34.** Clay-swelling test results from Hole 1124C. Higher clay-swelling times on the y-axis indicate a greater propensity for swelling. KCl acts as an anti-swelling agent.

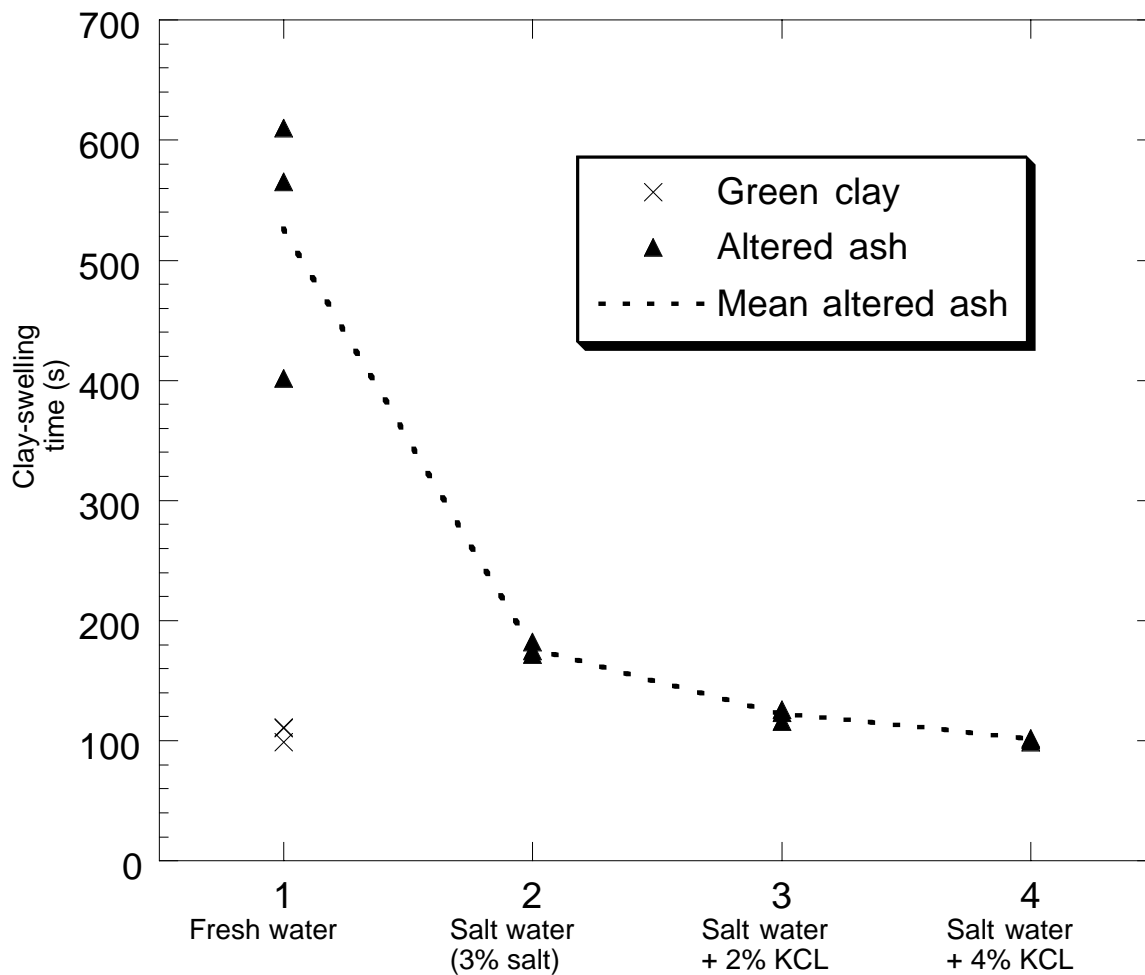
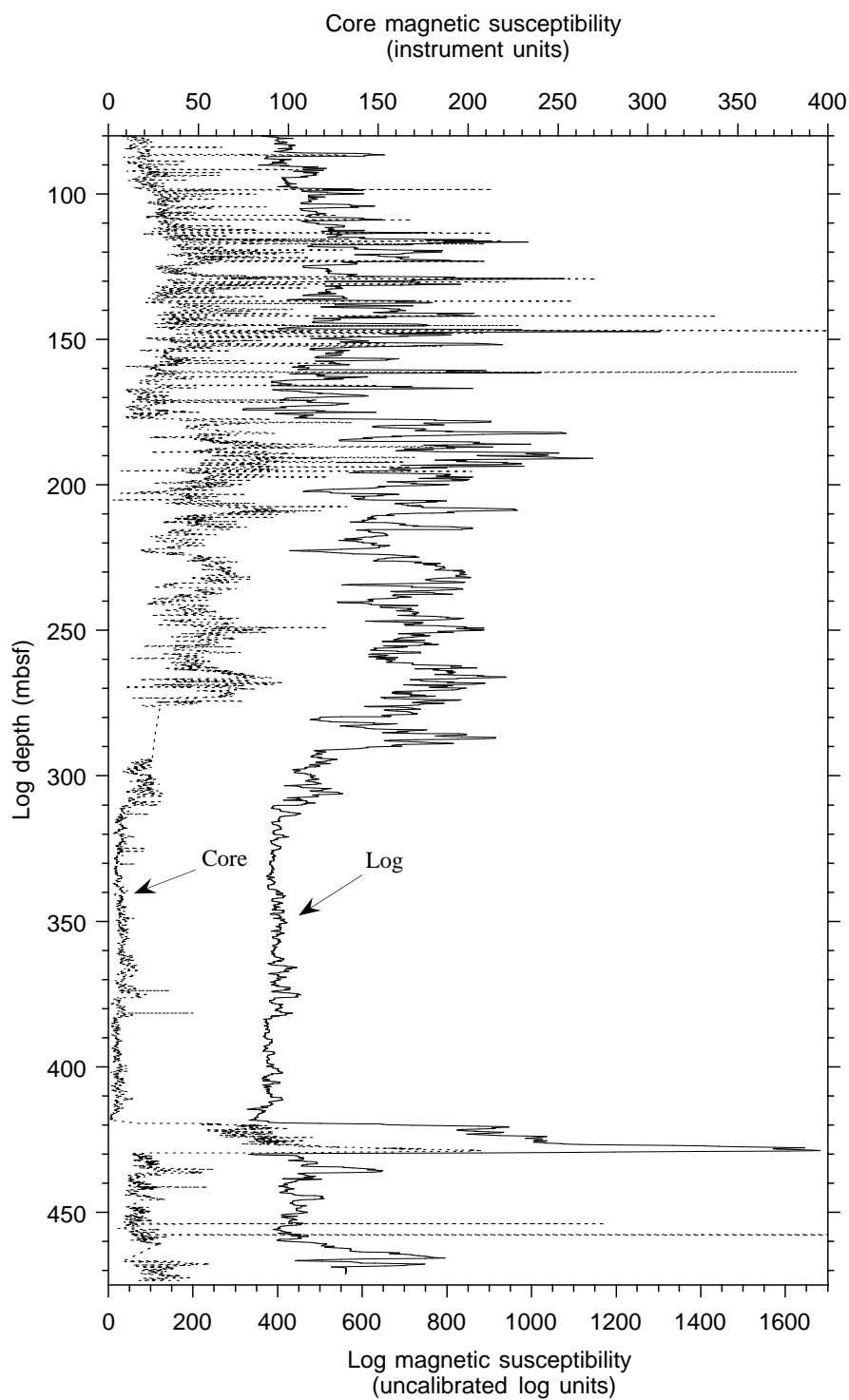
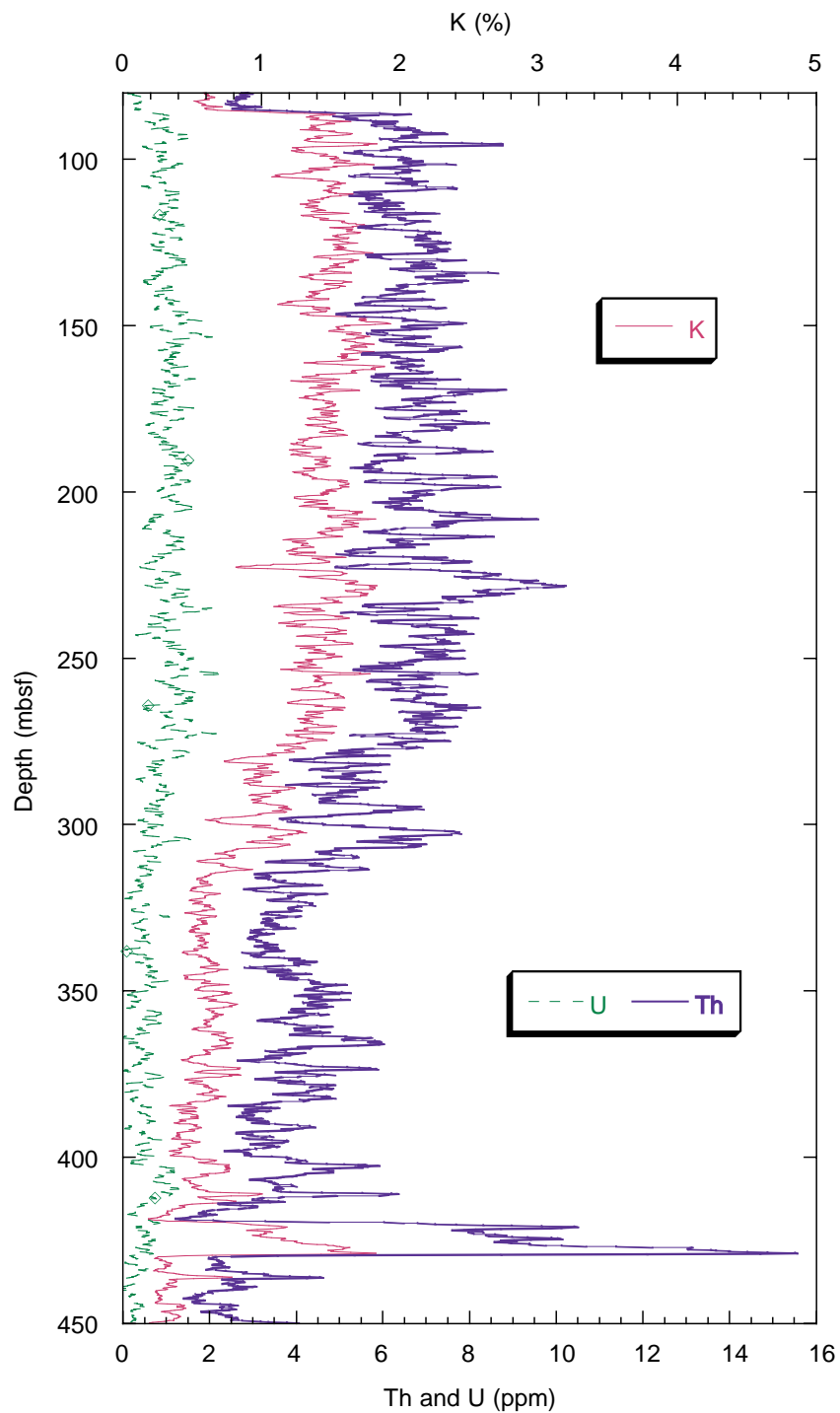


Figure F35. Comparison of log-based and core-based MS results.



**Figure F36.** Spectral gamma-ray results from Hole 1124C. Thorium values increase markedly in the brown mudstone, particularly toward its base.



**Figure F37.** FMS, gamma-ray, shallow resistivity, and MS results from the bottom of Hole 1124C. The brown mudstone and the predicted location of the K/T boundary are shown (see text for explanation).

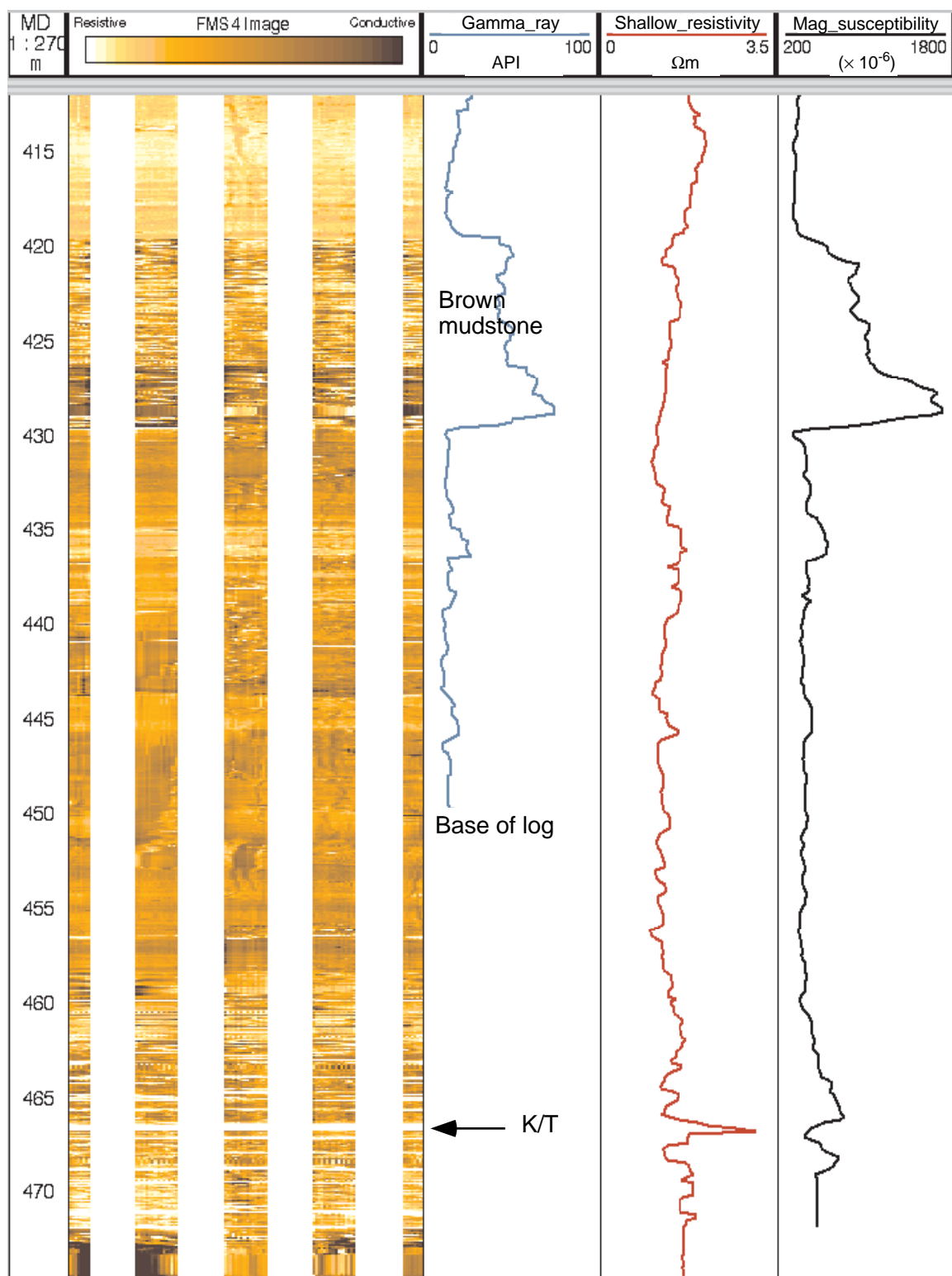


**Table T1.** Site 1124 seismic units and reflectors.

Reflector	Unit	Interval (ms TWT)	Time to base (ms TWT)	Assumed velocity (m/s)	Depth to reflector (m)	Thickness (m)	Cumulative thickness (m)	Character of reflections within units
Seabed					0	0	0	
R-1	A	85	85	1525	65	65	65	Discontinuous, subparallel
R-2	B1	100	185	1549	143	78	143	Faint, subparallel, rhythmic
R-3	B2	170	355	1650	293	150	293	Acoustically transparent
R-4	B3	134	489	1726	422	129	422	Semi-transparent, with "blotches"
Depth drilled to 485 m								
R-5	C1	110	599	1835	550	128	550	Strong, subparallel
	C2	46	645	1900	613	63	613	Acoustically transparent

**Table T2.** Site 1124 expanded coring summary. (See table note. Continued on next 13 pages.)

Core	Date (September 1998)	Time	Core depth (mbsf)		Length (m)		Recovery (%)	Section	Length (m)		Section depth (mbsf)		Catwalk samples	Comment
			Top	Bottom	Cored	Recovered			Liner	Curated	Top	Bottom		
181-1124A														
1H	25	1525	0.0	9.5	9.5	9.51	100.1		1	1.5	1.5	0.0	1.5	
									2	1.5	1.5	1.5	3.0	
									3	1.5	1.5	3.0	4.5	
									4	1.5	1.5	4.5	6.0	PAL
									5	1.5	1.5	6.0	7.5	
									6	1.5	1.5	7.5	9.0	PAL
									7	0.36	0.36	9.0	9.36	
									CC	0.15	0.15	9.36	9.51	PAL
										9.51	9.51		All to PAL	
					Totals:	9.5	9.51	100.10						
181-1124B														
1H	25	1730	0.0	5.4	5.4	5.41	100.2		1	1.5	1.5	0.0	1.5	
									2	1.5	1.5	1.5	3.0	IW, EDDY
									3	1.5	1.5	3.0	4.5	HS
									4	0.66	0.66	4.5	5.16	
									CC	0.25	0.25	5.16	5.41	PAL
										5.41	5.41			
2H	26	0540	5.4	9.9	4.5	4.48	99.6		1	1.5	1.5	5.4	6.9	
									2	1.5	1.5	6.9	8.4	IW, EDDY
									3	1.35	1.35	8.4	9.75	HS
									CC	0.13	0.13	9.75	9.88	PAL
										4.48	4.48			
					Totals:	9.9	9.89	99.90						
181-1124C														
1O	26	1525	0.0	8.0	0.0	0.0	N/A							
1X	26	1530	8.0	17.6	9.6	1.51	15.7		1	1.35	1.35	8.0	9.35	
									CC	0.16	0.16	9.35	9.51	PAL
										1.51	1.51		All to PAL	
2X	26	1630	17.6	27.2	9.6	7.68	80.0		1	1.29	1.29	17.6	18.89	
									2	0.71	0.71	18.89	19.6	
									3	1.5	1.5	19.6	21.1	
									4	0.94	0.94	21.1	22.04	IW
									5	1.5	1.5	22.04	23.54	HS
									6	1.5	1.5	23.54	25.04	
									CC	0.24	0.24	25.04	25.28	PAL
										7.68	7.68			
3H	26	1740	27.2	36.7	9.5	10.0	105.3		1	1.5	1.5	27.2	28.7	
									2	1.5	1.5	28.7	30.2	EDDY

**Table T2 (continued).**

Core	Date (September 1998)	Time	Core depth (mbsf)		Length (m)		Recovery (%)	Section	Length (m)		Section depth (mbsf)		Catwalk samples	Comment	
			Top	Bottom	Cored	Recovered			Liner	Curated	Top	Bottom			
4H	26	1845	36.7	46.2	9.5	9.74	102.5	3	1.5	1.5	30.2	31.7	IW HS PAL		
									4	1.5	1.5	31.7	33.2	IW	
									5	1.5	1.5	33.2	34.7	HS	
									6	1.5	1.5	34.7	36.2		
									7	0.81	0.81	36.2	37.01		
									CC	0.19	0.19	37.01	37.2	PAL	
										10.0	10.0				
5H	26	2010	46.2	55.7	9.5	9.99	105.2	1	1.5	1.5	36.7	38.2	All to PAL		
									2	1.5	1.5	38.2	39.7		
									3	1.5	1.5	39.7	41.2		
									4	1.5	1.5	41.2	42.7	IW	
									5	1.5	1.5	42.7	44.2	HS, EDDY	
									6	1.5	1.5	44.2	45.7		
									7	0.59	0.59	45.7	46.29		
									CC	0.15	0.15	46.29	46.44	PAL	
										9.74	9.74				
6H	26	2115	55.7	65.2	9.5	9.58	100.8	1	1.5	1.5	46.2	47.7	PAL		
									2	1.5	1.5	47.7	49.2		
									3	1.5	1.5	49.2	50.7	EDDY	
									4	1.5	1.5	50.7	52.2	IW	
									5	1.5	1.5	52.2	53.7	HS	
									6	1.5	1.5	53.7	55.2		
									7	0.69	0.69	55.2	55.89		
									CC	0.3	0.3	55.89	56.19	PAL	
										9.99	9.99				
7H	26	2240	65.2	74.7	9.5	9.99	105.2	1	1.5	1.5	65.2	66.7	PAL		
									2	1.5	1.5	66.7	68.2		
									3	1.5	1.5	68.2	69.7		
									4	1.5	1.5	69.7	71.2	IW	
									5	1.5	1.5	71.2	72.7	HS, EDDY	
									6	1.5	1.5	72.7	74.2		
									7	0.68	0.68	74.2	74.88		
									CC	0.31	0.31	74.88	75.19	PAL	
										9.99	9.99				
8H	26	2355	74.7	84.2	9.5	9.75	102.6								

**Table T2 (continued).**

Core	Date (September 1998)	Time	Core depth (mbsf)		Length (m)		Recovery (%)	Section	Length (m)		Section depth (mbsf)		Catwalk samples	Comment
			Top	Bottom	Cored	Recovered			Liner	Curated	Top	Bottom		
								1	1.5	1.5	74.7	76.2		
								2	1.5	1.5	76.2	77.7		
								3	1.5	1.5	77.7	79.2		
								4	1.5	1.5	79.2	80.7	IW	
								5	1.4	1.4	80.7	82.1	HS, EDDY	
								6	0.7	0.7	82.1	82.8		
								7	1.44	1.44	82.8	84.24		
								CC	0.21	0.21	84.24	84.45	PAL	
									9.75	9.75				
9H	27	0115	84.2	93.7	9.5	10.04	105.7							
								1	1.5	1.5	84.2	85.7		
								2	1.5	1.5	85.7	87.2		
								3	1.5	1.5	87.2	88.7	EDDY	
								4	1.5	1.5	88.7	90.2	IW	
								5	1.5	1.5	90.2	91.7	HS	
								6	1.5	1.5	91.7	93.2		
								7	0.71	0.71	93.2	93.91		
								CC	0.33	0.33	93.91	94.24	PAL	
									10.04	10.04				
10H	27	0220	93.7	103.2	9.5	9.12	96							
								1	1.5	1.5	93.7	95.2	EDDY	
								2	1.5	1.5	95.2	96.7		
								3	1.5	1.5	96.7	98.2		
								4	1.5	1.5	98.2	99.7	IW	
								5	1.5	1.5	99.7	101.2	HS	
								6	1.52	1.52	101.2	102.72		
								CC	0.1	0.1	102.72	102.82	PAL	All to PAL
									9.12	9.12				
11H	27	0335	103.2	112.7	9.5	9.85	103.7							
								1	1.5	1.5	103.2	104.7	EDDY	
								2	1.5	1.5	104.7	106.2		
								3	1.5	1.5	106.2	107.7		
								4	1.5	1.5	107.7	109.2	IW	
								5	1.5	1.5	109.2	110.7	HS	
								6	1.5	1.5	110.7	112.2		
								7	0.55	0.55	112.2	112.75		
								CC	0.3	0.3	112.75	113.05	PAL	
									9.85	9.85				
12H	27	0440	112.7	122.2	9.5	9.15	96.3							
								1	1.5	1.5	112.7	114.2		
								2	1.5	1.5	114.2	115.7		
								3	1.5	1.5	115.7	117.2		
								4	1.5	1.5	117.2	118.7		
								5	1.5	1.5	118.7	120.2	HS, EDDY	
								6	1.5	1.5	120.2	121.7		
								CC	0.15	0.15	121.7	121.85	PAL	All to PAL
									9.15	9.15				

**Table T2 (continued).**

Core	Date (September 1998)	Time	Core depth (mbsf)		Length (m)		Recovery (%)	Section	Length (m)		Section depth (mbsf)		Catwalk samples	Comment
			Top	Bottom	Cored	Recovered			Liner	Curated	Top	Bottom		
13H	27	0545	122.2	131.7	9.5	9.91	104.3		1	1.5	1.5	122.2	123.7	
									2	1.5	1.5	123.7	125.2	
									3	1.5	1.5	125.2	126.7	EDDY
									4	1.5	1.5	126.7	128.2	
									5	1.5	1.5	128.2	129.7	HS
									6	1.5	1.5	129.7	131.2	
									7	0.68	0.68	131.2	131.88	
									CC	0.23	0.23	131.88	132.11	PAL
										9.91	9.91			
14H	27	0650	131.7	141.2	9.5	9.51	100.1		1	1.5	1.5	131.7	133.2	
									2	1.5	1.5	133.2	134.7	
									3	1.5	1.5	134.7	136.2	
									4	1.5	1.5	136.2	137.7	IW, EDDY
									5	1.5	1.5	137.7	139.2	HS
									6	1.5	1.5	139.2	140.7	
									7	0.36	0.36	140.7	141.06	
									CC	0.15	0.15	141.06	141.21	PAL
										9.51	9.51			All to PAL
15H	27	0755	141.2	150.7	9.5	9.45	99.5		1	1.5	1.5	141.2	142.7	
									2	1.5	1.5	142.7	144.2	
									3	1.5	1.5	144.2	145.7	EDDY
									4	1.5	1.5	145.7	147.2	
									5	1.5	1.5	147.2	148.7	HS
									6	1.5	1.5	148.7	150.2	
									7	0.25	0.25	150.2	150.45	
									CC	0.2	0.2	150.45	150.65	PAL
										9.45	9.45			
16H	27	0900	150.7	159.2	8.5	8.72	102.6		1	1.5	1.5	150.7	152.2	
									2	1.5	1.5	152.2	153.7	
									3	1.5	1.5	153.7	155.2	
									4	1.5	1.5	155.2	156.7	
									5	1.5	1.5	156.7	158.2	HS, EDDY
									6	1.1	1.1	158.2	159.3	
									CC	0.12	0.12	159.3	159.42	PAL
										8.72	8.72			All to PAL
17X	27	1020	159.2	168.8	9.6	9.6	100		1	1.5	1.5	159.2	160.7	
									2	1.5	1.5	160.7	162.2	
									3	1.5	1.5	162.2	163.7	
									4	1.5	1.5	163.7	165.2	IW
									5	1.5	1.5	165.2	166.7	HS, HS
									6	1.5	1.5	166.7	168.2	

**Table T2 (continued).**

Core	Date (September 1998)	Time	Core depth (mbsf)		Length (m)		Recovery (%)	Section	Length (m)		Section depth (mbsf)		Catwalk samples	Comment
			Top	Bottom	Cored	Recovered			Liner	Curated	Top	Bottom		
18X	27	1125	168.8	178.4	9.6	9.58	99.8	7 CC	0.39	0.39	168.2	168.59	PAL	
									0.21	0.21	168.59	168.8		
									9.6	9.6				
									1	1.5	1.5	168.8	170.3	
									2	1.5	1.5	170.3	171.8	
									3	1.5	1.5	171.8	173.3	
									4	1.5	1.5	173.3	174.8	
									5	1.5	1.5	174.8	176.3	HS
									6	1.5	1.5	176.3	177.8	
19X	27	1240	178.4	188.0	9.6	9.87	102.8	7 CC	0.4	0.4	177.8	178.2	PAL	
									0.18	0.18	178.2	178.38		
									9.58	9.58				
									1	1.5	1.5	178.4	179.9	
									2	1.5	1.5	179.9	181.4	
									3	1.5	1.5	181.4	182.9	
									4	1.5	1.5	182.9	184.4	
									5	1.5	1.5	184.4	185.9	HS
									6	1.5	1.5	185.9	187.4	
									7	0.53	0.53	187.4	187.93	
20X	27	1345	188.0	197.7	9.7	9.67	99.7	7 CC	0.34	0.34	187.93	188.27	PAL	
									9.87	9.87				
									1	1.5	1.5	188	189.5	
									2	1.5	1.5	189.5	191	
									3	1.5	1.5	191	192.5	
									4	1.5	1.5	192.5	194	IW
									5	1.5	1.5	194	195.5	HS
									6	1.5	1.5	195.5	197	
									7	0.33	0.33	197	197.33	
									CC	0.34	0.34	197.33	197.67	PAL
21X	27	1450	197.7	207.3	9.6	9.76	101.7	7 CC	0.34	0.34	197.33	197.67	PAL	
									9.67	9.67				
									1	1.5	1.5	197.7	199.2	
									2	1.5	1.5	199.2	200.7	
									3	1.5	1.5	200.7	202.2	
									4	1.5	1.5	202.2	203.7	
									5	1.5	1.5	203.7	205.2	HS
									6	1.5	1.5	205.2	206.7	
									7	0.45	0.45	206.7	207.15	
									CC	0.31	0.31	207.15	207.46	PAL
22X	27	1600	207.3	216.9	9.6	9.76	101.7	7 CC	0.31	0.31	207.15	207.46	PAL	
									9.76	9.76				
									1	1.5	1.5	207.3	208.8	
									2	1.5	1.5	208.8	210.3	
									3	1.5	1.5	210.3	211.8	

**Table T2 (continued).**

Core	Date (September 1998)	Time	Core depth (mbsf)		Length (m)		Recovery (%)	Section	Length (m)		Section depth (mbsf)		Catwalk samples	Comment
			Top	Bottom	Cored	Recovered			Liner	Curated	Top	Bottom		
23X	27	1705	216.9	226.5	9.6	9.79	102	4	1.5	1.5	211.8	213.3	HS	IW
									1.5	1.5	213.3	214.8		
									1.5	1.5	214.8	216.3		
									0.28	0.28	216.3	216.58		
									0.48	0.48	216.58	217.06	PAL	
									9.76	9.76				
24X	27	1815	226.5	236.2	9.7	9.66	99.6	1	1.5	1.5	216.9	218.4	HS	IW
									1.5	1.5	218.4	219.9		
									1.5	1.5	219.9	221.4		
									1.5	1.5	221.4	222.9		
									1.5	1.5	222.9	224.4	HS	
									1.5	1.5	224.4	225.9		
									0.48	0.48	225.9	226.38		
									0.31	0.31	226.38	226.69	PAL	
									9.79	9.79				
25X	27	1920	236.2	245.8	9.6	9.78	101.9	1	1.5	1.5	226.5	228	HS	IW
									1.5	1.5	228	229.5		
									1.5	1.5	229.5	231		
									1.5	1.5	231	232.5		
									1.5	1.5	232.5	234		
									1.5	1.5	234	235.5		
									0.33	0.33	235.5	235.83		
									0.33	0.33	235.83	236.16	PAL	
									9.66	9.66				
26X	27	2030	245.8	255.4	9.6	9.7	101	1	1.5	1.5	236.2	237.7	HS	IW
									1.5	1.5	237.7	239.2		
									1.5	1.5	239.2	240.7		
									1.5	1.5	240.7	242.2		
									1.5	1.5	242.2	243.7		
									1.5	1.5	243.7	245.2		
									0.38	0.38	245.2	245.58		
									0.4	0.4	245.58	245.98	PAL	
									9.78	9.78				

**Table T2 (continued).**

Core	Date (September 1998)	Time	Core depth (mbsf)		Length (m)			Section	Length (m)		Section depth (mbsf)		Catwalk samples	Comment
			Top	Bottom	Cored	Recovered	Recovery (%)		Liner	Curated	Top	Bottom		
27X	27	2135	255.4	265.1	9.7	9.65	99.5	1	1.5	1.5	255.4	256.9	HS	PAL
								2	1.5	1.5	256.9	258.4		
								3	1.5	1.5	258.4	259.9		
								4	1.5	1.5	259.9	261.4		
								5	1.5	1.5	261.4	262.9		
								6	1.5	1.5	262.9	264.4		
								7	0.34	0.34	264.4	264.74		
								CC	0.31	0.31	264.74	265.05		
									9.65	9.65				
28X	27	2240	265.1	274.7	9.6	9.62	100.2	1	1.45	1.45	265.1	266.55	HS	PAL
								2	1.5	1.5	266.55	268.05		
								3	1.5	1.5	268.05	269.55		
								4	1.5	1.5	269.55	271.05		
								5	1.5	1.5	271.05	272.55		
								6	1.5	1.5	272.55	274.05		
								7	0.36	0.36	274.05	274.41		
								CC	0.31	0.31	274.41	274.72		
									9.62	9.62				
29X	27	2350	274.7	284.3	9.6	1.81	18.9	1	1.5	1.5	274.7	276.2	HS	PAL
								2	0.21	0.21	276.2	276.41		
								CC	0.1	0.1	276.41	276.51		
									1.81	1.81				All to PAL
30X	28	0100	284.3	294	9.7	0.15	1.5	CC	0.15	0.15	284.3	284.45	PAL	All to PAL
31X	28	0210	294	303.6	9.6	9.18	95.6	1	1.5	1.5	294	295.5	PAL	IW
								2	1.5	1.5	295.5	297		
								3	1.5	1.5	297	298.5		
								4	1.5	1.5	298.5	300		
								5	1.4	1.4	300	301.4		
								6	1.5	1.5	301.4	302.9		
								CC	0.28	0.28	302.9	303.18		
									9.18	9.18				
32X	28	0320	303.6	313.3	9.7	9.45	97.4	1	1.5	1.5	303.6	305.1	HS	PAL
								2	1.5	1.5	305.1	306.6		
								3	1.5	1.5	306.6	308.1		
								4	1.5	1.5	308.1	309.6		
								5	1.5	1.5	309.6	311.1		
								6	0.8	0.8	311.1	311.9		
								7	1.0	1.0	311.9	312.9		
								CC	0.15	0.15	312.9	313.05		

**Table T2 (continued).**

Core	Date (September 1998)	Time	Core depth (mbsf)		Length (m)		Recovery (%)	Section	Length (m)		Section depth (mbsf)		Catwalk samples	Comment
			Top	Bottom	Cored	Recovered			Liner	Curated	Top	Bottom		
33X	28	0425	313.3	322.9	9.6	9.48	98.8	1	9.45	9.45	313.3	314.8	HS	PAL
									1.5	1.5				
									1.5	1.5	314.8	316.3		
									1.5	1.5	316.3	317.8		
									1.5	1.5	317.8	319.3		
									1.5	1.5	319.3	320.8		
									1.5	1.5	320.8	322.3		
									0.31	0.31	322.3	322.61		
									0.17	0.17	322.61	322.78		
									9.48	9.48				
34X	28	0540	322.9	332.6	9.7	9.69	99.9	1	1.5	1.5	322.9	324.4	IW	HS
									1.5	1.5				
									1.5	1.5	324.4	325.9		
									1.5	1.5	325.9	327.4		
									1.5	1.5	327.4	328.9		
									1.5	1.5	328.9	330.4		
									1.5	1.5	330.4	331.9		
									0.42	0.42	331.9	332.32		
									0.27	0.27	332.32	332.59		
									9.69	9.69				
35X	28	0650	332.6	342.2	9.6	9.84	102.5	1	1.5	1.5	332.6	334.1	HS	PAL
									1.5	1.5				
									1.5	1.5	334.1	335.6		
									1.5	1.5	335.6	337.1		
									1.5	1.5	337.1	338.6		
									1.5	1.5	338.6	340.1		
									1.5	1.5	340.1	341.6		
									0.44	0.44	341.6	342.04		
									0.4	0.4	342.04	342.44		
									9.84	9.84				
36X	28	0800	342.2	351.9	9.7	9.61	99.1	1	1.5	1.5	342.2	343.7	HS	PAL
									1.5	1.5				
									1.5	1.5	343.7	345.2		
									1.5	1.5	345.2	346.7		
									1.5	1.5	346.7	348.2		
									1.5	1.5	348.2	349.7		
									1.5	1.5	349.7	351.2		
									0.36	0.36	351.2	351.56		
									0.25	0.25	351.56	351.81		
									9.61	9.61				
37X	28	0910	351.9	361.5	9.6	9.74	101.5	1	1.5	1.5	351.9	353.4	IW	HS
									1.5	1.5				
									1.5	1.5	353.4	354.9		
									1.5	1.5	354.9	356.4		
									1.5	1.5	356.4	357.9		

**Table T2 (continued).**

Core	Date (September 1998)	Time	Core depth (mbsf)		Length (m)		Recovery (%)	Section	Length (m)		Section depth (mbsf)		Catwalk samples	Comment
			Top	Bottom	Cored	Recovered			Liner	Curated	Top	Bottom		
38X	28	1025	361.5	371.2	9.7	9.66	99.6	5 6 7 CC	1.5	1.5	357.9	359.4	HS	
									1.5	1.5	359.4	360.9		
									0.33	0.33	360.9	361.23		
									0.41	0.41	361.23	361.64	PAL	
									9.74	9.74				
									1	1.5	361.5	363.0		
									2	1.5	363.0	364.5		
									3	1.5	364.5	366.0		
									4	1.5	366.0	367.5		
39X	28	1130	371.2	380.8	9.6	9.85	102.6	5 6 7 CC	1.5	1.5	367.5	369.0	HS	
									6	1.5	369.0	370.5		
									7	0.37	0.37	370.5	370.87	
									CC	0.29	0.29	370.87	371.16	PAL
									9.66	9.66				
									1	1.5	371.2	372.7		
									2	1.5	372.7	374.2		
									3	1.5	374.2	375.7		
									4	1.5	375.7	377.2		
40X	28	1240	380.8	390.4	9.6	9.37	97.6	5 6 7 CC	1.5	1.5	377.2	378.7	HS	
									6	1.5	378.7	380.2		
									7	0.46	0.46	380.2	380.66	
									CC	0.39	0.39	380.66	381.05	PAL
									9.85	9.85				
									1	1.5	380.8	382.3		
									2	1.5	382.3	383.8		
									3	1.5	383.8	385.3		
									4	1.5	385.3	386.8	IW	
41X	28	1400	390.4	400.1	9.7	9.57	98.7	5 6 7 CC	1.5	1.5	386.8	388.3	HS	
									6	1.5	388.3	389.8		
									7	0.27	0.27	389.8	390.07	
									CC	0.1	0.1	390.07	390.17	PAL
									9.37	9.37				All to PAL
									1	1.5	390.4	391.9		
									2	1.5	391.9	393.4		
42X	28	1515	400.1	409.7	9.6	9.74	101.5	5 6 7 CC	1.5	1.5	393.4	394.9		
									4	1.5	394.9	396.4		
									5	1.5	396.4	397.9	HS	
									6	1.5	397.9	399.4		
								CC	0.57	0.57	399.4	399.97	PAL	
									9.57	9.57				
								1	1.5	1.5	400.1	401.6		

**Table T2 (continued).**

Core	Date (September 1998)	Time	Core depth (mbsf)		Length (m)		Recovery (%)	Section	Length (m)		Section depth (mbsf)		Catwalk samples	Comment
			Top	Bottom	Cored	Recovered			Liner	Curated	Top	Bottom		
43X	28	1650	409.7	419.3	9.6	9.05	94.3	2	1.5	1.5	401.6	403.1		
									1.5	1.5	403.1	404.6		
									1.5	1.5	404.6	406.1		
									1.5	1.5	406.1	407.6	HS	
									1.5	1.5	407.6	409.1		
									0.37	0.37	409.1	409.47		
									0.37	0.37	409.47	409.84	PAL	
									9.74	9.74				
44X	28	1835	419.3	429	9.7	9.77	100.7	1	1.5	1.5	409.7	411.2		
									1.5	1.5	411.2	412.7		
									1.5	1.5	412.7	414.2	IW	
									1.5	1.5	414.2	415.7	HS	
									1.5	1.5	415.7	417.2		
									1.15	1.15	417.2	418.35		
									0.4	0.4	418.35	418.75	PAL	
									9.05	9.05				
45X	28	2020	429	438.7	9.7	9.72	100.2	1	1.5	1.5	419.3	420.8		
									1.5	1.5	420.8	422.3		
									1.5	1.5	422.3	423.8		
									1.5	1.5	423.8	425.3		
									1.5	1.5	425.3	426.8	HS	
									1.5	1.5	426.8	428.3		
									0.45	0.45	428.3	428.75		
									0.32	0.32	428.75	429.07	PAL	
									9.77	9.77				
46X	28	2205	438.7	448.3	9.6	7.18	74.8	1	1.5	1.5	429.0	430.5		
									1.5	1.5	430.5	432.0		
									1.5	1.5	432.0	433.5		
									1.5	1.5	433.5	435.0		
									1.5	1.5	435.0	436.5	HS	
									1.5	1.5	436.5	438.0		
									0.47	0.47	438.0	438.5		
									0.25	0.25	438.47	438.72	PAL	
									9.72	9.72				
47X	28	2345	448.3	457.9	9.6	9.26	96.5	1	1.5	1.5	438.7	440.2		
									1.5	1.5	440.2	441.7		
									1.5	1.5	441.7	443.2	IW	
									1.5	1.5	443.2	444.7	HS	
									0.84	0.84	444.7	445.54		
									0.34	0.34	445.54	445.88	PAL	
									7.18	7.18				

**Table T2 (continued).**

Core	Date (September 1998)	Time	Core depth (mbsf)		Length (m)		Recovery (%)	Section	Length (m)		Section depth (mbsf)		Catwalk samples	Comment
			Top	Bottom	Cored	Recovered			Liner	Curated	Top	Bottom		
								1	1.5	1.5	448.3	449.8		
								2	1.5	1.5	449.8	451.3		
								3	1.5	1.5	451.3	452.8		
								4	1.5	1.5	452.8	454.3		
								5	1.5	1.5	454.3	455.8	HS	
								6	1.5	1.5	455.8	457.3		
								CC	0.26	0.26	457.3	457.56	PAL	
									9.26	9.26				
48X	29	0150	457.9	467.4	9.5	5.52	58.1	1	1.5	1.5	457.9	459.4		
								2	1.5	1.5	459.4	460.9		
								3	1.5	1.5	460.9	462.4	HS	
								4	0.79	0.79	462.4	463.19		
								CC	0.23	0.23	463.19	463.42	PAL	
									5.52	5.52				
49X	29	0420	467.4	473.1	5.7	5.72	100.4	1	1.5	1.5	467.4	468.9		
								2	1.5	1.5	468.9	470.4		
								3	1.5	1.5	470.4	471.9	IW	
								4	1.12	1.12	471.9	473.02	HS	
								CC	0.1	0.1	473.02	473.12	PAL	
									5.72	5.72				
			Totals:		465.1	433.79	93.30							
181-1124D														
1O	30	0850	0.0	22.6	0.0	0.0	N/A							
1H	30	0950	22.6	32.1	9.5	9.56	100.6	1	1.5	1.5	22.6	24.1		
								2	1.5	1.5	24.1	25.6		
								3	1.5	1.5	25.6	27.1		
								4	1.5	1.5	27.1	28.6		
								5	1.5	1.5	28.6	30.1		
								6	1.5	1.5	30.1	31.6		
								7	0.37	0.37	31.6	31.97		
								CC	0.19	0.19	31.97	32.16	PAL	
									9.56	9.56				
2H	30	1055	32.1	41.6	9.5	7.75	81.6	1	1.5	1.5	32.1	33.6		
								2	1.5	1.5	33.6	35.1		
								3	1.5	1.5	35.1	36.6		
								4	1.5	1.5	36.6	38.1		
								5	1.5	1.5	38.1	39.6		
								6	0.07	0.07	39.6	39.67	PAL	All to PAL
								CC	0.18	0.18	39.67	39.85		
									7.75	7.75				
3H	30	1155	41.6	51.1	9.5	8.97	94.4							

**Table T2 (continued).**

Core	Date (September 1998)	Time	Core depth (mbsf)		Length (m)		Recovery (%)	Section	Length (m)		Section depth (mbsf)		Catwalk samples	Comment
			Top	Bottom	Cored	Recovered			Liner	Curated	Top	Bottom		
								1	1.5	1.5	41.6	43.1		
								2	1.5	1.5	43.1	44.6		
								3	1.5	1.5	44.6	46.1		
								4	1.5	1.5	46.1	47.6		
								5	1.5	1.5	47.6	49.1		
								6	1.24	1.24	49.1	50.34		
								CC	0.23	0.23	50.34	50.57	PAL	
											8.97	8.97		
4H	30	1300	51.1	60.6	9.5	8.52	89.7	1	1.5	1.5	51.1	52.6		
								2	1.5	1.5	52.6	54.1		
								3	1.02	1.02	54.1	55.12		
								4	1.5	1.5	55.12	56.62		
								5	1.5	1.5	56.62	58.12		
								6	1.4	1.4	58.12	59.52		
								CC	0.1	0.1	59.52	59.62	PAL	All to PAL
											8.52	8.52		
5H	30	1405	60.6	70.1	9.5	9.77	102.8	1	1.5	1.5	60.6	62.1		
								2	1.5	1.5	62.1	63.6		
								3	1.5	1.5	63.6	65.1		
								4	1.5	1.5	65.1	66.6		
								5	1.5	1.5	66.6	68.1		
								6	1.5	1.5	68.1	69.6		
								7	0.51	0.51	69.6	70.11		
								CC	0.26	0.26	70.11	70.37	PAL	
											9.77	9.77		
6H	30	1515	70.1	79.6	9.5	9.3	97.9	1	1.5	1.5	70.1	71.6		
								2	1.5	1.5	71.6	73.1		
								3	1.5	1.5	73.1	74.6		
								4	1.5	1.5	74.6	76.1		
								5	1.5	1.5	76.1	77.6		
								6	1.5	1.5	77.6	79.1		
								CC	0.3	0.3	79.1	79.4	PAL	
											9.30	9.30		
7H	30	1620	79.6	89.1	9.5	9.95	104.7	1	1.5	1.5	79.6	81.1		
								2	1.5	1.5	81.1	82.6		
								3	1.5	1.5	82.6	84.1		
								4	1.5	1.5	84.1	85.6		
								5	1.5	1.5	85.6	87.1		
								6	1.5	1.5	87.1	88.6		
								7	0.78	0.78	88.6	89.38		
								CC	0.17	0.17	89.38	89.55	PAL	
											9.95	9.95		

**Table T2 (continued).**

Core	Date (September 1998)	Time	Core depth (mbsf)		Length (m)		Recovery (%)	Section	Length (m)		Section depth (mbsf)		Catwalk samples	Comment
			Top	Bottom	Cored	Recovered			Liner	Curated	Top	Bottom		
8H	30	1725	89.1	98.6	9.5	9.01	94.8		1	1.5	1.5	89.1	90.6	
									2	1.5	1.5	90.6	92.1	
									3	1.5	1.5	92.1	93.6	
									4	1.41	1.41	93.6	95.01	
									5	1.5	1.5	95.01	96.51	
									6	1.5	1.5	96.51	98.01	
									CC	0.1	0.1	98.01	98.11	PAL
										9.01	9.01		All to PAL	
9H	30	1830	98.6	108.1	9.5	9.88	104		1	1.5	1.5	98.6	100.1	
									2	1.5	1.5	100.1	101.6	
									3	1.5	1.5	101.6	103.1	Liner patch
									4	1.5	1.5	103.1	104.6	Split liner
									5	1.5	1.5	104.6	106.1	Split liner
									6	1.5	1.5	106.1	107.6	Split liner
									7	0.6	0.6	107.6	108.2	Split liner
									CC	0.28	0.28	108.2	108.48	PAL
										9.88	9.88			
10H	30	1930	108.1	117.6	9.5	9.72	102.3		1	1.5	1.5	108.1	109.6	
									2	1.5	1.5	109.6	111.1	
									3	1.5	1.5	111.1	112.6	
									4	1.5	1.5	112.6	114.1	EDDY
									5	1.5	1.5	114.1	115.6	
									6	1.5	1.5	115.6	117.1	
									7	0.62	0.62	117.1	117.72	
									CC	0.1	0.1	117.72	117.82	PAL
										9.72	9.72		All to PAL	
11H	30	2035	117.6	127.1	9.5	9.89	104.1		1	1.5	1.5	117.6	119.1	
									2	1.5	1.5	119.1	120.6	
									3	1.5	1.5	120.6	122.1	
									4	1.5	1.5	122.1	123.6	
									5	1.5	1.5	123.6	125.1	
									6	1.5	1.5	125.1	126.6	
									7	0.72	0.72	126.6	127.32	
									CC	0.17	0.17	127.32	127.49	PAL
										9.89	9.89			
12H	30	2140	127.1	136.6	9.5	9.73	102.4		1	1.5	1.5	127.1	128.6	
									2	1.5	1.5	128.6	130.1	
									3	1.5	1.5	130.1	131.6	
									4	1.5	1.5	131.6	133.1	
									5	1.5	1.5	133.1	134.6	
									6	1.5	1.5	134.6	136.1	Liner patch

**Table T2 (continued).**

Core	Date (September 1998)	Time	Core depth (mbsf)		Length (m)		Recovery (%)	Section	Length (m)		Section depth (mbsf)		Catwalk samples	Comment
			Top	Bottom	Cored	Recovered			Liner	Curated	Top	Bottom		
13H	30	2240	136.6	146.1	9.5	10.04	105.7	7 CC	0.55	0.55	136.1	136.65	PAL	
									0.18	0.18	136.65	136.83		
									9.73	9.73				
									1	1.5	1.5	136.6	138.1	
									2	1.5	1.5	138.1	139.6	
									3	1.5	1.5	139.6	141.1	
									4	1.5	1.5	141.1	142.6	
14H	30	2355	146.1	155.6	9.5	9.75	102.6	CC	0.78	0.78	145.6	146.38	PAL	
									0.26	0.26	146.38	146.64		
									10.04	10.04				
									1	1.5	1.5	146.1	147.6	
									2	1.5	1.5	147.6	149.1	
									3	1.5	1.5	149.1	150.6	
									4	1.5	1.5	150.6	152.1	
									5	1.5	1.5	152.1	153.6	
15H	30	2355	155.6	165.1	9.5	9.75	102.6	CC	0.55	0.55	155.1	155.65	PAL	
									0.2	0.2	155.65	155.85		
									9.75	9.75				
Totals:			133	131.84	99.10									

Note: PAL = paleontology, IW = interstitial water, EDDY = geotechnical samples, HS = headspace. This table is also available in [ASCII format](#).

**Table T3.** Identification and abundance of nannofossils observed at Site 1124. (See table note. Continued on next three pages.)

**Table T3 (continued).**

**Table T3 (continued).**

Core, section, interval (cm)	Depth (mbsf)	Preservation	Group abundance	<i>Amauroliithus delicatus</i>	<i>Arkhangelskiella cymbiformis</i>	<i>Braunioria enomis</i>	<i>Calcidiscus leptoporus</i>	<i>Calcidiscus macintyrei</i>	<i>Calcidiscus premnacintyrei</i>	<i>Calcidiscus tropicus</i>	<i>Catinaster calyculus</i>	<i>Catinaster coelitus</i>	<i>Ceratolithus armatus</i>	<i>Ceratolithus cristatus</i>	<i>Chiasmolithus altus</i>	<i>Chiasmolithus bidens</i>	<i>Chiasmolithus danicus</i>	<i>Chiasmolithus oamaruensis</i>	<i>Chiasmolithus spp.</i>	<i>Cladiscoccus sublisticus</i>	<i>Coccolithus eopelagicus</i>	<i>Coccolithus miopelagicus</i>	<i>Coccolithus pelagicus</i>	<i>Coronocyclus nitescens</i>	<i>Crucilacolithus primus</i>	<i>Crucilacolithus tenuis</i>	<i>Cyclicargolithus abiseetus</i>	<i>Cyclicargolithus floridanus</i>	<i>Dicyococtites antarcticus</i>	<i>Dicyococtites bisectus</i>	<i>Dicyococtites productus</i>	<i>Discoaster adamanteus</i>	<i>Discoaster asymmetricus</i>	<i>Discoaster barbadiensis</i>	<i>Discoaster bolivi</i>	<i>Discoaster brouweri</i>	<i>Discoaster dellandrei</i>	<i>Discoaster druggii</i>	<i>Discoaster exilis</i>	<i>Discoaster intercalaris</i>	<i>Discoaster moorei</i>	<i>Discoaster quinqueramus</i>	<i>Discoaster pentanadiatus</i>	<i>Discoaster thiradiatus</i>	<i>Discoaster variabilis</i>	<i>Ericsonia formosa</i>	<i>Fasciculithus ulii</i>	<i>Fasciculithus pileatus</i>	<i>Fasciculithus tympaniformis</i>
25X-CC, 30-40	245.88	M C																																															
26X-CC, 27-37	255.4	P A	R																																														
27X-CC, 21-31	264.95	P C																																															
28X-CC, 21-31	274.62	P C																																															
29X-CC, 0-10	276.41	P C																																															
30X-CC, 0-15	284.3	B																																															
31X-CC, 18-28	303.08	M C																																															
32X-CC, 0-15	312.9	M C																																															
33X-CC, 7-17	322.68	M A	R																																														
34X-CC, 17-27	332.49	G A																																															
35X-CC, 30-40	342.34	G A																																															
36X-CC, 15-25	351.71	M A																																															
37X-CC, 31-41	361.54	G A																																															
38X-CC, 19-29	371.06	G C																																															
39X-CC, 29-39	380.95	G A																																															
40X-CC, 0-10	390.07	G A																																															
41X-CC, 47-57	399.87	G A																																															
42X-CC, 22-37	409.69	M A																																															
43X-1, 66	410.36	G A																																															
43X-2, 15	411.35	G A																																															
43X-2, 57	411.77	G A																																															
43X-6, 66	417.86	G A																																															
43X-CC, 30-40	418.65	M A																																															
44X-1, 100	420.3	G A																																															
44X-3, 1	422.31	M C																																															
44X-CC, 22-32	428.97	M C																																															
45X-1, 26	429.26	P A																																															
45X-1, 29	429.29	G A																																															
45X-CC, 15-25	438.62	G A																																															
46X-CC, 29-34	445.83	G C																																															
47X-CC, 16-26	457.46	M C																																															
48X-CC, 13-23	463.32	G C	R																																														
49X-1, 21-22	467.61	G A	C C																																														
49X-CC, 0-10	473.02	G A	C C																																														

Note: Preservation: G = good, M = moderate, and P = poor; total (group) and relative abundance of calcareous nannofossils: D = dominant, VA = very abundant, A = abundant, C = common, F = few, R = rare, and B = barren.

**Table T3 (continued).**

Core, section, interval (cm)	Depth (mbsf)	Preservation	Group abundance	<i>Geminithella rotula</i>	<i>Gephyrocapsa</i> (large)	<i>Gephyrocapsa</i> (medium)	<i>Gephyrocapsa parallela</i>	<i>Gephyrocapsa</i> (small)	<i>Helicosphaera carteri</i>	<i>Helicosphaera sellii</i>	<i>Hornbrookina teuriensis</i>	<i>Iseolithina fusca</i>	<i>Isthmolithus recurvus</i>	<i>Markalius inversus</i>	<i>Micula staurophora</i>	<i>Micula</i> spp.	<i>Minylitha convallis</i>	<i>Neochastozgus concinnus</i>	<i>Pseudosphaera cretacea</i>	<i>Pseudoemiliania lacunosa</i>	<i>Pyrocyclus</i> spp.	<i>Reticulofenestra asanoi</i>	<i>Reticulofenestra lockerii</i>	<i>Reticulofenestra</i> (medium)	<i>Reticulofenestra pseudounbilicus</i>	<i>Reticulofenestra</i> (small)	<i>Reticulofenestra umbilicus</i>	<i>Rhabdosphaera davigea</i>	<i>Sphenolithus abies</i>	<i>Sphenolithus belemnos</i>	<i>Sphenolithus capricornutus</i>	<i>Sphenolithus conicus</i>	<i>Sphenolithus delphinus</i>	<i>Sphenolithus heteromorphus</i>	<i>Sphenolithus moriformis</i>	<i>Sphenolithus neobies</i>	<i>Sphenolithus primus</i>	<i>Sphenolithus umbrellus</i>	<i>Syracosphera</i> spp.	<i>Thoracosphaera</i> spp.	<i>Thoracosphaera operculata</i>	<i>Toweius eminens</i>	<i>Toweius pertusus</i>	<i>Toweius tovae</i>	<i>Triquetorhabdulus carinatus</i>	<i>Umbilicosphaera shiozgei</i>	<i>Watsonellia barnesi</i>	<i>Zygohabiliithus bijugatus</i>
25X-CC, 30-40	245.88	M C F																																														
26X-CC, 27-37	255.4	P A																																														
27X-CC, 21-31	264.95	P C																																														
28X-CC, 21-31	274.62	P C																																														
29X-CC, 0-10	276.41	P C																																														
30X-CC, 0-15	284.3	B																																														
31X-CC, 18-28	303.08	M C																																														
32X-CC, 0-15	312.9	M C																																														
33X-CC, 7-17	322.68	M A																																														
34X-CC, 17-27	332.49	G A																																														
35X-CC, 30-40	342.34	G A																																														
36X-CC, 15-25	351.71	M A																																														
37X-CC, 31-41	361.54	G A																																														
38X-CC, 19-29	371.06	G C																																														
39X-CC, 29-39	380.95	G A																																														
40X-CC, 0-10	390.07	G A																																														
41X-CC, 47-57	399.87	G A																																														
42X-CC, 22-37	409.69	M A																																														
43X-1, 66	410.36	G A																																														
43X-2, 15	411.35	G A																																														
43X-2, 57	411.77	G A																																														
43X-6, 66	417.86	G A																																														
43X-CC, 30-40	418.65	M A																																														
44X-1, 100	420.3	G A																																														
44X-3, 1	422.31	M C																																														
44X-CC, 22-32	428.97	M C																																														
45X-1, 26	429.26	P A																																														
45X-1, 29	429.29	G A																																														
45X-CC, 15-25	438.62	G A																																														
46X-CC, 29-34	445.83	G C																																														
47X-CC, 16-26	457.46	M C																																														
48X-CC, 13-23	463.32	G C																																														
49X-1, 21-22	467.61	G A																																														
49X-CC, 0-10	473.02	G A																																														

**Table T4.** Nannofossil datum levels identified and age estimates used at Site 1124.

Depth (mbsf)	Bioevent	Age (Ma)	Reference
19.61	LO <i>Pseudoemiliania lacunosa</i>	0.42	Sato and Kameo, 1996
60.63	LO <i>Calcidiscus macintyreai</i>	1.60	Raffi et al., 1993
60.63	FO <i>Gephyrocapsa caribbeonica</i>	1.67	Raffi and Flores, 1995
70.14	LO <i>Discoaster brouweri</i>	1.96	Raffi and Flores, 1995
79.72	LO <i>Discoaster pentaradiatus</i>	2.30	Wei, 1993
89.25	LO <i>Discoaster surculus</i>	2.61	Raffi and Flores, 1995
98.43	LO <i>Reticulofenestra pseudoumbilicus</i>	3.82	Raffi and Flores, 1995
98.43	FO <i>Pseudoemiliania lacunosa</i>	4.0	Gartner, 1990
154.92	LO <i>Minylitha convallis</i>	7.73	Shackleton et al., 1995
183.22	FO <i>Minylitha convallis</i>	9.34	Raffi and Flores, 1995
183.22	LO <i>Cantinaster calculus</i>	9.64	Backman and Raffi, 1997
212.16	FO <i>Cantinaster coalitus</i>	10.79	Backman and Raffi, 1997
212.16	LO <i>Coccolithus miopelagicus</i>	10.94	Backman and Raffi, 1997
221.77	LO <i>Calcidiscus premacintyreai</i>	12.65	Raffi and Flores, 1995
240.97	LO <i>Sphenolithus heteromorphus</i>	13.52	Backman and Raffi, 1997
260.17	LO <i>Acme Discoaster deflandrei</i>	16.21	Raffi and Flores, 1995
280.35	FO <i>Geminolithella rotula</i>	19.8	Young et al., 1994
327.58	LO <i>Sphenolithus umbrellus</i>	23.6	Berggren et al., 1995b
327.58	LO <i>Dictyococcites bisectus</i>	23.9	Berggren et al., 1995b
337.41	LO <i>Sphenolithus delphix</i>	24.3	Berggren et al., 1995b
337.41	LO <i>Chiasmolithus altus</i>	26.1	Berggren et al., 1995b
410.86	FO <i>Sphenolithus distentus</i>	27.5	Berggren et al., 1995b
411.55	LO <i>Reticulofenestra umbilicus</i>	31.3	Morgans et al., 1996
414.82	LO <i>Ericsonia formosa</i>	32.8	Berggren et al., 1995b
417.86	Acme <i>Clasicoccus subdistichus</i>	33.3	Berggren et al., 1995b
419.82	FO <i>Isthmolithus recurvus</i>	35.5	Morgans et al., 1996
419.82	FO <i>Dictyococcites bisectus</i>	38	Berggren et al., 1995b
429.28	LO <i>Hornbrookina teuriensis</i>	58.3	Berggren et al., 1995b
442.22	FO <i>Fasciculithus tympaniformis</i>	59.7	Morgans et al., 1996
451.65	FO <i>Sphenolithus primus</i>	60.6	Berggren et al., 1995b
451.65	FO <i>Chiasmolithus bidens</i>	60.7	Berggren et al., 1995b
460.39	FO <i>Cruciplacolithus tenuis</i>	64.5	Berggren et al., 1995b
463.32	FO <i>Hornbrookina teuriensis</i>	64.9	Berggren et al., 1995b
467.61	LO <i>Micula</i> spp.	65	Berggren et al., 1995b

**Table T5.** Significant foraminiferal and bolboformid datums at Site 1124.

Foraminiferal events	Epoch	NZ stage	Age (Ma)	Core, section, interval (cm)	Depth (mbsf)
			181-		
FO <i>Globorotalia hirsuta</i>	Pleistocene	Wc	0.45	1124B-1H-1, 0-2 cm	0.02
LO <i>Globorotalia puncticuloides</i>	Pleistocene	Wc	~0.6	1124A-1H-1, 18-20	0.2
FO <i>Globorotalia truncatulinoides</i>	Pleistocene	Wn	~2	1124C-5H-CC	56.1
LO <i>Globorotalia tosaensis</i>	Pleistocene	Wc	~1	1124C-5H-5, 88-93 cm	53.1
LO <i>Globorotalia inflata triangula</i>	late Pliocene	Wn	~2	1124C-7H-CC	75.1
FO <i>Globorotalia crassula</i>	late Pliocene	Wm/Wn	2.6	1124C-5H-5, 88-93 cm	75.1
LO <i>Globorotalia crassaformis</i> (dextral)	late Pliocene	Wn	2.1	1124C-8H-3, 140-142 cm	80.1
FO <i>Globorotalia crassaformis</i> (dextral)	early Pliocene	Wp/Wm	3.0	1124C-8H-5, 10-12 cm	80.1
LO <i>Globorotalia crassaconica</i>	early Pliocene	Wp/Wm	3.0	1124C-9H-CC	94.1
FO <i>Globorotalia puncticuloides</i>	early Pliocene	Wp	3.6	1124C-10H-1, 76-78 cm	94.5
FO <i>Globorotalia inflata</i>	early Pliocene	Wo/Wp	3.7	1124C-10H-1, 76-78 cm	94.5
FO <i>Globorotalia inflata triangula</i>	early Pliocene	Wo/Wp	3.6	1124C-10H-1, 76-78 cm	94.5
LCO <i>Globorotalia pliozea</i>	early Pliocene	Wo/Wp	3.6	1124C-10H-1, 76-78 cm	94.5
LO <i>Globorotalia puncticulata</i>	early Pliocene	Wo/Wp	3.7	1124C-10H-1, 76-78 cm	94.5
FO <i>Globorotalia crassaconica</i>	early Pliocene	Wo	4.7	1124C-11H-CC	113.0
FO <i>Globorotalia puncticulata</i>	Miocene/Pliocene	Tk/Wo	5.2	1124C-11H-3, 74-78 cm	106.9
FO <i>Globorotalia pliozea</i>	late Miocene	Tk	5.4	1124C-11H-CC	113.0
LO <i>Globorotalia miotumida</i>	late Miocene	Tk	5.6	1124C-14H-2, 100-102 cm	134.2
FO <i>Sphaeroidinella paenedehisca</i>	late Miocene	Tt	~8	1124C-14H-CC	141.1
LO <i>Globoquadrina dehiscens</i>	late Miocene	e Tt	9.9	1124C-20X-CC	207.4
LO <i>Orbulina suturalis</i>	late Miocene	e Tt	~10.5	1124C-22X-CC	212.1
FO <i>Zeaglobigerina nepenthes</i>	middle Miocene	I Sw	11.8	1124C-21X-CC	207.4
LO <i>Globorotalia praemenardii</i>	middle Miocene	SI	13.2	1124C-22X-5, 124-128 cm	214.6
LO <i>Globorotalia amuria</i>	middle Miocene	SI/Sw	13	1124C-22X-5, 124-128 cm	214.6
FO <i>Globorotalia praemenardii</i>	middle Miocene	Sc	15.8	1124C-24X-CC	236.06
FO <i>Globigerinoides trilobus</i>	early Miocene	PI	19	1124C-29X-CC	276.4
LO <i>Catapsydrax dissimilis</i>	early Miocene	PI	16.7	1124C-28X-CC	274.6
FO <i>Sphaeroidinellopsis disjuncta</i>	early Miocene	m PI	18.5	1124C-22X-CC	212.1
LO <i>Globorotalia incognita</i>	early Miocene	PI	18.5	1124C-29X-CC	276.41
FO <i>Globorotalia incognita</i>	early Miocene	Po	21.6	1124C-29X-CC	276.41
FO <i>Cassidulina cuneata</i>	late Oligocene	Ld	~27	1124C-31X-CC	303.2
LO <i>Cibicidoides praemundulus</i>	late Oligocene	e/m Lw	23.8	1124C-40X-CC	390.1
LO <i>Subbotina angiporoidea</i>	early Oligocene	e Lwh	30	1124C-43X-CC	418.7
LCO <i>Paragloborotalia gemma</i>	early Oligocene	e Lwh	32	1124C-43X-CC	418.7
LO <i>Globigerinatheka index</i>	late Eocene	Ar	34.3	1124C-44X-1, 67-69 cm	420.0
LO <i>Ponticulospaera semiinvoluta</i>	late Eocene	Ar	34.8	1124C-44X-1, 67-69 cm	420.0
FO <i>Paragloborotalia gemma</i>	late Eocene	late Ar	35	1124C-43X-CC	418.7
LO <i>Nuttallides truempyi</i>	late Eocene	Ar	?34.3	1124C-44X-1, 67-69 cm	420.0
LO <i>Acarnania primitiva</i>	late Eocene	Ak	~36	1124C-44X-1, 67-69 cm	420.0
FO <i>Ponticulospaera semiinvoluta</i>	late Eocene	Ab	38.4	1124C-44X-5, 93-95 cm	426.2
FO <i>Globigerinatheka index</i>	middle Eocene	Dp	42.9	1124C-44X-6, 50-52 cm	427.3
LO <i>Gavelinella beccariiformis</i>	Paleocene	55	1124C-44X-CC (pink)*	429.1	
LO <i>Aragonaria quezzanensis</i>	Paleocene	Dt	55	1124C-45X-CC	438.7
FO <i>Morozovella conicotruncata</i>	middle Paleocene	Dt	60.9	1124C-45X-CC	438.7
FO <i>Morozovella angulata</i>	middle Paleocene	Dt	61	1124C-45X-CC	438.7
FO <i>Morozovella praecursoria</i>	middle Paleocene	Dt	~61.2	1124C-45X-CC	438.7
FO <i>Morozovella aff. trinidadensis</i>	early Paleocene	Dt	? ~63.0	1124C-45X-CC	438.7
FO <i>Globanomalina compressa</i>	early Danian	Dt	~63.5	1124C-47X-CC	457.6
LO <i>Globocorus daubjergensis</i>	early Danian	Dt	~63	1124C-47X-CC	457.6
LO <i>Globigerina fringa</i>	early Danian	Dt	63	1124C-47X-CC	457.6
LO <i>Globigerina eugubina</i>	earliest Danian	Dt	64.9	1124C-48X-CC	463.4
LO <i>Rugoglobigerina rugosa</i>	Maastrichtian	Mh/Dt	65	1124C-49X-CC	473.1
LO <i>Globorotalites michelinianus</i>	Maastrichtian	Mh/Dt	65	1124C-49X-CC	473.1

Note: \* = lower part of core catcher was colored pink. New Zealand stages: Wc = Castlecliffian, Wn = Nukumaruan, Wm = Mangapanian, Wp = Waipipian, Wo = Opoitian, Tk = Kapitean, Sw = Waiauan, SI = Lillburnian, Sc = Clifdeian, PI = Altonian, Po = Otaian, Ld = Duntroonian, Lw = Waitakian, Lwh = Whaingaroan, Ar = Runangan, Ak = Kaiatan, Ab = Bortonian, Dp = Porangan, Dt = Teurian, Mh = Haumurian, e = early, m = middle, l = late.

**Table T6.** Identification and abundance of planktonic foraminifers observed at Site 1124. (See table note. Continued on next page.)

**Table T6 (continued).**

Core, section, interval (cm)	Depth (mbfs)	Preservation	Abundance	<i>Globigerina bullloidies</i>	<i>Globigerina quinqueloba</i>	<i>Globigerinella glutinata</i>	<i>Globigerinoides ruber</i>	<i>Globorotalia inflata</i>	<i>Globorotalia truncatulinoides</i>	<i>Neogloboquadrina pachyderma</i>	<i>Orbulina universa</i>	<i>Globigerina falconensis</i>	<i>Globigerinoides conglobatus</i>	<i>Globorotalia crassula</i>	<i>Globorotalia punctulata</i>	<i>Neogloboquadrina dutertrei</i>	<i>Globorotalia crassula</i>	<i>Globorotalia tumida</i>	<i>Globorotalia punctuloides</i>	<i>Sphaeroidinella dehisces</i>	<i>Globorotalia crassaformis</i> (dextral)	<i>Globorotalia inflata triangula</i>	<i>Globorotalia piozea</i>	<i>Globorotalia crassaconica</i>	<i>Sphaeroidinellopsis paeneditensis</i>	<i>Globogaudringera dehisces</i>	<i>Globorotalia miotumida</i>	<i>Sphaeroidinellopsis disjuncta</i>	<i>Catapsydrax dissimilis</i>	<i>Acanina primitiva</i>	<i>Globigerinatethka index</i>	<i>Globorotaloides turrida</i>	<i>Ponticulaspiraera seminvoluta</i>	<i>Subbotina linaperta</i>	<i>Globanomalina compressa</i>	<i>Globocanusa daubjergensis</i>	<i>Subbotina simplicissima</i>	<i>Subbotina triloculoides</i>	<i>Globigerina fringa</i>	<i>Guembelitria cretacea</i>	<i>Hedbergella holmdelensis</i>	<i>Rugoglobigerina rugosa</i>	<i>Globigerinoides cf. trilobus</i>	<i>Globorotalia incognita</i>	<i>Globorotalia praemenardii</i>	<i>Globorotalia anulata</i>	<i>Globorotalia crassiformis</i> (sinistral)
31X-3, 93-96	297.93	P	T																																												
31X-C, 18-28	303.08		B																																												
33X-C, 7-17	322.68	M	T																																												
34X-C, 17-27	332.49	M	T																																												
35X-C, 30-40	342.34		B																																												
36X-C, 15-25	351.71	M	T																																												
37X-C, 31-41	361.54	M	T																																												
38X-C, 19-29	371.06		B																																												
40X-C, 0-10	390.07	P	T																																												
42X-3, 98-101	404.08	P	T																																												
42X-C, 22-37	409.69	G	F																																												
43X-C, 30-40	418.65	G	F																																												
44X-1, 67-69	419.97	G	F																																												
44X-5, 93-95	426.23	M	F																																												
44X-6, 50-52	427.3	M	F																																												
44X-C, 22-32	428.97		B																																												
45X-C, 15-25	438.62	M	F																																												
46X-C, 29-34	445.83	M	C																																												
47X-C, 16-26	457.46	P	R																																												
48X-3, 44-45	461.34	P	T																																												
48X-C, 13-23	463.32	M	R																																												
49X-C, 0-10	473.02	M	T																																												

Note: Preservation: G = good, M = moderate, and P = poor; total (group) and relative abundance of planktonic foraminifers: D = dominant, A = abundant, C = common, F = few/frequent, R = rare, T = trace, P = present, and B = barren.

**Table T7.** Identification and abundance of Paleocene and Late Cretaceous benthic foraminifers observed at Site 1124.

Core, section, interval (cm)	Depth	Preservation	Group abundance	<i>Alabamina creta</i>	<i>Aragonina quezzanensis</i>	<i>Buliminina navarroensis</i>	<i>Cassidulina cuneata</i>	<i>Cibicidoides praemunulus</i>	<i>Dorothia oxyacantha</i>	<i>Dorothia sp.</i>	<i>Dorothia trachioea</i>	<i>Gauymina sp.</i>	<i>Gavelinella beccariiformis</i>	<i>Globorotalites michelinianus</i>	<i>Gyroidina solitaria</i>	<i>Gyroidinoides globosus</i>	<i>Karerulina conversa</i>	<i>Neohabellina javisi</i>	<i>Nuttallina trumppi</i>	<i>Nuttallina thorealis</i>	<i>Pulena coryelli</i>	<i>Pulena quinqueloba</i>	<i>Quaanimorphina aliomorphinoidea</i>	<i>Rhabdostommina sp.</i>	<i>Saccammina pacifica</i>	<i>Spiropectammina aenata</i>	<i>Spiropectammina sp.</i>	<i>Spiropectammina spectabilis</i>	<i>Trilaxa</i> spp.
181-1124C-31X-CC, 18-28	303.08	P	R																										
40X-CC, 0-10	390.07	P	T																										
44X-CC, 22-32	428.97	G	C																										
45X-CC, 15-25	438.62	G	C	T	T	T																							
46X-CC, 29-34	445.83	M	T																										
47X-CC, 16-26	457.46	P	T																										
49X-CC, 0-10	473.02	G	C																										

Note: Preservation: G = good, M = moderate, and P = poor; total (group) abundance and relative abundance of radiolarians: C = common, F = few, R = rare, and T = trace.

**Table T8.** Identification and abundance of diatoms and silicoflagellates. (See table note. Continued on next three pages.)

Table T8 (continued).

Table T8 (continued).

Core, section, interval (cm)	Depth (mbst)	Diatom abundance	Silicoflagellate abundance
39X-CC, 29-39	380.95	F	<i>Actinocyclus curvatus</i>
40X-CC, 0-10	390.07	F	<i>Actinocyclus ehrenbergii</i>
41X-CC, 47-57	399.87	R	<i>Actinocyclus ellipticus</i>
42X-CC, 22-37	409.69	B	<i>Actinocyclus ingens</i>
43X-2, 35-36	401.73	B	<i>Actinopychthus senarius</i>
43X-2, 53-54	402.17	B	
43X-2, 10-11	411.29	B	
43X-CC, 30-40	418.65	B	
44X-1, 14-15	418.8	B	
44X-3, 102-102	419.67	B	
44X-CC, 22-32	428.97	B	
45X-1, 8-8	429.05	B	
45X-CC, 15-25	438.62	B	
46X-CC, 29-34	445.83	B	
47X-CC, 16-26	457.46	T	
48X-CC, 13-23	463.32	T	
49X-3, 135-150	467.82	B	
49X-CC, 0-10	473.02	B	
			<i>Asterolampra marylandica</i>
			<i>Aulacoseira granulata</i>
			<i>Azpeitia africana</i>
			<i>Azpeitia nodulifer</i>
			<i>Azpeitia oligocenica</i>
			<i>Bogorovia ventimini</i>
			<i>Cavatitius jouseanus</i>
			<i>Cestodiscus conveexus</i>
			<i>Cestodiscus novazaelandicus</i>
			<i>Cestodiscus sp.</i>
			<i>Chaetoceros resting spores</i>
			<i>Chaetoceros sp.</i>
			<i>Coscinodiscus descrescens</i>
			<i>Coscinodiscus radiatus</i>
			<i>Coscinodiscus rhombicus</i>
			<i>Crasspedodiscus sp.</i>
			<i>Denticulopsis dimorpha</i>
			<i>Denticulopsis sp.</i>
			<i>Diploneis sp.</i>
			<i>Eucampia antarctica</i>
			<i>Grammatophora sp.</i>
			<i>Hemiaulus claviger</i>
			<i>Hemiaulus polycystinorum</i>
			<i>Hemiaulus sp.</i>
			<i>Hemidiscus cuneiformis</i>
			<i>Hyalodiscus sp.</i>
			<i>Melosira architecturalis</i>
			<i>Nitzschia baronii</i>
			<i>Nitzschia challengeri</i>
			<i>Nitzschia fossils</i>
			<i>Nitzschia kerguelensis</i>
			<i>Nitzschia marina</i>
			<i>Nitzschia panduriformis</i>
			<i>Nitzschia reinholdii</i>
			<i>Nitzschia ritscherii</i>
			<i>Paralia sulcata</i>
			<i>Planktoniella sol</i>
			<i>Pseudoeunotia doliosus</i>
			<i>Pterotheca aculeifera</i>
			<i>Rixula reticulata</i>
			<i>Raphoneis amphiceros</i>
			<i>Raphoneis surireloides</i>
			<i>Rhizosol. habettata f. hiemalis</i>
			<i>Roella gelida</i> var. <i>schnaderi</i>
			<i>Roella gelida</i>

Note: Preservation: G = good, M = moderate, and P = poor; total (group) abundance and relative abundance of diatoms: C = common, F = few, R = rare, T = trace, and B = barren.

**Table T8 (continued).**

**Table T9.** Significant diatom datum levels.

Event	Age (Ma)	Core, section	Depth (mbsf)
181-1124C-			
LO <i>Nitzschia reinholdii</i>	0.65	2X-CC	25.18
LO <i>Nitzschia fossilis</i>	0.7	3H-CC	37.10
LO <i>Nitzschia barronii</i>	1.25	4H-CC	46.29
FO <i>Nitzschia fossilis</i>	7.6–7.7	14H-CC	146.06
LO <i>Rocella gelida</i>	22.4	31X-CC	303.08
LO <i>R. gelida</i> var. <i>schraderi</i>	23.7	34X-CC	332.49

**Table T10.** Identifications, range chart, and abundances of radiolarians. (See table note. Continued on next three pages.)

**Table T10 (continued).**

**Table T10 (continued).**

Note: Preservation: VG = very good, G = good, M = moderate, and P = poor; total (group) abundance and relative abundance of radiolarians: VA = very abundant, A = abundant, C = common, F = few, R = rare, VR = very rare, T = trace, and B = barren.

Table T10 (continued).

Core, section, interval (cm)	Depth (mbsf)	Preservation	Group abundance	<i>Cycladophora pilocenica</i>	<i>Dictyophimus hitundo</i>	<i>Lithopera bacca</i>	<i>Cyrtocapsella cf. tetrapera</i>	<i>Dorcaspyris</i> sp.	<i>Lamprocyclus matakohue</i>	<i>Liriospis</i> sp.	<i>Phomocytis alexandiae</i>	<i>Anthocytidium mariaeae</i>	<i>Lophocytis? cf. inaequalis</i>	<i>Lophocystis</i> sp. q.	<i>Lychnocanoma conica</i>	<i>Lychnocanoma elongata</i>	<i>Lychnocanoma</i> sp.	<i>Stichocorys neogriponensis</i>	<i>Stylosphaera timansi</i>	<i>Antiphormis gracilis</i>	<i>Botryostrobus</i> sp.	<i>Clathrocytis?</i> sp.	<i>Didymocytis prismatica</i>	<i>Dorcaspyris ateuchus</i>	<i>Gorgospyris</i> sp.	<i>Lithonellisa maurenae</i>	<i>Lophocytis? inaequalis</i>	<i>Lophocystis galenum</i>	<i>Lophophæna tekopua</i>	<i>Lychnocanoma neptunae</i>	<i>Periphæna</i> sp.	<i>Thecorys puriri</i>	<i>Valkyria pukapuka</i>	<i>Amphipyndax stocki</i>	<i>Botryoscorbus holissi</i>	<i>Calocystetta</i> sp.	<i>Dictyopora</i> sp.	<i>Lophocystis</i> sp.	<i>Lychnocanoma amphitrite</i>	<i>Lychnocanoma babylonis</i>	<i>Amphisphaera aotea</i>	<i>Dictyomitra</i> sp.	<i>Stichomitra symbatos</i>
31X-CC, 18-28	303.08	M VR																																									
32X-CC, 0-15	312.9	M R	T	T R	T T R	F T R	R R F R R	R R A F	T	T	T	R	R	T R R R	R	R	R	R	R	R	R	R	R	R	R	R	R	R	R	R	R	R	R										
33X-CC, 7-17	322.68	M C	R	F C R	F C R	F C R	R R A F	R R A F	T	T	T	T	T	T	T	T	T	T	T	T	T	T	T	T	T	T	T	T	T	T	T	T	T										
34X-CC, 17-27	332.49	G VA																																									
35X-CC, 30-40	342.34	G R																																									
36X-CC, 15-25	351.71	G R																																									
37X-CC, 31-41	361.54	M VR																																									
38X-CC, 19-29	371.06	M VR	T	T	T	T																																					
39X-CC, 29-39	380.95	G R																																									
40X-CC, 0-10	390.07	G VR																																									
41X-CC, 47-57	399.87	G VR																																									
42X-CC, 22-37	409.69	G R	R	T																																							
43X-CC, 30-40	418.65	P VR																																									
44X-CC, 22-32	428.97	B																																									
45X-CC, 15-25	438.62	G T																																									
46X-CC, 29-34	445.83	B																																									
47X-CC, 16-26	457.46	P T																																									
48X-3, 44-45	461.34	P VR																																									
48X-CC, 13-23	463.32	B																																									
49X-1, 21-22	467.61	P A																																									
49X-CC, 0-10	473.02	P A																																									

**Table T11.** Compilation of age data from magnetostratigraphic interpretation splice of Site 1124.

Chron/Event (base)	Depth (mcd)	Age (Ma)	Chron/Event (base)	Depth (mcd)	Age (Ma)
C1n (Brunhes)	28.85-33.75	0.78	C4Ar.1r	189.13	9.23
C1r.1r	39.85	0.99	C4Ar.1n	189.58	9.308
C1r.1n (Jaramillo)	43.25	1.07	C4Ar.3r	199.23	9.74
C1r.2r-1r	50.3	1.201	C5n.2n	234.93	10.949
C1r.2r-1n (Cobb Mtn.)	52.7	1.211	C5r.1r	235.38	11.052
C1r.2r	64.5	1.77	C5r.1n	236.98	11.099
C2n (Olduvai)	67.65	1.95	Hiatus	~237-238	~11-14 m.y.
C2r.1r	71.25	2.14	C5ACr	238.23	14.178
C2r.1n (Reunion)	71.6	2.15	C5ADn	245.23-249.53	14.612
C2r.2n	81.6	2.581	C5ADR	252.78	14.8
C2An.1n	89.15	3.04	C5Bn.1n	255.58	14.888
C2An.1r (Kaena)	90.6	3.11	C5Bn.1r	268.78	15.034
C2An.2n	91.55	3.22	Hiatus	~257	~15-16.5 m.y.
C2An.2r (Mammoth)	93.2	3.33	C5Cn.3n	269.43	16.726
C2An.3n	97.3	3.58	Unconformity	Below 288.23	~17.5-22.5 m.y.
C2Ar	106.6	4.18	C6Bn?	313.13	
C3n.1n (Cochiti)	108.95	4.29	C6Cn.1n?	326.23	
C3n.1r	111.6	4.48	C6Cn.1r	334.43	23.677
C3n.2n (Nunivak)	113.65	4.62	C6Cn.2n	338.08	23.8
C3n.2r	115.65	4.8	C6Cn.2r	350.18	23.999
C3n.3n (Sidufjall)	116.9	4.89	C6Cn.3n	355.73	24.118
C3n.3r	118.3	4.98	C6Cr	381.83	24.73
C3n.4n (Thvera)	12.15	5.23	C7n.1n	382.58	24.781
C3r	135.1	5.894	C7n.1r	385.08	24.835
C3An.1n	140	6.137	C7n.2n	388.73	25.183
C3An.1r	143.1	6.269	C7r	394.43	25.496
C3An.2n	148.45	6.567	C7An	398.58	25.648
C3Ar	154.7	6.935	C7Ar	401.93	25.823
C3Bn	156.3	7.091	C8n	413.08	26.554
C3Br.1r	157.25	7.135	C8r	420.73	27.027
C3Br.1n	158.25	7.17	C9n (in hiatus)	422.88	<27.972
C3B2.2r	161.55	7.341	C12r	425.38	33.058
C3Br.2n	162.1	7.375	C13n (in hiatus)	431.18	<33.545
C3Br.3r	162.6	7.432	Hiatus	440.93	~37-58 m.y.
C4n.1n	164.3	7.562	C27r	457.33-460.18	62.499
C4n.1r	166.8	7.65	C29n	472.68	64.745
C4n.2n	171.63	8.072	C29r	481.33	65.578
C4r.1r	175.73	8.225			
C4r.1n	176.03	8.257			
C4r.2r	180.53	8.699			
C4An	185.63	9.025			

Note: Ages are from Berggren et al. (1995), and ages of new intervals are from linear interpolation using adjacent points.

**Table T12.** Composite depth section, Site 1124. (See table note. Continued on next six pages.)

Leg	Site	Hole	Core	Type	Section	Section length (m)	Depth (mbsf)	Offset (m)	Composite depth (mcd)
181	1124	A	1	H	1	1.50	0.00	2.32	2.32
181	1124	A	1	H	2	1.50	1.50	2.32	3.82
181	1124	A	1	H	3	1.50	3.00	2.32	5.32
181	1124	A	1	H	4	1.50	4.50	2.32	6.82
181	1124	A	1	H	5	1.50	6.00	2.32	8.32
181	1124	A	1	H	6	1.50	7.50	2.32	9.82
181	1124	A	1	H	7	0.36	9.00	2.32	11.32
181	1124	A	1	H	CC	0.15	9.36	2.32	11.68
181	1124	B	1	H	1	1.50	0.00	0.00	0.00
181	1124	B	1	H	2	1.50	1.50	0.00	1.50
181	1124	B	1	H	3	1.50	3.00	0.00	3.00
181	1124	B	1	H	4	0.66	4.50	0.00	4.50
181	1124	B	1	H	CC	0.25	5.16	0.00	5.16
181	1124	B	2	H	1	1.50	5.40	0.90	6.30
181	1124	B	2	H	2	1.50	6.90	0.90	7.80
181	1124	B	2	H	3	1.35	8.40	0.90	9.30
181	1124	B	2	H	CC	0.13	9.75	0.90	10.65
181	1124	C	1	X	1	1.35	8.00	0.00	8.00
181	1124	C	1	X	CC	0.16	9.35	0.00	9.35
181	1124	C	2	X	1	1.29	17.60	0.00	17.60
181	1124	C	2	X	2	0.71	18.89	0.00	18.89
181	1124	C	2	X	3	1.50	19.60	0.00	19.60
181	1124	C	2	X	4	0.94	21.10	0.00	21.10
181	1124	C	2	X	5	1.50	22.04	0.00	22.04
181	1124	C	2	X	6	1.50	23.54	0.00	23.54
181	1124	C	2	X	CC	0.24	25.04	0.00	25.04
181	1124	C	3	H	1	1.50	27.20	-2.40	24.80
181	1124	C	3	H	2	1.50	28.70	-2.40	26.30
181	1124	C	3	H	3	1.50	30.20	-2.40	27.80
181	1124	C	3	H	4	1.50	31.70	-2.40	29.30
181	1124	C	3	H	5	1.50	33.20	-2.40	30.80
181	1124	C	3	H	6	1.50	34.70	-2.40	32.30
181	1124	C	3	H	7	0.81	36.20	-2.40	33.80
181	1124	C	3	H	CC	0.19	37.01	-2.40	34.61
181	1124	C	4	H	1	1.50	36.70	-1.48	35.22
181	1124	C	4	H	2	1.50	38.20	-1.48	36.72
181	1124	C	4	H	3	1.50	39.70	-1.48	38.22
181	1124	C	4	H	4	1.50	41.20	-1.48	39.72
181	1124	C	4	H	5	1.50	42.70	-1.48	41.22
181	1124	C	4	H	6	1.50	44.20	-1.48	42.72
181	1124	C	4	H	7	0.59	45.70	-1.48	44.22
181	1124	C	4	H	CC	0.15	46.29	-1.48	44.81
181	1124	C	5	H	1	1.50	46.20	-0.50	45.70
181	1124	C	5	H	2	1.50	47.70	-0.50	47.20
181	1124	C	5	H	3	1.50	49.20	-0.50	48.70
181	1124	C	5	H	4	1.50	50.70	-0.50	50.20
181	1124	C	5	H	5	1.50	52.20	-0.50	51.70
181	1124	C	5	H	6	1.50	53.70	-0.50	53.20
181	1124	C	5	H	7	0.69	55.20	-0.50	54.70
181	1124	C	5	H	CC	0.30	55.89	-0.50	55.39
181	1124	C	6	H	1	1.50	55.70	0.32	56.02
181	1124	C	6	H	2	1.50	57.20	0.32	57.52
181	1124	C	6	H	3	1.50	58.70	0.32	59.02
181	1124	C	6	H	4	1.50	60.20	0.32	60.52
181	1124	C	6	H	5	1.50	61.70	0.32	62.02
181	1124	C	6	H	6	1.50	63.20	0.32	63.52
181	1124	C	6	H	7	0.35	64.70	0.32	65.02
181	1124	C	6	H	CC	0.23	65.05	0.32	65.37
181	1124	C	7	H	1	1.50	65.20	2.54	67.74
181	1124	C	7	H	2	1.50	66.70	2.54	69.24
181	1124	C	7	H	3	1.50	68.20	2.54	70.74
181	1124	C	7	H	4	1.50	69.70	2.54	72.24
181	1124	C	7	H	5	1.50	71.20	2.54	73.74
181	1124	C	7	H	6	1.50	72.70	2.54	75.24
181	1124	C	7	H	7	0.68	74.20	2.54	76.74
181	1124	C	7	H	CC	0.31	74.88	2.54	77.42
181	1124	C	8	H	1	1.50	74.70	2.32	77.02

**Table T12 (continued).**

Leg	Site	Hole	Core	Type	Section	Section length (m)	Depth (mbfs)	Offset (m)	Composite depth (mcd)
181	1124	C	8	H	2	1.50	76.20	2.32	78.52
181	1124	C	8	H	3	1.50	77.70	2.32	80.02
181	1124	C	8	H	4	1.50	79.20	2.32	81.52
181	1124	C	8	H	5	1.40	80.70	2.32	83.02
181	1124	C	8	H	6	0.70	82.10	2.32	84.42
181	1124	C	8	H	7	1.44	82.80	2.32	85.12
181	1124	C	8	H	CC	0.21	84.24	2.32	86.56
181	1124	C	9	H	1	1.50	84.20	2.80	87.00
181	1124	C	9	H	2	1.50	85.70	2.80	88.50
181	1124	C	9	H	3	1.50	87.20	2.80	90.00
181	1124	C	9	H	4	1.50	88.70	2.80	91.50
181	1124	C	9	H	5	1.50	90.20	2.80	93.00
181	1124	C	9	H	6	1.50	91.70	2.80	94.50
181	1124	C	9	H	7	0.71	93.20	2.80	96.00
181	1124	C	9	H	CC	0.33	93.91	2.80	96.71
181	1124	C	10	H	1	1.50	93.70	4.27	97.97
181	1124	C	10	H	2	1.50	95.20	4.27	99.47
181	1124	C	10	H	3	1.50	96.70	4.27	100.97
181	1124	C	10	H	4	1.50	98.20	4.27	102.47
181	1124	C	10	H	5	1.50	99.70	4.27	103.97
181	1124	C	10	H	6	1.52	101.20	4.27	105.47
181	1124	C	10	H	CC	0.10	102.72	4.27	106.99
181	1124	C	11	H	1	1.50	103.20	6.19	109.39
181	1124	C	11	H	2	1.50	104.70	6.19	110.89
181	1124	C	11	H	3	1.50	106.20	6.19	112.39
181	1124	C	11	H	4	1.50	107.70	6.19	113.89
181	1124	C	11	H	5	1.50	109.20	6.19	115.39
181	1124	C	11	H	6	1.50	110.70	6.19	116.89
181	1124	C	11	H	7	0.55	112.20	6.19	118.39
181	1124	C	11	H	CC	0.30	112.75	6.19	118.94
181	1124	C	12	H	1	1.50	112.70	7.19	119.89
181	1124	C	12	H	2	1.50	114.20	7.19	121.39
181	1124	C	12	H	3	1.50	115.70	7.19	122.89
181	1124	C	12	H	4	1.50	117.20	7.19	124.39
181	1124	C	12	H	5	1.50	118.70	7.19	125.89
181	1124	C	12	H	6	1.50	120.20	7.19	127.39
181	1124	C	12	H	CC	0.15	121.70	7.19	128.89
181	1124	C	13	H	1	1.50	122.20	8.61	130.81
181	1124	C	13	H	2	1.50	123.70	8.61	132.31
181	1124	C	13	H	3	1.50	125.20	8.61	133.81
181	1124	C	13	H	4	1.50	126.70	8.61	135.31
181	1124	C	13	H	5	1.50	128.20	8.61	136.81
181	1124	C	13	H	6	1.50	129.70	8.61	138.31
181	1124	C	13	H	7	0.68	131.20	8.61	139.81
181	1124	C	13	H	CC	0.23	131.88	8.61	140.49
181	1124	C	14	H	1	1.50	131.70	10.19	141.89
181	1124	C	14	H	2	1.50	133.20	10.19	143.39
181	1124	C	14	H	3	1.50	134.70	10.19	144.89
181	1124	C	14	H	4	1.50	136.20	10.19	146.39
181	1124	C	14	H	5	1.50	137.70	10.19	147.89
181	1124	C	14	H	6	1.50	139.20	10.19	149.39
181	1124	C	14	H	7	0.36	140.70	10.19	150.89
181	1124	C	14	H	CC	0.15	141.06	10.19	151.25
181	1124	C	15	H	1	1.50	141.20	11.35	152.55
181	1124	C	15	H	2	1.50	142.70	11.35	154.05
181	1124	C	15	H	3	1.50	144.20	11.35	155.55
181	1124	C	15	H	4	1.50	145.70	11.35	157.05
181	1124	C	15	H	5	1.50	147.20	11.35	158.55
181	1124	C	15	H	6	1.50	148.70	11.35	160.05
181	1124	C	15	H	7	0.25	150.20	11.35	161.55
181	1124	C	15	H	CC	0.20	150.45	11.35	161.80
181	1124	C	16	H	1	1.50	150.70	11.83	162.53
181	1124	C	16	H	2	1.50	152.20	11.83	164.03
181	1124	C	16	H	3	1.50	153.70	11.83	165.53
181	1124	C	16	H	4	1.50	155.20	11.83	167.03
181	1124	C	16	H	5	1.50	156.70	11.83	168.53
181	1124	C	16	H	6	1.10	158.20	11.83	170.03
181	1124	C	16	H	CC	0.12	159.30	11.83	171.13
181	1124	C	17	X	1	1.50	159.20	11.83	171.03
181	1124	C	17	X	2	1.50	160.70	11.83	172.53

**Table T12 (continued).**

Leg	Site	Hole	Core	Type	Section	Section length (m)	Depth (mbsf)	Offset (m)	Composite depth (mcd)
181	1124	C	17	X	3	1.50	162.20	11.83	174.03
181	1124	C	17	X	4	1.50	163.70	11.83	175.53
181	1124	C	17	X	5	1.50	165.20	11.83	177.03
181	1124	C	17	X	6	1.50	166.70	11.83	178.53
181	1124	C	17	X	7	0.39	168.20	11.83	180.03
181	1124	C	17	X	CC	0.21	168.59	11.83	180.42
181	1124	C	18	X	1	1.50	168.80	11.83	180.63
181	1124	C	18	X	2	1.50	170.30	11.83	182.13
181	1124	C	18	X	3	1.50	171.80	11.83	183.63
181	1124	C	18	X	4	1.50	173.30	11.83	185.13
181	1124	C	18	X	5	1.50	174.80	11.83	186.63
181	1124	C	18	X	6	1.50	176.30	11.83	188.13
181	1124	C	18	X	7	0.40	177.80	11.83	189.63
181	1124	C	18	X	CC	0.18	178.20	11.83	190.03
181	1124	C	19	X	1	1.50	178.40	11.83	190.23
181	1124	C	19	X	2	1.50	179.90	11.83	191.73
181	1124	C	19	X	3	1.50	181.40	11.83	193.23
181	1124	C	19	X	4	1.50	182.90	11.83	194.73
181	1124	C	19	X	5	1.50	184.40	11.83	196.23
181	1124	C	19	X	6	1.50	185.90	11.83	197.73
181	1124	C	19	X	7	0.53	187.40	11.83	199.23
181	1124	C	19	X	CC	0.34	187.93	11.83	199.76
181	1124	C	20	X	1	1.50	188.00	11.83	199.83
181	1124	C	20	X	2	1.50	189.50	11.83	201.33
181	1124	C	20	X	3	1.50	191.00	11.83	202.83
181	1124	C	20	X	4	1.50	192.50	11.83	204.33
181	1124	C	20	X	5	1.50	194.00	11.83	205.83
181	1124	C	20	X	6	1.50	195.50	11.83	207.33
181	1124	C	20	X	7	0.33	197.00	11.83	208.83
181	1124	C	20	X	CC	0.34	197.33	11.83	209.16
181	1124	C	21	X	1	1.50	197.70	11.83	209.53
181	1124	C	21	X	2	1.50	199.20	11.83	211.03
181	1124	C	21	X	3	1.50	200.70	11.83	212.53
181	1124	C	21	X	4	1.50	202.20	11.83	214.03
181	1124	C	21	X	5	1.50	203.70	11.83	215.53
181	1124	C	21	X	6	1.50	205.20	11.83	217.03
181	1124	C	21	X	7	0.45	206.70	11.83	218.53
181	1124	C	21	X	CC	0.31	207.15	11.83	218.98
181	1124	C	22	X	1	1.50	207.30	11.83	219.13
181	1124	C	22	X	2	1.50	208.80	11.83	220.63
181	1124	C	22	X	3	1.50	210.30	11.83	222.13
181	1124	C	22	X	4	1.50	211.80	11.83	223.63
181	1124	C	22	X	5	1.50	213.30	11.83	225.13
181	1124	C	22	X	6	1.50	214.80	11.83	226.63
181	1124	C	22	X	7	0.28	216.30	11.83	228.13
181	1124	C	22	X	CC	0.48	216.58	11.83	228.41
181	1124	C	23	X	1	1.50	216.90	11.83	228.73
181	1124	C	23	X	2	1.50	218.40	11.83	230.23
181	1124	C	23	X	3	1.50	219.90	11.83	231.73
181	1124	C	23	X	4	1.50	221.40	11.83	233.23
181	1124	C	23	X	5	1.50	222.90	11.83	234.73
181	1124	C	23	X	6	1.50	224.40	11.83	236.23
181	1124	C	23	X	7	0.48	225.90	11.83	237.73
181	1124	C	23	X	CC	0.31	226.38	11.83	238.21
181	1124	C	24	X	1	1.50	226.50	11.83	238.33
181	1124	C	24	X	2	1.50	228.00	11.83	239.83
181	1124	C	24	X	3	1.50	229.50	11.83	241.33
181	1124	C	24	X	4	1.50	231.00	11.83	242.83
181	1124	C	24	X	5	1.50	232.50	11.83	244.33
181	1124	C	24	X	6	1.50	234.00	11.83	245.83
181	1124	C	24	X	7	0.33	235.50	11.83	247.33
181	1124	C	24	X	CC	0.33	235.83	11.83	247.66
181	1124	C	25	X	1	1.50	236.20	11.83	248.03
181	1124	C	25	X	2	1.50	237.70	11.83	249.53
181	1124	C	25	X	3	1.50	239.20	11.83	251.03
181	1124	C	25	X	4	1.50	240.70	11.83	252.53
181	1124	C	25	X	5	1.50	242.20	11.83	254.03
181	1124	C	25	X	6	1.50	243.70	11.83	255.53
181	1124	C	25	X	7	0.38	245.20	11.83	257.03
181	1124	C	25	X	CC	0.40	245.58	11.83	257.41

**Table T12 (continued).**

Leg	Site	Hole	Core	Type	Section	Section length (m)	Depth (mbsf)	Offset (m)	Composite depth (mcd)
181	1124	C	26	X	1	1.50	245.80	11.83	257.63
181	1124	C	26	X	2	1.50	247.30	11.83	259.13
181	1124	C	26	X	3	1.50	248.80	11.83	260.63
181	1124	C	26	X	4	1.50	250.30	11.83	262.13
181	1124	C	26	X	5	1.50	251.80	11.83	263.63
181	1124	C	26	X	6	1.50	253.30	11.83	265.13
181	1124	C	26	X	7	0.33	254.80	11.83	266.63
181	1124	C	26	X	CC	0.37	255.13	11.83	266.96
181	1124	C	27	X	1	1.50	255.40	11.83	267.23
181	1124	C	27	X	2	1.50	256.90	11.83	268.73
181	1124	C	27	X	3	1.50	258.40	11.83	270.23
181	1124	C	27	X	4	1.50	259.90	11.83	271.73
181	1124	C	27	X	5	1.50	261.40	11.83	273.23
181	1124	C	27	X	6	1.50	262.90	11.83	274.73
181	1124	C	27	X	7	0.34	264.40	11.83	276.23
181	1124	C	27	X	CC	0.31	264.74	11.83	276.57
181	1124	C	28	X	1	1.45	265.10	11.83	276.93
181	1124	C	28	X	2	1.50	266.55	11.83	278.38
181	1124	C	28	X	3	1.50	268.05	11.83	279.88
181	1124	C	28	X	4	1.50	269.55	11.83	281.38
181	1124	C	28	X	5	1.50	271.05	11.83	282.88
181	1124	C	28	X	6	1.50	272.55	11.83	284.38
181	1124	C	28	X	7	0.36	274.05	11.83	285.88
181	1124	C	28	X	CC	0.31	274.41	11.83	286.24
181	1124	C	29	X	1	1.50	274.70	11.83	286.53
181	1124	C	29	X	2	0.21	276.20	11.83	288.03
181	1124	C	29	X	CC	0.10	276.41	11.83	288.24
181	1124	C	31	X	1	1.50	294.00	11.83	305.83
181	1124	C	31	X	2	1.50	295.50	11.83	307.33
181	1124	C	31	X	3	1.50	297.00	11.83	308.83
181	1124	C	31	X	4	1.50	298.50	11.83	310.33
181	1124	C	31	X	5	1.40	300.00	11.83	311.83
181	1124	C	31	X	6	1.50	301.40	11.83	313.23
181	1124	C	31	X	CC	0.28	302.90	11.83	314.73
181	1124	C	32	X	1	1.50	303.60	11.83	315.43
181	1124	C	32	X	2	1.50	305.10	11.83	316.93
181	1124	C	32	X	3	1.50	306.60	11.83	318.43
181	1124	C	32	X	4	1.50	308.10	11.83	319.93
181	1124	C	32	X	5	1.50	309.60	11.83	321.43
181	1124	C	32	X	6	0.80	311.10	11.83	322.93
181	1124	C	32	X	7	1.00	311.90	11.83	323.73
181	1124	C	32	X	CC	0.15	312.90	11.83	324.73
181	1124	C	33	X	1	1.50	313.30	11.83	325.13
181	1124	C	33	X	2	1.50	314.80	11.83	326.63
181	1124	C	33	X	3	1.50	316.30	11.83	328.13
181	1124	C	33	X	4	1.50	317.80	11.83	329.63
181	1124	C	33	X	5	1.50	319.30	11.83	331.13
181	1124	C	33	X	6	1.50	320.80	11.83	332.63
181	1124	C	33	X	7	0.31	322.30	11.83	334.13
181	1124	C	33	X	CC	0.17	322.61	11.83	334.44
181	1124	C	34	X	1	1.50	322.90	11.83	334.73
181	1124	C	34	X	2	1.50	324.40	11.83	336.23
181	1124	C	34	X	3	1.50	325.90	11.83	337.73
181	1124	C	34	X	4	1.50	327.40	11.83	339.23
181	1124	C	34	X	5	1.50	328.90	11.83	340.73
181	1124	C	34	X	6	1.50	330.40	11.83	342.23
181	1124	C	34	X	7	0.42	331.90	11.83	343.73
181	1124	C	34	X	CC	0.27	332.32	11.83	344.15
181	1124	C	35	X	1	1.50	332.60	11.83	344.43
181	1124	C	35	X	2	1.50	334.10	11.83	345.93
181	1124	C	35	X	3	1.50	335.60	11.83	347.43
181	1124	C	35	X	4	1.50	337.10	11.83	348.93
181	1124	C	35	X	5	1.50	338.60	11.83	350.43
181	1124	C	35	X	6	1.50	340.10	11.83	351.93
181	1124	C	35	X	7	0.44	341.60	11.83	353.43
181	1124	C	35	X	CC	0.40	342.04	11.83	353.87
181	1124	C	36	X	1	1.50	342.20	11.83	354.03
181	1124	C	36	X	2	1.50	343.70	11.83	355.53
181	1124	C	36	X	3	1.50	345.20	11.83	357.03
181	1124	C	36	X	4	1.50	346.70	11.83	358.53

**Table T12 (continued).**

Leg	Site	Hole	Core	Type	Section	Section length (m)	Depth (mbsf)	Offset (m)	Composite depth (mcd)
181	1124	C	36	X	5	1.50	348.20	11.83	360.03
181	1124	C	36	X	6	1.50	349.70	11.83	361.53
181	1124	C	36	X	7	0.36	351.20	11.83	363.03
181	1124	C	36	X	CC	0.25	351.56	11.83	363.39
181	1124	C	37	X	1	1.50	351.90	11.83	363.73
181	1124	C	37	X	2	1.50	353.40	11.83	365.23
181	1124	C	37	X	3	1.50	354.90	11.83	366.73
181	1124	C	37	X	4	1.50	356.40	11.83	368.23
181	1124	C	37	X	5	1.50	357.90	11.83	369.73
181	1124	C	37	X	6	1.50	359.40	11.83	371.23
181	1124	C	37	X	7	0.33	360.90	11.83	372.73
181	1124	C	37	X	CC	0.41	361.23	11.83	373.06
181	1124	C	38	X	1	1.50	361.50	11.83	373.33
181	1124	C	38	X	2	1.50	363.00	11.83	374.83
181	1124	C	38	X	3	1.50	364.50	11.83	376.33
181	1124	C	38	X	4	1.50	366.00	11.83	377.83
181	1124	C	38	X	5	1.50	367.50	11.83	379.33
181	1124	C	38	X	6	1.50	369.00	11.83	380.83
181	1124	C	38	X	7	0.37	370.50	11.83	382.33
181	1124	C	38	X	CC	0.29	370.87	11.83	382.70
181	1124	C	39	X	1	1.50	371.20	11.83	383.03
181	1124	C	39	X	2	1.50	372.70	11.83	384.53
181	1124	C	39	X	3	1.50	374.20	11.83	386.03
181	1124	C	39	X	4	1.50	375.70	11.83	387.53
181	1124	C	39	X	5	1.50	377.20	11.83	389.03
181	1124	C	39	X	6	1.50	378.70	11.83	390.53
181	1124	C	39	X	7	0.46	380.20	11.83	392.03
181	1124	C	39	X	CC	0.39	380.66	11.83	392.49
181	1124	C	40	X	1	1.50	380.80	11.83	392.63
181	1124	C	40	X	2	1.50	382.30	11.83	394.13
181	1124	C	40	X	3	1.50	383.80	11.83	395.63
181	1124	C	40	X	4	1.50	385.30	11.83	397.13
181	1124	C	40	X	5	1.50	386.80	11.83	398.63
181	1124	C	40	X	6	1.50	388.30	11.83	400.13
181	1124	C	40	X	7	0.27	389.80	11.83	401.63
181	1124	C	40	X	CC	0.10	390.07	11.83	401.90
181	1124	C	41	X	1	1.50	390.40	11.83	402.23
181	1124	C	41	X	2	1.50	391.90	11.83	403.73
181	1124	C	41	X	3	1.50	393.40	11.83	405.23
181	1124	C	41	X	4	1.50	394.90	11.83	406.73
181	1124	C	41	X	5	1.50	396.40	11.83	408.23
181	1124	C	41	X	6	1.50	397.90	11.83	409.73
181	1124	C	41	X	CC	0.57	399.40	11.83	411.23
181	1124	C	42	X	1	1.50	400.10	11.83	411.93
181	1124	C	42	X	2	1.50	401.60	11.83	413.43
181	1124	C	42	X	3	1.50	403.10	11.83	414.93
181	1124	C	42	X	4	1.50	404.60	11.83	416.43
181	1124	C	42	X	5	1.50	406.10	11.83	417.93
181	1124	C	42	X	6	1.50	407.60	11.83	419.43
181	1124	C	42	X	7	0.37	409.10	11.83	420.93
181	1124	C	42	X	CC	0.37	409.47	11.83	421.30
181	1124	C	43	X	1	1.50	409.70	11.83	421.53
181	1124	C	43	X	2	1.50	411.20	11.83	423.03
181	1124	C	43	X	3	1.50	412.70	11.83	424.53
181	1124	C	43	X	4	1.50	414.20	11.83	426.03
181	1124	C	43	X	5	1.50	415.70	11.83	427.53
181	1124	C	43	X	6	1.15	417.20	11.83	429.03
181	1124	C	43	X	CC	0.40	418.35	11.83	430.18
181	1124	C	44	X	1	1.50	419.30	11.83	431.13
181	1124	C	44	X	2	1.50	420.80	11.83	432.63
181	1124	C	44	X	3	1.50	422.30	11.83	434.13
181	1124	C	44	X	4	1.50	423.80	11.83	435.63
181	1124	C	44	X	5	1.50	425.30	11.83	437.13
181	1124	C	44	X	6	1.50	426.80	11.83	438.63
181	1124	C	44	X	7	0.45	428.30	11.83	440.13
181	1124	C	44	X	CC	0.32	428.75	11.83	440.58
181	1124	C	45	X	1	1.50	429.00	11.83	440.83
181	1124	C	45	X	2	1.50	430.50	11.83	442.33
181	1124	C	45	X	3	1.50	432.00	11.83	443.83
181	1124	C	45	X	4	1.50	433.50	11.83	445.33

**Table T12 (continued).**

Leg	Site	Hole	Core	Type	Section	Section length (m)	Depth (mbsf)	Offset (m)	Composite depth (mcd)
181	1124	C	45	X	5	1.50	435.00	11.83	446.83
181	1124	C	45	X	6	1.50	436.50	11.83	448.33
181	1124	C	45	X	7	0.47	438.00	11.83	449.83
181	1124	C	45	X	CC	0.25	438.47	11.83	450.30
181	1124	C	46	X	1	1.50	438.70	11.83	450.53
181	1124	C	46	X	2	1.50	440.20	11.83	452.03
181	1124	C	46	X	3	1.50	441.70	11.83	453.53
181	1124	C	46	X	4	1.50	443.20	11.83	455.03
181	1124	C	46	X	5	0.84	444.70	11.83	456.53
181	1124	C	46	X	CC	0.34	445.54	11.83	457.37
181	1124	C	47	X	1	1.50	448.30	11.83	460.13
181	1124	C	47	X	2	1.50	449.80	11.83	461.63
181	1124	C	47	X	3	1.50	451.30	11.83	463.13
181	1124	C	47	X	4	1.50	452.80	11.83	464.63
181	1124	C	47	X	5	1.50	454.30	11.83	466.13
181	1124	C	47	X	6	1.50	455.80	11.83	467.63
181	1124	C	47	X	CC	0.26	457.30	11.83	469.13
181	1124	C	48	X	1	1.50	457.90	11.83	469.73
181	1124	C	48	X	2	1.50	459.40	11.83	471.23
181	1124	C	48	X	3	1.50	460.90	11.83	472.73
181	1124	C	48	X	4	0.79	462.40	11.83	474.23
181	1124	C	48	X	CC	0.23	463.19	11.83	475.02
181	1124	C	49	X	1	1.50	467.40	11.83	479.23
181	1124	C	49	X	2	1.50	468.90	11.83	480.73
181	1124	C	49	X	3	1.50	470.40	11.83	482.23
181	1124	C	49	X	4	1.12	471.90	11.83	483.73
181	1124	C	49	X	CC	0.10	473.02	11.83	484.85
181	1124	D	1	H	1	1.50	22.60	-3.62	18.98
181	1124	D	1	H	2	1.50	24.10	-3.62	20.48
181	1124	D	1	H	3	1.50	25.60	-3.62	21.98
181	1124	D	1	H	4	1.50	27.10	-3.62	23.48
181	1124	D	1	H	5	1.50	28.60	-3.62	24.98
181	1124	D	1	H	6	1.50	30.10	-3.62	26.48
181	1124	D	1	H	7	0.37	31.60	-3.62	27.98
181	1124	D	1	H	CC	0.19	31.97	-3.62	28.35
181	1124	D	2	H	1	1.50	32.10	-2.04	30.06
181	1124	D	2	H	2	1.50	33.60	-2.04	31.56
181	1124	D	2	H	3	1.50	35.10	-2.04	33.06
181	1124	D	2	H	4	1.50	36.60	-2.04	34.56
181	1124	D	2	H	5	1.50	38.10	-2.04	36.06
181	1124	D	2	H	6	0.07	39.60	-2.04	37.56
181	1124	D	2	H	CC	0.18	39.67	-2.04	37.63
181	1124	D	3	H	1	1.50	41.60	-0.78	40.82
181	1124	D	3	H	2	1.50	43.10	-0.78	42.32
181	1124	D	3	H	3	1.50	44.60	-0.78	43.82
181	1124	D	3	H	4	1.50	46.10	-0.78	45.32
181	1124	D	3	H	5	1.50	47.60	-0.78	46.82
181	1124	D	3	H	6	1.24	49.10	-0.78	48.32
181	1124	D	3	H	CC	0.23	50.34	-0.78	49.56
181	1124	D	4	H	1	1.50	51.10	0.42	51.52
181	1124	D	4	H	2	1.50	52.60	0.42	53.02
181	1124	D	4	H	3	1.02	54.10	0.42	54.52
181	1124	D	4	H	4	1.50	55.12	0.42	55.54
181	1124	D	4	H	5	1.50	56.62	0.42	57.04
181	1124	D	4	H	6	1.40	58.12	0.42	58.54
181	1124	D	4	H	CC	0.10	59.52	0.42	59.94
181	1124	D	5	H	1	1.50	60.60	2.08	62.68
181	1124	D	5	H	2	1.50	62.10	2.08	64.18
181	1124	D	5	H	3	1.50	63.60	2.08	65.68
181	1124	D	5	H	4	1.50	65.10	2.08	67.18
181	1124	D	5	H	5	1.50	66.60	2.08	68.68
181	1124	D	5	H	6	1.50	68.10	2.08	70.18
181	1124	D	5	H	7	0.51	69.60	2.08	71.68
181	1124	D	5	H	CC	0.26	70.11	2.08	72.19
181	1124	D	6	H	1	1.50	70.10	3.16	73.26
181	1124	D	6	H	2	1.50	71.60	3.16	74.76
181	1124	D	6	H	3	1.50	73.10	3.16	76.26
181	1124	D	6	H	4	1.50	74.60	3.16	77.76
181	1124	D	6	H	5	1.50	76.10	3.16	79.26
181	1124	D	6	H	6	1.50	77.60	3.16	80.76

**Table T12 (continued).**

Leg	Site	Hole	Core	Type	Section	Section length (m)	Depth (mbsf)	Offset (m)	Composite depth (mcd)
181	1124	D	6	H	CC	0.30	79.10	3.16	82.26
181	1124	D	7	H	1	1.50	79.60	4.06	83.66
181	1124	D	7	H	2	1.50	81.10	4.06	85.16
181	1124	D	7	H	3	1.50	82.60	4.06	86.66
181	1124	D	7	H	4	1.50	84.10	4.06	88.16
181	1124	D	7	H	5	1.50	85.60	4.06	89.66
181	1124	D	7	H	6	1.50	87.10	4.06	91.16
181	1124	D	7	H	7	0.78	88.60	4.06	92.66
181	1124	D	7	H	CC	0.17	89.38	4.06	93.44
181	1124	D	8	H	1	1.50	89.10	5.98	95.08
181	1124	D	8	H	2	1.50	90.60	5.98	96.58
181	1124	D	8	H	3	1.50	92.10	5.98	98.08
181	1124	D	8	H	4	1.41	93.60	5.98	99.58
181	1124	D	8	H	5	1.50	95.01	5.98	100.99
181	1124	D	8	H	6	1.50	96.51	5.98	102.49
181	1124	D	8	H	CC	0.10	98.01	5.98	103.99
181	1124	D	9	H	1	1.50	98.60	6.01	104.61
181	1124	D	9	H	2	1.50	100.10	6.01	106.11
181	1124	D	9	H	3	1.50	101.60	6.01	107.61
181	1124	D	9	H	4	1.50	103.10	6.01	109.11
181	1124	D	9	H	5	1.50	104.60	6.01	110.61
181	1124	D	9	H	6	1.50	106.10	6.01	112.11
181	1124	D	9	H	7	0.60	107.60	6.01	113.61
181	1124	D	9	H	CC	0.28	108.20	6.01	114.21
181	1124	D	10	H	1	1.50	108.10	6.51	114.61
181	1124	D	10	H	2	1.50	109.60	6.51	116.11
181	1124	D	10	H	3	1.50	111.10	6.51	117.61
181	1124	D	10	H	4	1.50	112.60	6.51	119.11
181	1124	D	10	H	5	1.50	114.10	6.51	120.61
181	1124	D	10	H	6	1.50	115.60	6.51	122.11
181	1124	D	10	H	7	0.62	117.10	6.51	123.61
181	1124	D	10	H	CC	0.10	117.72	6.51	124.23
181	1124	D	11	H	1	1.50	117.60	7.71	125.31
181	1124	D	11	H	2	1.50	119.10	7.71	126.81
181	1124	D	11	H	3	1.50	120.60	7.71	128.31
181	1124	D	11	H	4	1.50	122.10	7.71	129.81
181	1124	D	11	H	5	1.50	123.60	7.71	131.31
181	1124	D	11	H	6	1.50	125.10	7.71	132.81
181	1124	D	11	H	7	0.72	126.60	7.71	134.31
181	1124	D	11	H	CC	0.17	127.32	7.71	135.03
181	1124	D	12	H	1	1.50	127.10	8.95	136.05
181	1124	D	12	H	2	1.50	128.60	8.95	137.55
181	1124	D	12	H	3	1.50	130.10	8.95	139.05
181	1124	D	12	H	4	1.50	131.60	8.95	140.55
181	1124	D	12	H	5	1.50	133.10	8.95	142.05
181	1124	D	12	H	6	1.50	134.60	8.95	143.55
181	1124	D	12	H	7	0.55	136.10	8.95	145.05
181	1124	D	12	H	CC	0.18	136.65	8.95	145.60
181	1124	D	13	H	1	1.50	136.60	9.79	146.39
181	1124	D	13	H	2	1.50	138.10	9.79	147.89
181	1124	D	13	H	3	1.50	139.60	9.79	149.39
181	1124	D	13	H	4	1.50	141.10	9.79	150.89
181	1124	D	13	H	5	1.50	142.60	9.79	152.39
181	1124	D	13	H	6	1.50	144.10	9.79	153.89
181	1124	D	13	H	7	0.78	145.60	9.79	155.39
181	1124	D	13	H	CC	0.26	146.38	9.79	156.17
181	1124	D	14	H	1	1.50	146.10	10.31	156.41
181	1124	D	14	H	2	1.50	147.60	10.31	157.91
181	1124	D	14	H	3	1.50	149.10	10.31	159.41
181	1124	D	14	H	4	1.50	150.60	10.31	160.91
181	1124	D	14	H	5	1.50	152.10	10.31	162.41
181	1124	D	14	H	6	1.50	153.60	10.31	163.91
181	1124	D	14	H	7	0.55	155.10	10.31	165.41
181	1124	D	14	H	CC	0.20	155.65	10.31	165.96

Note: Most samples are from core catchers. This table is also available in [ASCII format](#).

**Table T13.** Splice tie points, Site 1124.

Site	Hole	Core	Type	Section	Depth in section (cm)			Site	Hole	Core	Type	Section	Depth in section (cm)			
					Depth (mbsf)	Depth (mcd)	Depth (mcd)						Depth (mbsf)	Depth (mcd)		
<b>Upper splice</b>																
1124	B	1	H	3	100	4.00	4.00	Tie to	1124	A	1	H	2	17	1.68	4.00
1124	A	1	H	7	34	9.34	11.66									
<b>Lower splice</b>																
1124	C	2	X	2	56	19.45	19.45	Tie to	1124	D	1	H	1	46.5	23.07	19.45
1124	D	1	H	6	80	30.90	27.28	Tie to	1124	C	3	H	2	98	29.68	27.28
1124	C	3	H	5	100	34.20	31.80	Tie to	1124	D	2	H	2	24	33.84	31.80
1124	D	2	H	5	56	38.66	36.62	Tie to	1124	C	4	H	1	140	38.10	36.62
1124	C	4	H	6	104	45.24	43.76	Tie to	1124	D	3	H	2	144	44.54	43.76
1124	D	3	H	6	42	49.52	48.74	Tie to	1124	C	5	H	3	4	49.24	48.74
1124	C	5	H	7	30	55.50	55.00	Tie to	1124	D	4	H	3	48	54.58	55.00
1124	D	4	H	5	122	57.84	58.26	Tie to	1124	C	6	H	2	74	57.94	58.26
1124	C	6	H	6	12	63.32	63.64	Tie to	1124	D	5	H	1	96	61.56	63.64
1124	D	5	H	5	20	66.80	68.88	Tie to	1124	C	7	H	1	114	66.34	68.88
1124	C	7	H	5	102	72.22	74.76	Tie to	1124	D	6	H	1	150	71.60	74.76
1124	D	6	H	5	144	77.54	80.70	Tie to	1124	C	8	H	3	68	78.38	80.70
1124	C	8	H	6	38	82.48	84.80	Tie to	1124	D	7	H	1	114	80.74	84.80
1124	D	7	H	5	16	85.76	89.82	Tie to	1124	C	9	H	2	132	87.02	89.82
1124	C	9	H	7	10	93.30	96.10	Tie to	1124	D	8	H	1	102	90.12	96.10
1124	D	8	H	5	92	95.93	101.91	Tie to	1124	C	10	H	3	94	97.64	101.91
1124	C	10	H	6	72	101.92	106.19	Tie to	1124	D	9	H	2	8	100.18	106.19
1124	D	9	H	6	66	106.76	112.77	Tie to	1124	C	11	H	3	38	106.58	112.77
1124	C	11	H	6	138	112.08	118.27	Tie to	1124	D	10	H	3	66	111.76	118.27
1124	D	10	H	6	124	116.84	123.35	Tie to	1124	C	12	H	3	46	116.16	123.35
1124	C	12	H	5	96	119.66	126.85	Tie to	1124	D	11	H	2	4	119.14	126.85
1124	D	11	H	6	116	126.26	133.97	Tie to	1124	C	13	H	3	16	125.36	133.97
1124	C	13	H	5	128	129.48	138.09	Tie to	1124	D	12	H	2	54	129.14	138.09
1124	D	12	H	6	68	135.28	144.23	Tie to	1124	C	14	H	2	84	134.04	144.23
1124	C	14	H	4	112	137.32	147.51	Tie to	1124	D	13	H	1	112	137.72	147.51
1124	D	13	H	6	124	145.34	155.13	Tie to	1124	C	15	H	2	108	143.78	155.13
1124	C	15	H	4	144	147.14	158.49	Tie to	1124	D	14	H	2	57	148.18	158.49
1124	D	14	H	6	2	153.62	163.93	Tie to	1124	C	16	H	1	140	152.10	163.93
1124	C	16	H	6	108	159.28	171.11									

Note: This table is also available in [ASCII format](#).

**Table T14.** Biostratigraphic events identified at Site 1124, using shipboard analysis data. (See table note. Continued on next page.)

	Events	Group	Age (Ma)	Core, section, interval (cm)	Depth (mbsf)	Depth (mcd)
1	LO <i>Globorotalia puncticuloides</i>	F	~0.6	1124A-1H-1, 18–20 cm	0.2	2.52
2	LO <i>Pseudoemiliania lacunosa</i>	N	0.42	1124C-2X-3, 146 cm	21.06	21.06
3	LO <i>Nitzschia reinholdii</i>	D	0.65	1124C-2X-CC	25.18	25.18
4	LO <i>Nitzschia barronii</i>	D	1.25	1124C-4H-CC	46.29	44.81
5	LO <i>Globorotalia tosaensis</i>	F	~1	1124C-5H-5, 88–93 cm	53.1	52.6
6	FO <i>Globorotalia crassula</i>	F	2.6	1124C-5H-5, 88–93 cm	53.1	52.6
7	FO <i>Globorotalia truncatulinoides</i>	F	~2	1124C-5H-CC	56.1	55.6
8	LO <i>Calcidiscus macintyrei</i>	N	1.60	1124C-6H-CC	65.18	65.5
9	FO <i>Gephyrocapsa caribbeanica</i>	N	1.67	1124C-6H-CC	65.18	65.5
10	LO <i>Discoaster brouweri</i>	N	1.96	1124C-7H-CC	75.09	77.41
11	FO <i>Cycladophora davisiана</i>	R	2.61	1124C-7H-CC	75.09	77.41
12	LO <i>Globorotalia inflata triangula</i>	F	~2	1124C-7H-CC	75.1	77.64
13	LO <i>Globorotalia crassaformis</i> (dextral)	F	2.1	1124C-8H-3, 140–142 cm	79.2	81.5
14	FO <i>Globorotalia crassaformis</i> (dextral)	F	3.0	1124C-8H-5, 10–12 cm	80.1	82.4
15	LO <i>Discoaster pentaradiatus</i>	N	2.30	1124C-8H-CC	84.35	87.15
16	LO <i>Globorotalia crassaconica</i>	F	3.0	1124C-9H-CC	94.1	98.4
17	LO <i>Discoaster surculus</i>	N	2.61	1124C-9H-CC	94.14	98.41
18	FO <i>Pseudoemiliania lacunosa</i>	N	4.0	1124C-9H-CC	94.14	98.41
19	FO <i>Globorotalia puncticuloides</i>	F	3.6	1124C-10H-1, 76–78 cm	94.5	98.8
20	FO <i>Globorotalia inflata</i>	F	3.7	1124C-10H-1, 76–78 cm	94.5	98.8
21	FO <i>Globorotalia inflata triangula</i>	F	3.6	1124C-10H-1, 76–78 cm	94.5	98.8
22	LCO <i>Globorotalia pliozea</i>	F	3.6	1124C-10H-1, 76–78 cm	94.5	98.8
23	LO <i>Reticulofenestra pseudoumbilicus</i>	N	3.82	1124C-10H-CC	102.72	106.99
24	FO <i>Globorotalia crassaconica</i>	F	4.7	1124C-11H-1, 89–91 cm	104.1	110.29
25	FO <i>Globorotalia puncticulata</i>	F	5.2	1124C-11H-3, 74–78 cm	106.9	113.09
26	FO <i>Globorotalia pliozea</i>	F	5.4	1124C-11H-CC	113.0	120.19
27	LO <i>Globorotalia puncticulata</i>	F	3.7	1124C-11H-CC	113.05	120.24
28	LO <i>Globorotalia miotumida</i>	F	5.6	1124C-14H-2, 100–120 cm	134.2	144.39
29	FO <i>Sphaeroidinella paenedehiscens</i>	F	~8	1124C-14H-CC	141.1	151.29
30	LO <i>Minylitha convallis</i>	N	7.73	1124C-16H-CC	159.3	171.13
31	LO <i>Catinaster calyculus</i>	N	9.64	1124C-19X-CC	188.17	200
32	FO <i>Minylitha convallis</i>	N	9.34	1124C-20H-CC	197.57	209.4
33	FO <i>Catinaster coalitus</i>	N	10.79	1124C-21X-CC	207.36	219.19
34	LO <i>Globoquadrina dehiscens</i>	F	10.1	1124C-20X-CC	207.4	219.23
35	FO <i>Zeaglobigerina nepenthes</i>	F	11.8	1124C-21X-CC	207.4	219.23
36	LO <i>Orbulina suturalis</i>	F	-10.5	1124C-22X-CC	212.1	223.93
37	FO <i>Sphaeroidinellopsis disjuncta</i>	F	18.5	1124C-22X-CC	212.1	223.93
38	LO <i>Globorotalia praemenardii</i>	F	13.2	1124C-22X-5, 124–128 cm	214.6	226.43
39	LO <i>Globorotalia amuria</i>	F	13	1124C-22X-5, 124–128 cm	214.6	226.43
40	LO <i>Coccolithus miopelagicus</i>	N	10.94	1124C-22X-CC	216.96	228.79
41	LO <i>Calcidiscus premacintyrei</i>	N	12.65	1124C-23X-CC	226.59	238.42
42	FO <i>Globorotalia praemenardii</i>	F	15.8	1124C-24X-CC	236.2	248.03
43	LO <i>Sphenolithus heteromorphus</i>	N	13.52	1124C-25X-CC	245.88	257.71
44	LO <i>Acme Discoaster deflandrei</i>	N	16.21	1124C-27X-CC	264.95	276.88
45	LO <i>Catapsydrax dissimilis</i>	F	16.7	1124C-28X-CC	274.6	286.43
46	FO <i>Globigerinoides trilobus</i>	F	19	1124C-29X-CC	276.4	288.23
47	LO/FO <i>Globorotalia incognita</i>	F	21.6–18.5	1124C-29X-CC	276.5	288.33
48	LO <i>Roccella gelida</i>	D	22.4	1124C-31X-CC	303.08	314.91
49	FO <i>Cassidulina cuneata</i>	F	~27	1124C-31X-CC	303.2	315.03
50	LO <i>Roccella gelida</i> var. <i>schraderi</i>	D	23.7	1124C-33X-CC	322.68	334.51
51	LO <i>Lychnocanoma conica</i>	R	28.75–30.10	1124C-33X-CC	322.68	334.51
52	LO <i>Sphenolithus umbrellus</i>	N	23.6	1124C-34X-CC	332.49	344.32
53	LO <i>Dictyococcites bisectus</i>	N	23.9	1124C-34X-CC	332.49	344.32
54	LO <i>Sphenolithus delphix</i>	N	24.3	1124C-34X-CC	332.49	344.32
55	LO <i>Chiasmolithus altus</i>	N	26.1	1124C-35X-CC	342.34	354.17
56	FO <i>Roccella vigilans</i>	D	30.24	1124C-40X-CC	390.07	402
57	LO <i>Cibicidoides praemundulus</i>	F	23.8	1124C-40X-CC	390.1	401.93
58	FO <i>Cavittatus jouseanus</i>	D	30.62	1124C-41X-CC	399.87	411.7
59	LO <i>Reticulofenestra umbilicus</i>	N	32.3	1124C-43X-2, 57 cm	411.77	423.6
60	LO <i>Ericsonia formosa</i>	N	32.8	1124C-43X-2, 57 cm	411.77	423.6
61	Acme <i>Clausicoccus subdistichus</i>	N	33.3	1124C-43X-6, 66 cm	417.86	429.69
62	FO <i>Isthmolithus recurvus</i>	N	36	1124C-43X-CC	418.65	430.48
63	FO <i>Dictyococcites bisectus</i>	N	38	1124C-43X-CC	418.65	430.48
64	LO <i>Subbotina angiporoidea</i>	F	30	1124C-43X-CC	418.7	430.53
65	LCO <i>Paragloborotalia gemma</i>	F	32	1124C-43X-CC	418.7	430.53
66	FO <i>Paragloborotalia gemma</i>	F	35	1124C-43X-CC	418.7	430.53
67	LO <i>Globigerinatheka index</i>	F	34.3	1124C-44X-1, 67–69 cm	420.0	431.83
68	LO <i>Ponticulasphaera semiinvoluta</i>	F	34.8	1124C-44X-1, 67–69 cm	420.0	431.83

**Table T14 (continued).**

Events	Group	Age (Ma)	Core, section, interval (cm)	Depth (mbsf)	Depth (mcd)
69 LO <i>Nuttallides truempyi</i>	F	?34.3	1124C-44X-1, 67–69 cm	420.0	431.83
70 LO <i>Acarinina primitiva</i>	F	~36	1124C-44X-1, 67–69 cm	420.0	431.83
71 FO <i>Ponticulospaera semiinvoluta</i>	F	38.4	1124C-44X-5, 93–95 cm	426.2	438.03
72 FO <i>Globigerinatheka index</i>	F	42.9	1124C-44X-6, 50–52 cm	427.3	439.13
73 LO <i>Gavelinella beccariiformis</i>	F	55	1124C-44X-CC	429.1	440.93
74 LO <i>Hornbrookina teuriensis</i>	N	58.3	1124C-45X-1, 29 cm	429.28	441.11
75 FO <i>Fasciculithus tympaniformis</i>	N	59.7	1124C-45X-CC	438.62	450.45
76 FO <i>Chiasmolithus bident</i>	N	60.7	1124C-45X-CC	438.62	450.45
77 LO <i>Aragonina quezzanensis</i>	F	55	1124C-45X-CC	438.7	450.53
78 FO <i>Morozovella conicotruncata</i>	F	60.9	1124C-45X-CC	438.7	450.53
79 FO <i>Morozovella angulata</i>	F	61	1124C-45X-CC	438.7	450.53
80 FO <i>Morozovella praecursoria</i>	F	~61.2	1124C-45X-CC	438.7	450.53
81 FO <i>Morozovella aff. trinidadensis</i>	F	? ~63.0	1124C-45X-CC	438.7	450.53
82 FO <i>Sphenolithus primus</i>	N	60.6	1124C-46X-CC	445.83	457.66
83 FO <i>Cruciplacolithus tenuis</i>	N	64.5	1124C-47X-CC	457.46	469.29
84 FO <i>Globanomalina compressa</i>	F	~63.5	1124C-47X-CC	457.6	469.43
85 LO <i>Globoconusa daubjergensis</i>	F	~63	1124C-47X-CC	457.6	469.43
86 LO <i>Globigerina fringa</i>	F	63	1124C-47X-CC	457.6	469.43
87 FO <i>Hornbrookina teuriensis</i>	N	64.9	1124C-48X-CC	463.32	475.15
88 LO <i>Globigerina eugubina</i>	F	64.9	1124C-48X-CC	463.4	475.23
89 LO <i>Micula</i> spp.	N	65	1124C-49X-1, 21 cm	467.61	479.44
90 LO <i>Rugoglobigerina rugosa</i>	F	65	1124C-49X-CC	473.1	484.93
91 LO <i>Globorotalites michelinianus</i>	F	65	1124C-49X-CC	473.1	484.93

Note: Most samples are from core catchers.

**Table T15.** Composition of interstitial waters, Site 1124.

Core, section, interval (cm)	Depth (mbsf)	Depth (mcd)	Cl <sup>-</sup> (mM)	pH	Alkalinity (mM)	Na <sup>+</sup> (mM)	Mg <sup>2+</sup> (mM)	Ca <sup>2+</sup> (mM)	SO <sub>4</sub> <sup>2-</sup> (mM)	HPO <sub>4</sub> <sup>2-</sup> (μM)	NH <sub>4</sub> <sup>+</sup> (μM)	H <sub>4</sub> SiO <sub>4</sub> (μM)	K <sup>+</sup> (mM)	Li <sup>+</sup> (μM)	Sr <sup>2+</sup> (μM)	
<b>181-1124B-</b>																
1H-2, 140-150	2.90	2.90	34.5	556	7.52	4.23	475	51.6	10.1	27.4	13.0	59	607	12.0	29	93
2H-2, 140-150	8.30	9.20	34.5	561	7.52	4.97	481	50.7	9.7	26.8	12.2	167	639	12.3	35	100
<b>181-1124C-</b>																
2X-4, 84-94	21.94	21.94	35.0	564	7.41	5.58	481	50.1	10.3	25.1	6.4	286	673	11.7	46	115
3H-4, 140-150	33.10	30.70	35.0	565	7.36	5.17	482	49.5	10.6	24.8	6.4	313	699	11.6	50	119
4H-4, 140-150	42.60	41.12	35.5	565	7.32	5.12	483	48.6	11.2	24.3	6.2	324	702	11.4	54	134
5H-4, 140-150	52.10	51.60	35.0	566	7.41	4.86	484	47.5	11.7	24.3	3.9	330	693	11.4	55	139
6H-4, 140-150	61.60	61.92	34.5	565	7.35	4.63	484	46.4	12.3	24.0	2.8	323	719	11.4	55	145
7H-4, 140-150	71.10	73.64	35.0	565	7.33	4.26	484	45.7	12.8	23.6	2.1	316	714	10.8	55	153
8H-4, 140-150	80.60	82.92	35.0	572	7.30	4.49	490	45.1	13.7	23.7	2.0	305	714	10.9	53	164
9H-4, 140-150	90.10	92.90	35.0	571	7.34	4.10	490	44.1	14.8	24.4	2.0	303	695	11.0	54	174
10H-4, 140-150	99.60	103.87	35.0	572	7.35	3.91	492	43.2	15.8	24.6	2.0	276	680	10.7	54	188
11H-4, 140-150	109.10	115.29	35.0	571	7.46	3.71	492	42.0	16.5	24.6	2.6	270	743	10.4	56	196
14H-4, 140-150	137.60	147.79	35.0	570	7.49	3.56	490	40.1	19.3	24.9	2.2	246	807	10.2	66	225
17X-4, 140-150	165.10	176.93	35.0	568	7.41	3.22	488	38.7	21.3	25.3	2.8	208	816	9.4	76	254
20X-4, 140-150	193.90	205.73	34.5	564	7.34	3.20	481	36.6	23.5	22.8	2.0	174	351	7.7	99	317
23X-4, 140-150	222.80	234.63	35.0	568	7.37	2.00	483	35.2	25.4	22.4	1.8	178	314	7.2	121	376
26X-4, 140-150	251.70	263.53	34.5	568	7.37	2.24	478	35.4	27.6	21.6	2.0	130	420	6.0	160	443
31X-4, 140-150	299.90	311.73	34.5	561	7.27	3.67	460	36.9	31.6	21.2	3.0	127	1036	5.5	240	515
34X-4, 135-150	328.75	340.58	35.0	572	7.10	3.34	472	35.2	31.6	21.5	2.2	164	1106	7.1	249	585
37X-4, 135-150	357.75	369.58	35.5	573	7.19	2.97	471	34.7	31.9	19.9	2.4	151	1155	7.1	252	598
40X-4, 135-150	386.65	398.48	35.5	578	7.07	4.08	474	33.6	33.7	19.7	2.4	160	1203	6.8	267	586
43X-3, 135-150	414.05	425.88	35.0	572	7.16	3.59	463	33.6	34.9	17.9	3.0	127	939	6.3	250	521
46X-3, 135-150	443.05	454.88	36.0	579	7.01	4.67	465	34.6	38.0	19.7	3.4	120	702	6.6	237	466
49X-3, 135-150	471.75	483.58	35.5	568	7.50	3.24	453	34.7	38.7	19.1	3.4	93	968	5.6	206	387

Note: This table is also available in [ASCII format](#).

**Table T16.** Inorganic carbon, carbonate, total carbon, total organic carbon, total nitrogen, total sulfur, and atomic organic carbon/nitrogen values for sediments from Holes 1124A, 1124B, and 1124C. ([See table note](#). Continued on next page.)

Core, section, interval (cm)	Depth (mbsf)	IC (%)	CaCO <sub>3</sub> (%)	TC (%)	TOC (%)	TN (%)	TS (%)	[C/N] <sub>a</sub> (%)
<b>181-1124A-</b>								
1H-2, 67-68	2.17	2.14	17.8	2.68	0.54	0.14	0.16	4.5
1H-4, 134-135	5.84	4.41	36.7					
1H-6, 103-104	8.53	4.96	41.3					
<b>181-1124B-</b>								
1H-1, 31-32	0.31	5.20	43.3					
1H-1, 107-108	1.07	2.40	20.0	2.87	0.47	0.13	n.d.	4.2
1H-3, 78-79	3.78	5.45	45.4					
2H-1, 54-55	5.94	5.77	48.1					
2H-3, 56-57	8.96	1.02	8.5	1.87	0.85	0.14	0.09	7.2
<b>181-1124C-</b>								
1X-1, 42-43	8.42	5.30	44.2	5.45	0.14	0.08	n.d.	2.1
2X-3, 120-121	20.80	8.16	68.0					
2X-6, 90-91	24.44	1.66	13.9	1.87	0.21	0.11	n.d.	2.3
3H-2, 51-52	29.21	4.48	37.3					
3H-2, 93-94	29.63	6.99	58.2					
3H-3, 90-91	31.10	1.10	9.2	1.45	0.35	0.12	0.03	3.3
3H-4, 83-84	32.53	1.53	12.8					
4H-1, 90-91	37.60	2.57	21.4					
4H-2, 90-91	39.10	6.31	52.6	6.49	0.17	0.07	n.d.	3.1
4H-5, 90-91	43.60	5.76	47.9					
5H-1, 119-120	47.39	3.57	29.7					
5H-2, 120-121	48.90	6.70	55.8	6.94	0.25	0.07	n.d.	4.1
5H-3, 120-121	50.40	4.16	34.7					
6H-1, 145-146	57.15	4.10	34.1					
6H-3, 100-101	59.70	6.19	51.6	6.34	0.15	0.08	n.d.	2.1
6H-5, 120-121	62.90	1.36	11.3	1.5	0.14	0.12	n.d.	1.4
7H-1, 98-99	66.18	7.75	64.6					
7H-3, 99-100	69.19	6.37	53.1					
7H-5, 100-101	72.20	4.18	34.9	4.56	0.38	0.09	0.05	5.2
8H-1, 68-69	75.38	4.30	35.8					
8H-3, 68-69	78.38	1.70	14.2	1.79	0.09	0.09	n.d.	1.1
8H-5, 68-69	81.38	7.47	62.2	7.7	0.23	0.07	n.d.	4
9H-1, 111-112	85.31	6.43	53.6					
9H-3, 112-113	88.32	2.28	19.0					
10H-1, 42-43	94.12	5.20	43.3	5.58	0.38	0.11	n.d.	4
10H-6, 50-51	101.70	1.48	12.4					
11H-3, 79-80	106.99	4.12	34.3					
11H-7, 13-14	112.33	0.50	4.2	0.89	0.39	0.08	n.d.	5.6
12H-2, 45-46	114.65	0.17	1.5	0.22	0.04	0.1	n.d.	0.5
12H-2, 77-78	114.97	2.35	19.6					
13H-2, 13-14	123.83	0.30	2.5					
13H-6, 40-41	130.10	3.29	27.4	3.72	0.43	0.07	n.d.	6.9
14H-4, 121-122	137.41	4.14	34.5					
14H-6, 117-118	140.37	0.41	3.4	0.66	0.25	0.07	n.d.	4.4
15H-1, 108-109	142.28	4.38	36.5	4.87	0.5	0.06	n.d.	9.9
15H-6, 110-111	149.80	1.12	9.3					
16H-1, 97-98	151.67	1.24	10.4					
16H-6, 60-61	158.80	0.18	1.5	0.62	0.44	0.09	n.d.	5.7
17X-1, 89-90	160.09	1.96	16.3	2.25	0.29	0.08	n.d.	4.4
17X-4, 90-91	164.60	1.23	10.3					
17X-6, 90-91	167.60	0.79	6.6					
18X-2, 56-57	170.86	3.07	25.6					
18X-4, 80-83	174.10	2.20	18.4					
19X-6, 88-89	186.78	1.87	15.6	2.13	0.26	0.07	n.d.	4.3
19X-6, 136-137	187.26	3.53	29.4					
20X-2, 50-51	190.00	0.68	5.6					
20X-4, 48-49	192.98	3.61	30.1					
21X-1, 80-81	198.50	1.37	11.4	1.69	0.32	0.08	n.d.	4.7
21X-4, 79-80	202.99	4.84	40.3					
22X-2, 90-91	209.70	0.65	5.4					
22X-4, 90-91	212.70	4.77	39.7	5.16	0.39	0.09	n.d.	5.4
23X-1, 47-48	217.37	3.73	31.0					
23X-5, 47-48	223.37	8.33	69.4					

**Table T16 (continued).**

Core, section, interval (cm)	Depth (mbsf)	IC (%)	CaCO <sub>3</sub> (%)	TC (%)	TOC (%)	TN (%)	TS (%)	[C/N] <sub>a</sub> (%)
24X-4, 79-80	231.79	1.17	9.8					
25X-1, 69-70	236.89	0.09	0.8	0.41	0.32	0.09	n.d.	4.2
25X-3, 69-70	239.89	6.39	53.3	6.78	0.38	0.07	n.d.	6.8
26X-2, 95-96	248.25	4.66	38.8					
26X-2, 123-124	248.53	0.58	4.8					
27X-2, 13-14	257.03	4.87	40.5					
27X-6, 125-126	264.15	0.59	4.9	0.7	0.11	0.09	n.d.	1.5
28X-2, 14-15	266.69	1.16	9.7					
29X-1, 14-15	274.84	0.91	7.6					
29X-2, 7-8	276.27	6.06	50.5	6.48	0.42	0.08	n.d.	6.1
31X-3, 84-85	297.84	5.54	46.2					
31X-5, 31-32	300.31	3.27	27.3					
32X-2, 102-103	306.12	0.47	3.9	0.87	0.4	0.09	n.d.	5.3
32X-4, 72-73	308.82	7.00	58.3					
33X-2, 58-59	315.38	6.85	57.0	7.4	0.55	0.08	n.d.	7.8
33X-2, 128-129	316.08	7.85	65.4					
34X-2, 75-76	325.15	7.15	59.6					
34X-5, 55-56	329.45	7.56	63.0					
35X-4, 111-112	338.21	7.82	65.2	8.37	0.55	0.1	n.d.	6.2
36X-1, 30-31	342.50	8.78	73.1					
36X-6, 74-75	350.44	3.89	32.4					
37X-3, 56-57	355.46	6.35	52.9	6.65	0.3	0.07	n.d.	4.7
37X-6, 59-60	359.99	6.77	56.4					
38X-2, 61-62	363.61	6.15	51.2					
38X-5, 101-102	368.51	8.27	68.9	8.24	n.d.	0.09	n.d.	—
39X-1, 113-114	372.33	8.31	69.2					
39X-4, 50-51	376.20	2.92	24.3					
40X-1, 96-97	381.76	7.75	64.5	7.76	0.01	0.07	n.d.	0.2
40X-4, 96-97	386.26	9.32	77.6					
43X-2, 26-27	411.46	5.68	47.3					
43X-5, 75-76	416.45	10.01	83.4	10.41	0.4	0.06	n.d.	8.2
44X-1, 60-61	419.90	5.70	47.5					
44X-4, 110-111	424.90	4.22	35.2	4.62	0.4	0.04	n.d.	12.6
44X-6, 40-41	427.20	3.13	26.1	3.41	0.28	0.04	n.d.	8.2
44X-6, 86-87	427.66	0.05	0.4	0.31	0.26	0.04	0.05	7.2
44X-7, 29-30	428.59	0.02	0.2	0.46	0.44	0.07	n.d.	7.9
45X-1, 9-11	429.09	10.22	85.1					
45X-6, 37-38	436.87	7.63	63.6					
46X-2, 51-52	440.71	10.31	85.9	10.31	n.d.	0.04	n.d.	—
46X-3, 96-97	442.66	10.60	88.3					
47X-3, 67-68	451.97	10.36	86.3					
47X-5, 49-50	454.79	9.57	79.7	9.91	0.34	n.d.	n.d.	—

Notes: Carbonate is calculated assuming that all inorganic carbon is calcite. n.d. = not detected. This table is also available in [ASCII format](#).

**Table T17.** List of index properties measured from Hole 1124C. (See table note. Continued on next two pages.)

Leg	Hole	Core	Section	Interval (cm)	Depth (mbsf)	Wet-water content (%)	Dry-water content (%)	Wet-bulk density (g/cm³)	Dry density (g/cm³)	Grain density (g/cm³)	Porosity (%)	Void ratio
181	1124C	1X	1	19-21	8.19	58.3	140.0	1.378	0.574	2.669	78.5	3.65
181	1124C	2X	1	51-53	18.11	46.5	86.9	1.532	0.820	2.696	69.6	2.29
181	1124C	2X	3	67-69	20.27	49.6	98.5	1.491	0.751	2.705	72.2	2.60
181	1124C	2X	6	105-107	24.59	49.4	97.7	1.497	0.757	2.731	72.3	2.61
181	1124C	3H	1	97-99	28.17	50.9	103.7	1.472	0.722	2.695	73.2	2.73
181	1124C	3H	2	72-74	29.42	44.6	80.6	1.561	0.864	2.707	68.1	2.13
181	1124C	3H	5	108-110	34.28	46.1	85.5	1.537	0.829	2.686	69.2	2.24
181	1124C	3H	6	118-120	35.88	47.7	91.1	1.521	0.796	2.727	70.8	2.43
181	1124C	4H	1	137-139	38.07	45.5	83.6	1.522	0.829	2.566	67.7	2.10
181	1124C	4H	3	92-94	40.62	48.3	93.5	1.503	0.777	2.671	70.9	2.44
181	1124C	4H	5	126-128	43.96	44.7	80.8	1.567	0.867	2.739	68.4	2.16
181	1124C	4H	6	133-135	45.53	47.1	88.9	1.526	0.808	2.705	70.1	2.35
181	1124C	5H	1	103-105	47.23	47.2	89.4	1.517	0.801	2.666	70.0	2.33
181	1124C	5H	2	83-85	48.53	43.9	78.2	1.554	0.872	2.613	66.6	2.00
181	1124C	5H	4	45-47	51.15	44.7	80.9	1.568	0.867	2.749	68.5	2.17
181	1124C	5H	5	52-54	52.72	46.7	87.6	1.529	0.815	2.689	69.7	2.30
181	1124C	6H	2	139-141	58.59	50.6	102.5	1.473	0.727	2.673	72.8	2.68
181	1124C	6H	4	7-9	60.27	47.9	91.8	1.502	0.783	2.627	70.2	2.35
181	1124C	6H	5	10-12	61.80	42.3	73.2	1.597	0.922	2.707	65.9	1.94
181	1124C	6H	6	122-124	64.42	44.6	80.5	1.567	0.869	2.736	68.3	2.15
181	1124C	7H	1	8-10	65.28	45.2	82.5	1.553	0.851	2.707	68.6	2.18
181	1124C	7H	3	36-38	68.56	43.6	77.2	1.575	0.889	2.694	67.0	2.03
181	1124C	7H	5	104-106	72.24	46.6	87.4	1.531	0.817	2.701	69.7	2.31
181	1124C	7H	6	124-126	73.94	43.5	77.1	1.555	0.878	2.591	66.1	1.95
181	1124C	8H	2	76-78	76.96	44.1	79.0	1.569	0.876	2.706	67.6	2.09
181	1124C	8H	4	130-132	80.50	44.5	80.2	1.570	0.871	2.742	68.2	2.15
181	1124C	8H	5	104-106	81.74	46.4	86.4	1.545	0.829	2.759	70.0	2.33
181	1124C	8H	7	9-11	82.89	49.0	95.9	1.498	0.765	2.692	71.6	2.52
181	1124C	9H	3	120-122	88.40	47.6	90.8	1.525	0.799	2.746	70.9	2.44
181	1124C	9H	4	131-133	90.01	43.4	76.8	1.589	0.899	2.757	67.4	2.07
181	1124C	9H	5	103-105	91.23	45.5	83.4	1.557	0.849	2.750	69.1	2.24
181	1124C	9H	6	34-36	92.04	46.7	87.7	1.527	0.814	2.685	69.7	2.30
181	1124C	10H	2	7-9	95.27	49.0	96.0	1.504	0.767	2.735	71.9	2.56
181	1124C	10H	4	134-136	99.54	48.0	92.2	1.511	0.786	2.694	70.8	2.43
181	1124C	10H	6	109-111	102.29	49.6	98.2	1.499	0.756	2.757	72.6	2.64
181	1124C	11H	1	27-29	103.47	47.5	90.5	1.524	0.800	2.727	70.7	2.41
181	1124C	11H	3	67-69	106.87	48.6	94.7	1.504	0.772	2.703	71.4	2.50
181	1124C	11H	5	139-141	110.59	47.5	90.6	1.513	0.794	2.664	70.2	2.36
181	1124C	12H	1	69-71	113.39	50.2	100.7	1.491	0.743	2.758	73.1	2.71
181	1124C	12H	3	29-31	115.99	51.0	103.9	1.474	0.723	2.710	73.3	2.75
181	1124C	12H	5	79-81	119.49	45.3	82.7	1.534	0.840	2.608	67.8	2.11
181	1124C	13H	1	69-71	122.89	50.0	100.0	1.496	0.748	2.773	73.0	2.71
181	1124C	13H	3	31-33	125.51	47.3	89.7	1.508	0.795	2.619	69.6	2.29
181	1124C	13H	5	84-86	129.04	47.7	91.2	1.513	0.791	2.679	70.5	2.39
181	1124C	14H	1	142-144	133.12	48.3	93.6	1.513	0.781	2.732	71.4	2.50
181	1124C	14H	3	133-135	136.03	47.0	88.5	1.535	0.814	2.747	70.4	2.38
181	1124C	14H	5	139-141	139.09	48.3	93.5	1.504	0.777	2.677	71.0	2.45
181	1124C	15H	1	79-81	141.99	49.1	96.3	1.502	0.765	2.727	72.0	2.57
181	1124C	15H	3	11-13	144.31	48.7	94.9	1.505	0.772	2.717	71.6	2.52
181	1124C	15H	5	77-79	147.97	43.2	75.9	1.554	0.883	2.558	65.5	1.90
181	1124C	16H	1	33-35	151.03	49.7	98.7	1.490	0.750	2.706	72.3	2.61
181	1124C	16H	3	79-81	154.49	45.5	83.4	1.543	0.841	2.671	68.5	2.18
181	1124C	16H	6	79-81	158.99	45.9	84.8	1.532	0.829	2.646	68.7	2.19
181	1124C	17X	2	81-83	161.51	50.2	100.6	1.482	0.739	2.693	72.6	2.65
181	1124C	17X	4	75-77	164.45	48.0	92.2	1.516	0.789	2.724	71.0	2.45
181	1124C	17X	6	124-126	167.94	49.9	99.6	1.483	0.743	2.677	72.2	2.60
181	1124C	18X	1	27-29	169.07	49.4	97.6	1.494	0.756	2.707	72.1	2.58
181	1124C	18X	3	139-141	173.19	45.3	82.9	1.553	0.849	2.715	68.7	2.20
181	1124C	18X	5	81-83	175.61	47.9	91.9	1.514	0.789	2.703	70.8	2.43
181	1124C	19X	2	134-136	181.24	36.0	56.3	1.697	1.086	2.694	59.7	1.48
181	1124C	19X	4	127-129	184.17	33.2	49.8	1.737	1.159	2.658	56.4	1.29
181	1124C	19X	6	68-70	186.58	35.6	55.3	1.689	1.088	2.636	58.7	1.42
181	1124C	20X	2	109-111	190.59	30.4	43.8	1.766	1.228	2.587	52.5	1.11
181	1124C	20X	4	78-80	193.28	30.0	42.8	1.786	1.251	2.619	52.2	1.09
181	1124C	20X	6	112-114	196.62	32.3	47.7	1.752	1.186	2.651	55.3	1.24
181	1124C	21X	2	73-75	199.93	29.3	41.5	1.793	1.267	2.604	51.3	1.06
181	1124C	21X	4	82-84	203.02	35.1	54.0	1.718	1.116	2.711	58.8	1.43

**Table T17 (continued).**

Leg	Hole	Core	Section	Interval (cm)	Depth (mbsf)	Wet-water content (%)	Dry-water content (%)	Wet-bulk density (g/cm <sup>3</sup> )	Dry density (g/cm <sup>3</sup> )	Grain density (g/cm <sup>3</sup> )	Porosity (%)	Void ratio
181	1124C	21X	6	96-98	206.16	32.0	47.1	1.769	1.202	2.689	55.3	1.24
181	1124C	22X	2	77-79	209.57	33.8	51.2	1.742	1.153	2.718	57.6	1.36
181	1124C	22X	4	72-74	212.52	30.0	42.9	1.795	1.256	2.649	52.6	1.11
181	1124C	22X	6	65-67	215.45	28.9	40.6	1.813	1.290	2.640	51.1	1.05
181	1124C	23X	2	81-83	219.21	32.2	47.5	1.770	1.200	2.708	55.7	1.26
181	1124C	23X	4	46-48	221.86	32.7	48.5	1.763	1.187	2.712	56.2	1.29
181	1124C	23X	5	69-71	223.59	34.9	53.7	1.723	1.121	2.719	58.8	1.43
181	1124C	24X	2	86-88	228.86	33.5	50.3	1.747	1.162	2.710	57.1	1.33
181	1124C	24X	4	87-89	231.87	32.0	47.0	1.776	1.208	2.711	55.4	1.24
181	1124C	24X	6	38-40	234.38	33.3	49.9	1.744	1.164	2.687	56.7	1.31
181	1124C	25X	2	65-67	238.35	31.3	45.6	1.787	1.227	2.708	54.7	1.21
181	1124C	25X	3	98-100	240.18	31.2	45.4	1.794	1.234	2.726	54.7	1.21
181	1124C	25X	5	112-114	243.32	31.5	46.1	1.784	1.221	2.710	54.9	1.22
181	1124C	26X	1	120-122	247.00	32.6	48.4	1.767	1.191	2.725	56.3	1.29
181	1124C	26X	3	129-131	250.09	32.2	47.5	1.775	1.203	2.724	55.8	1.26
181	1124C	26X	5	124-126	253.04	30.2	43.2	1.814	1.267	2.722	53.5	1.15
181	1124C	27X	1	135-137	256.75	28.7	40.3	1.841	1.312	2.712	51.6	1.07
181	1124C	27X	3	137-139	259.77	30.6	44.0	1.804	1.252	2.713	53.8	1.17
181	1124C	27X	5	122-124	262.62	29.5	41.8	1.808	1.274	2.659	52.1	1.09
181	1124C	28X	1	131-133	266.41	30.9	44.6	1.783	1.233	2.666	53.8	1.16
181	1124C	28X	3	135-137	269.40	30.6	44.1	1.794	1.246	2.684	53.6	1.16
181	1124C	28X	5	129-131	272.34	30.9	44.7	1.790	1.237	2.691	54.0	1.18
181	1124C	29X	1	105-107	275.75	29.2	41.3	1.822	1.289	2.688	52.0	1.09
181	1124C	31X	1	100-102	295.00	38.0	61.2	1.669	1.035	2.714	61.8	1.62
181	1124C	31X	3	147-149	298.47	36.4	57.2	1.693	1.077	2.702	60.2	1.51
181	1124C	31X	5	74-76	300.74	42.3	73.3	1.596	0.921	2.701	65.9	1.93
181	1124C	32X	1	89-91	304.49	38.4	62.4	1.661	1.022	2.714	62.3	1.65
181	1124C	32X	3	75-77	307.35	40.8	69.0	1.622	0.960	2.716	64.7	1.83
181	1124C	32X	5	97-99	310.57	48.3	93.4	1.503	0.777	2.670	70.9	2.43
181	1124C	32X	7	60-62	312.50	39.8	66.1	1.629	0.981	2.674	63.3	1.73
181	1124C	33X	1	56-58	313.86	43.4	76.6	1.572	0.890	2.666	66.6	2.00
181	1124C	33X	3	89-91	317.19	43.9	78.3	1.562	0.876	2.654	67.0	2.03
181	1124C	33X	5	126-128	320.56	40.9	69.2	1.615	0.954	2.689	64.5	1.82
181	1124C	34X	1	92-94	323.82	41.9	72.0	1.596	0.928	2.671	65.3	1.88
181	1124C	34X	3	84-86	326.74	37.1	59.0	1.672	1.051	2.666	60.6	1.54
181	1124C	34X	5	54-56	329.44	36.0	56.3	1.699	1.087	2.702	59.8	1.49
181	1124C	35X	1	92-94	333.52	36.3	56.9	1.689	1.076	2.680	59.8	1.49
181	1124C	35X	3	25-27	335.85	35.2	54.2	1.710	1.109	2.684	58.7	1.42
181	1124C	35X	6	71-73	340.81	36.6	57.8	1.688	1.070	2.701	60.4	1.53
181	1124C	36X	2	37-39	344.07	34.5	52.8	1.719	1.125	2.680	58.0	1.38
181	1124C	36X	4	84-86	347.54	29.4	41.6	1.824	1.288	2.700	52.3	1.10
181	1124C	36X	6	50-52	350.20	32.9	48.9	1.747	1.173	2.668	56.0	1.28
181	1124C	37X	2	58-60	353.98	30.1	43.1	1.831	1.280	2.772	53.8	1.17
181	1124C	37X	4	24-26	356.64	30.7	44.3	1.794	1.243	2.689	53.8	1.16
181	1124C	37X	6	37-39	359.77	29.0	40.9	1.835	1.302	2.716	52.1	1.09
181	1124C	38X	2	84-86	363.84	30.2	43.2	1.812	1.266	2.714	53.4	1.14
181	1124C	38X	4	73-75	366.73	27.1	37.1	1.875	1.367	2.712	49.6	0.98
181	1124C	38X	6	63-65	369.63	27.0	37.0	1.870	1.365	2.694	49.3	0.97
181	1124C	39X	2	67-69	373.37	25.3	33.9	1.917	1.431	2.721	47.4	0.90
181	1124C	39X	4	101-103	376.71	27.1	37.1	1.857	1.354	2.660	49.1	0.96
181	1124C	39X	6	45-47	379.15	29.2	41.2	1.875	1.328	2.851	53.4	1.15
181	1124C	40X	2	83-85	383.13	28.9	40.7	1.832	1.302	2.701	51.8	1.07
181	1124C	40X	4	61-63	385.91	31.4	45.7	1.781	1.223	2.689	54.5	1.20
181	1124C	40X	6	73-75	389.03	35.4	54.8	1.706	1.102	2.688	59.0	1.44
181	1124C	41X	2	56-58	392.46	31.0	44.9	1.831	1.264	2.835	55.4	1.24
181	1124C	41X	4	31-33	395.21	24.8	33.0	1.909	1.435	2.672	46.3	0.86
181	1124C	41X	6	131-133	399.21	21.5	27.4	2.011	1.579	2.730	42.2	0.73
181	1124C	42X	2	91-93	402.51	24.1	31.8	1.932	1.466	2.691	45.5	0.84
181	1124C	42X	4	95-97	405.55	24.2	31.9	1.932	1.464	2.694	45.6	0.84
181	1124C	42X	6	41-43	408.01	21.9	28.1	1.997	1.559	2.723	42.8	0.75
181	1124C	43X	2	86-88	412.06	22.0	28.2	1.981	1.545	2.689	42.5	0.74
181	1124C	43X	4	51-53	414.71	20.0	24.9	2.039	1.632	2.710	39.8	0.66
181	1124C	43X	6	76-78	417.96	21.9	28.1	1.994	1.557	2.716	42.7	0.74
181	1124C	44X	2	49-51	421.29	31.1	45.2	1.771	1.220	2.642	53.8	1.17
181	1124C	44X	4	59-61	424.39	25.5	34.3	1.903	1.417	2.697	47.5	0.90
181	1124C	44X	6	80-82	427.60	36.4	57.3	1.659	1.055	2.571	59.0	1.44
181	1124C	45X	1	71-73	429.71	24.5	32.4	1.936	1.462	2.720	46.3	0.86
181	1124C	45X	3	62-64	432.62	23.6	30.8	1.943	1.485	2.685	44.7	0.81
181	1124C	45X	5	101-103	436.01	20.0	25.0	2.036	1.629	2.704	39.7	0.66
181	1124C	45X	7	40-42	438.40	19.8	24.7	2.036	1.633	2.692	39.3	0.65

**Table T17 (continued).**

Leg	Hole	Core	Section	Interval (cm)	Depth (mbsf)	Wet-water content (%)	Dry-water content (%)	Wet-bulk density (g/cm <sup>3</sup> )	Dry density (g/cm <sup>3</sup> )	Grain density (g/cm <sup>3</sup> )	Porosity (%)	Void ratio
181	1124C	46X	1	130-132	440.00	23.9	31.4	1.957	1.489	2.742	45.7	0.84
181	1124C	46X	3	80-82	442.50	24.4	32.2	1.933	1.462	2.706	46.0	0.85
181	1124C	46X	5	65-67	445.35	24.8	32.9	1.928	1.451	2.718	46.6	0.87
181	1124C	47X	1	115-117	449.45	28.5	39.9	1.845	1.319	2.711	51.4	1.06
181	1124C	47X	3	133-135	452.63	24.8	32.9	1.925	1.448	2.710	46.6	0.87
181	1124C	47X	5	131-133	455.61	23.7	31.0	1.961	1.497	2.738	45.3	0.83
181	1124C	48X	1	58-60	458.48	21.8	27.9	1.985	1.552	2.692	42.4	0.74
181	1124C	48X	3	100-102	461.90	23.3	30.4	1.955	1.499	2.699	44.4	0.80

Note: This table is also available in [ASCII format](#).